The Hashemite Kingdom of Jordan
Scientific Research Support Fund
The Hashemite University

JJEES

Jordan Journal of Earth and Environmental Sciences

Volume (12) Number (2)

JJEES is an International Peer-Reviewed Research Journal

ISSN 1995-6681 jjees.hu.edu.jo June 2021

Jordan Journal of Earth and Environmental Sciences (JJEES)

JJEES is an International Peer-Reviewed Research Journal, Issued by Deanship of Scientific Research, The Hashemite University, in corporation with, the Jordanian Scientific Research Support Fund, the Ministry of Higher Education and Scientific Research.

Editorial Board:

Associate Editorial Board: (Arranged Alphabetically)

International Advisory Board: (Arranged Alphabetically)

Editorial Board Support Team:

Submission address:

Manuscripts should be submitted electronically to the following e-mail:

jjees@hu.edu.jo

For more information and previous issues:

www.jjees.hu.edu.jo

Hashemite Kingdom of Jordan

Scientific Research Support Fund

Hashemite University

Jordan Journal of Earth and Environmental Sciences

JJEES

An International Peer-Reviewed Scientific Journal

Financed by the Scientific Research Support Fund

Volume 12 Number (2)

http:// jjees.hu.edu.jo/

ISSN 1995-6681

Cover page photo: Bedding plane with abundant largely articulated valves of the brackish-water bivalve Eomiodon preserved in life position. Kimmeridgian at Santa Cruz, Lusitanian Basin, Portugal. Photographed by Prof. Dr. Franz Fürsich

JJEES
Jordan Journal of Earth and Environmental Sciences

JJEES

JJEES (2021) 12 (2): 99-105
ISSN 1995-6681

Jordan Journal of Earth and Environmental Sciences

Effectiveness of water harvesting technique on selected pastoral shrub: a case of the Syrian Badia (Qaryatien)

Mahmoud Al Hamdan*[1], Wafaa Aboud[2], Boshra Khozam[1], Issam AlKhouri[3]

[1]*General Commission for Scientific Agricultural Researches, Homs, Syria.*
[2]*Al Baath University, Homs, Syria.*
[3]*Department of soil and land reclamation, Faculty of Agriculture, Al Baath University, Syria.*

Received 15 August 2020; Accepted 10 October 2020

Abstract

This research intends to cast light on the importance of water harvesting in the Syrian Badia, a region with an extreme shortage of water resources. The study was carried out during the rainy season of 2010 at the research centre of Mehassa (Qaryatien) in the Syrian Badia. Semi-circular ponds with 40m-diameter were constructed, parallel to the contour lines for water harvesting. Blank ponds with no embankment were simultaneously dug at similar dimensions. The impact of slope steepness of the water ponds on the harvested water volume was evaluated using slopes of 5% and 2%. Both ponds (constructed and blank) were planted with three types of pastoral shrubs *Atriplex halimus, Atriplex lecoclada,* and *Salaola vermiculate***.** The water balance study showed that the constructed ponds preserved excess water of 51.10% for all types of pastoral plants compared with the blanks. It also revealed that the field capacity of the soil in the water ponds increased by 11.11% compared with blanks, with the highest values for soils with a slope of 5% relative to 2%, which will support the growth of more pastoral shrubs. It was noticed that the consumption of water for the pastoral plants cultivated in the constructed ponds increased at the 5% slope more than that at the slope of 2%**.**

Keywords: water balance, pastoral plants, water harvesting techniques, Syrian Badia (Qaryatien).

1. Introduction

Water is considered as one of the most important limiting factors for agricultural production in arid and semi-arid areas, and the stability of the population in these areas. The exploitation and the misuse of water resources lead to a significant reduction in land productivity and desertification. Rainwater harvesting has been a viable alternative to cope with the increasing water demands for irrigation and drinking purposes, especially in these arid and semi-arid regions (Jack and Osman, 1995).

The water harvesting system is dependent on the source and the form of runoff and the used method to concentrate and collect water. The main element of rainwater harvesting techniques is the knowledge of the ratio between runoff area and water collection area. Usually, the water is stored and the plant is cultivated (in cultivated areas), provided that the soil has sufficient water to supply the cultivated crops until rainfall season (Abdel Al, 1994).

The general principle of water harvesting systems is that there are two major areas: the surface runoff area (the catchment area) and the storage area (agricultural area). The water harvesting area can be divided into macro-catchments, micro catchments and floodwater harvesting (IDRC et al., 1993).

Studies conducted in the Syrian Badia for the use of water harvesting and propagation techniques showed that the quantity of water harvested in reservoirs during the period 1995-1998 ranged from 11,900 to 22,000 m^3 (Arar, 1993). These waters are suitable for irrigating crops, watering livestock and humans use after treatment. These quantities can be sufficient to water 66000 sheep for three months at a rate of 8 litres/sheep/day, and enough to cultivate 2000 hectares at a rate of 100 litres. The use of water harvesting techniques also resulted in an emergence of associated plant species, and to an increased rate of pastoral plants, by reducing runoff and rehabilitating of vegetation. Besides, it reduces agricultural soil erosion to 40% on the catchments in which the ponds were constructed (Somme and Abdel-Al, 2002).

Despite the lack of rainfall in arid and semi-arid areas, the soils are susceptible to a high rate of erosion due to flash floods and a lack of vegetative cover. Therefore these characteristics of dry areas require caution when a particular water harvesting technique is selected (UNEP, 1982; Joddi, 1999).

Water harvesting can help to conserve natural resources, particularly soil and vegetation, with implications for good livestock feedstuffs (ICARDA, 1997).

The use of rainwater harvesting in arid and semi-arid areas, where precipitation often occurs fora few months, it is probably one of the most effective means to secure water for human, animal, and plants. Though, rainwater harvesting is associated with some uncontrollable factors such as climatic conditions or soil conditions. However, the good investment and the use of available rainwater, no matter how much little it is, provide basic sources of water in some cases (Arab

* Corresponding author e-mail: alhamdan1978@hotmail.com

Organization for Agricultural Development, 1999).

The main objective of this project is to rationalize the use of water in the Syrian Badia due to the lack of water resources, using methods and techniques that contribute to increasing their productivity and efficiency. The most important of these methods is water harvesting with a simple technique and low costs that can effectively contribute to improving the management of natural resources (water, soil, vegetation), particularly improved vegetation cover and the provision of a livestock feed base, as well as the water supply for livestock and domestic use of water (Arar, 1995).

2. Materials and Methods

2.1. Location of the study area

This study was carried out at the Agricultural Scientific Research Center in Mehassa, 120 km northeast of Damascus and 15 km south of Qaryatien Town. It is located at 37.2°,14',37'' longitude, 34.08°,13',34'' latitude and (735) m altitude, with a total area of 7000 ha (Figure 1).

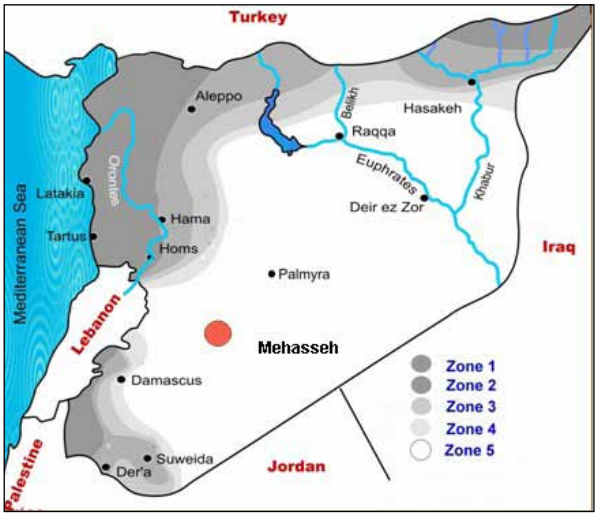

Figure 1. Location map of the studied site. (Ministry of agriculture in Syria)

Note: (Zone from 1 to 5 in the map: is the areas of agricultural stability in Syria, and this map indicates that the study area is outside the borders of the fifth agricultural stability zone, where the rainfall rate is less than 200 mm. So that the studied area consider a marginal area (Badia).

The site is characterized by a hot and dry climate in summer and a cold one in winter with low rainfall of 114 mm per year. This study was carried out during the rainy season of 2010, where rainfall was monitored at the experiment site. The highest rainfall rate was during January with 27.7 mm, and the total rainfall in this season was 78.2 mm. In January, runoff occurred at a rainfall intensity of 11.89 mm/h (Table 1).

2.2. Field work

Two hillsides with different slopes(5% and 2%) were selected, and several semi-circular bunds were established on the contour lines directly at the studied slopes, using the Nevo device which is available In the study site. The ponds of a 40m diameter were drawn, and then a special tractor was used to dig the lines of the contour and open the ponds. The blank was drawn without making an edge. The height of the top edge reached (80) cm and the lowest point reached (60) cm at a slope of 5%; taking into account the unification of the diameters of the bunds and the blank (40) meters. The spacing between the bunds on the contour line was(10) meters and the distance between the contour line was(10) meters. The catchment areas were unified so that each bund on each contour line is isolated from the adjacent bund in the same contour line, and the other bunds on the second contour line. Therefore the catchment area is the square of semi-circular bund with a radius of (20) m.

The bunds and the blank were cultivated in different types of pastoral plants *(Atriplex halimus - Atriplex lecoclada - Salsola vermiculata*), on a 2.5 m spacing between one plant and the other, in the lower third of the arch after a light rainfall of (2) mm. Neutron probe tube was planted on the depth of (50) cm in each section to measure the moisture of soil after the rainfall and periodically every two weeks for each treatment (bund–blank), due to the type of planted shrubs. A rain intensity gauge was put to measure the rainfall intensity (mm/h), and mineral reservoirs were distributed in the experiment to estimate the amount of runoff water.

Table 1. Climatic characteristics of the studied site during 2010.

Month / Climatic element	Jan.	Feb.	Mar.	Apr.	May	June	July	Aug.	Sep.	Oct.	Nov.	Dec.
Rainfall (mm)	27.7	9.6	13.6	20.4	0.4	0	0	0	0	3	0	3.5
Total rainfall mm78.2												
Minimum Temperature	3.9-	6.3-	3.1-	2.2	4.2	9.8	11.8	16.2	11.2	4.4	1.8-	4.5-
Maximum Temperature	19.7	24.8	29	28.4	32.9	33	38.5	39.3	34.7	33.1	26.1	3.7-
Evaporation (mm/month)	6.93	6.91	6.92	6.91	6.89	27.5	28.1	27.05	27.15	27.24	27.36	27.3
Monthly eva-transpiration	42	61	86	136	223	222	217	224	196	143	80	41
Wind speed (m/sec)	3.8	3.8	3.6	4.1	4.3	4.6	4.4	6	3.6	3.2	3.1	4.5
Relative humidity (%)	74.1	64.2	57.9	51.4	35	44.2	45.3	49.1	48.7	50.3	68.0	73.1
Solar Brightness	116.95	136.97	192.79	242.52	269.35	270.20	271.5	268.90	209.31	175.46	154.97	117.19

2.3. Transactions and Reversals

The experiment was designed in a complete randomized design, where Treatment 1 included "Topography slope" of two slopes; 2% and 5%. On the other hand, the Treatment 2 included the "Type of plant" where three types of pastoral plants were selected**;** *Atriplex halimus, Atriplex lecoclada,* and *Salsola vermiculata*. Three replications were adopted for each treatment at every studied slope, thus the number of experiments were experimental pieces at the studied slopes Figure 2. The area of the experimental piece (the area of a semicircular with a diameter of 40 m) was 628 m^2.

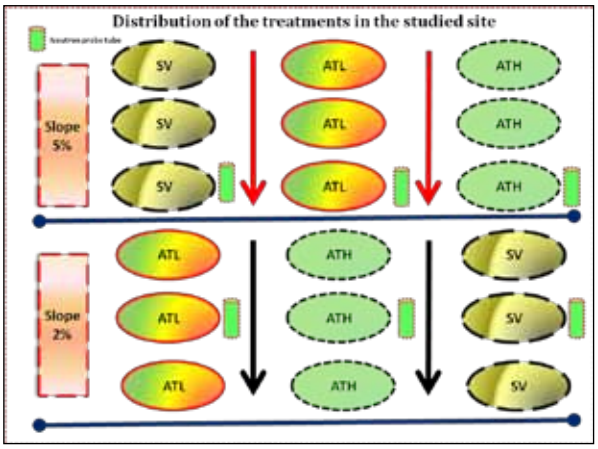

Figure 2. Distribution of treatments in the studied site (SV: *Salsola vermiculata* shrubs, ATL: *Atriplex lecoclada* shrubs, ATH: *Atriplex halimus* shrubs) (Jirdi, 1992)

2.4. Measurements

2.4.1. Physical and hydrological-Physical analyses (Jirdi, 1992)

The physical and hydrological-physical analyses included the following:

1. Determination of the moisture of the soil (%).
2. Determination of the bulk density (g/cm3).
3. The rate of water percolation in soil by the form of a double roller.
4. Calculate the total porosity%.
5. Determination of field capacity%.
6. Determination of permanent wilting point%.
7. Calculation of available water%.

2.4.2 Field measurements

1. Soil samples were taken from the ponds before planting, and from the blank at the depth of (0-25 cm) to conduct some laboratory analysis related to the study.
2. Measuring the amount of rain precipitation by a metric meter installed beside the experiment.
3. Determination of moisture at the depth of (0-45cm) after each rainfall by a Neutron probe device, and Table 2 shows the tracking of the moisture readings(%) of the studied soil.
4. Water storage is estimated and calculated from the following relationship (Kheder et al., 1996):

   $Ws = W * Bd * H * S * 10000$

   Where Ws is the water storage (m^3 / ha), W is the soil moisture (measured as part of one), Bd is the Bulk Density(g / cm^3), H is the depth of the studied depth (m), and S is the Plot Area (m^2).
5. Determination of rainfall intensity mm/h using the rain gauge installed at the experiment site.
6. Determination of runoff using runoff coefficient (Somme and Abdel-al, 2002) as follows:
   Total annual runoff = Runoff coefficient (K)* Total annual precipitation
7. The efficiency or percentage of water storage (%) was computed by calculation of the following relationship:
   Water storage efficiency (%) = (% water storage after the runoff - %water storage before runoff) / (% water storage after the runoff
8. The amount of runoff of the rainwater (cr) was calculated using the following relationship:

   $cr = (s* c* e)$

   where cr is the amount of surface runoff of the rainwater contained in the studied catchment (Liter), s is the amount of runoff of rainwater (L/m2) collected ina tank, c is the concentration of the flow solution (g/L) which is harvested ina tank, and e is the soil water storage efficiency (%)
9. Estimation of the water budget of the soil at the studied catchment (Darwish, 2009):

   The water budget equation= water inflow - outflow

   P + Q inflow = ET + ΔS + Q outflow

   $\Delta S = P- (I + ET)$

   Where ΔS is the Change in water storage in studied soil, P is the total precipitation of rainfall water in the catchment area (mm), I is the soil percolation (mm/ hr), and ET is the Monthly Evapotranspiration (mm/ month) which is calculated by using of one of the used mathematical relationships (the relationship of penman), and here its value was estimated by using the program ETo calculator.
10. Assessment of water balance of the studied pastoral plants and calculation of water consumption of the cultivated pastoral plants (Darwish, 2009):

    $ET = ET_o * K_C$

    Where ET is the water requirement for crop (mm/ day), ETo is the reference evapotranspiration (mm/day), and Kc is the crop coefficient.
11. Calculation of crop coefficient for pastoral plants:

    $K_C = ET / ET_o$

Table 2. Weight waters values by kind of agriculture at slope 5%, 2%.

Plant	Treatment	Weight moisture Readings (%)		Bulk density (g/cm^3)
		Before runoff	After Runoff	
Atriplex HalimusATH (slope2%)	bund	8.75	16.26	1.25
	blank	8.32	13.86	1.25
Atriplex HalimusATH (slope5%)	bund	8.98	18.19	1.25
	blank	6.70	12.78	1.25
Atriplexe lecoclada ATL (slope2%)	bund	7.47	14.76	1.25
	blank	7.17	12.94	1.25
Atriplexe lecoclada ATL (slope5%)	bund	10.19	16.19	1.25
	blank	7.36	11.66	1.25
Salsola vermiculata SV (slope2%)	bund	8.85	12.72	1.25
	blank	8.57	10.29	1.25
Salsola vermiculataSV (slope5%)	bund	9.26	14.41	1.25
	blank	8.75	16.26	1.25

3. Results and discussion

Water storage and the efficiency of water storage in the soil is presented in Table 3. It showed significant increases in water storage and the efficiency of water storage in the soil of the constructed ponds compared with the blank (without edges). Also, the results showed, The storage of water and the efficiency of water storage increased with increasing slope steepness from 35.73% To 50.60% For 5%, and from 30.41% to 46.21% for slope2%, respectively (Table 3).

Table 3. Water storage and the efficiency of water storage in the soil at the studied slopes (5%, 2%).

Plant	Treatment	Water storage m^3/ha		Water storage efficiency %	L.S.D*
		Before runoff	After runoff		
ATH (slope2%)	bund	492.00	914.69	46.21	7.28**
	blank	468.00	779.46	39.96	
ATH (slope5%)	bund	505.50	1023.47	50.60	10.25**
	blank	376.70	718.77	47.59	
ATL (slope2%)	bund	420.00	830.26	49.41	6.60**
	blank	403.50	728.10	44.58	
ATL (slope5%)	bund	574.50	911.23	37.06	8.95**
	blank	414.00	655.68	36.86	
SV (slope2%)	bund	498.00	715.65	30.41	5.31**
	blank	482.00	579.00	16.75	
SV (slope5%)	bund	520.90	810.53	35.73	7.63**
	blank	498.00	658.79	25.77	

*** L.S.D is the indicator of statistical analysis represents the Least Significant Difference at 5% Significant level.**

Comparison of soil properties and hydrological parameters in response to different water harvesting techniques is tabulated in Table 4. It shows that the field capacity of the soil increased about (5.48%) and (1%) at the slopes 5% and 2%, so that, the available water at the constructed ponds raised in all cultivated plants compared with the blank, and their values at slope 5% were higher than at the slope 2%. The reason may be due to the surface runoff of rainwater carries with it the soil and some of the transported organic materials that collect behind the ponds of the water harvesting technique, and this affects the improvement of the soil texture and its ability to save water, at last, this led to increasing the field capacity.

Table 4. Some physical properties of soil studied at two slopes (5% and 2%).

Type of plant	Slope (%)	Treatment	Field capacity before runoff (%)	Field capacity after runoff (%)	Permanent wilt point before runoff (%)	Permanent wilt pointafter runoff%%	Available water before runoff (%)	Available water after runoff (%)
Atriplex Halimus ATH	5%	bund	19.9	20.99	5.0	4.08	14.9	16.91
		blank	19.0	20.90	5.1	4.2	13.9	16.7
	2%	bund	20.2	20.39	8.8	8.79	11.4	12.69
		blank	20.0	20.01	7.4	7.32	12.6	12.69
Atriplexe lecoclada ATL	5%	bund	20.5	21.3	5.5	4.28	15	17.02
		blank	20.0	21.2	6.0	5.29	14	15.91
	2%	bund	20.5	20.8	5.2	5.01	15.30	15.79
		blank	19.8	19.83	4.15	4.11	15.65	15.72
Salsola vermiculata SV	5%	bund	20	20.04	7.9	7.8	14.68	14.83
		blank	19.9	20.00	5.22	5.17	14.68	12.24
	2%	bund	20	22.5	5.8	5.44	14.2	17.06
		blank	19	20.8	5.5	5.23	13.5	15.57

On the other hand, the amount of runoff water in the studied catchments was estimated from the volume of the collected water inside the distributed mineral reservoirs behind the bunds at the studied slopes, and the results were presented in Table (5).

The results In Table (5) showed, that water storage in the soil at all cultivated types of plants, has increased behind the bunds compared with the blank and its values at slope 5%was higher than its values at the slope 2%.

Table 5. Amount of runoff water and water storage efficiency at studied slopes (5% and 2%).

Plant	Treatment	Square of Catchment area (m^2)	Water storage (m^3/ha)	Water storage efficiency (%)	Concentration of runoff water (g/L)	Amount of surface runoff (m^3/ha)	L.S.D
ATH (slope5%)	bund	628	1023.47	50.60	0.62	511.87	5.21**
	balk	628	718.77	47.59	0.15	81.70	
ATH (slope2%)	bund	628	914.69	46.21	1.2	807.67	7.55**
	balk	628	779.46	39.96	0.65	322.38	
ATL (slope5%)	bund	628	911.23	37.06	0.5	268.87	5.41**
	balk	628	655.68	36.86	0.24	92.36	
ATL (slope2%)	bund	628	830.26	49.41	0.3	195.97	4.22**
	balk	628	728.10	44.58	0.08	41.35	
SV (slope5%)	bund	628	810.53	35.73	0.5	230.58	4.88**
	balk	628	658.79	25.77	0.24	64.88	
SV (slope2%)	bund	628	715.65	30.41	0.3	103.96	4.33**
	balk	628	579.00	16.75	0.08	12.35	

The water balance was estimated for the studied catchments at all studied slopes (5% and 2%) according to the type of cultivated plants Table (6), first, The Water balance of soil was10782.3 m^3/ha in all types of cultivated plants. It was calculated by subtracting the total value of water lost to soil (percolation) from the total value of the collected water catchment area. (12117.9-1335.6), however, The soil balance of the studied slopes (5% and 2%) has increased for all types of cultivated plants behind the ponds compared with blank after the surface runoff of the rainwater by (11227.9-10723.9 = 504) m^3/ha, and in the rate of (4.48%).On the other hand, the water budget for the soil of the catchment areas at the studied slopes behind the pond sat all types of cultivated plants before the occurrence of runoff at the beginning of rainy season was (4766.10) m^3 /ha, it decreased at the end of the rainy season period (4388.95) m^3/ha, and in the rate of (7.92%). Also, the water budget for the soil of the catchment areas at the studied slopes behind the blank at all types of cultivated plants before the occurrence of runoff at the beginning of rainy season was (4389.40) m^3/ha, where it decreased at the end of the rainy season period (1799.02) m^3/ha, and in the rate of (59.02%). The water budget of the studied soil at the two studied slopes (5% and 2%) increased by (59.01%) behind the constructed ponds on all types of cultivated plants. The use of water harvesting techniques by ponds in the studied area contributed to collecting of runoff water inside the soil of the catchments and to ensure sufficient quantity of available water for cultivated plants to follow up its growth by (51.10%) compared with blank (Tables 6-7).

Table 6. Water balance of the soil in the studied catchments at the two slopes (5%, 2%).

Type of plant	Slope (%)	Treatment (bund – blank)	Moisture before runoff (m^3/ha)	Moisture after runoff (m^3/ha)	Annual rainfall (m^3/ ha)	Infiltration (mm/h)	Amount of runoff (m^3/ha)	Evaporation (mm/month)	Evapo-transpiration calculated according to penman equation (mm/month)	**Water balance of the soil before runoff**	**Water balance of the soil after runoff**
Atriplex Halimus	2 %		492.00	914.69	782	3.6	807.67	69.3	420	784.7	1233.06
		bund	468.00	779.46	782	3.6	322.38	69.3	420	760.7	612.54
	5 %	blank	505.50	1023.47	782	4.8	511.87	69.3	420	798.2	1046.04
		bund	376.70	718.77	782	4.8	81.70	69.3	420	669.4	311.17
Atriplex Lecoclada	2 %	blank	420.00	830.26	782	3.6	195.97	69.3	420	712.7	536.93
		bund	403.50	728.10	782	3.6	41.35	69.3	420	696.2	280.15
	5 %	blank	573.50	911.23	782	4.8	268.87	69.3	420	866.2	690.80
		bund	414.00	655.68	782	4.8	92.36	69.3	420	706.7	258.74
Salsola vermiculata	2 %	blank	498.00	715.65	782	3.6	103.96	69.3	420	790.7	330.31
		bund	482.00	579.00	782	3.6	12.35	69.3	420	774.7	102.05
	5 %	blank	520.90	810.53	782	4.8	230.58	69.3	420	813.6	551.81
		bund	489.00	658.79	782	4.8	64.88	69.3	420	781.7	234.37
Total			5643.1	9325.63	9384	504	2733.94	831.6	5040	10723.97	11227.97

Table 7. Water balance of the pastoral plants behind the bunds and blank at the studied slopes (5%, 2%).

Type of plant	Slope (%)	Treatment (bund – blank)	Water storage before runoff (m^3/ ha)	Evaporation from soil (mm/day)	Given water (m^3/ha)			Water storage afterrunoff (m^3/ha)	Monthly consumption (m^3/ha)	**Annual consumption (rainy season) (m^3/ha)**	**ET_o reference evaporation (m^3/ha)**		
					Irrigation	Rain fall	Total				Penman	Blany cridel	Ivanove
Atriplex Halimus	2 %	bund	49250.	69.3	0	277	277	914.69	21.193	635.79	480	435	420
		blank	468.00	69.3	0	277	277	779.46	17.485	524.56	480	435	420
	5 %	bund	505.50	69.3	0	277	277	1023.5	24.369	731.07	480	435	420
		blank	376.70	69.3	0	277	277	718.77	18.506	555.17	480	435	420
Atriplex Lecoclada	2 %	bund	420	69.3	0	277	277	830.26	20.779	623.36	480	435	420
		blank	403.5	69.3	0	277	277	728.1	17.923	537.7	480	435	420
	5 %	bund	573.5	69.3	0	277	277	911.23	18.361	550.83	480	435	420
		blank	414	69.3	0	277	277	655.68	15.159	454.78	480	435	420
Salsola vermiculata	2 %	bund	498	69.3	0	277	277	715.65	14.358	430.75	480	435	420
		blank	482	69.3	0	277	277	579	10.337	310.1	480	435	420
	5 %	bund	520.9	69.3	0	277	277	810.53	16.758	502.73	480	435	420
		blank	489	69.3	0	277	277	658.79	5.6597	169.79	480	435	420
Total					0	3324.00	3324.00	9325.66	200.89	6026.63	5760.00	5220.00	5040.00

4. Conclusions

The study of water balance in the system (soil-plant) by using large semi-circular bunds of water harvesting technique led to the following:

1. The water balance of the studied soil increased by (59.01%), in the constructed ponds at slopes of 5% and 2%, and for all types of cultivated plants compared with blank.
2. The field capacity of the soil in the ponds increased by11.11%for all types of cultivated plants compared with blank(without bunds). Their values were higher at a 5% slope sites relative to those at a slope 2%, thus the available water increased to the pastoral shrubs.
3. The use of water harvesting technique by bunds, in the studied area, contributed to collecting of runoff water of the rainwater inside the soil of the catchments, and this ensures sufficient quantity by (51.10%) of available water for cultivated plants to follow up the growth compared with blank (without bunds).
4. The consumption of water for the whole pastoral plants behind the bunds increased at the slope 5% more than the slope 2%.
5. For the first time in the studied area, the value of the crop coefficient (KC) was calculated for *Atriplex halimus***,** *Atriplex lecoclada***,** and the *salsola vermiculata***.**

References

Abdel Al, A. (1994). Topography of catchments in the Syrian Baddia. Directorate of Irrigation and Water Use, Ministry of Agriculture and Agrarian Reform, Damascus.

Al-Jirdi, A. (1992). Soil Physics, the Faculty of Agriculture, Aleppo University Publications.

Arab Organization for Agricultural Development (AOAD) (1999). Strengthening Joint Research in Developing Water Use Efficiency in the Arab States, Khartoum, 90 pages.

Arar, A. (1995). Methods and Methods of Reducing Water Use in Arab Agriculture, National Meeting of Agriculture Sector Officials in the Arab World, Khartoum, pp. 9-40.

Arar, A.(1993).optimization of water use in arid areas, FAO expert consultation on water harvesting for improved agriculture production- 21-25 Nov, 1993-Cairo-Egypt

Darwish, E.E. (2009). Water Balance of Soil and its Relation to Agricultural Production, Journal of the Faculty of Arts 99: 466-506.

International center for agricultural researches in a dry area (ICARDA). (1997). Economic of water harvesting and storage in the Mahesseh watersheds. Aleppo, Syria.

IDRC, Abdulal, A. (1993). Integrated watershed development, Syria, IDRC, Canada.

Jack, K., and Osman, F. (1995). Freshwater development and utilization seminar on options and strategies for freshwater development and utilization in Arab countries. 26-28 June, Amman, Jordan.

Joddi, O. (1999). Hydrology and water harvesting, a training course in the Ministry of Agriculture and Agrarian Reform, Syrian Arab Republic.

Kheder, A., Kangoo, A., Haifa, S. (1996). Irrigation and Agricultural Drainage, Faculty of Agricultural Engineering, Tishreen University Publications, p. 133.

Somme, G. and Abdel-al, A. (2002). Micro catchment water Harvesting for improved Vegetative cover in Syrian Baddia.

UNEP. (1982). Rain and Storm water Harvesting in Rural Areas, Tycooly International Publishing Ltd., Dublin.

JJEES

Jordan Journal of Earth and Environmental Sciences

JJEES (2021) 12 (2): 106-112
ISSN 1995-6681

Source rock evaluation of the Chia Gara Formation in the Bekhme-1 well, Harir District, Kurdistan Region, Iraq

Rzger Abdula*[1, 2], Sardar Fatah[3], Gardun Salih[1], Mohammed Mustafa[1], Muhammed Ali[4]

[1]Department of Petroleum Geoscience, Soran University, Soran, Iraq
[2]Petroleum and Mining Engineering Department, Tishk International University, Erbil, Iraq
[3]Department of Geology, College of Science, University of Sulaimani, Sulaymaniyah, Iraq
[4]Directorate of Oil and Mining in Garmian (Kalar), Sulaymaniyah, Iraq

Received 27 May 2020, Accepted 21 November 2020

Abstract

Rock-Eval pyrolysis technique has been done for 18 cutting rock samples of the Chia Gara Formation (Middle Tithonian-Berriasian) from Bekhme-1 Well on High Folded Zone, Erbil District, Kurdistan Region of Iraq. The range and average of total carbon content (TOC), free Hydrocarbon (S1) are 0.84-2.87, 1.56 wt. % and 0.07-0.94, 0.61 mg HC/g rock respectively; indicating fair to good source rock. The average genetic potential (S1+S2) is 4.12, 4.15, and 4.13 mg HC/g rock for upper, middle, and lower parts, respectively. These values represent moderate potentiality. This study approved that the kerogen is a mixture of type II/III and type III. The combination of production index (range: 0.22-0.15; average:0.15), and T_{max} values (range:438-449°C) illustrate that the stage of maturity for the Chia Gara Formation is early mature. There is no evidence for the oil crossover effect in Bekhme-1 Well because none of the S1/TOC values is greater than one; therefore, it appears that the organic matter just started to enter the oil window.

Keywords: Chia Gara, rock evaluation, Kerogen, Harir, Iraq

1. Introduction

Kurdistan Region became a host of many international oil companies in the last decade. They have tried to explore new oil or gas field, also upgrade hydrocarbon reserves. By that time, the Kurdistan Region has been subdivided by many areas known as "Block"; which are awarded by specialized oil companies (Fatah et al., 2020). In 2007, the Magyar Olajes Gazipari Nyr (formerly known as MOL Plc), through its subsidiary, Kalegran Limited Company awarded exploration of Akri-Bijeel Block. The Bekhme-1 Well is the second discovery well that was been drilled in this block (Csontos et al., 2011). The Chia Gara Formation, with a thickness of 300 m occurs within the interval 1458-1158 m under the surface. The Bekhme-1 Well is located in the eastern part of the Akri-Bijeel Block in northern Iraq, about 10 km north-west of Harir Town in Erbil Governorate, the capital city of the Kurdistan Region of Iraq. It is situated on latitude 36° 40' 33.05'' North and longitude 44° 17' 47.60'' East (Figure 1).

The study of the organic matter content of the Chia Gara Formation has been investigated by several researchers, for instant: Odisho and Othman (1992) believed that this rock unit might represent a good source rock in the northern part of Iraq. Others e.g. Mohialdeen (2008), Mohialdeen et al.(2013a), Hakimi et al. (2017), Abdula et al. (2017) approved that the organic-rich limestone and shale of the Chia Gara Formation considered a very good to excellent source rock for hydrocarbon generation. The average total organic carbon (TOC wt.%) content for the Chia Gara Formation is 1.5 wt.%, and it contains kerogen types II and III, indicating marine and non-marine organic matter, proposing oil and gas prone sources (Ali, 2018).

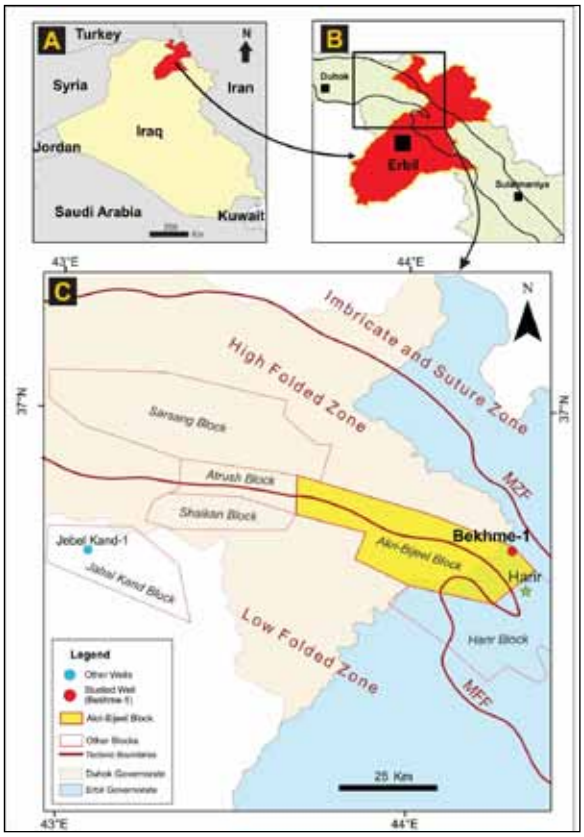

Figure 1. Location map of the studied well. A. The main map of Iraq showing with an indication of Erbil Governorate. B. Close view of Erbil and other cities with an indication of the study area. C. Location map of Bekhme-1 Well within Akri-Bijeel Block with relevant to other surrounding blocks.

* Corresponding author e-mail: rzger.abdulkarim@tiu.edu.iq

The petroleum system of Jabal Kand Oil Field which is located nearby Akri-Bijeel Field shows that the formations such as the Sargelu and younger, the Chia Gara, are immature and have not generated any oil, depending on vitrinite reflectance (Ro) <0.55% (Abdula, 2017a). Oil-source correlation and biomarker characteristics of oils and oil/bitumen seeps reveal that there is a genetic relationship between these oils and extracted organic matter from the Chia Gara source rock (Mohialdeen et al., 2013b; Al-Jaafary and Hadi, 2015; Edilbi, 2016). The Chia Gara Formation in Atrush, Sarsang, and Shaikhan oilfields can be considered as good to excellent source rock; its TOC content ranges from 1.14-8.50 wt.% with an average of 1.85 wt.%, 3.91 wt.%, and 6.94 wt.% in Atrush-1, Mangesh-1, and Shaikhan-8 wells, respectively (Mamaseni et al., 2019).

This study aims to report the organic geochemical characteristics and hydrocarbon potentiality of the Chia Gara Formation within the Bekhme-1 Well.

2. Materials and Methods

Eighteen cutting rock samples of the Chia Gara Formation were collected from the Bekhme-1 Well at different depths and different spacing ranges (Table 1). The samples were stored at the Geological Survey Office in Erbil, Kurdistan Region. The collected samples represent the different lithologies of the Chia Gara Formation. These lithologies are common in limestone and shale. The samples have been analyzed at Kurdistan Institution for Strategic Studies and Scientific Research (KISSR) in Sulaymaniyah, Kurdistan Region.

2.1. Rock-Eval pyrolysis

This test is performed for all samples. Initially, the representative cutting samples were cleaned of contaminations and washed with distilled water, then oven-dried at 40 °C for 24 hours. The washed-out samples were crushed to become a powder, then taken about 100 mg of sample to be analyzed by Rock-Eval 6 apparatus. The Rock-Eval test involves the continuous heating of a sample ranging from 100 °C-850 °C in an inert atmosphere (Helium or Nitrogen Gas) (Lafargue et al., 1998). The heating program is: starting from 100 °C, then retain the sample at 300 °C for 3 minutes, and then increased the temperature to 850 °C at a rate of 25 °C/min. The details of this technique and parameters are documented in Behar et al. (2001). The measured parameters include TOC (wt.%), S1 (mg HC/g rock), S2 (mg HC/g rock), and T_{max} (°C) are quoted in Table 1. Additional parameters such as Hydrogen Index (HI=S2/TOC x 100) and Production Index (PI=S1/(S1+S2)) are calculated from these measured values and are also shown in Table 1.

3. Geological Setting

The Mountain Front Flexure (MMF) and Main Zagros Fault (MZF) are considered as the two prominent tectonic features of the Zagros orogenic belt, which separate the Low Folded Zone from the High Folded Zone and the Imbricate Zone (Koshnaw et al., 2017). Bekhme-1 Well situated on the High Folded Zone (Figure 1). Northern Iraq has been affected by several transversal fault systems, which are the Hadar-Bekhme Fault Zone and the Anah-Qalat Dizeh Fault Zone that underwent a sinistral strike-slip movement during the Quaternary (Reif et al., 2012).

Table 1. Rock-Eval pyrolysis data for samples of the Chia Gara Formation in the Bekhme-1 Well in the Kurdistan Region, Iraq (Ali, 2018).

Sample No.	Depth (m)	TOC (wt.%)	S1	S2	T_{max}	HI	PI	GP
1	1158	0.84	0.83	2.92	439	348	0.22	3.75
2	1178	1.05	0.94	3.96	444	377	0.19	4.90
3	1198	1.02	0.65	2.81	441	275	0.19	3.46
4	1218	1.20	0.62	4.51	444	376	0.12	5.13
5	1218	1.28	0.12	2.74	445	214	0.04	2.86
6	1238	1.24	0.63	4.00	439	323	0.14	4.63
7	1258	1.03	0.71	3.40	438	330	0.17	4.11
8	1278	1.03	0.59	2.99	440	290	0.16	3.58
9	1298	1.24	0.66	3.56	439	287	0.16	4.22
10	1318	1.58	0.71	3.59	441	227	0.17	4.30
11	1338	1.90	0.69	3.99	439	210	0.15	4.68
12	1358	1.85	0.65	3.40	440	184	0.16	4.05
13	1378	2.11	0.71	3.79	441	180	0.16	4.50
14	1398	1.71	0.54	3.00	439	175	0.15	3.54
15	1418	1.76	0.58	3.02	439	172	0.16	3.60
16	1438	1.57	0.52	2.55	439	162	0.17	3.07
17	1458	2.87	0.82	5.27	443	184	0.14	6.09
18	1458	2.73	0.07	3.96	449	145	0.02	4.03
	Min.	0.84	0.07	2.55	438	145	0.02	2.86
	Max.	2.87	0.94	5.27	449	377	0.22	6.09
	Average	1.56	0.61	3.53	441	248	0.15	4.14

TOC: Total Organic Carbon (wt.%); S1: Free hydrocarbon (mg HC/gm rock); S2: Generation potential (mg HC/gm rock); T_{max}: Temperature of maximum peak of S2 (C°); HI: Hydrogen Index (100 x S2/TOC); PI: Production Index {S1/(S1+S2)}; GP: Genetic Potential or Petroleum Potential (S1+S2)

From Bijeel Anticline towards Aqra and Bakurman (Figure 2), it is quite common to find steep southerly dips in the Mesozoic section on the southern limb of the anticline. A lot of thrust exposures were found at the southern limbs, and one at the northern limb, which suggests that thrusts underlie the limbs of major folds (Csontos et al., 2012).

The obtainable geological and geophysical data designate that the Akri-Bijeel Block comprises Cenozoic marine and non-marine Cretaceous carbonate and marl strata (Figure 3) that are more than 1.4 Km thick which, in turn, rest conformably on the Jurassic marine sedimentary strata (~0.8 Km thick). The Bekhme-1 Well reached a total depth of 4560 m in hard formations and it was sampled from about 1158 to 2290 m with a generally good recovery, but the well-log history designates that some of the cuttings' runs had incomplete or no recovery (Ali, 2018). The Chia Gara Formation (Middle Tithonian-Berriasian) type locality is located at the Chia Gara Anticline, south of Amadia Town in the High Folded Zone of Northern Iraq with a thickness of 232 m (Bellen et al., 1959).

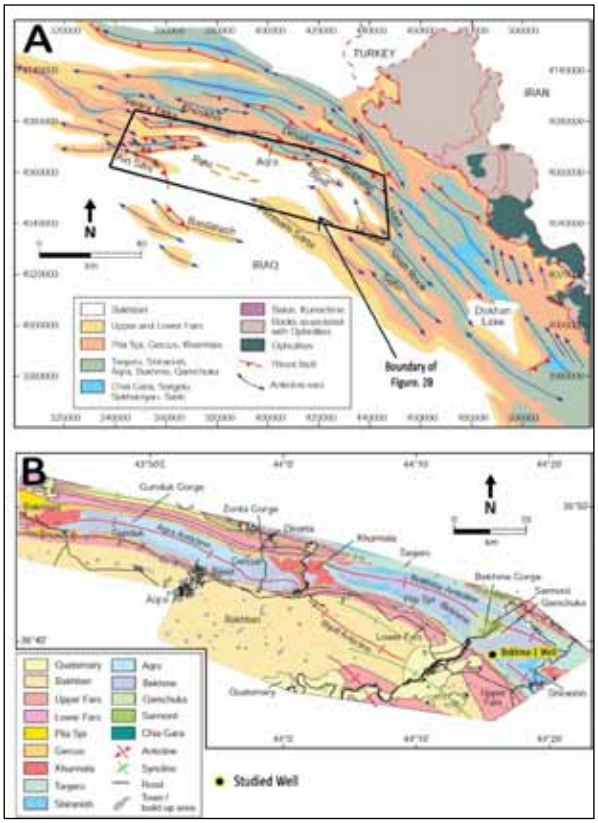

Figure 2. A. Schematic geologic map of Northern part of Iraq showing generalized geologic formations and trends of anticline axes (after Csontos et al., 2012). B. Detailed geological map of the area with an indication of the studied well, the map showing the two main anticlines to the north that correspond to the Aqra (western) and the Bekhme (eastern) (after Csontos et al., 2012).

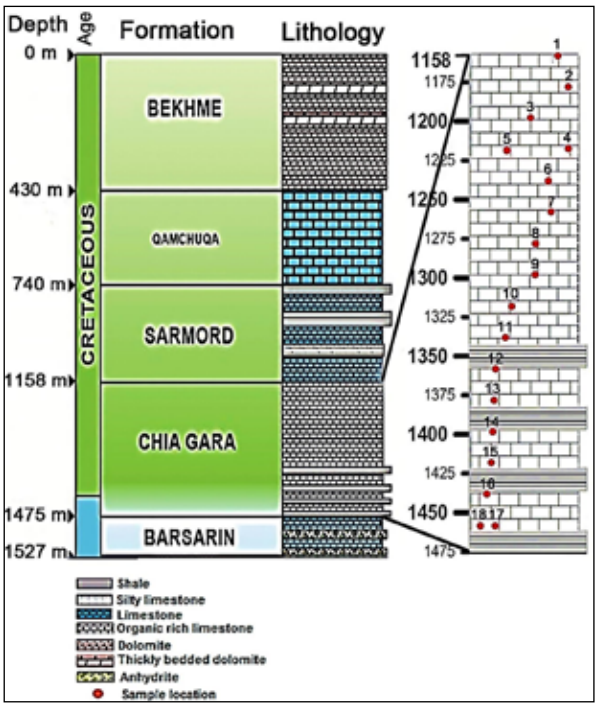

Figure 3. Stratigraphic column of Bekhme-1 Well showing the summary of well lithology with measured depth and sample locations (Ali, 2018).

The stratigraphic sequence of the Chia Gara Formation in Bekhme Gorge and Rowanduz area is characterized by intercalation of dark grey thin to thickly bedded limestone with black fissile shale (Al-Qayim and Saadalla, 1992).

The depositional environment of the Chia Gara Formation was supposed to be the beginning of the toe of the slope to the deep open marine environment (Bellen et al., 1959; Buday, 1980; Edilbi, 2010). The study of clay minerals showed that rocks of the Chia Gara mainly consist of kaolinite and illite in different proportions, which indicates deposition during a transgressive episode of sea level (TST) (Edilbi and Sherwani, 2019). Leanza (1996) correlated the lithological facies of the Chia Gara Formation with Vaca Muerta Formation in the Argentine Andes. Many horizons of both formations were found to be consisting of dark brown marly shales comprising several big-sized ("Phacoids") calcareous concretions all of them were deposited in a highly bituminous environment, signifying a primary short-term depositional control on their formation (Howarth, 1992; Leanza, 1996). This might characterize an extremely bituminous worldwide occurrence worth being considered as a high-resolution chemical-stratigraphic event (Kauffman, 1988).

4. Results and Discussion

4.1. Total organic carbon

Generally, the Total Organic Carbon (TOC wt.%) in a rock sample; describes the quantity of organic carbon within a rock unit, including both kerogen and bitumen. This parameter is used for measuring the quantity, but not the quality of organic carbon in the rock sample (Hunt, 1996; Peters et al., 2005). However, a sufficient amount of TOC increases the sediment chance to be a good source rock concerning the type of initial input of the organic matter and degree of maturity (Tissot and Welte, 1984; Peters and Cassa, 1994). To produce oil, the carbon has to be connected to hydrogen in a source rock (Demaison and Moore, 1980; Peters, 1986; Dembicki Jr, 2009). In Barker's (1996) opinion, the 1.0 wt.% TOC is the lower limit for a productive source rock as it would never yield enough oil to trigger primary migration from a source rock of less than 1.0 wt.% (Figure 4).

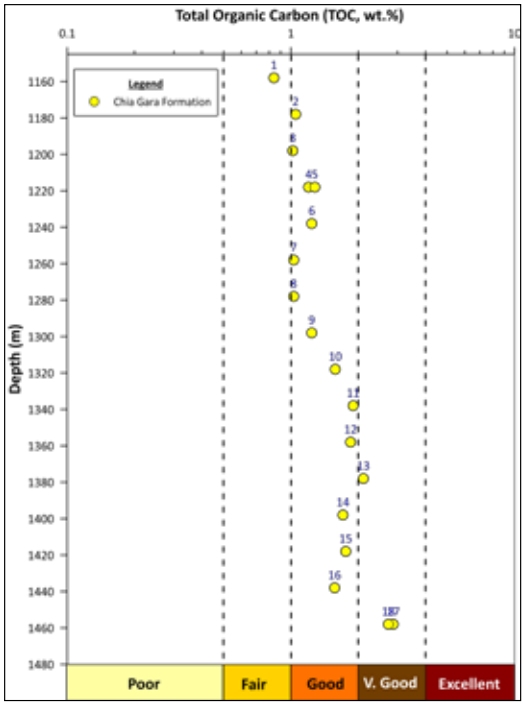

Figure 4. TOC wt.% versus depth indicates that the lower part is richer than the upper part.

To ensure the contamination effect upon the TOC, all the samples have been plotted on the cross plot of TOC versus S1 (Figure 5) dependingly, it's clear that all the samples are clean and not contaminated by drilling fluid.

Rock-Eval data for samples in the Bekhme-1 Well show that TOC wt.% values range from 0.84 wt.% to 2.87 wt.% with an average of 1.56 wt.% (Table 1) (Ali, 2018). This range represents a good to very good source rock at the lower part and a good source rock at the middle and upper parts (Figure 4) depending on the assumptions described by Peters (1986) and Peters and Cassa (1994).

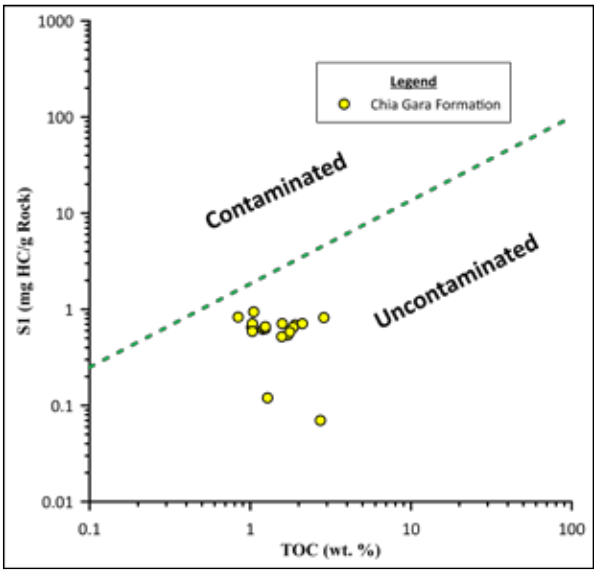

Figure 5. Cross plot of TOC wt.% versus S1 shows that all the samples are uncontaminated by drilling fluid (Osli et al., 2019).

4.2. Genetic potential

A genetic potential includes the total amount of free hydrocarbon already formed from kerogen (S1) and the amount of hydrocarbon left (S2) that has not been yet converted. Mathematically, this could be expressed as S1+S2 (mg HC/g rock) (Tissot and Welte, 1984). Genetic potential is not a measure of hydrocarbon character although it can be used to determine the consistency of prospective organic matter (Pitman et al., 1987).

Depending on Rock-Eval data, the analyzed samples of Chia Gara Formation contain S1 ranges from 0.07 to 0.94 and S2 ranges from 2.55 to 5.27 mg HC/g rock. Consequently, the genetic potential (GP) ranges from 2.86 to 6.09 with an average of 4.14 mg HC/g rock (Table 1). The average genetic potential values are 4.12, 4.15, and 4.13 for upper, middle, and lower parts, respectively. These genetic potential values are almost the same and indicate a fair to good potentiality (Figure 6).

4.3. Hydrogen index

The quality of organic matter depends on the amount of hydrogen that exists. For petroleum to be generated, the carbon needs to be associated with hydrogen in a source rock (Dembicki Jr, 2009). The HI values fluctuate back and forth (Table 1) due to the organic matter's hydrogen content, but generally, the lower part of the Chia Gara Formation contains a low amount of HI content (Figure 7).

A low-hydrogen organic matter commonly has a high T_{max}, and a high-hydrogen organic matter has a low T_{max} (Hunt, 1996). The hydrogen index values are lower in the deeper horizons which may indicate that hydrocarbon started to generate hydrocarbon within the lower horizon, but it is not initiated in the upper horizons yet (Figure 7). As a consequence of generating hydrocarbon, the amount of hydrogen decreases (Hunt, 1996).

The oil crossover effect appears when S1/TOC is more than 1, but none of the values is greater than one; therefore, it appears that the organic matter just started to enter the oil window (Figure 8).

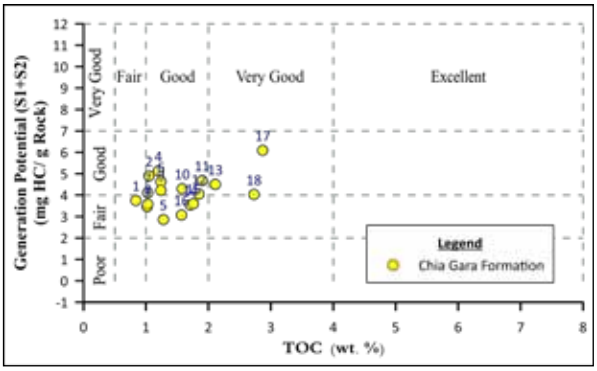

Figure 6. Cross plot of TOC wt.% versus Generation Potential (GP) shows the fair to good potentiality (Alaug et al., 2014).

4.4. Kerogen type

Kerogen type determination in source rock is the initial task because different types of organic matter have different potentialities for hydrocarbon generation (Tissot and Welte, 1978; 1984). The cross plot of TOC wt.% versus S2 (Figure 9) points out the kerogen types II/III and III (Dahl et al., 2004; Allen et al., 2008) which indicates mixed oil-gas prone and gas-prone (Figure 9). The plot of HI vs. T_{max} also points out the existence of types II/III and III kerogens (Hunt, 1996) (Figure 10). The HI values of these samples range between 145 and 377 mg HC/g TOC (Table 1), which also suggests mixed oil-gas-prone and terrestrial gas-prone (Tissot and Welte, 1984; Peters and Cassa, 1994). The quality of organic matter increases from the lower part to the upper part according to their HI values (Figure 7). The organic matters belong to Type III (HI average 172 mg HC/g TOC), mixed Type II and III (average 254 mg HC/g TOC), and Type II (HI average 319 mg HC/g TOC) for lower, middle, and upper parts, respectively (Tissot and Welte, 1984; Peters and Cassa, 1994).

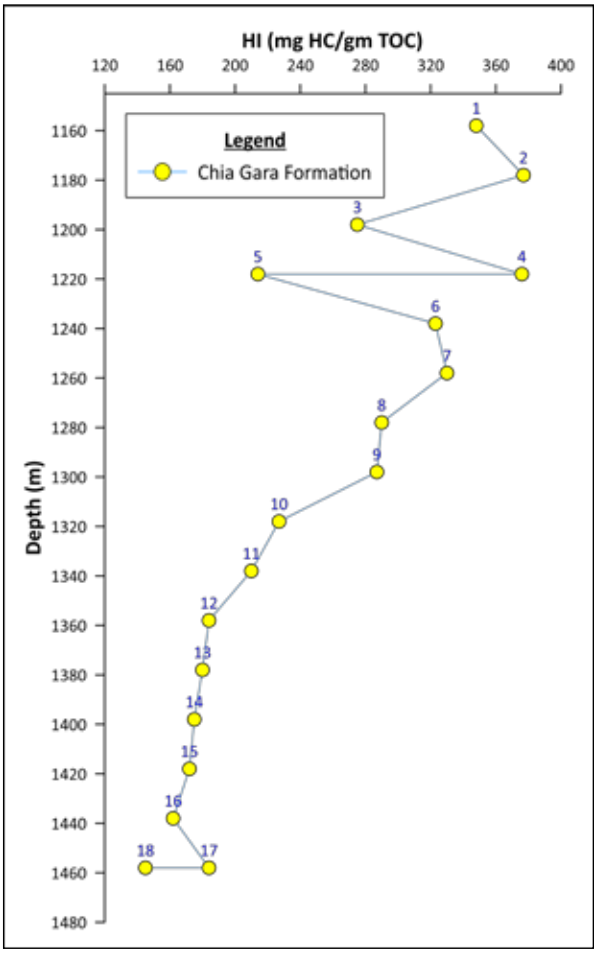

Figure 7. Hydrogen index versus depth shows that hydrogen index values within the lower part (deeper) are lower than the upper part (shallower).

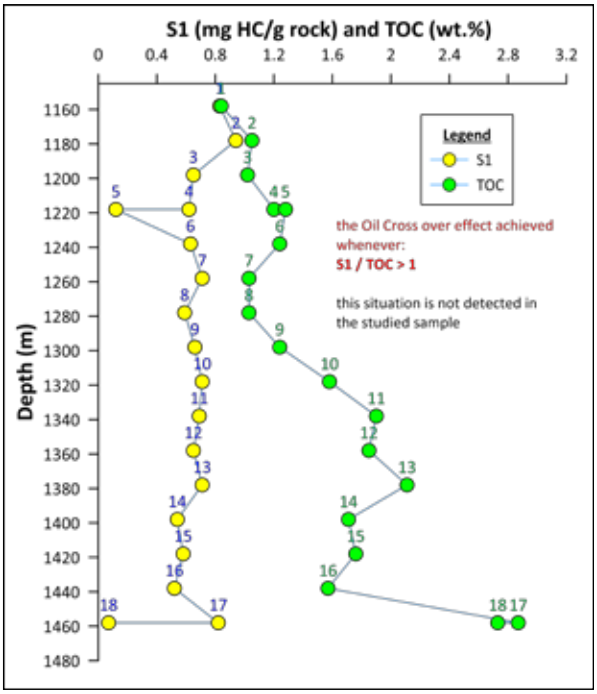

Figure 8. S1 (mg HC/g rock) and TOC (wt.%) versus depth displays that S1/TOC values are less than 1.

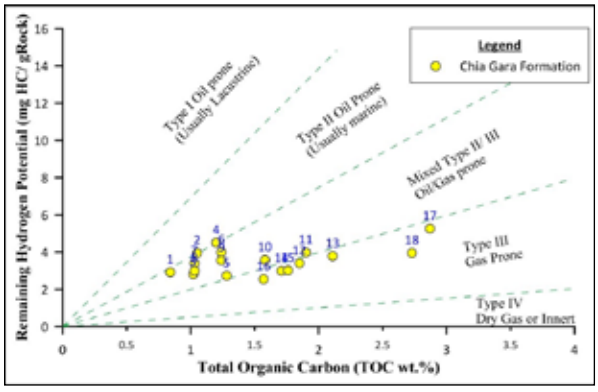

Figure 9. Total Organic Carbon (TOC) vs. S2 diagram of kerogen types shows that the Chia Gara Formation samples lie in the field of type II/III and III kerogens (modified from Dahl et al., 2004; Allen et al., 2008).

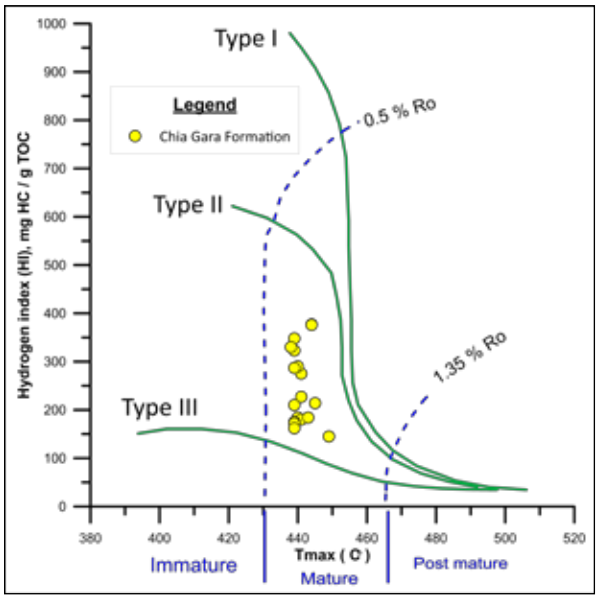

Figure 10. T_{max} vs. HI kerogen shows that the samples are types III and a mixture of II and III and they lie in the mature field (Hunt,1996).

4.5. Maturity

Rock-Eval T_{max} (°C) is the temperature at which the S2 (mg HC/g rock) peak during pyrolysis reaches its maximum amount of hydrocarbon production (Espitalié et al., 1984). Tissot and Welte (1984) and Hunt (1996) recognized factors that affect T_{max} values such as type of organic matter, contamination, and the mineral matrix. Tissot et al. (1987) proposed that T_{max} is a strong maturation predictor between 420 °C and 460 °C in Type II kerogen and between 400 °C and 600 °C in Type III terrestrially derived kerogen.

The T_{max} values range between 438 and 449 °C with an average of 441 °C. This range is within early mature for Type III kerogen (Peters and Cassa, 1994; Bacon et al., 2000). The production index values range between 0.02 and 0.22 with an average of 0.15. These values when combined with T_{max} values indicate an early mature stage (Peters and Cassa, 1994).

T_{max} vs. PI plot shows the Chia Gara Formation samples are located in the early mature zone and started to enter the oil window zone (Figure 11). The same situation is also approved when samples are plotted in the cross plot of T_{max}

versus HI (Figure 10).

The study of Chia Gara Formation by Edilbi (2010) and Abdula (2017a) approved that the maturity increase from the west (Banik: T_{max} values range between 438 and 441 °C with an average of 440 °C) toward the east (Barsarin: T_{max} values range between 449 and 486 °C with an average of 463 °C) of their study area. Increasing maturity toward the east of the studied well may be related to the higher burial that the formation has experienced as documented by Edilbi's (2010) isopach map and consequently experienced higher temperature and pressure. According to Abdula (2017b), the current borehole temperature is 85.8 °C at 4060.2 m below the ground level, but palaeotemperature could be higher. The 1D basin modelling of the Bekhme-1 Well displays that the Chia Gara Formation reached a maximum depth of 2700 m around 75 Ma (Figure 12).

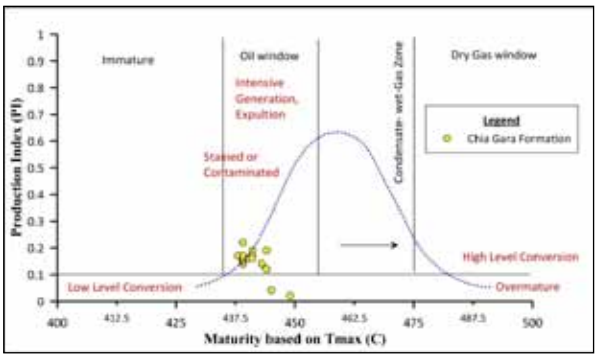

Figure 11. T_{max} vs. Production Index (PI) diagram of the Chia Gara Formation (adapted from Atta-Peters et al., 2015).

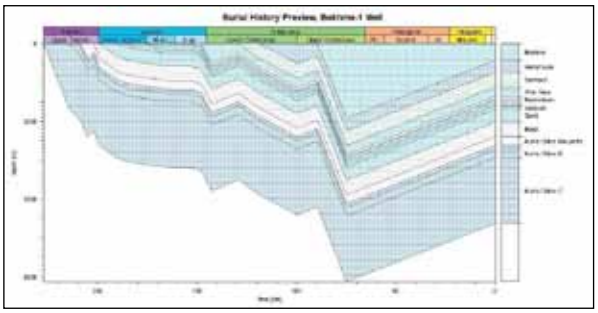

Figure 12. Thermal, burial and subsidence history curves at Bekhme-1 Well (Abdula et al., 2020).

5. Conclusions

The Chia Gara Formation in Bekhme-1 Well can be considered as a fair to good source rock in the lower part and a good source rock in the middle and upper parts, where the average of TOC content is 1.55 wt.%. The organic matter content belongs to kerogen types II/III and III. The average genetic potential (S1 + S2) value is 4.12, 4.15, and 4.13 mg HC/g rock for upper, middle, and lower parts, respectively. These values indicate a moderate potentiality. The maturity level based on the production index values (0.02-0.22)and T_{max} values (average of 441 °C) indicate an early mature stage. There is no evidence for the oil crossover effect for the analyzed samples because none of the S1/TOC values is greater than one; therefore, it appears that the organic matter just started to enter the oil window.

Acknowledgments

The authors would like to thank three anonymous reviewers for their valuable comments that improved the article.

References

Abdula, R.A. (2017a). Petroleum system modeling of Jabal Kand Oil Field, Northern Iraq. ZANCO Journal of Pure and Applied Sciences 29(2): 88–95.

Abdula, R.A. (2017b). Geothermal gradients in Iraqi Kurdistan deduced from bottom hole temperatures. Egyptian Journal of Petroleum 26: 601–608.

Abdula, R.A., Hassan, H.Y., Martin, M. (2020). Petroleum system modeling of Akri-Bijeel Oil Field, northern Iraq: Insights from 1D Basin Modeling. UKH Journal of Science and Engineering 4(2): 166–177.

Abdula, R.A., Ali, M.A., Ahmed, M.M., Hamad, H.R. (2017). Rock-Eval pyrolysis results from the Bijeel-1 Well, Kurdistan Region, Iraq. ZANCO Journal of Pure and Applied Sciences 29(3): 29–38.

Alaug, A.S., Mahmoud, M.S., Deaf, A.S., Al-Ameri, T.K. (2014). Palynofacies, organic geochemical analyses and hydrocarbon potential of some Upper Jurassic-Lower Cretaceous rocks, the Sabatayn-1 Well, Central Yemen. Arabian Journal of Geosciences 7(6): 2515–2530.

Ali, M. (2018). Geochemical evaluation of organic matter in Jurassic source rocks, Bekhme-1 Well, Erbil Governorate, Kurdistan Region, Iraq. Iraqi Bulletin of Geology and Mining 14(2): 49–59.

Al-Jaafary, A.S. and Hadi, A. (2015). Hydrocarbon potential, thermal maturation of the Jurassic sequences, and the genetic implication for the oil seep in North Thrust Zone, North Iraq. Arabian Journal of Geosciences 8(10): 8089–8105.

Allen, T.L., Fraser, T.A., Osadetz, K.G. (2008). Rock-Eval/TOC data for 18 wells, PeelPlateau and Plain, Yukon Territory (65º 50' to 67º 00' N; 133º 45' to 135º 15' W). Yukon Geological Survey, Open-File 2008-1, 14 p. plus spreadsheet(s):http://ygsftp.gov.yk.ca/publications/openfile/2008/of2008_1.pdf, accessed 2/8/2010.

Al-Qayim, B. and Saadallah, A. (1992). Petrology of Jurassic Chia Gara Formation, Northern Iraq. Journal of the Geological Society of Iraq 25 (2): 162–181.

Atta-Peters, D., Achaegakwo, C.A., Garrey, P. (2015). Palynofacies, organic geochemical analyses and hydrocarbon potential of the Takoradi 11-1 Well, Saltpond Basin, Ghana. Petroleum and Coal 57(5): 478–499.

Bacon, C.A., Calver, C.R., Boreham, C.J., Leaman, D.E., Morrison, K.C., Revill, A.T., Volkman, J.K. (2000). The petroleum potential of onshore Tasmania-a review. Geological Survey Bulletin 71. Mineral Resources Tasmania.

Barker, C. (1996). Thermal modeling of petroleum generation: theory and applications. New York, Amsterdam; Elsevier. 1st edition, 45: 1–512.

Behar, F., Beaumont, V., Penteado, H.L. De B. (2001). Rock-Eval 6 technology: Performances and developments. Oil and Gas Science and Technology Rev. IFP 56(2): 111-134.

Bellen, R.C. Van, Dunnington, H.V., Wetzel, R., Morton, D. (1959). Lexique Stratigraphique International. 3, Asie, Fascicule 10a Iraq, Paris.

Buday, T. (1980). The Regional Geology of Iraq: Stratigraphy and Paleogeography. Dar Al-Kutub Publishing House, University of Mosul, Mosul.

Csontos, L., Pocsai, T., Sasvari, A., and Koncz, I. (2011). Geology and petroleum systems of Akri-Bijeel Block, Kurdistan region of Iraq. MOL Scientific Magazine 2011 (1): 16–23.

Csontos, L., Sasvári, A. Pocsai, T., Kósa, L., Salae, A.T., and Ali, A. (2012). Structural evolution of the Northwestern Zagros, Kurdistan Region, Iraq—Implications on oil migration. GeoArabia 17(2): 81–116.

Dahl, B., Bojesen-Koefoed, J.A., Holm, A., Justwan, H., Rasmussen, E., Thomsen, E. (2004). A new approach to interpreting Rock-Eval S2 and TOC data for kerogen quality assessment. Organic Geochemistry 35: 1461–1477.

Demaison, G.J. and Moore, G. (1980). Anoxic environments and oil source bed genesis. AAPG Bulletin 64(8): 1179–1209.

Dembicki Jr, H. (2009). Three common source rock evaluation errors made by geologists during prospect or play appraisals. AAPG Bulletin 93(3): 341–356.

Edilbi, A.N.F. and Sherwani, G.H. (2019). Petrography and source rock potential of Chia Gara Formation (Late Jurassic–Early Cretaceous) in Northern Iraq and Kurdistan Region. Journal of Petroleum Exploration and Production Technology 9: 1801–1818.

Edilbi, A.N.F. (2016). The role of the Baluti Formation within Triassic Petroleum Systems in Kurdistan; Akre-Bijeel Block, Gara and Ora anticlines: An organic geochemical and basin modeling approach. PhD thesis, University of Aberdeen.

Edilbi, A.N. (2010). Stratigraphy and petroleum potential of Chia Gara Formation (Tithonian- Berriasian) in selected sections in North Iraq. Master thesis, Salahaddin University.

Espitalié, J., Marquis, F., Barsony, I. (1984). Geochemical logging. In Voorhees, K.J. (ed.), Analytical pyrolysis: techniques and application. London, Butterworths, pp. 276–304.

Fatah, S.S., Salih, D.A., Kalaitzidis, S., Mohialdeen, I.M., Khanaqa, P.A. (2020). Organic geochemical and petrographical characteristics of the lower part of Sarmord Formation, M-2 Well, Miran Oil Field, Kurdistan, NE Iraq: Implications for hydrocarbon generation potential and thermal maturation. Journal of Zankoy Sulaimani 22 (1), pp. 39-58.

Hakimi, M.H., Mohialdeen, I.M.J., Al-Ahmed, A.A., El-Nady, M.M. (2017). Thermal modeling and hydrocarbon generation of the Late Jurassic-Early Cretaceous Chia Gara source rock in the Iraqi Kurdistan region, northern Zagros Fold Belt. Egyptian Journal of Petroleum **27(4). DOI:** 10.1016/j.ejpe.2017.10.007.

Howarth, M.K. (1992). Tithonian and Berriasian ammonites from the Chia Gara Formation in northern Iraq. Paleontology 35(3): 597–655.

Hunt, J.M. (1996). Petroleum geochemistry and geology. Second edition, New York, W. H. Freeman, and Company.

Kauffman, E.G. (1988). Concepts and methods of high-resolution event stratigraphy. Annual Review of Earth and Planetary Sciences 16: 605-654.

Koshnaw, R.I., Horton, B. K., Stockli, D. F., Barber, D. E., Tamar-Agha, M. Y., Kendall, J.J. (2017). Neogene shortening and exhumation of the Zagros fold-thrust belt and foreland basin in the Kurdistan region of northern Iraq. Tectonophysics 694: 332-355.

Lafargue, E., Marquis, F., Pillot, D. (1998). Rock-Eval 6 applications in hydrocarbon exploration, production and in soil contamination studies. Revue De L'institut Français Du Pétrole (IFP) 53(4): 421–437.

Leanza, H.A. (1996). The Tithonian ammonite genus *Chigaroceras* Howarth (1992) as a bioevent marker between Iraq and Argentina. GeoResearch Forum 1(1996): 451-458.

Mamaseni, W.J., Naqshabandi, S.F., Al-Jaboury, F.Kh. (2019). Hydrocarbon Generation Potential of Chia Gara Formation in Three Selected Wells, Northern Iraq. Open Geosciences, 11(1): 77-88.

Mohialdeen, I.M.J., Hakimi, M.H., Al-Beyati, F.M. (2013a). Geochemical and petrographic characterization of late Jurassic-early Cretaceous Chia Gara Formation in Northern Iraq: Palaeoenvironment and oil-generation potential. Marine and Petroleum Geology 43: 166–177.

Mohialdeen, I.M.J., Hakimi M.H., Al-Beyati, F.M. (2013b). Biomarker characteristics of certain crude oils and the oil-source rock correlation for the Kurdistan oilfields, Northern Iraq. Arabian Journal of Geosciences 8(1) DOI: 10.1007/s12517-013-1228-3.

Mohialdeen, I.M.J. (2008). Source rock appraisal and oil/source correlation for the Chia Gara Formation, Kurdistan-north Iraq. PhD dissertation, University of Sulaimani, Iraq.

Odisho, K.Y. and Othman, R.S. (1992). Preliminary geochemical evaluation of hydrocarbon source rocks in the northern part of Iraq. Iraqi Geological Journal 25: 136–153.

Osli, L.N, Shalaby, M.R., Islam, M.A. (2019). Hydrocarbon generation modeling and source rock characterization of the Cretaceous-Paleocene Taratu Formation, Great South Basin, New Zealand. Journal of Petroleum Exploration and Production Technology 9(1): 125–139.

Peters, K.E. (1986). Guidelines for evaluating petroleum source rock using programmed pyrolysis. AAPG Bulletin 70(3): 318–329.

Peters, K.E. and Cassa, M.R.(1994). Applied source rock geochemistry. Chapter 5, In Magoon, L.B. and Dow, W.G. (Eds.), The petroleum system—from source to trap. AAPG Memoir 60: 93–120.

Peters, K.E., Walters, C.C. and Moldowan, J.M. (2005). The biomarker Guide (2nd ed.) 1-2, United Kingdom, Cambridge University Press.

Pitman, J.K., Franczyk, K.J., Andres, D.E. (1987). Marine and non-marine gas-bearing rocks in Upper Cretaceous Blackhawk and Nelson formations, eastern Uinta Basin, Utah-sedimentology, diagenesis, and source rock potential. AAPG Bulletin 71(1): 76–94.

Reif, D., Decker, K., Grasemann, B., Peresson, H. (2012). Fracture patterns in the Zagros fold-and-thrust belt, Kurdistan Region, Iraq. Tectonophysics 576–577: 46–62.

Tissot, B.P., Pelet, R., Ungerer, P.H. (1987). Thermal history basins, maturation indices and kinetics of oil and gas generation. AAPG Bulletin 71: 1445–1466.

Tissot, B.P. and Welte, D.H. (1984). Petroleum formation and occurrence—A new approach to oil and gas exploration. 2ndedition: Springer Verlag, Berlin.

JJEES

JJEES (2021) 12 (2): 113-121
ISSN 1995-6681

Jordan Journal of Earth and Environmental Sciences

Depositional environment, microfacies analysis and planktonic foraminifera of oil shale deposits in the Wadi Al-Shallala Area, NW Jordan.

Hanan Al-Soud and Habes Al-Mashakbeh*

Department of Applied Earth and Environmental Sciences, Institute of Earth and Environmental Sciences, Al al-Bayt University, Jordan.

Received 4 May 2020; Accepted 15 October 2020

Abstract

This paper discusses the depositional environment, microfacies analysis and planktonic foraminifera of oil shale deposits exposed in the Wadi Al-Shallala area. The study is based on the analysis of 29 samples collected from a 7 m thick section. The data obtained from the microfacies analysis and the micropaleontological study of the Wadi Al-Shallala section shows that oil shale occurs within the Muwaqqar Chalk-Marl Formation (MCM). Four microfacies associations MF1 to 4 are recognized; Foraminifera-Bioclastic, Mudstone/Wackestone (MF1), Bioclastic-Foraminifera-Wackestone/Packestone (MF2), Subbotina-Foraminifera Packestone (MF3), and Peloidal Wackestone (MF4).

The benthic and planktonic foraminifera that were recognized in the studied thin sections are *Nodosaria* sp., *Subbotina* sp., *Lenticulina* sp., *Acarinina* sp., *A.soldadoensis*, and *A. aspensis*.This study identifies nine species of planktonic foraminifera that belong to five genera, and the Paleocene-Eocene age is assigned to the studied section based on the occurrence of certain planktonic foraminifera, e.g. (*Acarinina esnaensis*, *A. strabocella*, *A. interposita*, *A. soldadoensis*, *A. aspensis*, *Pearsonites broedermanni*, *Turborotalita carcoselleensis*, *Praemurica pseudoinconstans*, *Morozovella praeangulata*, *Subbotina cancellata*, *Planorotalites capdevilensis*, and *P. pseudoscitula*). In comparison, the variation in the index of oceanity shows that the sea level (continental shelf) slightly fluctuated over the time of the deposition of the oil shale. The bathymetry's average (water paleodepth) of the exposed oil shale section is about 120 m.

The current study indicates that the Paleocene-Eocene oil shales were deposited in a shallow-water carbonate to moderate circulation of the open shelf.

Keywords: Microfacies, Oil Shale, Foraminifera, Planktonic Percentages (P/B), Index of Oceanity, Jordan.

1. Introduction

Oil shale deposits in Jordan are grey to dark-grey fine-coloured, well-bedded sedimentary rocks of Late Cretaceous to Early Cenozoic age, containing organic matter that produces a significant amount of oil and gas upon destructive distillation. Numerous geological studies have shown that there are several oil shale deposits within the country (Alali, 2006, and Alali et al., 2015). The most significant oil shale deposits exist in 26 different locations throughout the country, with the 8 most important deposits located in the west-central area of the country. Other significant deposits are located in the Yarmouk area near the northern border, and the Ma'an district in southern Jordan (Hamarneh et al., 2006).

The Wadi Al-Shallala oil shale deposits were not analyzed in detail, most of the research concentrated on the oil shale microfacies. In this research, in support of microfacial analysis, the contents of oil shale microfossils in the Wadi AL-Shallala area (Figure 1) were extracted and described. Microfacies and micropaleontological analyses of source rocks are an essential method for studying sediment deposition environment like oil shale.

In Wadi Ashajara, northern Jordan, Al-Atawneh (2018) studied the depositional environment of the Eocene oil shale. Jarrar (1989) provided ideas on the sources of organic matter and the depositional setting. Other studies focused on the sources, depositional environment, quality, geochemistry and commercial production of Jordanian oil shales (Abed, 1982; Abed and Amireh, 1983; Hufnagel, 1985; Abed et al., 2005; Mehdawi and Mustafa, 2008; El-Hasan, 2008; Jaber et al., 2008; Ali Hussein et al., 2015; Hakimi et al., 2016; and Beik et al., 2017).

Ahmad et al., 2020 studied the stratotype section of the Wadi Shallala Formation, including the upper part of Umm Rijam Chert Limestone Formation and Wadi Shallala Formation from the northwestern part of Jordan for their contents of calcareous nannofossils and isotopes for the first time. Forty-two calcareous nannofossil species belonging to the Nannotetrina fulgens (NP15/CP13) Zone assigned to the Middle Eocene age where determined.

The main objective of the present study is to investigate the depositional environment, and microfacies analysis, coupled with the foraminifera of oil shale deposits in the Wadi Al-Shallala area.

* Corresponding author e-mail: Habes2819@aabu.edu.jo

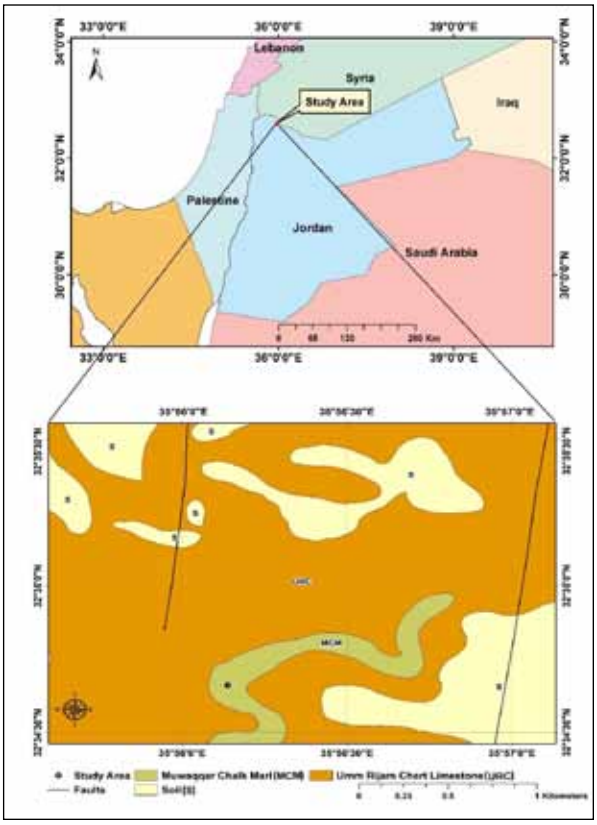

Figure 1. Location of study area (Modified after Moh'd, 2000).

2. Geological setting

Jordan was located at the Neo-Tethys Ocean's southern edge in the Cretaceous to Eocene. During that time interval, the sedimentation took place on a broad, shallow shelf that covered the northern edge of the Arabian Plate (Martin, 2001; Powell and Moh'd, 2011). A thick sequence of chalk, marl, and limestone is accumulated over the northern and central parts of Jordan. This sedimentary system, influenced by the subsequent closure of Neo-Tethys, associated with the continuous shifting of the African Arabian Plate toward the Eurasian Platelet to the formation of basins proper for oil shales deposition (Barjous and Mikbel, 1990).

Furthermore, tectonic movements along with broad structural features such as the Syrian Arc (Mart, 1987) and shifts in eustatic sea level (Haq and Al-Qahtani, 2005) also influenced the depositional environment.

The Jordanian oil shale is considered to be naturally bituminous marls with variable colours of grey to black with typical rather blue colour when weathered, in addition to the light content of fine-grained foraminifera content.

The exposed rocks in the present study are the Muwaqqar Chalk Marl Formation (MCM) and Umm Rijam Chert Limestone Formation. MCM is the oldest rock unit exposed in the study area and has a steeped topographical slope, high escarpments and flat bottom wadis with a dendritic drainage pattern (Moh'd, 2000). It is composed of yellowish marl, pale chalky marl, chalk and marly limestone with some carbonate concretions from bottom to top.

The thickest oil shale intervals occur in the lower part of the MCM and are typical for the Late Cretaceous to early Paleogene (Hamarneh et al., 1998).

3. Materials and Methods

The research area is Wadi Al-Shallala, which is situated in the north of Jordan, where it forms an extension of the Yarmouk River Basin (Thnebat, 2003).

The present study is based on one exposed oil shale section in the area, which estimated to be about 7 m thick. It is about 12 km northeast of Irbid City and about 5 km northwest of A-Ramtha City between 32° 34' 28" N; 35° 55' 6" E and 32° 35' 32" N; 35° 57' 8" **(**Figure 1**)**.

Twenty-nine samples were collected at regular distances of 25 cm from bottom to top for laboratory analysis, and 29 thin sections were made for petrographical analysis. The petrographic and microfacies study was conducted using a Nikon light microscope in the Department of Applied Earth and Environmental Sciences, Al al-Bayt University. The oil shale in the exposed section of the Wadi Al-Shallala consists of a sequence of grey to dark-grey-coloured marls, chalky marls and marly limestones, while the weathered surface gives light-blue colour **(**Figure 2**)**. The allochemical constituents were identified and classified based on Dunham (1962) and Flügel (1982). Microfacies are named according to Dunham's (1962) classification and are compared with the Ramp Microfacies (SMF) of Wilson (1975) and Flügel (2004) for the interpretation of the depositional environments. Samples were treated with a 3% hydrogen peroxide (H_2O_2) solution then washed over a 63 µm sieve for foraminifer analysis and dried at 50° C in an oven. The samples were sieved using a series of sieves after further drying. Foraminifera was picked from a specified fraction under a binocular microscope. Calculation of the index of oceanity carried out mathematically for each sample, then averaged for each microfacies type. The mean values of each microfacies type were represented on the Gibson graph to estimate the bathymetry of the oil shale deposition.

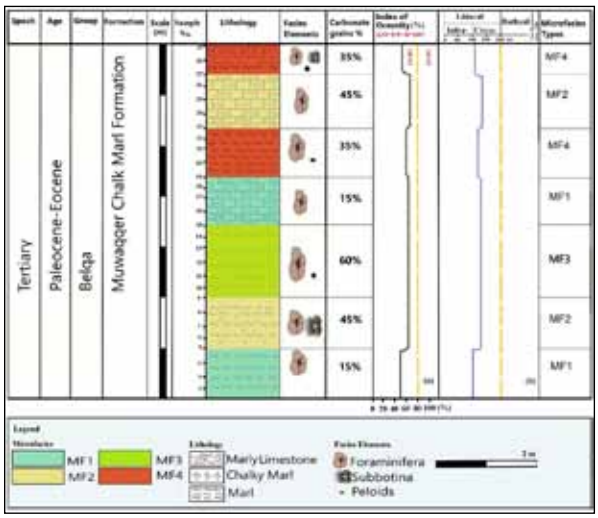

Figure 2. Lithological columnar section including curve of the variation of the oceanity index (a) and the bathymetry (b) of the Wadi Al-Shallala oil shale section.

In this article, the foraminifer taxonomy and descriptions are based on Brasier (1980), Loeblich et al. (1994), Olsson et al. (1999), Berggren et al. (2006) and Wade et al. (2011). Thin sections, labelled s-mf1-29, used for this study are deposited in the Department of Applied Earth and Environmental Sciences, Al al-Bayt University.

4. Results and Discussion

4.1. Microfacies Analysis:

Four major microfacies types were identified from bottom to top in the section of Wadi Al-Shallala:

MF1: Foraminifera-Bioclastic, Mudstone/Wackestone (Figures 3 a-d)

The Foraminifera-Bioclastic, Mudstone/Wackestone Microfacies **(**Figure 3a**)** consists of thin-bedded dark grey marls and marly limestone. This microfacies is represented by nine thin sections of the studied section. The total thickness of the microfacies is 2m (ca. 28% of the section) repeated two times from the base at samples no. 1–5 and 16–19 of the studied section, respectively (Figure 2). This type of microfacies is dominated by a lime-mud matrix, including 15% of carbonate grains. Bioclastic and mostly foraminifera are the dominant grains. This facies is mainly composed of fine- to medium-grained bioclastics in a micrite matrix: *Nodosaria* sp. (Figure 3b) and *Lenticulina* sp. (Figure 3c). Owing to cementation, the influence of diagenesis processes is well defined (Figure 3d). Röhl et al. (1991) interpreted the type of this microfacies type as being primarily deposited in a low-energy lagoon. Also, the Mudstone to Wackestone microfacies is interpreted as a restricted lagoon to the marine shelf, according to Wilson (1975) and Flügel (1982).

MF2: **Bioclastic-Foraminifera-Wackestone/Packestone (**Figures 4 a-d)

This microfacies type comprises chalky marl with some marly limestone levels consisting of 45% carbonate grains, represented by nine thin sections of the studied section. The total thickness of the Bioclastic-Foraminifera-Wackestone/Packestone microfacies is 2 m (ca. 28% of the section) repeated two times from the base at samples no. 6–9 and 24–27 of the studied section respectively (Figures 2,4a). The well-preserved carbonate grains predominantly include foraminifera bioclastic fragments, fragmented bones (Figure 4b); *Acarinina* sp., and *Subbotina* sp. (Figure 4c). Most of the grains are rounded to subrounded and incorporated in the micrite matrix. This microfacies type is characterized by different assemblages of skeletal debris.

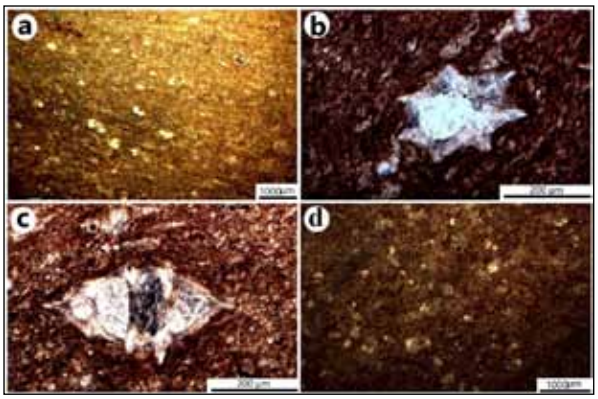

Figure 3. A. MF1-Foraminifera-Bioclastic, Mudstone-Wackestone. B. MF1-*Nodosaria* sp. C. MF1-*Lenticulina* sp. D. MF1-Well defined cementation.

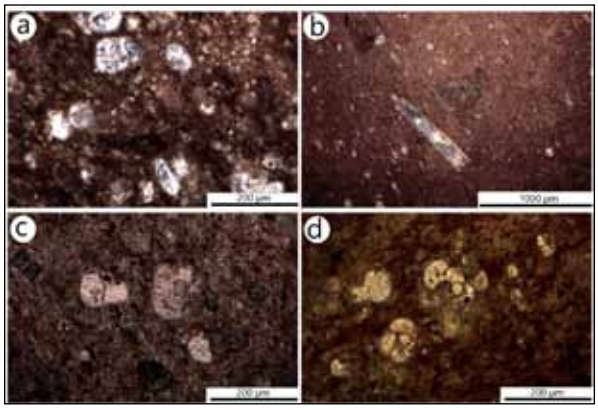

Figure 4. A. MF2-Bioclastic-Foraminifera-Wackestone/Packstone. B. MF2-Fragmented bones; C. MF2-*Acarinina* sp. D. MF2-*Acarinina soldadoensis* (Brönnimann 1952).

Acarinina soldadoensis (Brönnimann 1952) (Figure 4d) is a planktonic foraminifer, recognizing in this type of microfacies. This *Acarinina soldadoensis* (Brönnimann 1952) was identified by comparing the image of the thin section with all the nearby external morphology depicted through the images and it turned out that it is similar to the image of the species *Acarinina soldadoensis* mentioned in page 159 of Postuma (1971). The first occurrence of *Acarinina soldadoensis* (Brönnimann 1952) is at the base of the P4c subzone, Thanetian, 57.8Ma (Olsson et al. 1999), and the last occurrence is within the E7 zone, 45.72–50.20Ma, Lutetian (Wade et al. 2011). The suggested depositional environment for this type of facies is shallow neritic waters of moderate open circulation; it may have been formed in swales in the proximity of shoals in a high-energy environment.

MF3-Subbotina-Foraminifera Packestone(Figures 5a-b)

This facies type (Figure 5a) primarily consists of marlstone, light-brown to dark-grey, dull to light-grey, thin to medium-bedded, interbedded with greenish marl. *Subbotina*-Foraminifera Packestone microfacies is represented by six thin sections in the studied section. The total thickness of the microfacies is 1.5 m (ca. 21% of the section) recognized at samples no. 10–15 of the studied section, respectively (Figure 2), consisting of 60% carbonate grains.

The well-preserved grains are mainly comprised of rounded *Subbotina* sp. and *Acarinina* sp. *Acarinina aspensis* (Colom, 1954) (Figure 5b) is a planktonic foraminifera that identifies in this type of microfacies. This *Acarinina aspensis* (Colom, 1954) was identified by comparing the image of the thin section with all the nearby external morphology depicted through the slides and it turned out that it is similar to the image of the species *Acarinina aspensis* mentioned in Figure No. 7, page 175 of Postuma (1971). The first occurrence of *Acarinina aspensis* is at the base of the E7a subzone,50.2Ma, Ypresian, and the last occurrence was in the middle part of the E7a subzone,49.3Ma, Ypresian (Berggren et al., 2006). Owing to cementation, the influence of the diagenesis processes is well depicted (Figure 5b).

These microfacies are believed to have deposited in a shallow subtidal lagoonal environment of the inner shelf as indicated by the restricted faunal assemblage. Such microfacies are identical to those described by Wilson (1975) and Flügel (2004).

MF-4: Peloidal Wackestone (Figures 5c-d)

The Peloidal Wackestone Microfacies (Figures 5c, 5d) comprises thin-bedded dark-grey to dark grey to green marl. This microfacies is represented by six thin sections from the studied section. The total thickness of the microfacies is 1.5 m (ca. 21% of the section) repeated two times from the base at samples no. 20–23 and 28–29 of the studied section, respectively (Figure 2). This facies consists mainly of micritic limestone with 35% carbonate grains, often sub sorted peloids, bones, bioclastics and some foraminifera; typically, reasonably retained. These are usually the result of indurated carbonate mud due to erosion. The marl is greenish-grey to dark-grey, locally red-brown and cream to dark-brown. A few fossils were recognized in some shale beds such as; foraminifera, ostracods, and pelecypods. Owing to dissolution, the influence of diagenesis processes is well defined (Figures 5c, 5d). The proposed environment for this facies type is shallow neritic water of open circulation at or just below wave base.

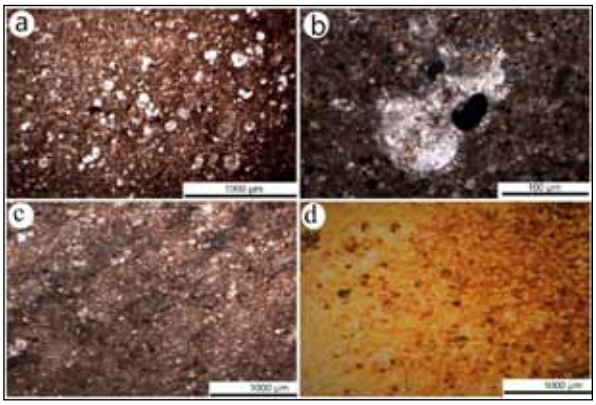

Figure 5. A. MF3-Foraminifera Packstone Subbotina sp. B. MF3-*Acarinina aspensis* (Colom 1954). C and d. MF4-Peloidal Wackestone.

The rock facies changes vertically in the exposed oil shale deposits from foraminifera-bioclastic, mudstone/wackestone in the lowermost part to peloidal wackestone in the uppermost part. Therefore, it is divided into seven units, based on the lithology and fossil contents; from the bottom to top, it begins with the marly unit (Unit 1) containing mainly benthonic and planktonic foraminifera. The marly unit composed of foraminifera-bioclastic, mudstone/wackestone microfacies represented by samples no. 1-5. Chalky marl (Unit 2) immediately above the marly unit is existed comprising predominantly of foraminifera and bioclastic fragments. The chalky marl composed of dominantly Bioclastic-Foraminifera-Wackestone/ Packestone microfacies represented by samples no. 6-9.

The following upwardly unit is marl (Unit-3) consisting mainly of *Subbotina* sp. and *Acarinina* sp. The marly unit composed of *Subbotina*-foraminifera packstone represented by samples no. 10-15.

Marly limestone (Unit 4) immediately above the marly unit is existed comprising predominantly of benthonic and planktonic foraminifera. The marly limestone composed of dominantly foraminifera-bioclastic, mudstone/wackestone microfacies represented by samples no.16-19.

The following unit is marl (Unit-5) consisting mainly of sub sorted peloids, bones, bioclastic, and some foraminifera. The marly unit composed of peloidal wackestone microfacies represented by samples no. 20-23. Marly limestone (Unit 6) immediately above the marly unit is existed comprising of foraminifera and bioclastic fragments. The marly limestone composed of dominantly bioclastic-foraminifera-wackestone/packstone microfacies represented by samples no. 24-27. The uppermost unit is marly to marly limestone (Unit-7) composed dominantly of peloids, bones, bioclastic, and some foraminifera. The marly and marly limestone unit includes peloidal wackestone microfacies represented by samples no. 28-29.

4.2. Index of Oceanity (I.O)

Benthic and planktonic foraminifera are typical constituents of a broad variety of shallow to deep-water marine environments. The proportion of planktonic foraminifera in the sediment to the total amount of foraminifera referred to as the plankton/benthos ratio. The quantitative relationship between the number of plankton to the total number of individuals in the sediment (benthic + plankton) is also known as oceanity index (Gibson, 1989). The proportion of the planktonic foraminiferal assemblage usually increases with the depth of water (De Swaaf et al. 1999). This proxy may be used as a fundamental and effective method to estimate the paleo-water depth at deposition and/ or the distance from the shore (Gibson, 1989; Van der Zwaan et al., 1990).

The (I.O) allows for the evaluation of bathymetry because in the marine waters the maximum productivity for planktonic foraminifers is far from a coast, but on the continental platforms, the benthic foraminifers proliferate. Foraminiferal planktonic and benthic abundances were counted and planktonic percentages (P/B) were calculated from the section studied in the oil shale deposits. The calculated values of the (I.O) for each sample and the mean for each microfacies type were shown in (Table 1) and (Figure 2a). The mean values of each microfacies type were correlated and compared with the Gibson graph (Figure 6) to assign approximately the bathymetry of the oil shale deposition (Figure 2b).

The mean values of the (I.O) of the studied section from the bottom are MF1= 53%, MF2= 62%, MF3 = 62%, MF1 = 62%, MF4 = 61%, MF2 = 63%, MF4 =57%. The mean of (I.O) in all samples from the studied section is about 60%. As a consequence of the relative sea-level changes, the I.O probably records slight variations in the oil shale samples.

Table 1. The mean values of the I.O and the estimated bathymetry of each recognized Microfacies types of study area.

MF types (Top)	I.O	Bathymetry(m)
MF4	57	110
MF2	63	132
MF4	61	124
MF1	62	128
MF3	62	128
MF2	62	128
MF1	53	105
Mean	60	120

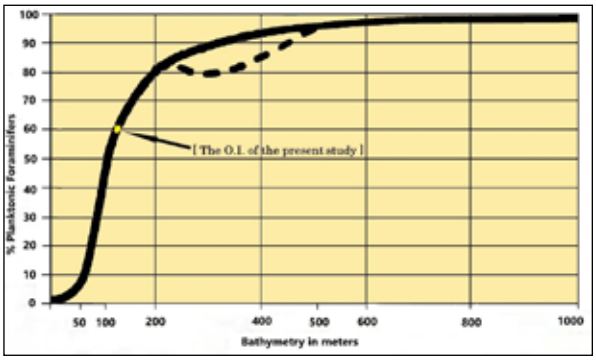

Figure 6. Index of oceanity (after Gibson, 1989).

The (I.O) from several depths transects across the United States shows that the middle-to-outer neritic transition at ~100 m is marked by 20–60% planktonic foraminifera and increases at ~200 m to 60–90% planktonic foraminifera (Gibson, 1989). The (I.O) at depth ~200 m is marked by 80% planktonic foraminifera and increases at > 200 m to 80–100% planktonic foraminifera based on the Gibson graph. Karoui-Yaakoub et al. (2016) used the Gibson model to reconstruct the bathymetry or the bottom water conditions of the Nukhul section (Egypt).

The approximate values of the bathymetry of the studied section from the bottom are MF1= 105 m, MF2= 128 m, MF3 = 128 m, MF1 = 128 m, MF4 = 124 m, MF2 = 132 m, MF4 =110 m. The mean of the bathymetry in the whole samples of the present section is about 120 m.

4.3. Planktonic Foraminifera

In the present study, the Cretaceous scheme of Caron (1985), the Palaeocene–Eocene scheme of Olsson et al., (1999) and new planktonic Foraminifera of (Hemleben et al., 1989) are adopted and the classification of the foraminifera is based on Loeblich and Tappan (1964). Fourteen species of planktonic foraminifera belong to nine genera are identified in this study;

(*Acarinina esnaensis*, *A. strabocella*, *A. interposita*, *A. soldadoensis*, *A. aspensis*, *Pearsonites broedermanni*, *Turborotalita carcoselleensis*, *Praemurica pseudoinconstans*, *Morozovella praeangulata*, *Subbotina cancellata*, *Planorotalites capdevilensis*, and *P. pseudoscitula*, *Planoglobanomalina* sp., *Globanomalina* sp.).

The most important identified planktonic Foraminifera species were photographed by a Scanning Electron Microscope (SEM) and are illustrated in (Figure 7).

Based on the range of the studied fourteen species of planktonic Foraminifera, the Paleocene to Eocene age were assigned as follows: Paleocene: (*Acarinina esnaensis*, *A. strabocella*, *Pearsonites broedermanni*, *Praemurica pseudoinconstans*, *Morozovella praeangulata*, and *Subbotina cancellata*) and Eocene: (*Acarinina esnaensis*, *A. interposita*, *A. soldadoensis*, *A. aspensis*, *Pearsonites broedermanni*, *Turborotalita carcoselleensis*, *Planorotalites capdevilensis*, *P. pseudoscitula*, and *Subbotina corpulenta*).

The study of (Futyan, 1976) determines the age of the oil shale deposits in Jordan somewhat differently, he assigned its age from Turonian, Santonian, Campanian, Maastrichtian, Paleocene to Eocene. Yassini, (1979) reported that the Muwaqqar Formation was deposited during the period of Maastrichtian-Late Eocene age. They are as follows: Maastrichtian: (*Globotruncana* zone); Paleocene*:* (*Morozovella*, *Planorotalites*, *Subbotina*, *Globoconusa*); Lower Eocene: (*Morozovella* zone). Al-Mashakbeh, (2012) identified three zones from the oil shale deposits in central Jordan during the Maastrichtian-Eocene age. The zones are: Maastrichtian: (*Pseudoguembelina*, *Racemiguembelina* and *Gansserina* zone); Paleocene: (*Morozovella*, *Praemurica*, *Subbotina*, and *Parvularugoglobigerina* zone); Lower Eocene: (*Acarinina*, and *Morozovella* zone).

4.4. Depositional Environments:

Oil shale originates in anoxic environments where the need for oxygen in the water column is greater than the availability (Demaison and Moor, 1980; Hay, 1995). Jordanian oil shales were deposited under restricted conditions of circulation. It is proposed that a set of physical barriers developed during the period of oil shale deposition, that enhanced the restricted conditions. The anoxic conditions that contributed to the deposition of Wadi Al-Shallala oil shale in the Yarmouk sub-basins may have resulted from syndepositional subsidence of fault bound throughout. The low diversity in the benthonic foraminiferal assemblage implies a low-oxygen environment, deposited under low-energy conditions. The variability in P/B ratios indicates fluctuations in sea level and that demonstrates the variation of the environment from shallow to open sea (Figure 8).

Microfacies diversity suggests a sea-level fluctuation from a shallow, restricted marine to an open marine depositional environment. The Mudstone/Wackestone Microfacies was deposited on the continental shelf. The Wackestone Microfacies type was deposited in open marine, shallow water. The Wackestone/Packstone microfacies was deposited in a shallow, restricted marine environment with limited water circulation and low energy. The Packestone Microfacies type concurrently accumulated in areas with similar quiet water sedimentation to those found in open sea shelf environments, and these conditions were ideal for retaining organic matter.

According to the aforementioned microfacies types, the depositional environment of the Wadi Al-Shallala oil shale can be attributed to a shallow continental shelf in a restricted marine and an open marine environment (Al-Soud, 2020). The present study confirms the results of previous studies that the Jordanian oil shales were deposited in a shallow, calm restricted environment, with limited open water circulation (e.g. Abed and Amireh, 1983; Mehdawi and Mustafa, 2008; Alqudah et al., 2014; Khrewesh, 2014; Ali Hussein et al., 2015; Beik et al., 2017, Al-Atawneh, 2018). Many authors have linked deposits of oil shale to MCM (Bender, 1974; Powell, 1989; Abed et al., 2005; Mihdawi and Mustafa, 2007). The age assignment of the MCM in previous studies are ranging from Maastrichtian to Paleocene age (e.g. Bender, 1974; Yassini, 1980; Powell, 1989), whereas Khrewesh (2014) used ammonites for assigning the MCM in Jebal Khuzayma in southeastern Jordan a Maastrichtian age. Basha (1982) gave an Eocene age based on foraminifera to the bituminous

marl layers of central east Jordan. The variations of the age assignment of MCM in Jordan may be due to the different geographic locations of the studied sections or attributed to the materials used for age determination.

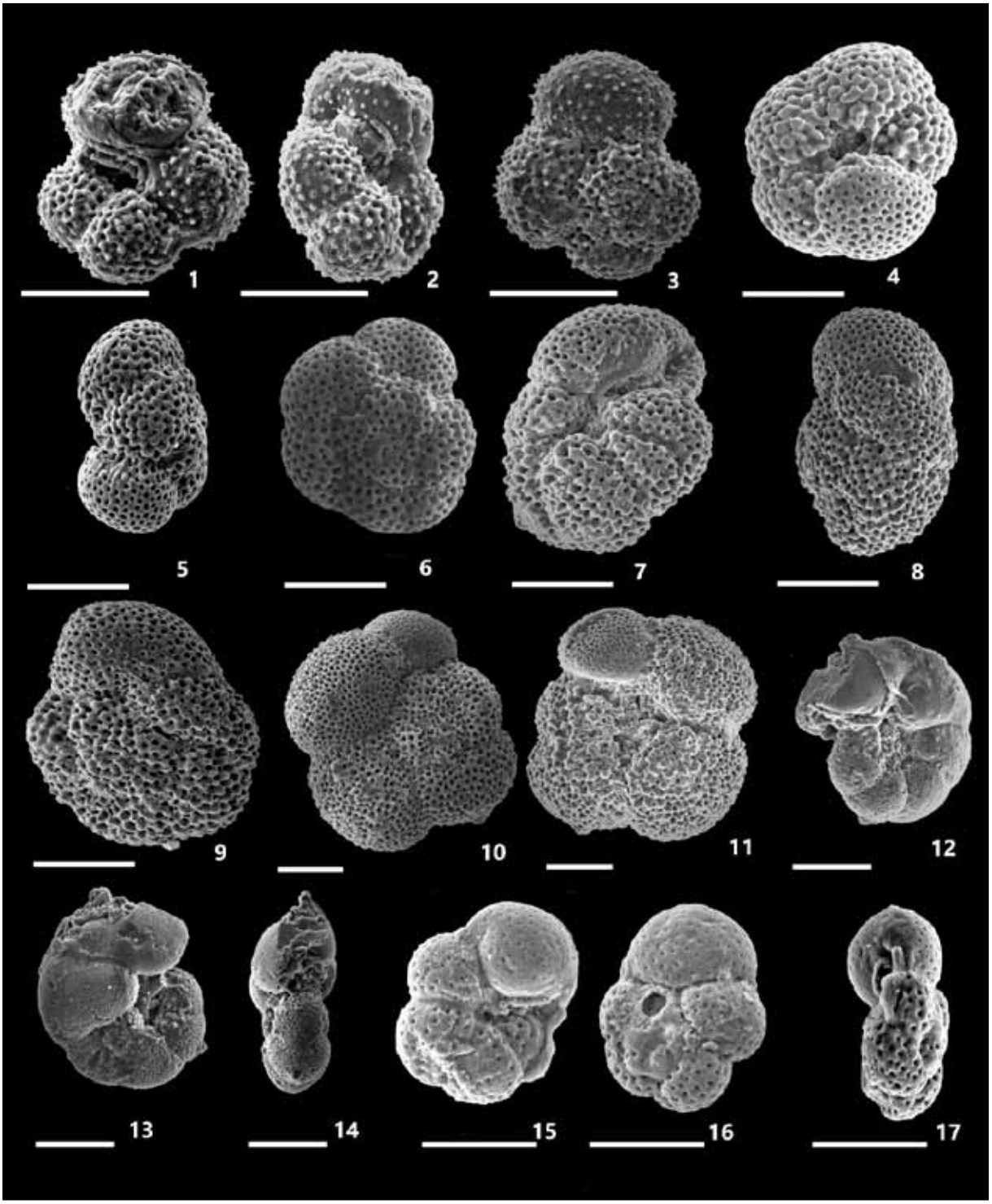

Figure 7. SEM photographs of selected planktonic foraminiferal species from the studied section.The scale barsof all Figures equal 100 µm. 1-3: *Acarinina esnaensis* (LeRoy 1953). 4-6: *Acarinina strabocella* (Loeblich and Tappan 1957). 7-9: *Pearsonites broedermanni* (Cushman and Bermudez 1949). 10-11: *Turborotalita carcoselleensis* (Toumarkine and Bolli, 1975). 12-14: *Planoglobanomalina* sp. 15-17: *Globanomalina* sp.

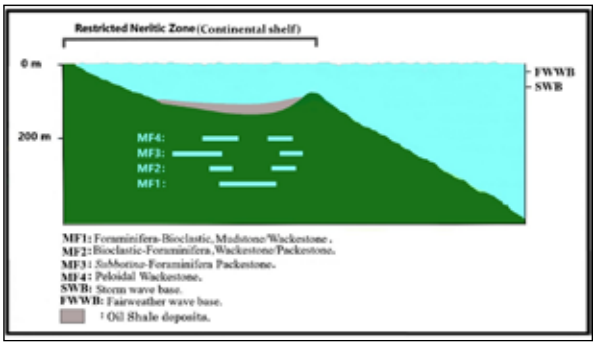

Figure 8. Depositional model of the study.

The average depth in all samples of the present section was around 120 m. Analysis based on planktonic percentages (P/B) or I.O indicated that oil shale deposition occurred in the continental shelf environment, which is following the results of the microfacies analysis (Al-Soud, 2020).

5. Conclusions

Four main microfacies types are distinguished and described; Foraminifera-Bioclastic, Mudstone/Wackestone (**MF1**), Bioclastic-Foraminifera-Wackestone/Packestone (**MF2**), Subbotina-Foraminifera Packestone (**MF3**), and Peloidal Wackestone (**MF4**). The average water depth of the exposed oil shale section is about 120 m.

The benthic foraminifera that was recognized in the present study are Nodosaria sp., and Lenticulina sp. The planktonic foraminifera that was recognized in the present study are; Acarinina esnaensis, A. strabocella, A. interposita, A. soldadoensis, A. aspensis, Pearsonites broedermanni, Praemurica pseudoinconstans, Morozovella praeangulata, Subbotina cancellata, S. corpulenta, Turborotalita carcoselleensis, Planorotalites capdevilensis, P. pseudoscitula, Planoglobanomalina sp., and Globanomalina sp. The Paleocene-Eocene age is assigned to the studied oil shale section. Microfacies analysis and I.O or planktonic percentages (P/B) indicate that the exposed oil shale section was deposited within a shallow marine and moderate circulation of an open marine shelf.

Acknowledgements

The authors would like to thank Prof. Abdalla Abu Hamad (University of Jordan) and Prof. Hendrik Klein (Saurierwelt Paläontologisches Museum, Germany) for the review of the manuscript and their suggestions and useful amendments. This article is part of the M.Sc thesis of the first author.

References

Abed, A.M. (1982). On the hydrocarbons of some Jordanian oil shales. Dirasat 9: 63-79.

Abed, A.M. and Amireh, B.S. (1983). Petrography and geochemistry of some Jordanian oil shales from north Jordan. Journal of Petroleum Geology 5(3): 261-274. http://dx.doi.org/10.1111/j.1747-5457.1983.tb00571.x.

Abed, A. M., Arouri, K. R., Boreham, C. J. (2005). Source rock potential of the phosphorite–bituminous chalk–marl sequence in Jordan. Marine and Petroleum Geology 22(3): 413-425. https://doi.org/10.1016/j.marpetgeo.2004.12.004.

Ahmad, F., Faris, M., Farouk, S. (2020). Calcareous Nannofossil Biostratigraphy and Carbon Isotopes from the Stratotype Section of the Middle Eocene Wadi Shallala Formation, Northwestern Jordan. Jordan Journal of Earth and Environmental Sciences 11 (2): 103-112.

Alali, J., Abdelfattah, A. S., Yasin, S. M., Al Omari, W. (2015). Oil Shale in Jordan. Natural Resources Authority of Jordan, 26 pp.

Alali, J. (2006). Jordan oil shale, availability, distribution, and investment opportunity. In International Conference on Oils Shale: Recent Trends in Oil Shale pp. 7-9.

Al-Atawneh, M. S. (2018). Depositional Environment of Eocene Oil Shale from Wadi Ashajara. M.Sc. Thesis, Yarmouk University, Jordan.

Ali Hussein, M., Alqudah, M., Blessenohl, M., Podlaha, O. G., Mutterlose, J. (2015). Depositional environment of Late Cretaceous to Eocene organic-rich marls from Jordan. GeoArabia 20(1): 191-210.

Al-Mashakbeh, H. (2012). Micropaleontology and Biostratigraphy of Some Oil Shale Deposits in Jordan, Ph.D. Thesis, University of Jordan, Jordan.

Alqudah, M., Hussein, M. A., Podlaha, O. G., den Boorn, S. V., Kolonic, S., Mutterlose, J. (2014). Calcareous nannofossil biostratigraphy of Eocene Oil shales from central Jordan. GeoArabia 19(1): 117-140.

Al-Soud, H. (2020). Microfacies analysis, Micropaleontology and Paleoenvironment of Oil Shale Deposits in Wadi Al-Shallala – Jordan. M. Sc. Thesis, Al al-Bayt University, Jordan.

Barjous, M. and Mikbel, S. (1990). Tectonic evolution of the Gulf of Aqaba-Dead Sea transforms fault system. Tectonophysics 180(1): 49-59. https://doi.org/10.1016/0040-1951(90)90371-E.

Basha, S. (1982). Stratigraphy, palaeogeography and oil possibilities of the Azraq Sirhan Turayf basin (Jordan-Saudi Arabia). Dirasat 9: 85-106.

Beik, I., Gómez, V.G., Podlaha, O.G., Mutterlose, J. (2017). Microfacies and depositional environment of Late Cretaceous to Early Paleocene oil shales from Jordan. Arabian Journal of Geosciences 10(15): 346. https://doi.org/10.1007/s12517-017-3118-6.

Bender, F. (1974). Geology of Jordan. Supplementary Edition in English with Minor Revisions. Gebrueder Borntraeggger, Berlin, 196pp.

Berggren, W.A., Pearson, P.N., Huber, B.T., Wade, B.S. (2006). Taxonomy, biostratigraphy and phylogeny of Eocene Acarinina. Atlas of Eocene Planktonic Foraminifera. Cushman Foundation Special Publication 41: 257-326.

Brasier, M.D. (1980). Microfossils. George Allen and Unwin, London, 193 pp.

Brönnimann, P. (1952). Trinidad Paleocene and lower Eocene Globigerinidae. Bulletin of American Paleontology 34(143): 1-34.

Caron, M. (1985). Cretaceous Planktonic Foraminifera. In: Bolli, H. M., Saunders, J. B. and Perch-Nielsen, K. (Eds), Plankton Stratigraphy. Cambridge University Press, Cambridge: 17- 86.

Colom, G. (1954). Estudio de las biozonas con foraminíferos del Terciario de Alicante. Boletín del Instituto Geológico y Minero de España 66: 1-279.

Cushman, J. A. and Bermudez, P. J. (1949). Some Cuban species of Globorotalia. Contributions from the Cushman Laboratory for Foraminiferal Research 25: 26-45.

De Swaaf, M. E., De Rijk, T. C., Eggink, G., Sijtsma, L. (1999). Optimisation of docosahexaenoic acid production in batch cultivations by Crypthecodinium cohnii. Journal of Biotechnology 70(1-3): 185-192. https://doi.org/10.1016/S0079-6352(99)80111-8

Demaison, G.J. and Moore, G.T. (1980). Anoxic environments and oil source bed genesis. AAPG Bulletin 64(8): 1179-1209. https://doi.org/10.1306/2F91945E-16CE-11D7-8645000102C1865D.

Dunham, R.J. (1962). Classification of Carbonate Rocks According to Depositional Texture. In: Ham, W.E. (Ed.), Classification of Carbonate Rocks, AAPG, Tulsa, 108-121.

El-Hasan, T. (2008). Geochemistry of redox-sensitive trace elements and its implication on the mode of formation of the Upper Cretaceous oil shales, Central Jordan. Neues Jahrbuch für Geologie und Paläontologie, Abhandlungen 249(3): 333-344. https://doi.org/10.1127/0077-7749/2008/0249-0333.

Flügel, E. (1982). Introduction to facies analysis. In Microfacies Analysis of Limestones (pp. 1-26). Springer, Berlin, Heidelberg. https://doi.org/10.1007/978-3-642-68423-4_1.

Flügel, E. (2004). Microfacies analysis of carbonate rocks. Analysis, interpretation and application. Springer, Berlin. https://doi.org/10.1007/978-3-662-08726-8

Futyan, A.I. (1976). Late Mesozoic and early Cainozoic benthic foraminifera from Jordan. Paleontologie (Prague) 13: 517–537.

Gibson, T. G. (1989). Planktonic benthonic foraminiferal ratios: modern patterns and Tertiary applicability. Marine Micropaleontology 15(1-2): 29-52. https://doi.org/10.1016/0377-8398(89)90003-0.

Hakimi, M. H., Abdullah, W. H., Alqudah, M., Makeen, Y. M., Mustapha, K. A. (2016). Reducing marine and warm climate conditions during the Late Cretaceous, and their influence on organic matter enrichment in the oil shale deposits of North Jordan. International Journal of Coal Geology 165: 173-189. https://doi.org/10.1016/j.coal.2016.08.015.

Hamarneh, Y., Alali, J., Sawaged, S. (1998). Oil shale resources development in Jordan. Natural Resources Authority, Hashemite Kingdom of Jordan, Amman.

Hamarneh, Y., Jamal, A., Suzan, S. (2006). Oil shale resources development in Jordan (PDF). Natural Resources Authority of Jordan.

Haq, B.U. and Al-Qahtani, A.M. (2005). Phanerozoic cycles of sea-level change on the Arabian Platform. GeoArabia 10(2): 127-160.

Hay, W.W. (1995). Paleoceanography of Marine Organic Carbon-Rich Sediments. In A.-Y. Huc (Ed.), Paleogeography, Paleoclimate, and Source Rocks. AAPG Studies in Geology Series no. 40: 21-59. https://doi.org/10.1007/978-3-642-68423-4_1.

Hemleben, C., Spindler, M., Anderson, O. R. (1989). Modern planktonic Foraminifera. New York: Springer Verlag, 363 pp. Free-floating forms are the worldwide markers in the geological time scale. https://doi.org/10.1007/978-1-4612-3544-6

Hufnagel, H. (1985). Oil shale in Jordan. Natural resources and development 22: 46-62.

Jaber, J.O., Sladek, T.A., Mernitz, S., Tarawneh, T. M. (2008). Future policies and strategies for oil shale development in Jordan. Jordan Journal of Mechanical and Industrial Engineering 2(1): 31-44.

Jarrar, M. (1989). Composition, Stratigraphy and depositional environment of kerogenous limestone of Wadi AL-Shallala. Master thesis, Yarmouk University, Jordan.

Karoui-Yaakoub, N., Mtimet, M.S., Grira, C., Guesmi, W., Bejaoui, S. (2016). Planktonic foraminiferal biostratigraphy and paleoenvironment of the Danian/Selandian in west-central Sinai (Egypt), implications from the Nukhul section. Arabian Journal of Geosciences 9(7): 1-15. https://doi.org/10.1007/s12517-016-2513-8

Khrewesh, A.M., Hamad, A.A., Abed, A.M. (2014). Late Cretaceous Muwaqqar Formation Ammonites in Southeastern Jordan. Jordan Journal of Earth and Environmental Sciences 6(2): 77-83.

LeRoy, L.W. (1953). Biostratigraphy of the Maqfi Section, Egypt. Memoir Geological Socity of America 54: 1-73. https://doi.org/10.1130/MEM54-p1

Loeblich Jr., A.R. and Tappan, H. (1994). Foraminifera of the Sahul Shelf and Timor Sea. Cushman Foundation for Foraminiferal Research. Special Publication 31: 661.

Loeblich, A.R. and Tappan, H. (1957). Planktonic foraminifera of Paleocene and early Eocene Age from the Gulf and Atlantic coastal plains. In: Loeblich, A.R., Jr., Tappan, H., Beckmann, J.P., Bolli, H. M., Montanaro Gallitelli, E. Troelsen, J.C. (Eds.), Studies in Foraminifera. U.S. National Museum Bulletin 215: 173-198.

Loeblich, A.R. and Tappan, H. (1964). Treatise on Invertebrate Paleontology (Vol. 1 and 2). The Geological Society of America and The University of Kansas Press, Lawrence.

Mart, Y. (1987). Superpositional tectonic patterns along the continental margin of the southeastern Mediterranean: a review. Tectonophysics 140(2-4): 213-232. https://doi.org/10.1016/0040-1951(87)90230-7

Martin, A.Z. (2001). Late Permian to Holocene paleofacies evolution of the Arabian Plate and its hydrocarbon occurrences. GeoArabia 6(3): 445-504.

Mehdawi, H. and Mustafa, H. (2008). Geochemistry and evaluation of organic matter of the oil shale from Muwaqqar formation (Maastrichtian- Paleocene) in the area between Wadi Zahar and Wadi Abu Ziyad , NW- Jordan. Abhath AL-Yarmouk 17 (1B): 233-257.

Moh'd, B. K. (2000). The Geology of Irbid and Ash Shuna Ash Shamaliyya (Waqqas): Map Sheets No. 3154-II and 3154-III. Hashemite Kingdom of Jordan, Natural Resources Authority, Geology Directorate, Geological Mapping Division.

Olsson, R. K., Berggren, William A., Hemleben, C., Huber, Brian T. (1999). "Atlas of Paleocene Planktonic Foraminifera." Smithsonian Contributions to Paleobiology 1 -252. https://doi.org/10.5479/si.00810266.85.1.

Postuma, J. (1971). Manual of Planktonic Foraminifera. Elsevier Publishing Co. Amsterdam 420.

Powell, J. H. (1989). Stratigraphy and sedimentation of the Phanerozoic rocks in central and south Jordan, part B: Kurnub, Ajlun and Belqa Groups. (Geology Directorate, Natural Resources Authority, Amman, Jordan), Bulliten 11, 130 pp.

Powell, J.H. and Moh'd, B.K. (2011). Evolution of Cretaceous to Eocene alluvial and carbonate platform sequences in central and south Jordan. GeoArabia 16(4): 29-82.

Röhl, U., Dumont, T., von Rad, U., Martini, R., Zaninetti, L. (1991). Upper Triassic tethyan carbonates off northwest Australia (Wombat Plateau, ODP Leg 122). Facies 25(1): 211-251. https://doi.org/10.1007/BF02536760

Thnebat M.A. (2003). Hydrological study of Wadi Al-Shallala Yarmouk Basin, Master thesis. University of Jordan, Amman, Jordan.

Van der Zwaan, G. J., Jorissen, F. J., De Stigter, H. C. (1990). The depth dependency of planktonic/benthic foraminiferal ratios: constraints and applications. Marine Geology 95(1): 1-16. https://doi.org/10.1016/0025-3227(90)90016-D

Wade, B.S., Pearson, P.N., Berggren, W.A., Pälike, H. (2011). Review and revision of Cenozoic tropical planktonic foraminiferal biostratigraphy and calibration to the geomagnetic polarity and astronomical time scale. Earth-Science Reviews 104(1-3): 111-142. https://doi.org/10.1016/j.earscirev.2010.09.003

Wilson, J.L. (1975). Carbonate Facies in Geologic History. Springer, Berlin, pp. 471. https://doi.org/10.1007/978-1-4612-6383-8

Yassini, I. (1979). Maastrichtian-Lowe Eocene biostratigraphy and the planktonic foraminiferal biozonation in Jordan. Revista española de micropaleontología 11: 5-57.

JJEES

JJEES (2021) 12 (2): 122-133
ISSN 1995-6681

Jordan Journal of Earth and Environmental Sciences

Treatment of real olive mill wastewater by sole and combination of H_2O_2, O_3, and UVA: effect of doses and ratios on organic content and biodegradability

Dheaya Alrousan

Department of Water Management and Environment, Prince EL-Hassan Bin Talal Faculty for Natural Resources and Environment, The Hashemite University, Jordan.

Received 8 October 2020; Accepted 25 October 2020

Abstract

Given the rapidly growing olive oil agroindustry, many countries in the coming future will face the same challenge of olive mill wastewater (OMW) management as the Mediterranean countries currently do. Ozonation and ozone-based advanced oxidation processes (AOPs) could represent a promising complementary or alternative solution for OMW treatment. One critical parameter that significantly influences the efficiency and the cost of ozone processes is the chemical dosages and ratios. This research investigated OMW treatment by sole and combination of H_2O_2, O_3, and UVA irradiation, in a glass tube photoreactor and by applying a wide range of H_2O_2 and O_3 dosages and ratios. The treatment efficiency was evaluated based on the reduction of dissolved organic carbon (DOC) and the change in biodegradable organic content expressed by BOD_5 and biodegradability. The highest DOC reduction in this study was ≈ 40% by UVA/ peroxonation, while the highest enhancement in BOD_5 (209%) and biodegradability (254%) was achieved by dark peroxonation. However, a wide range of doses combination can result in the same degree of change in DOC reduction or BOD_5 and biodegradability enhancement. This lab-based study demonstrates the potential of the studied systems to significantly reduce the organic fraction of real OMW and increase the biodegradability, which offering a new spectrum to optimize the chemical dosages based on the purpose of the treatment.

Keywords: Olive mill wastewater, ozonation, peroxonation, biodegradability, AOPs

1. Introduction

The countries around the Mediterranean basin hold 97% of global olive oil production (Saez et al., 2020). Unfortunately, high production is always combined with large quantities of wastewater as a byproduct, where around 30 million m^3 of olive mill wastewater (OMW) is generated annually in the Mediterranean region alone (Pedrero et al., 2020). Even though the OMW amount is not relatively high, most countries' legislations prohibits OMW's direct discharge in water bodies (Al-Bsoul et al., 2020). Still, whenever that happened, it has caused catastrophic environmental consequences due to the high OMW pollution impact, which is assumed to be 100 – 200 times to that of the domestic wastewater (El-Abbassi et al., 2013). Moreover, the amount of OMW generated worldwide is expected to increase in the coming future because of the rapidly growing agroindustry of olive oil production in countries outside the Mediterranean, such as Argentina, Australia, and Chile (Pedrero et al., 2020).

The OMW characteristics are affected by several factors, such as olive type, degree of fruit maturity, and the oil extraction method (Erses Yay et al., 2012). However, it is generally characterized by a dark brown color, unpleasant odor, low pH, high organic and suspended solids content, and similarly high levels of phenolic compounds (Ioannou-Ttofa et al., 2017; Ahmed et al., 2019). The simplest and most common practices followed for OMW treatment at low cost, and unskilled labor are evaporation ponds. Despite the suitability of evaporation ponds in the Mediterranean countries where the evaporation rates are high during the summer period, the leakages and infiltration into groundwater, in addition to odor and breading of insects, are some of evaporation ponds disadvantages (Saez et al., 2020; Erses Yay et al., 2012; Khoufi et al., 2009). In the context of; i) the high organic and phenolic content of OMW, ii) the seasonal OMW generation during a few months of the year, iii) and the geographically scattering of the olive mills (Ioannou-Ttofa et al., 2017; Ahmed et al., 2019), different treatment methods have been considered to overcome those limitations, which includes, but not limited to, electrocoagulation (Niazmand et al., 2020), membrane processes (Akdemir and Ozer, 2009), adsorption (Azzam et al., 2013), electrocatalysis (UĞUrlu et al., 2019), and biological treatment (Bertin et al., 2004). Unfortunately, most of the proposed OMW treatment processes are either inefficient or cost-ineffective (Ochando-Pulido et al., 2017).

In the last two decades, several remarkable studies have addressed the application of advanced oxidation processes (AOPs) for OMW treatment in particular (Al-Bsoul et al., 2020; Iboukhoulef et al., 2019; Hodaifa et al., 2019; García and Hodaifa, 2017). The key advantage of AOPs over other treatment options is their ability to non-selectively degrade various types of organic and inorganic compounds rather

* Corresponding author e-mail: dheaya@hu.edu.jo

than transform them into another phase by relying on hydroxyl radicals ($OH^{\bullet}$) formation (Ioannou-Ttofa et al., 2017; Pérez-Lucas et al., 2020). Despite the widespread use of ozone for water and wastewater treatment, a limited number of studies considered the use of ozone and ozone-based AOPs for OMW treatment (Iboukhoulef et al., 2019; Bar Oz et al., 2018) (Miranda et al., 2001; Al-Bsoul et al., 2020; Lafi et al., 2009). Nevertheless, considering the in situ costs of ozone generation, ozonation is not generally advised as a standalone solution for reducing organic content (Daghrir et al., 2016). However, combining ozone with irradiation or hydrogen peroxide (H_2O_2) is well reported to enhance treatment efficiency (Oturan and Aaron, 2014; Bethi et al., 2016; Li et al., 2015). The critical parameters to be optimized that are significantly influencing the efficiency and cost are the chemical dosages and the OMW organic content. The optimization depends on the treatment's purpose, which could be; 1) reducing the organic content if high purity effluent water is needed or there are restrictions on the effluent dissolved organic load, 2) or increasing the biodegradability and the biodegradable fraction for biogas production, or as a complementary step for biological treatment.

This study aims to examine the efficiency of ozone-based AOPs to treat real OMW and experimentally determine the optimum oxidants dosages and initial dissolved organic carbon concentration in the light of organic content reduction and biodegradability enhancement. The AOPs that are particularly examined in this study are O_3/dark, O_3/UVA, H_2O_2/dark, H_2O_2/UVA, O_3/H_2O_2, and O_3/H_2O_2/UVA.

2. Theory

Ozone has a high oxidation potential (Barzegar et al., 2019) and can attack organic compounds either directly (ozonolysis) by oxidizing particular organic compounds or indirectly by generating $OH^{\bullet}$ (Pérez-Lucas et al., 2020). The O_3 attack mode depends on the treatment conditions such as the pH and the organic and inorganic constituents. In ozonolysis, O_3 selectively attack organic compounds that have high electron density sites (Pérez-Lucas et al., 2020), such as the carbon-carbon double bond, aromatic rings, and the functional groups containing nitrogen (N), oxygen (O), sulfur (S), and phosphorus (P) (Michael-Kordatou et al., 2018). The ozonolysis reactions include the oxidation-reduction, dipolar cycloaddition, electrophilic substitution, and nucleophilic addition (Dai et al., 2015). Those reactions transform organic compounds into smaller molecular weight saturated intermediates rather than leading to full mineralization (Iboukhoulef et al., 2019). Regardless of numerous suggested reaction pathways for the indirect ozone mode of action to generate $OH^{\bullet}$, there is a general agreement that the hydroxide ions (OH^-) initiate the O_3 decomposition chain (natural decomposition) (Equation 1) (Oturan and Aaron, 2014). However, this is only true in pure water as other various compounds or actions can act as initiators of O_3 decomposition, which can be generalized in the form of Equation 2 (chemically assisted decomposition). The decomposition initiators include but not limited to, humic substances, formate (Gardoni et al., 2012), transition metal ions (Kasprzyk-Hordern et al., 2003), activated carbon (Farzadkia et al., 2014), phenols and amines (Wert et al., 2009), and UV irradiation (UV photo-ozonation) in the range of 200 – 360 nm (Equation 3) (Oturan and Aaron, 2014; Bustos-Terrones et al., 2016).

$$3O_3 + OH^- + H^+ \rightarrow 2OH^{\bullet} + O_3^{\bullet-} + 4O_2 \quad \text{Eq. 1}$$

$$O_3 + H_2O + \text{decomposition initiator} \rightarrow \text{series of reactions} \rightarrow OH^{\bullet} \quad \text{Eq. 2}$$

$$O_3 + H_2O + h\nu \rightarrow 2\,OH^{\bullet} + O_2 \quad \text{Eq. 3}$$

Hydrogen peroxide, in particular, gained huge interest as O_3 decomposer (Equation 4) (researchers often name this process by peroxonation, wet peroxide ozonation, and perozonation) (Miklos et al., 2018; Oturan and Aaron, 2014; Li et al., 2015; Englehardt et al., 2013). The peroxonation process utilizes the direct ozone and hydrogen peroxide oxidation power and the generated hydroxyl radicals' mineralization capability.

$$2O_3 + H_2O_2 \rightarrow 2OH^{\bullet} + 3O_2 \quad \text{Eq. 4}$$

Even though H_2O_2 is considered as relatively inexpensive and environmentally friendly oxidant, it has limited application as sole organic content reduction because of its weak oxidation potential (Oturan and Aaron, 2014). However, similar to ozone, H_2O_2 can be decomposed to generate hydroxyl radicals where this decomposition can be initiated and promoted by; transitional metals (Fe, Cu, Co, etc.) (Yazdanbakhsh et al., 2015), activated carbon (Kurniawan and Lo, 2009), TiO_2 (Moreira et al., 2018), zero-valent iron (ZVI) (Yazdanbakhsh et al., 2015) and UV irradiation in the range of 200 to 300 nm (Equation 5) (Oturan and Aaron, 2014).

$$H_2O_2 + h\nu \rightarrow 2\,OH^{\bullet} \quad \text{Eq. 5}$$

The peroxonation process efficiency can be further improved by combining it with UV irradiation (UV peroxonation), which boosts the $OH^{\bullet}$ generation (Hassanshahi and Karimi-Jashni, 2018; Bethi et al., 2016; Wang and Xu, 2012). In most of the studies, the employed UV is high energy and short wavelength source such as; UVC (Guo et al., 2018), UV-ABC (Antonio da Silva et al., 2018), VUV (Yuval et al., 2017), UVAB (Huang et al., 2018), and gamma irradiation (Ebrahimi et al., 2018) with limited interest in using the near-ultraviolet irradiation (Nie et al., 2010; Dong et al., 2019; Celeiro et al., 2018).

One critical parameter in ozone-based AOPs are the oxidants dosages, as using inappropriate doses of H_2O_2 or O_3 may act as hydroxyl radicals scavenger (Equation 6 (Elmolla and Chaudhuri, 2010) and Equation 7 (Barzegar et al., 2019)) by reacting with the very reactive hydroxyl radicals ($OH^{\bullet}$) (E^0 = 2.8 V) (Yazdanbakhsh et al., 2015) and producing the less reactive hydroperoxyl radicals () (E^0 = 1.7 V) (Kurniawan and Lo, 2009). The hydroperoxyl radicals have even lower oxidation power than ozone (E^0 = 2.07 V) (Barzegar et al., 2019) or hydrogen peroxide (E^0 = 1.78 V) (Oturan and Aaron, 2014).

$$H_2O_2 + OH^{\bullet} \rightarrow HO_2^{\bullet} + H_2O \quad \text{Eq. 6}$$

$$O_3 + OH^{\bullet} \rightarrow HO_2^{\bullet} + O_2 \quad \text{Eq. 7}$$

3. Material and methods

3.1. Olive mill wastewater

OMW in this study was obtained during the milling campaign of 2017/2018 from Al Zyoud Olive Oil Mill, located in Alzarqa (middle – north of Jordan) that uses a three-phase continuous olive oil extraction (Rapanelli International, Italy). Fresh samples of OMW were collected from the decenter outlet in 20 L polyethylene containers, transferred to the laboratory within 20 min, filtered through a 0.45 µm membrane, and stored at 3-5 ℃. The main physicochemical characteristics of the filtered OMW are summarized in Table 1.

Table 1. Olive mill wastewater characteristics

parameter	unit	Value ± Standard deviation
Chemical oxygen demand (COD)	mg/L	38750 ± 320
Biochemical oxygen demand (BOD_5)	mg/L	2221 ± 160
Dissolved organic carbon (DOC)	mg/L	11413.4 ± 373.8
Total solids (TS)	mg/L	41870 ± 770
Total suspended solids (TSS)	mg/L	28350 ± 460
pH	-	4.52 ± 0.38
Conductivity	mS/cm	10.4 ± 0.25
Turbidity	NTU	57.8 ± 3.52 (NTU)

3.2. Materials

All chemicals used were of high purity grade and sourced from Sigma Aldrich and BDH. For TOC standards preparation, potassium hydrogen phthalate was supplied by Nacalai Tesque Inc. Hydrogen peroxide 35% strength was supplied by BDH, AnalaR. Ozone was produced in situ using OZ-3G ozone generator (Ozonefac Ltd., China) with a variable ozone outlet concentration and a constant air flow rate of 5 L/min.

3.3. Analytical methods

The treatment efficiency was evaluated by measuring the dissolved organic carbon (DOC) and the biochemical oxygen demand (BOD_5). DOC was used rather than the chemical oxygen demand (COD) to minimize hydrogen peroxide interference with COD measurements (Elmolla and Chaudhuri, 2010), and was evaluated using Shimadzu 5000 TOC/V with auto-sampler. The injected sample volume was 50 µL, and the catalyst used was the regular sensitivity Pt catalyst. The samples' biodegradable organic content was determined by measuring the BOD_5 using BOD_5 EVO System 6 (VELP Scientifica, Inc). The BOD_5 samples have all been subjected to extended aeration in the dark for 15 min before being tested to avoid any measurements interfering caused by ozone residue. All samples in this study were analyzed in triplicate unless otherwise stated.

3.4. Experimental setup

The experiments were carried out in a custom-built borosilicate glass tube photoreactor with concentrated parabolic collectors (Figure 1). Full details of the photoreactor modules are described in our previous publication (Alrousan and Dunlop, 2020). Even the reactor was initially designed for experiments under solar irradiation; it was used with artificial UVA lamps in this study for future research comparison purposes.

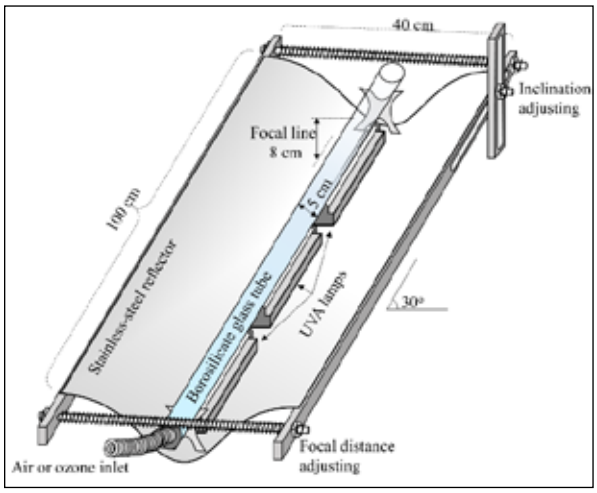

Figure 1. Glass tubes photoreactor with concentrated parabolic collectors

The photoreactor was illuminated from below using three 11W UVA lamps (TL11W/05 Philips lamp, Holland). The lamps emitted radiation between 300 – 460 nm with maximum emission at 365 nm and average incident UVA intensity of 55.4 ± 6.3 W/m^2. The glass tube total capacity is 1.96 L; however, due to the inclination angle and to ensure room for gas bubbling, the volume of OMW treated in each experimental batch was 1.5 L. The glass tube was wrapped in aluminum foil for studies without irradiation. Depending on the experiments' purpose, air or air with ozone was continuously fed to the tube reactor. For experiments with hydrogen peroxide, hydrogen peroxide was added as a single dosage to the OMW at the beginning of each experiment with different concentrations. OMW was diluted with distilled water to give initial DOC concentration from 1000 - 4000 mg/L (corresponds to DOC_0 of 83.3 – 333.3 mM). All experiments were carried out for three hours, and 500 ml samples were withdrawn before and after the treatment for physiochemical analysis. Table 2 describes the systematic approach to the experimental conditions.

Table 2. Matrix of experimental conditions.a

Experiment	O_3 dosage (mM)	H_2O_2 dosage (mM)	Illumination conditions
Dark/aerated	0.00	0.00	dark
UVA/aerated	0.00	0.00	UVA
Ozonation (O_3/dark)	37.5 -150	0.00	dark
Ozone photolysis (O_3/UVA)	37.5 -150	0.00	UVA
H_2O_2-peroxidation (H_2O_2/dark)	0.00	66.7 -266.7	dark
(H_2O_2/UVA)	0.00	66.7 -266.7	UVA
Peroxonation (H_2O_2/O_3/dark)	37.5 -150	66.7 -266.7	dark
Photo-peroxonation (H_2O_2/O_3/UVA)	37.5 -150	66.7 -266.7	UVA

[a] The nominal DOC0 for all experiments ranged from (83.3 – 333.3 mM), real values were slightly different from that

3.5. Calculations and data representation

The biodegradability (abbreviated as Bio) was represented by the ratio of BOD_5 to DOC values, as expressed in Equation 8.

$$Bio = \frac{BOD_5}{DOC}$$

The change in TOC, BOD_5, and biodegradability was expressed in normalized form as in the general Equation 9, where M_0 and M_f are the measured values before and after the treatment, respectively.

$$E_M = \frac{M_f}{M_0} \quad \text{Eq. 9}$$

The independent variables; H_2O_2 dosage, O_3 dosage, and the initial dissolved organic carbon (DOC_0) of the tested OMW, were normalized in the form of a molar fraction (X) by dividing the value of each independent variable (measured by mM) by the summation of all independent variables (Equation 10 - Equation 12).

$$X_{H_2O_2} = \frac{H_2O_2\ dosage}{H_2O_2\ dosage + O_3\ dosage + DOC_0} \quad \text{Eq. 10}$$

$$X_{O_3} = \frac{O_3\ dosage}{H_2O_2\ dosage + O_3\ dosage + DOC_0} \quad \text{Eq. 11}$$

$$X_{DOC_0} = \frac{DOC_0}{H_2O_2\ dosage + O_3\ dosage + DOC_0} \quad \text{Eq. 12}$$

All 3D plots were created using Origin 2019b software (OriginLab Corporation, Northampton, USA) with a built-in Thin Plate Spline (TPS) algorithm.

4. Results and discussion

4.1. Control experiments

In control experiments, diluted OMW with various initial organic content was subjected for three hours to different light exposure conditions (dark and UVA irradiation) with and without aeration. No change in OMW organic content was noticed for experiments without aeration, even under UVA irradiation (data not shown). As can be observed from Figure 2a, there was a very slight reduction in DOC and BOD_5 (≈ 1.4% and ≈ 3.6%, respectively) under dark aeration conditions with almost no effect of the initial OMW organic content (DOC_0). However, there is no reason for this tiny reduction except the air stripping of the purgeable dissolved organic carbon (PDOC), such as the volatile and low boiling organic compounds, which are commonly found in OMW and cause odor problems in the vicinities of the olive mills (Azbar et al., 2004). Based on the relatively higher reduction in BOD_5 compared to DOC, it can be assumed that the bulk of PDOCs in the studied OMW are biodegradable compounds.

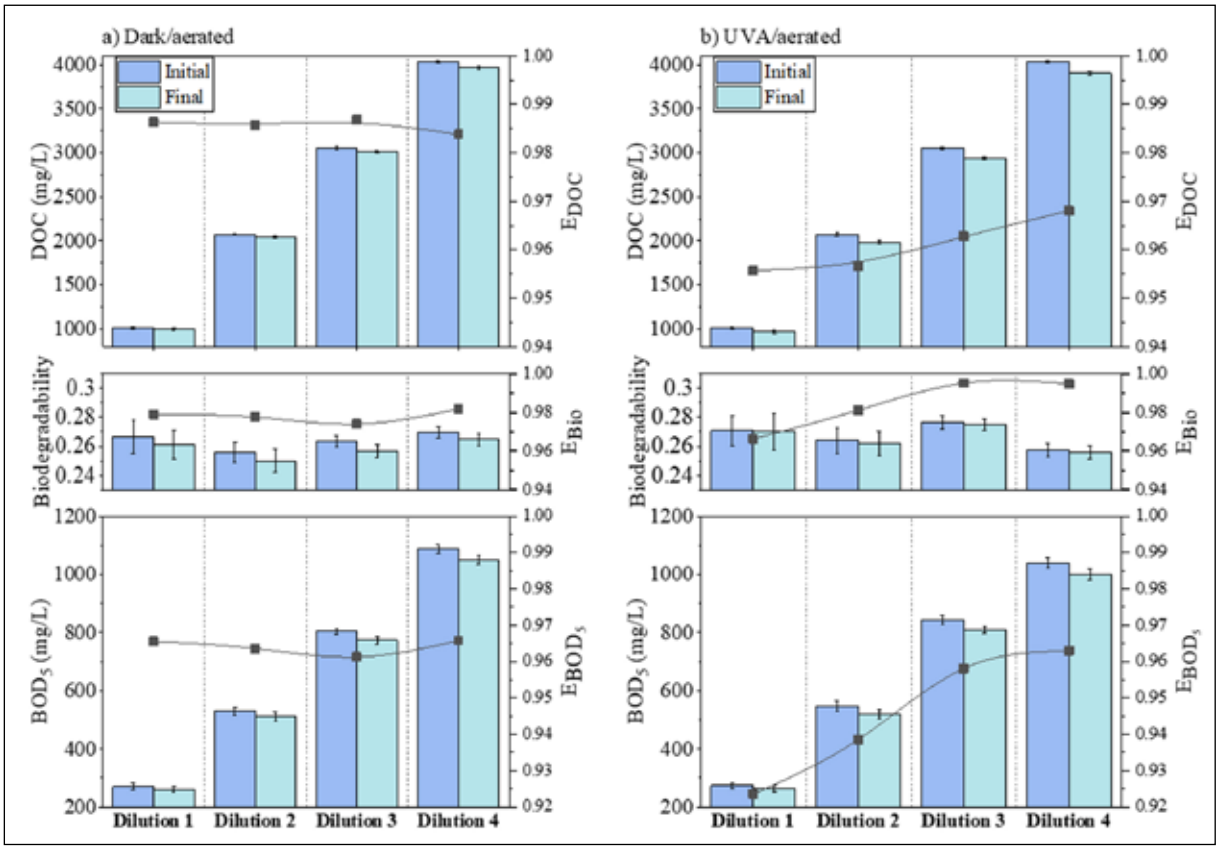

Figure 2. Change in DOC, biodegradability, and BOD5 using different OMW dilutions under dark and UVA aeration.

Referring to Figure 2b, the DOC and BOD_5 reduction (Max. ≈ 4.4% and ≈ 7.6%, respectively) became more than twice under UVA irradiation compared to those in the dark. This enhancement might be accredited to OMW organics' photolytic decomposition or the air stripping of the photolytic decomposition intermediates. It is well proven that organic compounds, most of the time, are more subjected to photolysis (Antonio da Silva et al., 2018). Furthermore, olive oil is well reported to contain natural photosensitizers (Ali et al., 2020), and so expected the wastewater generated from the extraction process. Even increasing DOC_0 is expected to amplify the degradation by providing more photosensitizers; it was found to slightly reduce the E_{DOC} and E_{BOD5}, which could be linked to the light penetration reduction (Nguyen and Juang, 2015). According to García and Hodaifa (García and Hodaifa, 2017), one of the critical barriers for UV penetration in OMW is the turbidity. Regardless of the photolysis capability to affect the organic content in different wastewaters (industrial, municipal, and greywater) (Gulyas et al., 2005), the findings in this study are in agreement with the reported insufficiency of photolysis to promote the pollutants mineralization even at a higher intensity or longer irradiation time (Moreira et al., 2018; Otálvaro-Marín et al., 2019).

4.2. Ozonation and ozone photolysis

ozonation and ozone photolysis have been evaluated at different O_3 doses (37.5-150 mM) and DOC_0 values (83.3 to 333.3 mM). The change in DOC, BOD_5, and biodegradability in this section was represented graphically by 3D surface plots as a function of O_3 dosage and DOC_0 value (shown in the graphs insets), and 2D plots as a function of ozone dosage molar fraction (X_{O3}). Although it is not widely common in AOPs to represent the results as a function of oxidant molar fraction, it was found to be an excellent parameter to explain the findings in this study, as will be seen. A similar, but not exact conclusion was drawn by Buffle et al. (Buffle et al., 2006), who investigated the effect of ozone dose on wastewater treatment from different sources and found the efficiency better described by the ozone molar ratio (O_3 dosage/DOC_0).

4.2.1. Organic content reduction (E_{DOC})

As can be observed from Figure 3 a and b, ozonation and ozone photolysis showed a higher DOC reduction in comparison to the corresponding control experiments (dark/aerated and UVA/aerated) in the previous section, where 10% and 17% DOC reduction by ozonation and UVA ozonation, respectively, been achieved under the best conditions.

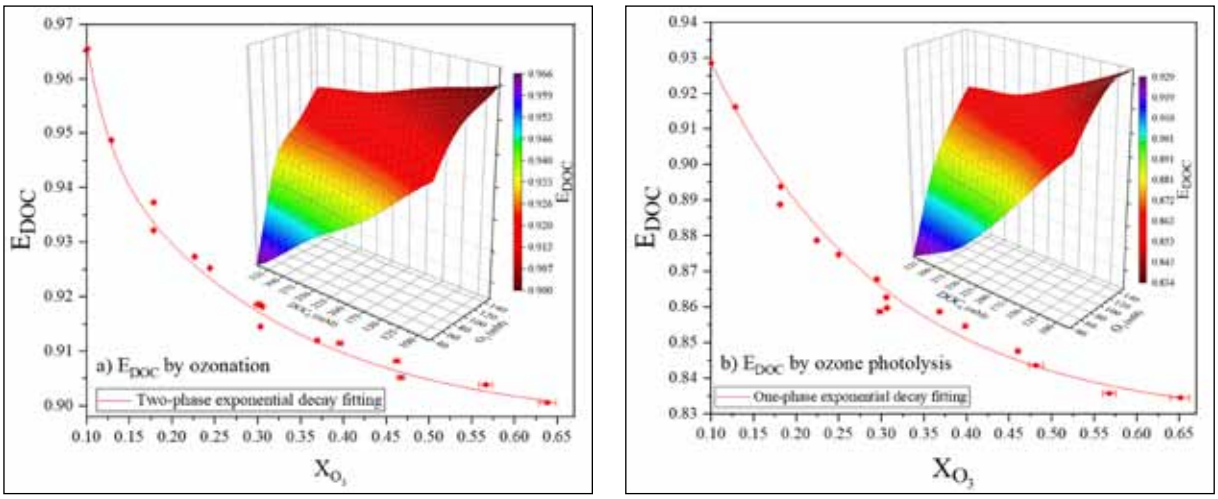

Figure 3. Effect of O_3 dosage molar ratio (X_{O3}) on DOC reduction (E_{DOC}) by; a) ozonation and b) ozone photolysis, the insets show the 3D surface plots of E_{DOC} as a function of O_3 dosage and DOC_0 value.

In general, the efficiency of all AOPs that are combined with aeration is linked to at least three mechanisms: 1) complete mineralization, 2) air stripping of the purgeable intermediates, and 3) air stripping of the unoxidized starting organics (< 1.4% in this study). In ozone-based processes, in particular, the first two mechanisms are dependent on direct ozone oxidation, and $OH^{\bullet}$ generated from ozone decomposition (natural (Equation 1), chemically assisted (Equation 2), and photo-assisted (Equation 3)). Indeed natural ozone decomposition favors alkaline conditions (Oturan and Aaron, 2014), which is not the situation in this study (pH of OMW = 4.52 ± 0.38). However, various constitutes present in OMW may initiate O_3 decomposition, as explained before. In addition to the $OH^{\bullet}$ provided by photo-assisted ozone decomposition (Equation 3), organic photolysis should not be neglected as it showed a significant effect in UVA/aerated control experiments.

As shown in Figure 3 insets, E_{DOC} is reduced by either increasing the O_3 dosage or reducing the DOC_0. According to the literature, there is a general agreement that increasing ozone dose will lead to a higher degree of degradation (Daghrir et al., 2016; Bustos-Terrones et al., 2016; Khataee et al., 2017). However, there are different opinions about the effect of the initial pollutant concentration, where some authors reported an increase in degradation with higher DOC (Bustos-Terrones et al., 2016), and some others reported the opposite (Khataee et al., 2017). Nevertheless, the effect of both parameters (O_3 dose and DOC_0) on E_{DOC} can be interlinked by their ratio represented by ozone dosage molar fraction (X_{O3}). The appropriateness of X_{O3} can be noticed by the low scattering of equal ratio points in Figure 3. As can be observed, the low range X_{O3} showed a higher impact on DOC reduction than the high range. Increasing X_{O3} from 0.1 to 0.3, for instance, reduced E_{DOC} by 5% and

7% in ozonation and ozone photolysis, respectively. On the other hand, doubling X_{O3} from 0.3 to 0.6 did not reduce E_{DOC} by more than 3% in either system. The decay in E_{DOC} by increasing X_{O3} is attributed to OH• scavenging induced by excessive ozone ratio (Equation 7) (Barzegar et al., 2019) or by the inorganic constitutes of OMW that are reported by authors to act as OH• scavengers (such as , and) (Kasprzyk-Hordern et al., 2003; Al-Bsoul et al., 2020). Another hypothesis explained by Li et al. (Li et al., 2015) is related to the degradation process being controlled by the dissolved O_3 concentration in water rather than O_3 fed to the system. Still, the organic content reduction in this study was lower than that reported elsewhere regarding OMW by ozonation ((Lafi et al., 2009; Iboukhoulef et al., 2019) or UV/ozonation (Lafi et al., 2009; Miranda et al., 2001). Variation in DOC reduction effectiveness among studies is mainly associated with the water matrix components, the ozone dosage, and the UV source. Unfortunately, no studies examined OMW degradation by ozone under UVA irradiation up to our knowledge. Previous studies of the cited literature (Lafi et al., 2009; Miranda et al., 2001) have used high energy low wavelength light sources in their work.

The E_{DOC} in ozonation (Figure 3a) and ozone photolysis (Figure 3b) could be modeled by a two-phase exponential decay relationship of X_{O3} (Equation 13). However, the ozone photolysis can be simplified to a one-phase exponential decay with a correlation coefficient (R^2) higher than 0.98. The fitting parameters are shown in Table 3.

$$EDOC = \alpha + \beta_1 e^{-\left(\frac{X_{O3}}{k_1}\right)} + \beta_2 e^{-\left(\frac{X_{O3}}{k_2}\right)} \quad \text{Eq. 13}$$

Where α represents the offset, β_1 and β_2 are phase 1 and 2 amplitudes, and k_1 and k_2 are phase 1 and 2 ratio constants, respectively.

Table 3. Two-phase exponential decay fitting parameters for ozonation and ozone photolysis

Parameters/system	ozonation	ozone photolysis
α	0.896	0.828
β_1	0.934	0.165
k_1	0.025	0.204
β_2	0.082	-
k_2	0.220	-
R^2	0.981	0.987

4.2.2. Change in BOD_5 and biodegradability

In ozonation, E_{BOD5} showed low and high optimum values with respect to ozone dosage and initial organic content. Those values were corresponding to 0.15 and 0.45 X_{O3} (Figure 4a). The change in BOD5 (either reduction or enhancement) describes the net difference between the biodegradable intermediates remain in the water and the biodegradable organics that escape the water, entirely (in the form of CO_2 and H_2O) or partially mineralized (purgeable and volatile intermediates). In the light of DOC reduction, it is possible to assume that the first fraction of organic components in OMW to be attacked by ozone are the easily biodegradable compounds such as amino acids, simple carbohydrates, and fats. For low X_{O3} values (< 0.15), the ozone attack causes higher actual mineralization or more purgeable intermediates than causing biodegradable intermediates accumulation. By increasing X_{O3} above 0.15, refractory organics break down and become more biodegradable but with very low reactivity toward ozone, leading to the accumulation of biodegradable intermediates (Antonio da Silva et al., 2018). Similar findings have been reported by Andreozzi et al. (Andreozzi et al., 2008) when they investigated OMW treatment by ozone. In that study, treating OMW for 1 hr by ozone reduced the phenolic content by 56.8% while the COD reduction did not exceed 8.1%. Despite the presence of low optimum E_{BOD5}, no similar optimum value was noticed for E_{Bio} (Figure 4b) as the E_{DOC} reduction effect dumped it in that X_{O3} range. At $X_{O3} > 0.45$, BOD_5 and biodegradability become inversely proportional to X_{O3}, but to a lesser degree than their rising rate. Several authors referred that to the formation of biorecalcitrant intermediates (Amor et al., 2019).

In UVA ozonation, BOD_5 and biodegradability (Figure 5 a and b) increased by increasing the O_3 to DOC_0 ratio without showing any optimum value. This phenomenon of biodegradability enhancement by ozone photolysis is widely reported in the literature (Yazdanbakhsh et al., 2015; Bar Oz et al., 2018) and attributed to the accumulation of the biodegradable intermediate as explained.

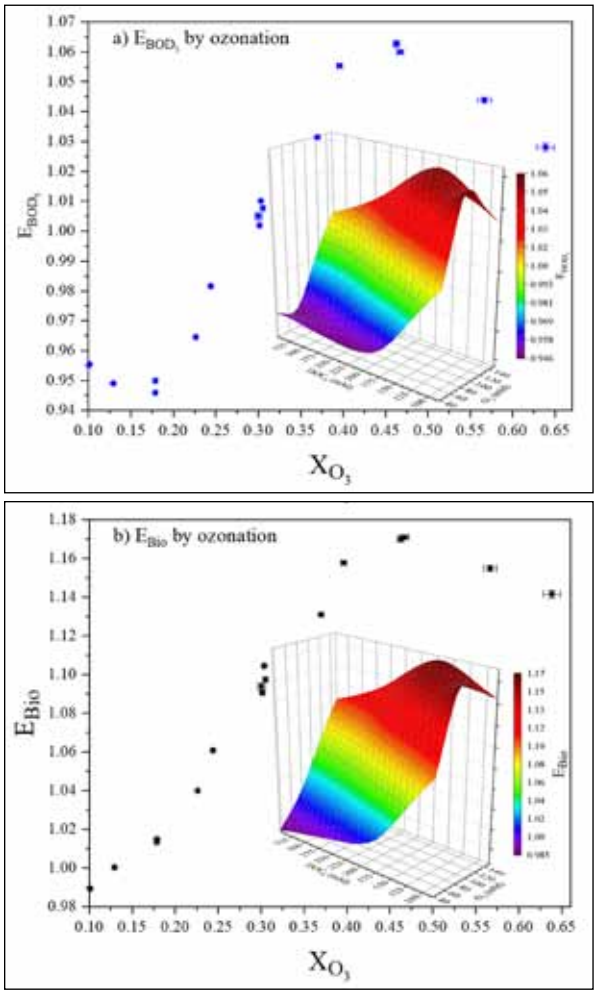

Figure 4. Effect of O_3 dosage molar ratio (X_{O3}) on the change of BOD_5 (E_{BOD5}) and biodegradability (E_{bio}) by ozonation, the insets show the 3D surface plots of E_{BOD5} and E_{bio} as a function of O_3 dosage and DOC_0 value.

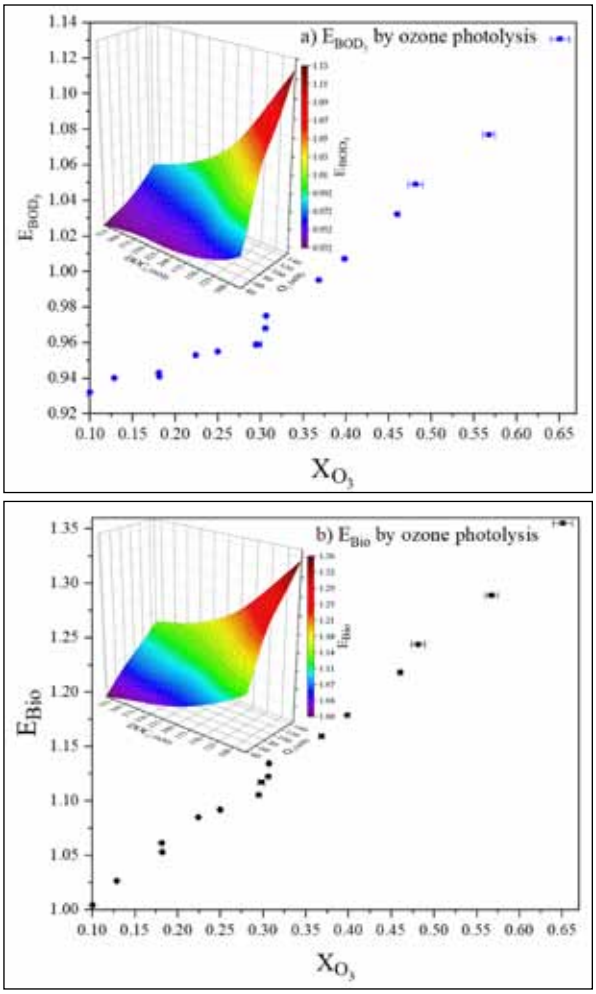

Figure 5. Effect of O_3 dosage molar ratio (X_{O3}) on the change of BOD_5 (E_{BOD5}) and biodegradability (E_{bio}) by ozone photolysis, the insets show the 3D surface plots of E_{BOD5} and E_{bio} as a function of O_3 dosage and DOC_0 value.

4.3. Treatment by H_2O_2/Dark and H_2O_2/UVA

The effect of H_2O_2 dosage and initial organic content on OMW treatment was evaluated in the dark and under UVA irradiation by applying H_2O_2 doses from 66.7 to 266.7 mM on diluted OMW with initial organic content (DOC_0) ranged from 83.3 to 333.3 mM. The change in DOC, BOD_5, and biodegradability was presented by 3D surface plots (insets of the figures in this section) and 2D plots as a function of H_2O_2 dosage molar fraction (X_{H2O2}) and will be discussed based on that. Different from ozonation, it is more common by researchers to represent the efficiency in H_2O_2-based treatment using the ratio of H_2O_2 dose to the organic content measured as DOC (Souza et al., 2014), COD (Quispe-Arpasi et al., 2018), or TOC (Barrera et al., 2012). Similar to ozonation and ozone photolysis, the DOC reduction in H_2O_2/Dark and H_2O_2/UVA increased by increasing the H_2O_2 dosage or reducing DOC_0. As shown in Figure 6 a and b, it was possible to achieve 4.7% and 11.8% DOC reduction by H_2O_2/Dark and H_2O_2/UVA, respectively, under the best conditions. Nevertheless, the efficiency in both systems is low in comparison to the corresponding control experiments. The low capacity of H_2O_2 to cause a significant reduction in organic content is consistent with those published (Nie et al., 2010; Guo et al., 2018; Celeiro et al., 2018; Lamsal et al., 2011), where it is often linked to the low oxidation potential of H_2O_2 (Oturan and Aaron, 2014) and the high energy required to decompose it photolytically (Equation 5) (Dong et al., 2019; Celeiro et al., 2018).

Interestingly, the DOC reduction was paired with a significant change in BOD_5 (Figure 7 a and b), which indicates that DOC reduction in H_2O_2/Dark experiments is due only to the formed purgeable intermediates as no possible source of $OH^{\bullet}$ generation during the dark experiments is expected. In addition to the purgeable intermediate formation hypothesis, the DOC reduction in H_2O_2/UVA treatment is probably related to the photolysis of either the organics initially present in OMW or the generated oxidation intermediates and, to a lesser extent, to the $OH^{\bullet}$ generated from H_2O_2 photodecomposition (Equation 5). Despite that H_2O_2 decomposition requires UV irradiation in the range of 200 to 300 nm (Equation 5) (Oturan and Aaron, 2014), based on the absorption coefficient values in Lachheb et al. work (Lachheb et al., 2017), H_2O_2 can absorb up to 0.1 of the lamp emissions in the current study, which may result in a small amount of $OH^{\bullet}$ to be produced.

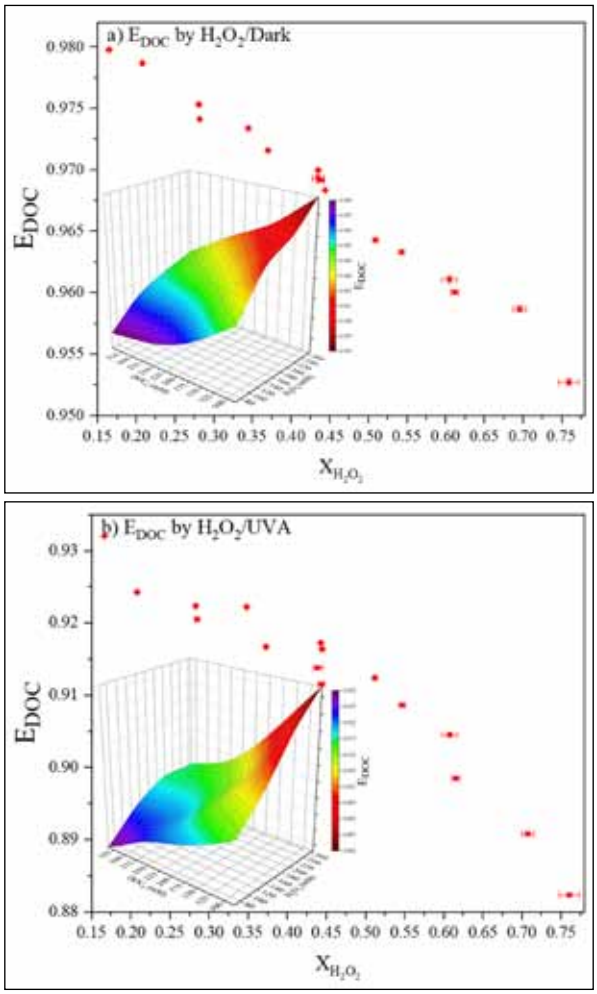

Figure 6. Effect of H_2O_2 dosage molar ratio (X_{H2O2}) on DOC reduction E_{DOC}) by; a) H_2O_2/Dark and b) H_2O_2/UVA, the insets show the 3D surface plots of E_{DOC} as a function of H_2O_2 dosage and DOC_0 value.

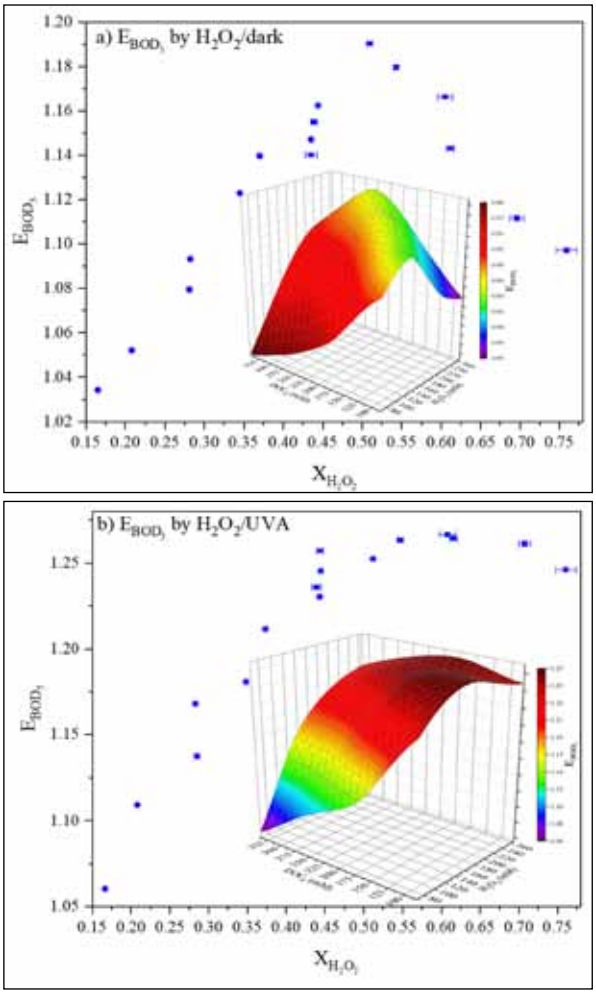

Figure 7. Effect of H_2O_2 dosage molar ratio (X_{H2O2}) on the change of BOD_5 (E_{BOD5}) by; a) H_2O_2/Dark and b) H_2O_2/UVA, the insets show the 3D surface plots of E_{BOD5} as a function of H_2O_2 dosage and DOC_0 value.

In H_2O_2/Dark, E_{BOD5} (Figure 7a) and E_{bio} (Figure 8a) showed an upper optimum value at 0.51 X_{H2O2} (1.19 and 1.23, $E_{BOD5,}$ and E_{bio}, respectively), which after this decreased dramatically. On the other hand, during H_2O_2/UVA treatment, E_{BOD5} (Figure 7b) and E_{bio} (Figure 8b) kept increasing with X_{H2O2} to 0.6 (at which E_{BOD5} = 1.27 and E_{bio} = 1.42), above 0.6 X_{H2O2}, E_{BOD5} slightly decreased while the E_{bio} remained unchanged. The improvement in BOD_5 and biodegradability is due to the accumulation of the intermediates and their toxicity (Bar Oz et al., 2018; Khoufi et al., 2009), as explained before in ozonation.

4.4. Peroxonation and UVA/peroxonation

The peroxonation and UVA/peroxonation treatment was carried out by applying different combinations of H_2O_2 and O_3 dosages (83.3 to 333.3 mM and 37.5-150 mM, respectively) on diluted OMW with different initial organic content (83.3 to 333.3 mM). Those combinations produced H_2O_2: O_3 ratio of 0.44 - 7.1, H_2O_2: DOC_0 ratio of 0.19 - 3.18, and O_3: DOC_0 ratio of 0.11 - 1.87, which include even a wider range of the examined ratios in the literature (Miklos et al., 2018; Oturan and Aaron, 2014; Li et al., 2015; Englehardt et al., 2013). The E_{DOC}, E_{BOD5}, and E_{bio} results were depicted against ozone and hydrogen peroxide molar fraction on 3D surface plots with XY projection to visualize all parameters' effect. It is noteworthy that the initial dissolved organic carbon molar fraction is implicitly represented in the plots by the complementary of X_{O3} plus X_{H2O2} to unity.

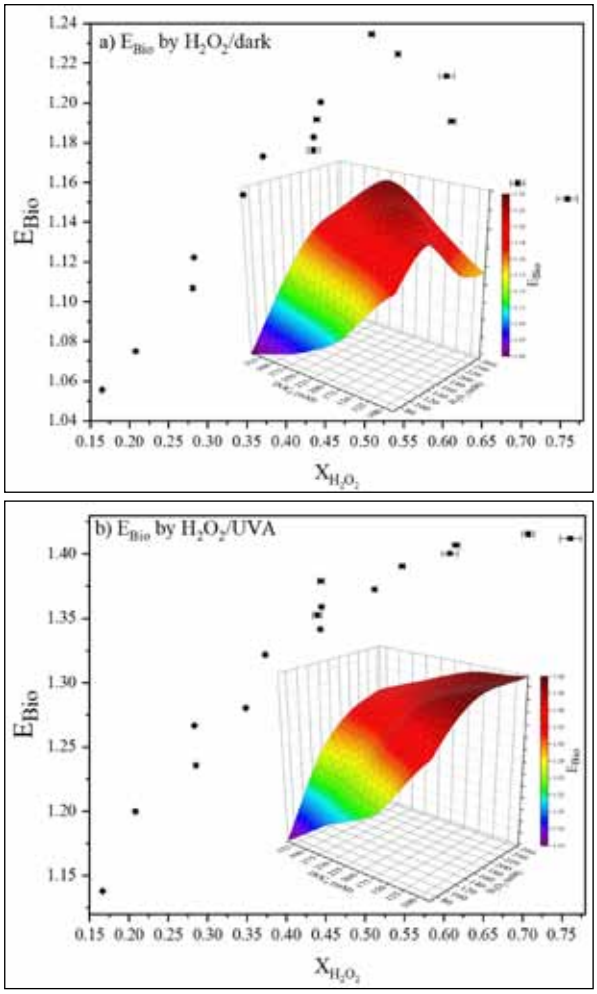

Figure 8. Effect of H_2O_2 dosage molar ratio (X_{H2O2}) on the change of biodegradability (E_{bio}) by; a) H_2O_2/Dark and b) H_2O_2/UVA, the insets show the 3D surface plots of E_{bio} as a function of H_2O_2 dosage and DOC_0 value.

4.4.1. Organic content reduction (E_{DOC})

As can be seen in Figure 9, the peroxonation and UVA peroxonation are more effective in DOC reduction than the treatment by ozone or hydrogen peroxide alone with or without UVA irradiation. The enhancement is mainly attributed to ozone decomposition by H_2O_2 (Equation 4) (Hassanshahi and Karimi-Jashni, 2018; Bethi et al., 2016; Wang and Xu, 2012). However, one shall keep in mind that the DOC reduction is caused by the complete mineralization and transforming the OMW organics into purgeable intermediates. The complete mineralization and intermediates formation involves synergistic and competitive pathways that can enhance or inhibit the DOC reduction efficiency. The main two competitive pathways include the $OH^{\cdot}$ scavenging by H_2O_2 (Equation 6) (Englehardt et al., 2013; Kurniawan and Lo, 2009) or O_3 (Equation 7) (Barzegar et al., 2019) and the interaction of oxidants with organic matters (Englehardt et al., 2013).

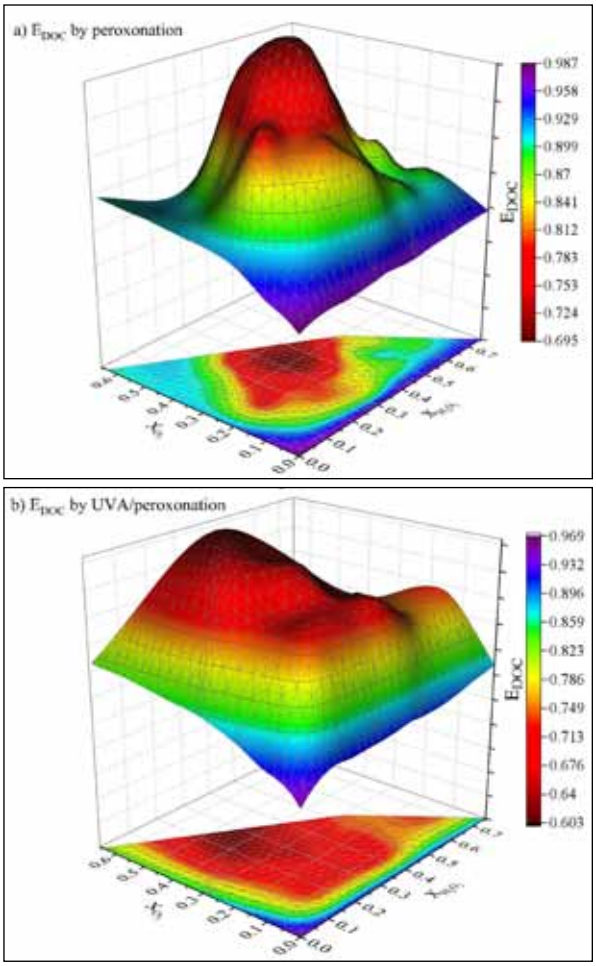

Figure 9. Effect of H_2O_2 and O_3 molar ratios (X_{H2O2} and X_{O3}) and the initial dissolved organic carbon (DOC_0) concentration on DOC reduction (E_{DOC}) by; a) peroxonation, b) UVA/peroxonation.

Theoretically, the optimum H_2O_2: O_3 molar ratio to generate OH• is 1:2 (Englehardt et al., 2013). However, several different ratios were obtained in this study. In peroxonation, the highest DOC reduction (≈ 30%) was between 0.28 - 0.4 X_{H2O2} and 0.25 - 0.4 X_{O3}, which corresponds to 0.7 – 1.6 H_2O_2: O_3 molar ratio. On the other hand, the DOC reduction in UVA/peroxonation was higher than peroxonation alone, where ≈ 40% DOC reduction was achieved with a shift in the preferred X_{H2O2} and X_{O3} range to 0.18 - 0.32 and 0.33 – 0.5 (corresponds to 0.22 – 0.97 H_2O_2: O_3 molar ratio), respectively. The enhancement in UVA/peroxonation is expected because of the organics photolysis and the OH• generated from H_2O_2 and O_3 photodecomposition (Equation 3 and Equation 5). Nevertheless, in UVA/peroxonation, it was possible to achieve more than 35% DOC reduction in all experiments regardless of the ozone or hydrogen peroxide molar ratio.

4.4.2. Change in BOD_5 and biodegradability

The OMW BOD_5 value for peroxonation treatment (Figure 10a) showed a substantial increase relative to treatment with ozone or hydrogen peroxide separately, where approximately more than 1.4% E_{BOD5} was obtained for the whole tested range except for those with X_{H2O2} > 0.5. Moreover, the maximum increase in the biodegradable fraction (E_{BOD5} values > 2) was achieved in two distinct intervals of ozone and hydrogen peroxide molar ratios; 1) between 0.08 - 0.2 X_{H2O2} and 0.1 - 0.4 X_{O3}, and 2) between 0.08 - 0.4 X_{H2O2} and 0.1 - 0.2 X_{O3}. On the one hand, E_{bio} in peroxonation (Figure 10b) increased over the whole range with a maximum value of 2.54. Nevertheless, it was possible to achieve about 100% enhancement in biodegradability for all X_{H2O2} and X_{O3} between 0.1- 0.4. As the optimal O_3 and H_2O_2 range for biodegradability enhancement are completely different from the optimal range for DOC reduction, it can be inferred that BOD_5 enhancement is due to direct oxidation by H_2O_2 and O_3, which did not contribute to mineralization or the formation of purgeable intermediates but rather caused accumulation of biodegradable intermediates.

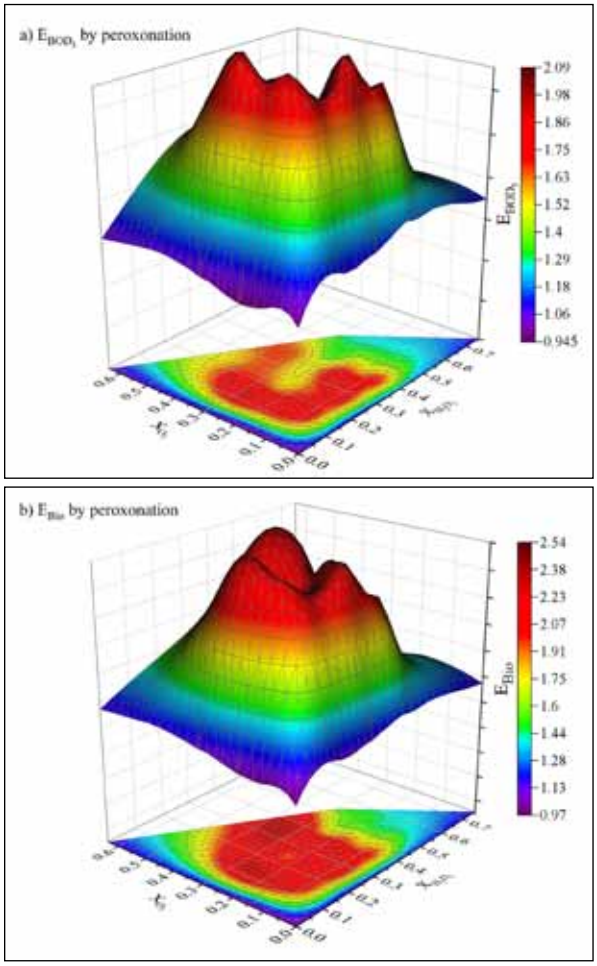

Figure 10. Effect of H_2O_2 and O_3 molar ratios (X_{H2O2} and X_{O3}) and the initial dissolved organic carbon (DOC_0) concentration during peroxonation on; a) the change in BOD_5 (E_{BOD5}) and b) the change in biodegradability (E_{bio}).

On the other hand, UVA/peroxonation was less efficient in improving OMW biodegradable content (Figure 11a) or improving the biodegradability (Figure 11b) in comparison to peroxonation, where it showed a maximum of 1.38 and 2.12 E_{BOD5} and E_{bio}, respectively. The lower efficiency implies that UVA/peroxonation has a higher affinity to attacks the biodegradable compounds. As can be seen from the same figure (Figure 11a), improving E_{BOD5} is favoring X_{H2O2} > 0.2 and X_{O3}< 0.5, which is the same range for biodegradability enhancement (Figure 11b). The use of very high doses of ozone (X_{O3} > 0.5) has a detrimental effect on OMW's biodegradable fraction. Even though ozone removes refractory phenolic compounds, thus improving E_{BOD5} by

decomposing the polyphenolic chain into smaller molecules, it may also generate numerous intermediates, which may disrupt the bacterial population within OMW (Bar Oz et al., 2018; Khoufi et al., 2009). It is worth to mention that even with the high biodegradability improvement by peroxonation and UVA/peroxonation, the final OMW biodegradability in any system never exceeded 0.67 (measured by BOD_5/TOC).

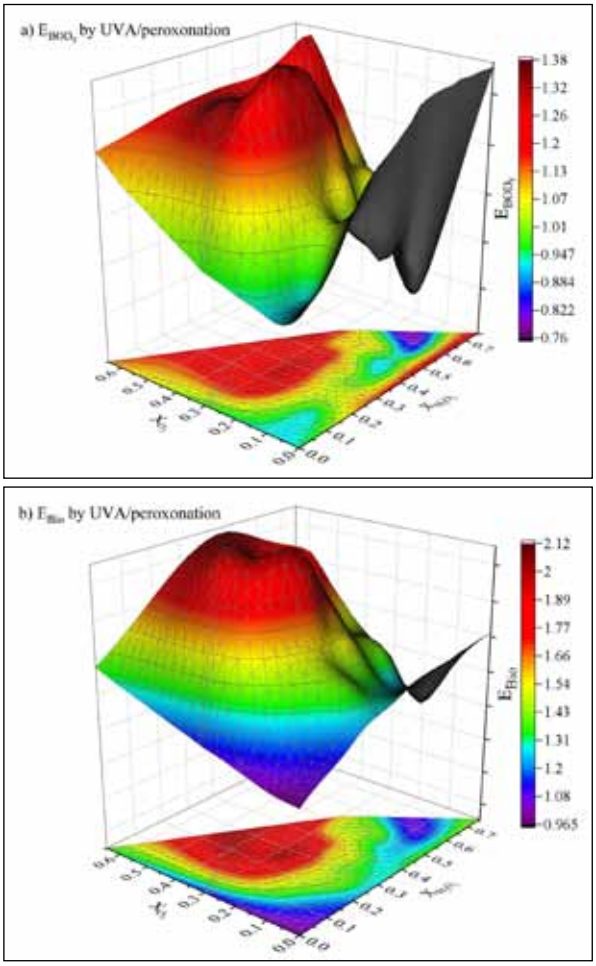

Figure 11. Effect of H_2O_2 and O_3 molar ratios (X_{H2O2} and X_{O3}) and the initial dissolved organic carbon (DOC_0) concentration during UVA/peroxonation on; a) the change in BOD_5 (E_{BOD5}) and b) the change in biodegradability (E_{bio}).

5. Conclusions

Photolysis, ozonation (O_3/dark), ozone photolysis (O_3/UVA), H_2O_2-peroxidation (H_2O_2/Dark), H_2O_2 photo-peroxidation (H_2O_2/UVA), peroxonation (H_2O_2/O_3/dark), and photo-peroxonation (H_2O_2/O_3/UVA) were employed for OMW treatment. Using hydrogen peroxide as standalone or in combination with UVA irradiation showed to be infeasible for OMW DOC reduction. However, it could be a good choice for biodegradability enhancement, particularly under UVA irradiation. In ozonation and UVA ozonation, increasing the ozone dosage or reducing the initial OMW organic content enhanced the treatment efficiency. UVA/peroxonation showed the highest DOC reduction, while peroxonation showed the highest improvement in biodegradability. The combination of H_2O_2, O_3, and UVA has a synergetic and competitive effect on OMW organic content reduction and biodegradability change. However, the ratios of H_2O_2, O_3, and DOC_0 have numerous effects on OMW treatment efficiency. The appropriate ratio estimation is essential to wither apply the studied processes as an alternative or complementary treatment. This study also provides clear and valuable information regarding applying the tested systems as a pre or post-treatment when combined with other technologies according to the specific needs. For example, UVA peroxonation has high efficiency in reducing the organic content, making it more suitable as a polishing step for the biological treatment effluent. On the other hand, peroxonation significantly enhanced OMW biodegradability, making it a right pretreatment choice to improve biological wastewater treatment.

It was impossible to run this number of experiments under real sun conditions during the same milling campaign period in this stage of the project. Further experiments will be carried out in the second stage of the project to optimize OMW mineralization and biodegradability and to confirm the practical feasibility of tested systems under solar irradiation.

References

Ahmed, P. M., Fernández, P.M., de Figueroa, L.I.C., Pajot, H. F. (2019). Exploitation Alternatives of Olive Mill Wastewater: Production of Value-Added Compounds Useful for Industry and Agriculture. Biofuel Research Journal 6: 980-94.

Akdemir, E. O., and Ozer, A. (2009). Investigation of Two Ultrafiltration Membranes for Treatment of Olive Oil Mill Wastewater. Desalination 249: 660-66.

Al-Bsoul, A., Al-Shannag, M., Tawalbeh, M., Al-Taani, A. A., Lafi, W. K., Al-Othman, A., Alsheyab, M. (2020). Optimal Conditions for Olive Mill Wastewater Treatment Using Ultrasound and Advanced Oxidation Processes. Science of the Total Environmen 700: 134576.

Ali, H., Iqbal, M. A., Atta, B. M., Ullah, R., Khan, M. B. (2020). Phenolic Profile and Thermal Stability of Monovarietal Extra Virgin Olive Oils Based on Synchronous Fluorescence Spectroscopy. Journal of Fluorescence 30: 939-47.

Alrousan, D. M. A. and Dunlop, P. S. M. (2020). Evaluation of Ozone-Based Oxidation and Solar Advanced Oxidation Treatment of Greywater. Journal of Environmental Chemical Engineering 8(5) 104309. https://doi.org/10.1016/j.jece.2020.104309

Amor, C., Marchão, L., Lucas, M.S., Peres, J.A. (2019). Application of Advanced Oxidation Processes for the Treatment of Recalcitrant Agro-Industrial Wastewater: A Review. Water 11(2), 205; https://doi.org/10.3390/w11020205

Andreozzi, R., Canterino, M., Somma, I. Di., Giudice, R. Lo., Marotta, R., Pinto, G., Pollio, A. (2008). Effect of Combined Physico-Chemical Processes on the Phytotoxicity of Olive Mill Wastewaters. Water Research 42(6-7): 1684-1692. https://doi.org/10.1016/j.watres.2007.10.018.

da Silva, D.A., Cavalcante, R. P., Cunha, R. F., Junior, A. M., de Oliveira, S. C. (2018). Optimization of Nimesulide Oxidation Via a Uv-Abc/H2o2 Treatment Process: Degradation Products, Ecotoxicological Effects, and Their Dependence on the Water Matrix. Chemosphere 207: 457-68.

Azbar, N., Bayram, A., Filibeli, A., Muezzinoglu, A., Sengul, F., Ozer, A. (2004). A Review of Waste Management Options in Olive Oil Production. Critical Reviews in Environmental Science and Technology 34: 209-47.

Azzam, M.O. J., Al-Gharabli, S.I., Al-Harahsheh, M.S. (2013). Olive Mills Wastewater Treatment Using Local Natural Jordanian Clay. Desalination and Water Treatment 53: 627-36.

Oz, Y. B., Mamane, H., Menashe, O., Cohen-Yaniv, V., Kumar, R., Kruh, L. I., Kurzbaum, E. (2018). Treatment of Olive Mill Wastewater Using Ozonation Followed by an Encapsulated Acclimated Biomass. Journal of Environmental Chemical Engineering 6: 5014-23.

Barrera, M., Mehrvar, M., Gilbride, K.A., McCarthy, L. H., Laursen, A. E., Bostan, V., Pushchak, R. (2012). Photolytic Treatment of Organic Constituents and Bacterial Pathogens in Secondary Effluent of Synthetic Slaughterhouse Wastewater. Chemical Engineering Research and Design 90: 1335-50.

Barzegar, G., Wu, J., Ghanbari, F. (2019). Enhanced Treatment of Greywater Using Electrocoagulation/Ozonation: Investigation of Process Parameters. Process Safety and Environmental Protection 121: 125-32.

Bertin, L., Berselli, S., Fava, F., Petrangeli-Papini, M., Marchetti, L. (2004). Anaerobic Digestion of Olive Mill Wastewaters in Biofilm Reactors Packed with Granular Activated Carbon and "Manville" Silica Beads. Water Research 38: 3167-78.

Bethi, B., Sonawane, S.H., Bhanvase, B. A., Gumfekar, S. P. (2016). Nanomaterials-Based Advanced Oxidation Processes for Wastewater Treatment: A Review. Chemical Engineering and Processing - Process Intensification 109: 178-89.

Marc-Olivier, B., Jochen, S., Sébastien, M., Martin, J., von Gunten, U.. (2006). Ozonation and Advanced Oxidation of Wastewater: Effect of O3 Dose, pH, DOM and HO• -Scavengers on Ozone Decomposition and HO• Generation. Ozone: Science and Engineering 28: 247-59.

Bustos-Terrones, Y., Rangel-Peraza, J. G., Sanhouse, A., Bandala, E. R., Torres, L. G. (2016). Degradation of Organic Matter from Wastewater Using Advanced Primary Treatment by O3 and O3/UV in a Pilot Plant. Physics and Chemistry of the Earth, Parts A/B/C, 91: 61-67.

Celeiro, M., Hackbarth, F. V., de Souza, S. M. A. G. U., Llompart, M., Vilar, V. J. P. (2018). Assessment of Advanced Oxidation Processes for the Degradation of Three UV Filters from Swimming Pool Water. Journal of Photochemistry and Photobiology A: Chemistry 351: 95-107.

Daghrir, R., Gherrou, A., Noel, I., Seyhi, B. (2016). Hybrid Process Combining Electrocoagulation, Electroreduction, and Ozonation Processes for the Treatment of Grey Wastewater in Batch Mode. Journal of Environmental Engineering 142: 04016008.

Dai, Q., Chen, L., Chen, W., Chen, J. (2015). Degradation and Kinetics of Phenoxyacetic Acid in Aqueous Solution by Ozonation. Separation and Purification Technology 142: 287-92. https://doi.org/10.1016/j.seppur.2014.12.045.

Dong, W., Sun, S-P., Yang, X., Zhou, K., Li, Y., Wang, X., Wu, Z., Wu, W. D., Chen, X D. (2019). Enhanced Emerging Pharmaceuticals Removal in Wastewater after Biotreatment by a Low-Pressure UVA/Feiii-EDDS/H2O2 Process under Neutral pH Conditions. Chemical Engineering Journal 366: 539-49.

Ebrahimi, Izadyar, Mazeyar Parvinzadeh Gashti, Mojtaba Sarafpour. (2018). Photocatalytic Discoloration of Denim Using Advanced Oxidation Process with H2O2/UV. Journal of Photochemistry and Photobiology A: Chemistry 360: 278-88.

El-Abbassi, A., A. Hafidi, M. Khayet, M. C. García-Payo. (2013). Integrated Direct Contact Membrane Distillation for Olive Mill Wastewater Treatment. Desalination 323: 31-38.

Elmolla, Emad S., Malay Chaudhuri. (2010). Photocatalytic Degradation of Amoxicillin, Ampicillin and Cloxacillin Antibiotics in Aqueous Solution Using UV/TiO2 and UV/H2O2/TiO2 Photocatalysis. Desalination 252: 46-52.

Englehardt, J. D., T. Wu, G. Tchobanoglous. (2013). Urban Net-Zero Water Treatment and Mineralization: Experiments, Modeling and Design Water Research 47: 4680-91.

Erses Yay, A. Suna, H. Volkan Oral, Turgut T. Onay, Orhan Yenigün. (2012). A Study on Olive Oil Mill Wastewater Management in Turkey: A Questionnaire and Experimental Approach, Resources. Conservation and Recycling 60: 64-71.

Farzadkia, Mahdi, Yousef Dadban Shahamat, Simin Nasseri, Amir Hossein Mahvi, Mitra Gholami, Ali Shahryari. (2014). Catalytic Ozonation of Phenolic Wastewater: Identification and Toxicity of Intermediates. Journal of Engineering 2014: 1-10.

García, Cristina Agabo, Gassan Hodaifa. (2017). Real Olive Oil Mill Wastewater Treatment by Photo-Fenton System Using Artificial Ultraviolet Light Lamps. Journal of Cleaner Production 162: 743-53.

Gardoni, D., A. Vailati, R. Canziani. (2012). Decay of Ozone in Water: A Review. Ozone: Science & Engineering 34: 233-42.

Gulyas, H., H. B. Jain, A. L. Susanto, M. Malekpur, K. Harasiuk, I. Krawczyk, P. Choromanski, M. Furmanska. (2005). Solar Photocatalytic Oxidation of Pretreated Wastewaters: Laboratory Scale Generation of Design Data for Technical-Scale Double-Skin Sheet Reactors. Environmental Technology 26: 501-14.

Guo, K., Z. Wu, S. Yan, B. Yao, W. Song, Z. Hua, X. Zhang, X. Kong, X. Li, J. Fang. (2018). Comparison of the UV/Chlorine and UV/H2O2 Processes in the Degradation of Ppcps in Simulated Drinking Water and Wastewater: Kinetics, Radical Mechanism and Energy Requirements. Water Research 147: 184-94.

Hassanshahi, N., and A. Karimi-Jashni. (2018). Comparison of Photo-Fenton, O3/H2O2/UV and Photocatalytic Processes for the Treatment of Gray Water. Ecotoxicology and Environmental Safety 161: 683-90.

Hodaifa, G., Gallardo, P. A. R., García, C. A., Kowalska, M., Seyedsalehi, M. (2019). Chemical Oxidation Methods for Treatment of Real Industrial Olive Oil Mill Wastewater. Journal of the Taiwan Institute of Chemical Engineers 97: 247-54.

Huang, W., Bianco, A., Brigante, M., Mailhot, G. (2018). Uva-Uvb Activation of Hydrogen Peroxide and Persulfate for Advanced Oxidation Processes: Efficiency, Mechanism and Effect of Various Water Constituents. Journal of Hazardous Materials 347: 279-87.

Iboukhoulef, H., Douani, R., Amrane, A., Chaouchi, A., Elias, A. (2019). Heterogeneous Fenton Like Degradation of Olive Mill Wastewater Using Ozone in the Presence of BiFeO3 Photocatalyst. Journal of Photochemistry and Photobiology A: Chemistry, 383. Elsevier, 2019, 383, □10.1016/j.jphotochem.2019.112012□. □hal-02359982□.

Ioannou-Ttofa, L., Michael-Kordatou, I., Fattas, S. C., Eusebio, A., Ribeiro, P., M. Rusan, A. R. Amer, S. Zuraiqi, M. Waismand, C. Linder, Z. Wiesman, J. Gilron, D. Fatta-Kassinos. (2017). Treatment Efficiency and Economic Feasibility of Biological Oxidation, Membrane Filtration and Separation Processes, and Advanced Oxidation for the Purification and Valorization of Olive Mill Wastewater. Water Research 114: 1-13.

Kasprzyk-Hordern, B., Ziółek, M., Nawrocki, J. (2003). Catalytic Ozonation and Methods of Enhancing Molecular Ozone Reactions in Water Treatment. Applied Catalysis B: Environmental 46: 639-69.

Khataee, A., Kıranşan, M, Karaca, S., Sheydaei, M. (2017). Photocatalytic Ozonation of Metronidazole by Synthesized Zinc Oxide Nanoparticles Immobilized on Montmorillonite. Journal of the Taiwan Institute of Chemical Engineers 74: 196-204.

Khoufi, S., Aloui, F., Sayadi, S. (2009). Pilot Scale Hybrid Process for Olive Mill Wastewater Treatment and Reuse, Chemical Engineering and Processing: Process Intensification 48: 643-50.

Kurniawan, T. A., and Lo, W. H. (2009). Removal of Refractory Compounds from Stabilized Landfill Leachate Using an Integrated H2O2 Oxidation and Granular Activated Carbon (Gac) Adsorption Treatment. Water Research 43: 4079-91.

Lachheb, H., Guillard, C., Lassoued, H., Haddaji, M., Rajah, M., Houas, A. (2017). Photochemical Oxidation of Styrene in Acetonitrile Solution in Presence of H2O2, TiO2 /H2O2 and Zno/H2o2. Journal of Photochemistry and Photobiology A: Chemistry 346: 462-69.

Lafi, W. K., Shannak, B., Al-Shannag, M., Al-Anber, Z., Al-Hasan, M. (2009). Treatment of Olive Mill Wastewater by Combined Advanced Oxidation and Biodegradation. Separation and Purification Technology 70: 141-46.

Lamsal, R., Walsh, M. E., Gagnon, G. A. (2011). Comparison of Advanced Oxidation Processes for the Removal of Natural Organic Matter. Water Researc, 45: 3263-9.

Li, G.; He, J.; Wang, D.; Meng, P.; Zeng, M. (2015). Optimization and Interpretation of O3 and O3/H2O2 Oxidation Processes to Pretreat Hydrocortisone Pharmaceutical Wastewater. Environmental Technology 36: 1026-34.

Michael-Kordatou, I., Karaolia, P. Fatta-Kassinos, D. (2018). The Role of Operating Parameters and Oxidative Damage Mechanisms of Advanced Chemical Oxidation Processes in the Combat against Antibiotic-Resistant Bacteria and Resistance Genes Present in Urban Wastewater. Water Research 129: 208-30.

Miklos, D. B., Remy, C., Jekel, M., Linden, K. G., Drewes, J. E., Hubner, U. (2018). Evaluation of Advanced Oxidation Processes for Water and Wastewater Treatment - a Critical Review. Water Research 139: 118-31.

Miranda, M.A., Amat, A.M., Arques, A. (2001). Abatement of the Major Contaminants Present in Olive Oil Industry Wastewaters by Different Oxidation Methods: Ozone and/or Uv Radiation Versus Solar Light. Water Science and Technology 44: 325-30.

Moreira, N. F. F., Narciso-da-Rocha, C., Polo-Lopez, M. I., Pastrana-Martinez, L. M., Faria, J. L., Manaia, C. M., Fernandez-Ibanez, P., Nunes, O. C., Silva, A. M. T. (2018). Solar Treatment (H2o2, TiO2-P25 and Go-TiO2 Photocatalysis, Photo-Fenton) of Organic Micropollutants, Human Pathogen Indicators, Antibiotic Resistant Bacteria and Related Genes in Urban Wastewater. Water Research 135: 195-206.

Nguyen, A. T., and Juang, R. S. (2015). Photocatalytic Degradation of P-Chlorophenol by Hybrid H2O2 and TiO2 in Aqueous Suspensions under UV Irradiation. Journal of Environmental Management 147: 271-7.

Niazmand, R., Jahani, M., Sabbagh, F., Rezania, S. (2020). Optimization of Electrocoagulation Conditions for the Purification of Table Olive Debittering Wastewater Using Response Surface Methodology. Water 12. 12(6), 1687; https://doi.org/10.3390/w12061687.

Nie, Y., Hu, C. Zhou, L., Qu, J., Wei, Q., Wang, D. (2010). Degradation Characteristics of Humic Acid over Iron Oxides/Fe0 Core-Shell Nanoparticles with UVA/H2O2. Journal of Hazardous Materials 173: 474-9.

Ochando-Pulido, J. M., Pimentel-Moral, S., Verardo, V., Martinez-Ferez, A. (2017). A Focus on Advanced Physico-Chemical Processes for Olive Mill Wastewater Treatment. Separation and Purification Technology 179: 161-74.

Otálvaro-Marín, H. L., González-Caicedo, F., Arce-Sarria, A., Mueses, M. A., Crittenden, J. C., Machuca-Martinez, F. (2019). Scaling-up a Heterogeneoush2o2/Tio2/Solar-Radiation System Using the Damköhler Number. Chemical Engineering Journal 364: 244-56. https://doi.org/10.1016/j.cej.2019.01.141.

Oturan, M. A., and Aaron, J-J. (2014). Advanced Oxidation Processes in Water/Wastewater Treatment: Principles and Applications. A Review. Critical Reviews in Environmental Science and Technology 44(23): 2577-641. DOI:10.1080/10643389.2013.829765

Pedrero, F., Grattan, S. R., Ben-Gal, A., Vivaldi, G A. (2020). Opportunities for Expanding the Use of Wastewaters for Irrigation of Olives. Agricultural Water Management 241. https://doi.org/10.1016/j.agwat.2020.106333.

Pérez-Lucas, G., Aliste, M., Vela, N., Garrido, I., Fenoll, J., Navarro, S. (2020). Decline of Fluroxypyr and Triclopyr Residues from Pure, Drinking and Leaching Water by Photo-Assisted Peroxonation. Process Safety and Environmental Protection 137: 358-65.

Quispe-Arpasi, D., Souza, R. de, Stablein, M., Liu, Z., Duan, N., Lu, H., Zhang, Y., Alessandra, A. L. de O., Ribeiro, R., Tommaso, G. (2018). Anaerobic and Photocatalytic Treatments of Post-Hydrothermal Liquefaction Wastewater Using H2o2, Bioresource Technology Reports, 3: 247-55. https://doi.org/10.1016/j.biteb.2018.08.003.

Saez, J. A., M. D. Perez-Murcia, A. Vico, M. R. Martinez-Gallardo, F. J. Andreu-Rodriguez, M. J. Lopez, M. A. Bustamante, J. C. Sanchez-Hernandez, J. Moreno, R. Moral. (2020). Olive Mill Wastewater-Evaporation Ponds Long Term Stored: Integrated Assessment of in Situ Bioremediation Strategies Based on Composting and Vermicomposting. Journal of Hazardous Materials 402: 123481.

Souza, B. S., Dantas, R. F., Cruz, A., Sans, C., Esplugas, S., Dezotti, M. (2014). Photochemical Oxidation of Municipal Secondary Effluents at Low H2O2 Dosage: Study of Hydroxyl Radical Scavenging and Process Performance. Chemical Engineering Journal 237: 268-76. https://doi.org/10.1016/j.cej.2013.10.025

Uğurlu, M., Yilmaz, S. İ., Vaızoğuiiar, A. (2019). Removal of Color and Cod from Olive Wastewater by Using Three-Phase Three-Dimensional (3d) Electrode Reactor, Materials Today: Proceedings, 18: 1986-95.

Wang, J. L., and Xu, L. J. (2012). Advanced Oxidation Processes for Wastewater Treatment: Formation of Hydroxyl Radical and Application. Critical Reviews in Environmental Science and Technology 42: 251-325. DOI:10.1080/10643389.2010.507698

Wert, E. C., Rosario-Ortiz, F. L., Snyder, S. A. (2009). Effect of Ozone Exposure on the Oxidation of Trace Organic Contaminants in Wastewater. Water Research 43: 1005-14.

Yazdanbakhsh, A., Mehdipour, F., Eslami, A., Maleksari, H. S., Ghanbari, F. (2015). The Combination of Coagulation, Acid Cracking and Fenton-Like Processes for Olive Oil Mill Wastewater Treatment: Phytotoxicity Reduction and Biodegradability Augmentation, Water Science and Technology, 71(7): 1097-105.

Yuval, A., Eran, F., Janin, W., Oliver, O., Yael, D. (2017). Photodegradation of Micropollutants Using V-UV/UV-C Processes; Triclosan as a Model Compound, Science of the Total Environment, 601-602: 397-404.

JJEES

JJEES (2021) 12 (2): 134-144
ISSN 1995-6681

Jordan Journal of Earth and Environmental Sciences

Analysis of socio-economic and housing characteristics In some selected slum area in Lagos State Metropolis, Nigeria using Geographical Information System

Oluwaseun Okimiji*[1], Oludare Adedeji[1],
Olusegun Oguntoke[1], Olufunke Shittu[2], Moses Aborisade[3], Obioma Ezennia[1]

[1]Department of Environmental Management and Toxicology, Federal University of Agriculture, Nigeria.
[2]Department of Microbiology, Federal University of Agriculture, Nigeria
[3]School of Environmental Science and Engineering, Tianjin University, China

Received 2 April 2019; Accepted 29 October 2020

Abstract

This study aims to evaluate the socio-economic and housing characteristic of residents in the slums of Lagos Metropolis. A multi-stage sampling method was used, whereby systematic and simple random sampling procedures were adopted. Data was collected using a valid questionnaire and face-to-face open interviews with household residents in Bariga, Oworonshoki, Makoko, and Iwaya slums. The obtained data were subjected to descriptive statistics using statistical package for social science version 20 and Geographical Information System based Multi-Criteria Decision Analysis. Results of the socio-economic characteristic of residents showed that 32.5 % had no formal education, out of which 39.5 % of the respondents were business persons while 77.0 % are in the low-income class. Housing characteristics revealed that 32.0 percent of the respondents were owner-occupier while 27.0 % are rental-tenant. About 30.0 percent of the houses occupied by most of the respondents were built from 1981 to 1995, and 30.5 percent had lived in the slum for more than ten years. Most of the respondents occupied one-room apartments (73.0 %), and about 58.5 % of houses are built with concrete. This study suggests that a comprehensive approach to slum upgrading is necessary by engaging local governments in partnership-based planning, community participation, and infrastructure improvement; this can be achieved by improving the security of tenure through regularization of land rights and improving the provision of basic services, incentives for community management, access to health, education and new housing areas should be built. Thus, the approach should be carried out to consider the needs and desires of the urban poor.

Keywords: Slums, Settlements, Socio-economic peculiarity, Housing, Urban planning, GIS.

1. Introduction

Housing is among the major determinants of a city structure that profoundly influences the community's health, efficiency, social behaviour, satisfaction, and general welfare (Omole, 2010). Furthermore, adequate shelter has always been the major consequential need for human existence (Oladapo, 2006). Hence, the provision of appropriate housing, especially for the urban poor, constitutes a major constraint to the growth of most African countries and developing nations at large (Lawanson, 2005). More so, in the sub-Sahara African region, countries are faced with the shortage of urban infrastructure deficiency, good housing, urban poverty, growing urban populations, and prevalence of informal housing practices (Habitat International Coalition, 2006). Omole (2010) notes that most of the housing conditions-related problems found most especially in Lagos, Nigeria, resulting largely from inadequately planned land use and non-secure land tenure, poor construction, weak development control, and cultural lifestyles of the inhabitants, and low level of socio-economic attributes.

Moreover, Cohen (2006) discovered that socio-economic factors affect societal organizations, such as the nature of work, demographic structures, people's lifestyles, and the choice better to understand the pattern and trends of urban change. Furthermore, International Housing Coalition (2007) reported that the urban population is escalating among the sub-Sahara African countries, whereby about 75 and 99 percent of urban residents in most African cities live in squalid slums of ramshackle housing. UN-Habitat (2003) ascertain that slum expansion is fuelled by an emulsion of rapid rural to- urban migration, spiraling urban poverty, the inability of the urban poor to access affordable land for housing, and insecure land tenure. However, Owoeye and Omole (2012) documented that the environmental conditions faced in slums manifest themselves in various forms such as overcrowding, the emergence of unsanitary housing, and the general deterioration in the environment's quality. World Bank (2008) reported that slums result from unrealistic regulatory frameworks and ill-conceived policies.

Slums are found to arise from failed policies, bad governance, corruption, inappropriate regulation, dysfunctional land markets, unresponsive financial systems, and a fundamental lack of political will (Chang, 2009). Although, cities are struggling to accommodate their rising

* Corresponding author e-mail: princessokimiji@yahoo.com

populations and address the multidimensional challenges like infrastructure and urban sprawl developments (Soyinka et al., 2016). Hence, slumming conditions have become a global concern and one key factor driving rapid urbanization (Davis, 2004). United Nations Human Settlement Program (UNHSP, 2003) projected that the global number of slum dwellers would have increased to about two billion in the next thirty years. Rahman et al. (2010) reported that the poor's environmental conditions lead to the decay of inner cities and the growth of shantytowns, especially in the peri-urban areas. These living conditions in slums are usually unhygienic and contrary to all planned urban growth norms. They are vulnerable to all forms of pollutions such as air pollution, noise pollution, traffic congestion, and surface water pollution. Therefore, this study examines residents' socio-economic attributes and housing characteristics around slum settlements within Lagos metropolis to determine the contributing factors responsible for poor environmental conditions in the slums.

2. Materials and Methods

2.1. Study Area

The study was carried out in four selected slums within Lagos Metropolis, Nigeria, around Longitudes 3 ̊249 'E and latitudes 6 ̊279 'N with a coastline of approximately 180 km (Odunuga et al., 2012). The state has a total land area of 3577.28 km2, out of which 22 percent is wetland and a population density of approximately 5926 persons per km2 (Oshodi, 2013). Lagos state population is estimated to be 24.5 million in 2015 (UNHSP, 2003) and 29 million by 2020 (Lagos Water Corporation, 2011), with a growth rate of 3.2 and 8 percent (World Bank, 2013). The state's geology consists of coastal plain sands and a tidal flat with alluvium (BRNCC, 2012), while vegetation is a tropical rainforest zone, consisting of mangrove swamps, freshwater swamps, lagoons, and creeks. Relief occupies a low-lying topography of 1– 4 % slope, an elevation of 0–2 m above sea level (Awosika et al., 2000) represented by the dendritic drainage system of river Ogun, Adiyan, and Ossa (Idowu and Martins, 2007). The state is ranked 15th globally in terms of the population vulnerable to coastal flooding because over 70 percent of its population live in unplanned settlements such as slums (Adelekan, 2010), this is not surprising as only 45.2 percent of its built-up areas are connected with drains (Nwigwe and Emberga, 2014), and only less than 30 percent of the existing drains are maintained (Aderogba, 2012). There is two distinct climatic seasons experience in the state; dry and wet (rainy). It also experiences high air temperatures ranging from 30.0 ˚C to 38.0 ˚C (Adejuwon, 2004). Figure 1 presents the map of the study area indicating the sample locations.

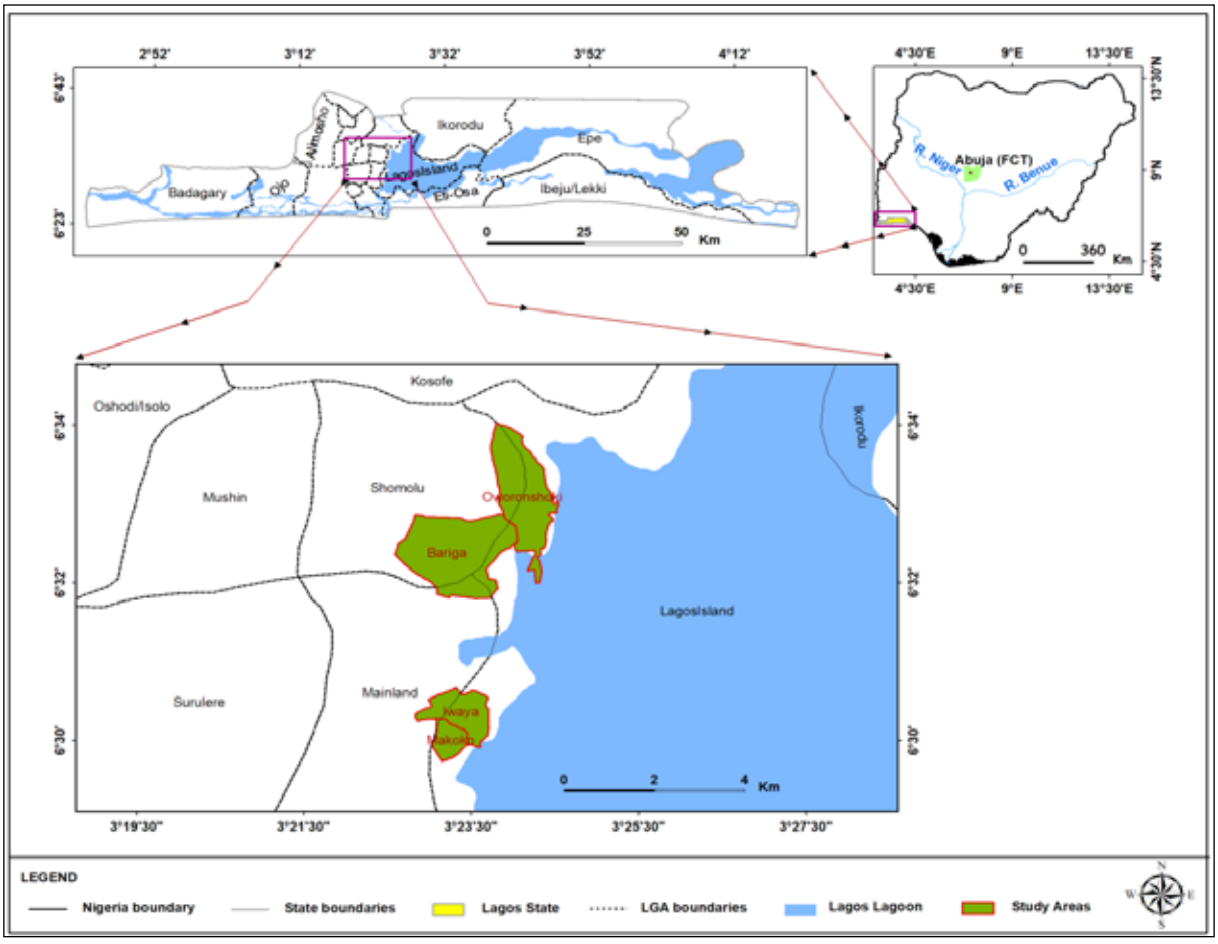

Figure 1. Location map of the study area.

2.2. Research Approach and Design

Primary and secondary data were used. Primary data were derived from a field survey of the slum settlement. In contrast, secondary data includes relevant literature such as books and journals, internet materials, land use maps of the study area, documents from community participation, and government agencies.

2.3. Sampling Location

A total of four selected slum settlements were designated for this study in the Lagos metropolis. These slums were randomly selected from the list of slum settlement identified by officials of the Lagos state environmental protection agency (LSEPA) after excluding settlement that is not closed to the coastal area. The aim is to target slums that are located close to the coastal area. The names of the slums are Bariga, Oworoshoki, Makoko, and Iwaya.

2.4. Survey

A multi-stage sampling procedure was employed in selecting the study area. A descriptive survey design was also adopted because it allows the establishment of unique characteristics of the inhabitants and developing a detailed picture and intensive knowledge of the study area. More so, a reconnaissance survey of the study area was also carried out. A systematic sampling method was used in selecting the houses; the first house was randomly selected and the subsequent house at an interval of the fifth house. Simple random sampling was used in selecting a household head. In a situation where the household head was not available, the wife or a grown-up child was chosen.

Moreover, this field survey study was designed and administrated to different slums located around the Lagos metropolis' coastal areas. The questionnaire was pre-tested to assure reliability and validity issues. Hence, a pilot survey was conducted in early July 2015 because it provides useful information regarding the study in processes, resource management, and scientific evidence (Van Teijlingen et al., 2001). Hill (1998) also suggested 10 to 30 participants for pilots in survey research. Therefore, this study makes use of 10 to 40 participants by using the formula stipulated by Berenson et al. (2006);

$$n = \frac{Z2\ XS2}{D2}$$

n = is the minimum sample size

z = is the value of the distribution function (for normal distribution z = 1.96 while for alpha = 0.05)

s = is the population standard deviation

d = is the acceptable standard error of the mean (the standard error of the mean is estimated as the sample standard deviation divided by the square root of the sample size).

Furthermore, the preliminary fieldwork conducted also sought the household's agreement to participate in the study. Trained interviewers visited more than 250 individual households and obtained the necessary information from a responsible adult. Two hundred (200) households out of the original list of 280 agreed to participate in the survey representing a response rate of 71.4 %. Seventy households out of 280 who agreed to participate were chosen from each slum location in Lagos metropolis. They were provided with questionnaires containing detailed questions about residents' socio-economic characteristics, physical characteristics of residential buildings, and the availability of basic amenities.

This sample size (70 households out of the total 280 households) gives a 95 % confidence level with a margin of error of 5 % using the formula suggested by Cochran (1963);

$$\text{Sample size} = \frac{Distributionof\ 50\ \%}{\frac{((MarginofError\ \%)Squared}{ConfidenceLevelScore)Squared}}$$

Finite Population Correction:

$$\text{True Sample} = \frac{SamplesizexPopulation}{Samplesize(Population-1)Squared}$$

Population = 1,000

$$\text{Sample size} = \frac{0.5\ x\ (1-0.5\ ))}{\frac{((0.05)2}{(1.96)2}}$$

$$\text{Sample size} = \frac{0.25}{((0.025512)2}$$

$$\text{Sample size} = \frac{0.25}{((0.00065077)2}$$

Sample size = 384.16

$$\text{True Sample} = \frac{384.16\ x\ 1000}{384.16\ +1000-1}$$

$$\text{True Sample} = \frac{384160.3024}{1383.1603}$$

True Sample = 277.7409 (True sample size was rounded up to the nearest whole number).

Table 1. Sampling source and population Estimation.

Slum locations	Estimation of population	Pilot survey	Total number of questionnaire per location
Bariga	250	10	70
Oworoshoki	250	10	70
Makoko	250	10	70
Iwaya	250	10	70
Total	1,000	40	280

More so, the true sample size was rounded up to 278, but in other to get an equal number of questionnaires per location, 70 questionnaires were distributed. However, the survey was conducted for six months: the month of October to March from 2015 to 2016. Coordinates were recorded at each sampling site using the Garmin GPS device (GPSMAP 76CSX model).

2.5. Statistical Analysis

The data obtained were subjected to descriptive analyses (frequency, percentage, and chart) using the social sciences statistical package (SPSS version 20.1). The advanced analysis employed in this study is Geographical Information System

(GIS) based Multi-Criteria Decision Analysis (MCDA) Arc Map 10.1 to analyze the questionnaire's information and produce a spatial analysis of the study area.

2.6. Spatial Analysis of the Study Area Using Multi-Criteria Analysis (MCA) in GIS

The methodology used in data collection (Figure 2) incorporated those of Abbot (2000); Karanja (2010), and Tyler (2011), whereby data collected consist of two main parts: capturing the social information from the communities using a questionnaire and capturing the spatial information using GIS. Households were interviewed across the settlement while social information was subsequently recorded in a spreadsheet. The spatial information was derived from satellite imagery of the settlement, sourced from the global land cover facility (GLCF), and questionnaire data were integrated into GIS software for the evaluation. Ascertaining the key issues of low-income settlements based on measurements includes using the following:

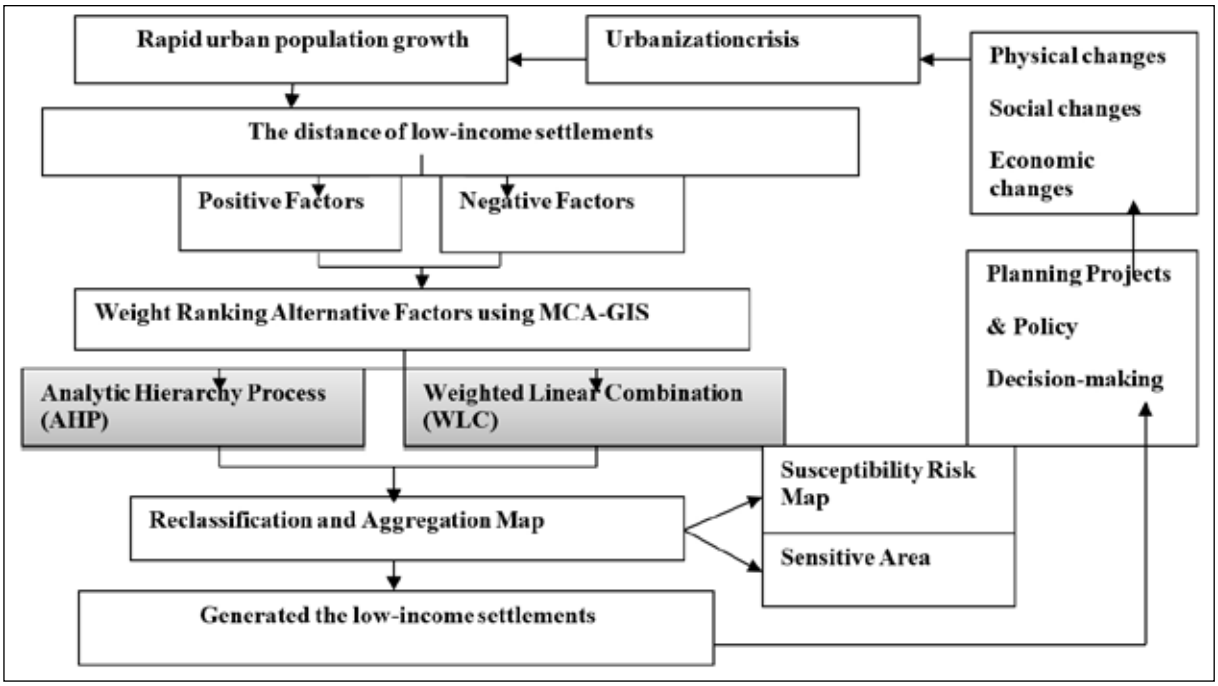

Figure 2. GIS-based spatial decision-making procedures (Shummadtayar et al., 2013).

2.6.1. Analytical Hierarchy Process (AHP)

For measuring individual participant data, Saaty (1977) reported that the AHP could be derived by taking the principal eigenvector of a square reciprocal matrix of pair-wise comparisons between the criteria and dealing with the relative importance of the two criteria involved in determining suitability for an individual with the size of areas recommended for prioritization (Malczewski, 1999).

2.6.2. Weighted Linear Combination (WLC)

Measures the different scales so that all factor maps will be positively correlated with suitability (Figure 2). A linear scaling method was applied, typically using the minimum and maximum values as scaling points for standardization. Factors were combined, followed by a summation of the results to yield a suitability map (Anagnostopoulos, 2009).

3. Results and Discussion

3.1. Socio-Economic Characteristics of Residents

The respondents' socio-demographic characteristics (Table 2) showed that gender (female) were 54.0; 58.0; 60.0, and 56.0 % for Bariga, Oworoshoki, Makoko and Iwaya, respectively. And about 46.0 % (Bariga), 42.0 % (Oworoshoki), 40.0 % (Makoko), and 44.0 % (Iwaya) accounts for male gender across the slums. The high values recorded for females across the slums could be attributed to the assertion that men have the right to marry more than one wife, making females dominant in the settlement.Marital status of the respondents revealed that 52.0; 52.0; 34.0 and 36.0 (Bariga, Oworoshoki, Makoko, Iwaya) percent were still single and about (Bariga) 20.0 %, (Oworoshoki) 28.0 %, (Makoko) 44.0 % and (Iwaya) 48.0 % were married while others 28.0; 20.0; 22.0 and 16.0 percent were either widow or widower. Hence, most of the respondents who are still single could be due to the living conditions because even the married ones among the respondents are complaining about their poor marriage life and how they could not afford two square meals per day.

The educational level of the respondents depicts that 20.0 % (Bariga), 12.0 % (Oworoshoki), 62.0 % (Makoko), and 28.0 % (Iwaya) had no formal education, which means that they cannot read or write. About 38.0; 54.0; 4.0; and 26.0 percent (Bariga, Oworoshoki, Makoko and Iwaya) attended tertiary institution and 8.0; 14.0; 30.0; and 28.0 percent had primary education certificate while 34.0 % (Bariga), 20.0 % (Oworoshoki), 4.0 % (Makoko) and 18.0 % (Iwaya) stopped at the secondary school education. The implication of the low level of education of the people in the area weakens the importance of a healthy environment whereby the majority of the respondents are poor, and their low monthly income depicts a high level of poverty among the respondents (Ayoola and Amole, 2014). Therefore, it can be deduced that residents in the slum area will be living below the minimum environmental standards

Common occupations of the respondent are businessmen and women (20.0; 22.0; 8.0 and 32.0 %) at Bariga, Oworoshoki, Makoko and Iwaya respectively; apart from the civil servant that constituted 42.0 % (Bariga), 46.0 % (Oworoshoki), 6.0 % (Makoko) and 16.0 % (Iwaya). About 36.0; 26.0; 4.0 and 30.0 percent were student while 2.0 %, 6.0 %, 10.0 % and 22.0 % are pensioner, this shows that the occupational and income distributions are closely related. Hence, the nature of occupation determines their level of income. More so, occupation characteristics portray the settlements as typical slum emerging areas with sprout growth from rural-urban migration.

Concerning the monthly income range, respondents in Bariga (64.0 %), Oworoshoki (76.0 %), Makoko (82.0 %), and Iwaya (86.0 %) were within the low-income range, and about 32.0; 24.0; 18.0 and 14.0 percent were in the middle-income range while only 4.0 % (Bariga) of the respondents can boost of being in the high-income range (Table 2). This study shows that the poorer residents are the low-income earner, so they prefer staying in the slum area because of cheaper livelihood. Lawanson and Olanrewaju (2012) also documented that about 70 % of the 17 million Lagos metropolis residents are considered poor and can only survive by participating in informal activities.

Table 2. Socio-Economic Characteristics.

Demographic Characteristics	Bariga		Oworonshoki		Makoko		Iwaya		Total Freq	Total (%)
	Freq	%	Freq	%	Freq	%	Freq	%		
Gender										
Male	23	46.0	21	42.0	20	40.0	22	44.0	86	43
Female	27	54.0	29	58.0	30	60.0	28	56.0	114	57
Marital Status										
Single	26	52.0	26	52.0	17	34.0	18	36.0	87	43.5
Married	10	20.0	14	28.0	22	44.0	24	48.0	70	35
Others	14	28.0	10	20.0	15	22.0	8	16.0	43	21.5
Educational Level										
No Formal Education	10	20.0	10	12.0	31	62.0	14	28.0	65	32.5
Primary Education	4	8.0	7	14.0	15	30.0	14	28.0	40	20
Secondary Education	17	34.0	10	20.0	2	4.0	9	18.0	38	19
Tertiary Institution	19	38.0	23	54.0	2	4.0	13	26.0	57	28.5
Occupation of Respondents										
Businessperson	10	20.0	13	22.0	4	8.0	16	32.0	79	39.5
Civil Servant	21	42.0	23	46.0	3	6.0	8	16.0	55	27.5
Student	18	36.0	11	26.0	2	4.0	15	30.0	46	23
Pensioner	1	2.0	3	6.0	5	10.0	11	22.0	20	10
Monthly Income Range										
Low	32	64.0	38	76.0	41	82.0	43	86.0	154	77
Middle	16	32.0	12	24.0	9	18.0	7	14.0	44	22
High	2	4.0	-	-	-	-	-	-	2	1

Source: Field Work, Lagos Metropolis slums 2015/2016.

3.2. Residential Building Characteristics

Figure 3a shows that about 32; 14; 31, and 23 percent of the respondents in Bariga, Oworoshoki, Makoko, and Iwaya were owner-occupier. The values recorded for owner-occupier tenancy status are not surprising because most of the respondents occupy land space without land tenure certification to erect buildings and structures.

The common tenancy status among the respondent (Figure 3b) is the rental tenant accounting for 24 % (Bariga), 27 % (Oworoshoki), 25 % (Makoko), and 24 % (Iwaya), respectively. The findings from this study confirm the assertion reported by the FNG-National Housing Policy (2004) that the most predominant form of tenure in many Nigerian cities is rental accommodation, providing over ninety percent of the country's housing sector (Olanrewaju, 1997). Hence, Ogunleye (2011) also ascertained that a significant proportion of low-income people in developing world cities live in rental housing.

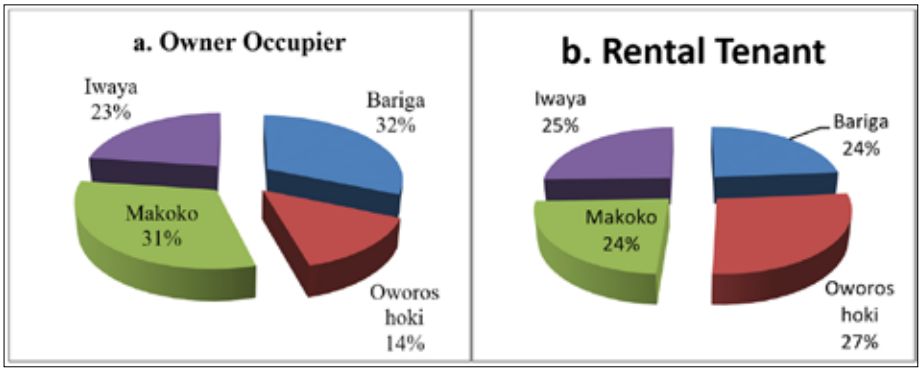

Figure 3 a. Owner-occupier tenancy status. b. Rental-tenant tenancy status.
Source: Field Work, Lagos Metropolis slums 2015/2016

The age of most building occupied. showed in Table 3 revealed that 2.0; 6.0; 14.0, and 18.0 percent of the buildings were built from 1960 to 1976 in Bariga, Oworoshoki, Makoko, and Iwaya, respectively. Hence, 24.0 %, 10.0 %, 36.0 % and 26.0 % of the houses were constructed from 1977 to 1980, followed by 2.0 % (Bariga), 48.0 % (Oworoshoki), 38.0 % (Makoko) and 32.0 % (Iwaya) built from 1981 to 1995. About 34.0 % (Bariga) of the houses are built from 1996 to 2010, and 38.0; 36.0; 12.0, and 24.0 percent were erected from 2011 up to date. These signify that buildings increase in the slum settlement, which gives rise to poor environmental conditions in the slum.

Concerning the duration of occupancy, 16.0; 12.0; 18.0 and 18.0 percent of respondents reported that they have lived in the slum for 1 to 4 years and about 6.0 % (Bariga), 28.0 % (Oworoshoki), 36.0 % (Makoko), and 22.0 % (Iwaya) revealed that they had stayed in the slum for 5 to 7 years. Although 28.0; 20.0; 42.0, and 32.0 percent had lived for about 8 to 10 years, followed by those who lived for 11 to 15 years (22.0; 22.0 and 14.0 %) respectively. Hence, most of the respondents in Bariga (28.0 %), Oworoshoki (8.0 %), Makoko (20.0 %), and Iwaya (8.0 %) had lived in the slum for 16 years and above. These results revealed that the populations of the slum dwellers are increasing daily due to rural-urban migration.

Most of the respondents' common accommodation unit is squatting with friends and families, which constitute 6.0 %, 10.0 %, 2.0 %, and 4.0 % (Bariga, Oworoshoki, Makoko, and Iwaya), respectively. About 42.0; 64.0; 96.0 and 90.0 percent occupied one-room apartment. More so, 30.0 %, 12.0 %, 2.0 % and 4.0 % of the respondents occupied two rooms apartment. Hence, 16.0 % (Bariga), 10.0 % (Oworoshoki) and 2.0 % (Iwaya) are occupying three room's apartment while 6.0 % (Bariga) and 4.0 % (Oworoshoki) occupied four rooms apartment (Table 3). Generally, most slum dwellers are in the low-income range, which corroborates with the assertion that they cannot afford a comfortable apartment. NBS (2009) reported that the Nigerian Government Urban Survey in 1970 shows that 70 % of Lagos households lived in one-room housing units. By 2007 the figure had marginally risen to 72.3 percent.

Table 3. Physical Characteristics of Buildings.

Physical Characteristics of Buildings	Bariga		Oworonshoki		Makoko		Iwaya		Total Freq	Total (%)
	Freq	%	Freq	%	Freq	%	Freq	%		
Age of Building Occupied										
1960-1976	1	2.0	3	6.0	7	14.0	9	18.0	20	10
1977-1980	12	24.0	5	10.0	18	36.0	13	26.0	48	24
1981-1995	1	2.0	24	48.0	19	38.0	16	32.0	60	30
1996-2010	17	34.0	-	-	-	-	-	-	17	8.5
2011 till date	19	38.0	18	36.0	6	12.0	12	24.0	55	27.5
Duration of Occupancy										
1-4yrs	8	16.0	6	12.0	9	18.0	9	18.0	32	16
5-7yrs	3	6.0	14	28.0	18	36.0	11	22.0	46	23
8-10yrs	14	28.0	10	20.0	21	42.0	16	32.0	61	30.5
11-15yrs	11	22.0	11	22.0	-	-	7	14.0	29	14.5
16yrs and above	14	28.0	4	8.0	10	20.0	4	8.0	32	16
Accommodation Unit Occupied										
Squatting	3	6.0	5	10.0	1	2.0	2	4.0	11	5.5
One-room apartment	21	42.0	32	64.0	48	96.0	45	90.0	146	73
Two rooms apartment	15	30.0	6	12.0	1	2.0	2	4.0	24	12
Three rooms apartment	8	16.0	5	10.0	-	-	1	2.0	14	7
Four rooms apartment	3	6.0	2	4.0	-	-	-	-	5	2.5

Source: Field Work, Lagos Metropolis slums 2015/2016.

Figure 4 shows that most respondents' buildings are block and cemented surface (36 and 18%) for Makoko and Iwaya, respectively. About 72 (Bariga), 72 (Oworoshoki), 16 (Makoko), and 74 (Iwaya) percent occupied buildings built with concrete. Hence, 28%, 28%, 30%, and 8% of the respondents occupied mud and cemented surface buildings while only 18% (Makoko) stayed in wooden and board steel surface buildings. This study's findings corroborate with Olotuah (2005), who reported that 75% of the dwelling unit in Nigeria's urban centres are substandard, and the dwellings are sited in slum areas.

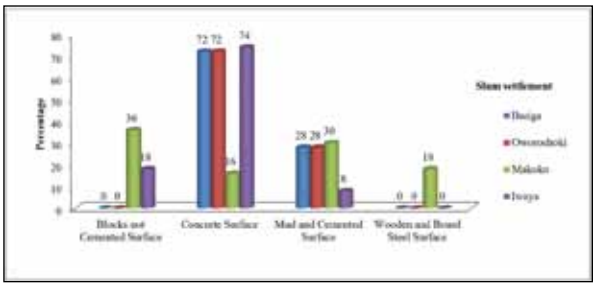

Figure 4. Types of buildings occupied by the respondents.
Source: Field Work, Lagos Metropolis slums 2015/2016.

Household size of most respondent showed in Figure 5 revealed that 26 (Bariga), 32 (Oworoshoki), 4 (Makoko), and 34 (Iwaya) percent accounts for 1 to 2 persons per room and about 6; 14; 2; and 14 percent accounted for 3 to 4 persons per room. Hence, 48 %; 36 %; 40 %, and 36 % for Bariga, Oworoshoki, Makoko, and Iwaya consist of 5 to 8 persons per room while 20; 18; 54 and 16 percent constitutes nine persons and above per room. This study's results conform with Oshodi (2010), who reported that living conditions are worse among poor households living in informal settlements with an occupancy ratio of 8 to 10 persons per room.

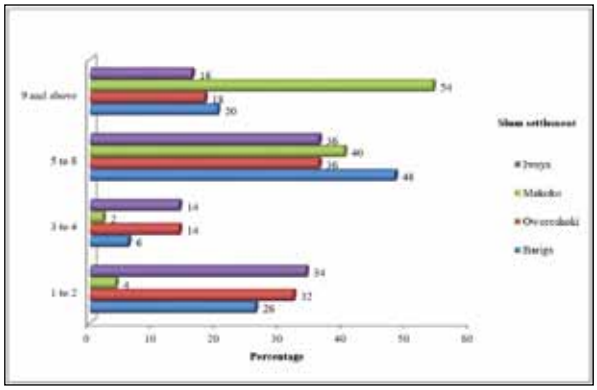

Figure 5. The household size of the respondents.
Source: Field Work, Lagos Metropolis slums 2015/2016

3.3. Availability of Basic Amenities

Table 4 shows that electricity availability in the slum settlement accounted for 100% (Bariga), 100% (Oworoshoki), 100% (Makoko), and 96% (Iwaya), respectively, while only 4.0 % (Iwaya) of the respondents complained of unavailability of electricity. Hence, 60.0; 58.0; 70.0 and 74.0 percent of the respondents had access to toilet facilities, while 40.0%, 42.0%, 30.0%, and 26.0% (Bariga, Oworoshoki, Makoko, and Iwaya) do not have toilet facilities in their houses, this implies that the respondents who do not have access to toilet facilities make use of public toilets. Most of the respondents (22.0; 32.0; 86.0 and 70.0%) in Bariga, Oworoshoki, Makoko, and Iwaya do not have waste disposal methods; they usually dump their generated waste in an open dump while 78.0%; 68.0%; 14.0%, and 30.0% of the respondent had access to waste disposal methods whereby they dump their generated waste inside a pit before burying the waste. This finding also conforms with Ackleman and Anderson (2008), who documented that basic infrastructures' unavailability causes widespread environmental damages.

Table 4. Basic Amenities Availability.

Availability of Amenities	Bariga		Oworonshoki		Makoko		Iwaya		Total Freq	Total (%)
	Freq	%	Freq	%	Freq	%	Freq	%		
Electricity										
No	-	-	-	-	-	-	2	4.0	2	1
Yes	50	100.0	50	100.0	50	100.0	48	96.0	198	99
Toilet facilities										
No	20	40.0	21	42.0	15	30.0	13	26.0	69	34.5
Yes	30	60.0	29	58.0	35	70.0	37	74.0	131	65.5
Waste disposal method										
No	11	22.0	16	32.0	43	86.0	35	70.0	105	52.5
Yes	39	78.0	34	68.0	7	14.0	15	30.0	95	47.5

Source: Field Work, Lagos Metropolis slums 2015/2016.

Figure 6 depicts the medium of water provision across the study area. Private water provision constitutes about 60; 42; 18 and 26 percent for Bariga, Oworoshoki, Makoko, and Iwaya, respectively, while 22 %; 16 %; 42 %, and 24 % accounts for public-private provision, this means that the residents contributes money in constructing central borehole for the community. Hence, government water provision consists of 18 % (Bariga), 42 % (Oworoshoki), 40 % (Makoko) and 50 % (Iwaya) respectively. The implication of this is that most of the respondents use the water provided by the government. The results from this study corroborate with the United Nations (2010). Who reported that a sustainable water supply is increasingly difficult in urban areas due to population growth and urbanization, poor management, and ageing infrastructure.

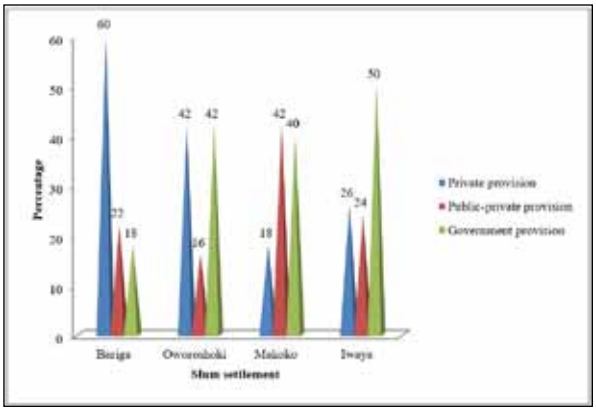

Figure 6. The medium of water provision in the study area. Source: Field Work, Lagos Metropolis slums 2015/2016.

The cooking methods shown in Figure 7 revealed that 22; 4; 6, and 22 percent of the respondents in Bariga, Oworoshoki, Makoko, and Iwaya use fuelwood for cooking because they believe it is cheaper than gas or kerosene. This result agrees with Gwatkin et al. (2000), who reported that people using and exposed to fuelwood are higher in South Western Nigeria's low-income settlement. About 16%; 16%; 54%, and 26 % use coal for cooking, which is the most common cooking method among the slum dwellers. Although 20% (Bariga), 46% (Oworoshoki), 16% (Makoko) and 40% (Iwaya) uses kerosene stove for cooking. Thus, the respondent reported that the kerosene stove is affordable and economical. Hence, 2; 18; 18 and 6 percent of the respondents use electric stoves once electricity is available Hence 40%, 16%, 6%, and 6% (Bariga, Oworoshoki, Makoko, and Iwaya) uses gas stove for cooking. Although most of the respondents reported that it is expensive to maintain, but it aids fast cooking. The findings from this study conforms with Olufemi et al. (2012), who ascertained that urban areas, especially the low-income settlement, use multiple cooking methods than the rural areas.

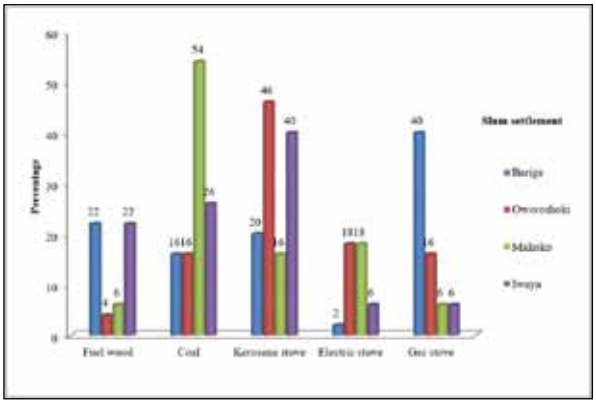

Figure 7. Methods of cooking of the respondents. Source: Field Work, Lagos Metropolis slums 2015/2016.

Figure 8 shows the means of transportation around the study area. Hence, 18 percent of the respondents in Makoko make use of canoe as means of transportation, and about 12 % (Bariga), 22 % (Oworoshoki), 60 % (Makoko), and 44 % (Iwaya) use the footpath. However, 12; 22 and 18 percent of the respondents use motorcycles while 38 %, 34 %, and 38 % use commercial buses. Hence, 50 and 32 percent of the respondents in Bariga and Oworoshoki use tricycles popularly known as Keke Napep. These findings could be attributed to the assertion that low-income dwellers are faced with a high level of poverty. More so, Samuel and Silvester (2002) reported that the cost of urban infrastructure and services (transport and others) has become unaffordable to most urban slum dwellers due to widespread poverty and low-income levels.

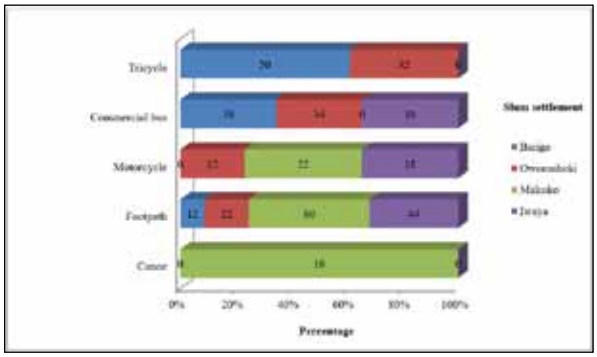

Figure 8. Means of transportation of respondents. Source: Field Work, Lagos Metropolis slums 2015/2016.

4. Spatial Analysis of the Study Area Using Multi-Criteria Analysis (MCA)

4.1. False Composite Colour (FCC) and Classified Image Of 1984

Figure 9a depicts the False composite colour image of 1984. The classification used for the map was the bare ground represented by grey colour and the built-up area represented by the red colour. In contrast, the blue colour represents the water bodies. Thus, as in the period (1984), the rate of urbanization is at the lowest peak.

Figure 9b shows the classified image of 1984. Hence, the different land cover and land use types used for the map classifications were vegetation/wetland, which represents the green colour, the built-up area represents the grey colour. In contrast, water bodies represent the blue colour. Generally, as of this period, the urban areas have started witnessing an increase in development; this confirms the assertion made by Shummadtayar (2013), who reported that spatial analysis provides representative information about settlement natural and human-made features.

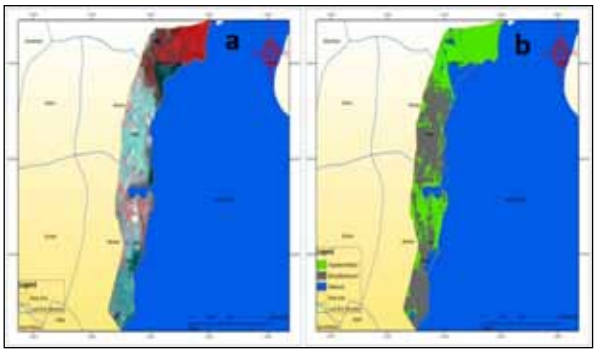

Figure 9. a. False composite image of 1984. b. Classified image of 1984. Source: Field Work, Lagos Metropolis slums 2015/2016.

4.2. False Composite Colour (FCC) and Classified Image Of 2014

The false composite color image of 2014 showed in Figure 10a revealed that the urbanization process takes a higher dimension, whereby most urban areas are witnessing changes in land use and land cover types. Hence, the bare ground represents the grey colour, and the red colour represented the built-up area, while the blue colour represents the water bodies on the map. Figure 10b shows the classified image of 2014. The vegetation/wetland is represented by green color. The built-up area represents grey color, while water bodies represent a blue color on the map.

Most importantly, as at this period, there is an increase in a built-up area with buildings extending towards the lagoon and several changes due to urban city expansion processes and the quest for development. Similarly, researches have shown that multi-criteria analysis is good for the decision-making process. These confirm the assertion stipulated by Temiz and Tecim (2009). They reported the combined use of GIS and multi-criteria decision methods (MCDM) for forestry management in Izmir, Turkey, which allows forest managers to visualize solutions proposed by MCDM and better understand the problem they confront in the study area.

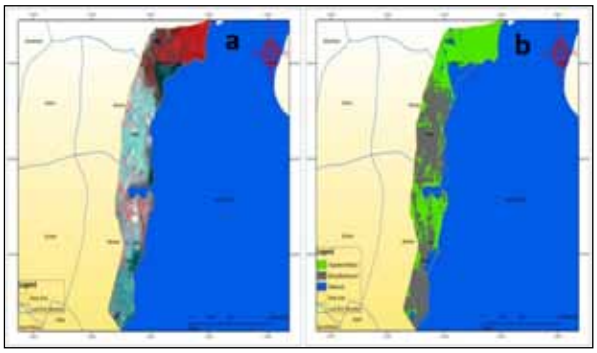

Figure 10. a. False composite image of 2014. b. The classified image of 2014. Source: Field Work, Lagos Metropolis slums 2015/2016.

4.3.1. Socio-Economic Characteristics of Residents Survey

Figure 11a shows that few of the respondents belong to the high-income earners in Bariga. In contrast, most of the respondents are still on the moderate-income level across the study area, represented with green colour on the map. In contrast, the other areas of Makoko, Iwaya, Bariga, and Oworoshoki, represented with red colour belong to the low-income earners; this implies that people prefer to live in slum settlements with a cheaper and affordable livelihood.

Figure 11b depicts that Makoko and Bariga settlements are faced with poor underdeveloped slums while Iwaya and Oworoshoki are among the poorest slum settlements in this study. Although few parts of Bariga had a little developed area, most of the slum settlements in this study need government intervention by partnering with the private sector to upgrade the settlement. More so, there is a notion that multi-criteria analysis is suitable for urban susceptibility environmental criteria used in evaluating and eliminating long-term effects of the informal settlement. Hence, thus conforms with Liu et al. (2007), who carried out a study using these methods by integrating GIS and multi-criteria analysis in the Hanyang lake area located in Wuhan city China where a comprehensive method is used in analyzing the suitability of future land use according to specified requirements, preferences, and predictions that were uncovered in Liu et al., 2007 research work.

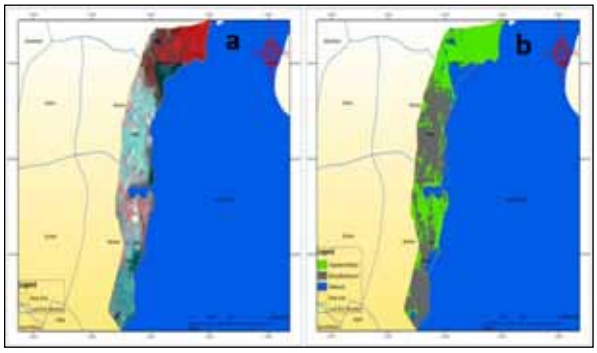

Figure 11. a. Monthly income range. b. Undeveloped areas. Source: Field Work, Lagos Metropolis slums 2015/2016.

4.3.2. Residential Building Characteristics Survey

Building types shown in Figure 12a revealed that Iwaya and Bariga had more cemented surface buildings than the other slum settlement. In contrast, block and cemented surface buildings are found across the study area. The mud buildings are found in Makoko, Iwaya, Bariga, and Oworoshoki, respectively. Generally, the building types found across the slum settlement are of substandard quality due to the poor living standard among the slum dwellers.

Figure 12b shows that the house structures are of low quality across the study area marked with yellow colour on the map. The green colour represents areas with moderate housing structures in Makoko, Iwaya, Bariga, and Oworoshoki respectively is still part of the sentence before adding full-stop. this means that most of the houses had little availability of basic amenities. Hence, the areas that are represented with red colour signify areas with high quality of housing structure. The high level of poor housing quality could be attributed to the lack of security of tenure.

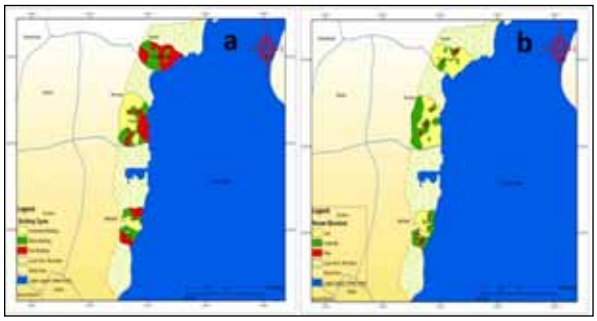

Figure 12. Figure 12. a. Building types. b. House structures. Source: Field Work, Lagos Metropolis slums 2015/2016.

5. Conclusions

This study concluded that poor housing conditions and lack of good financing schemes in upgrading the settlements contribute to the high rate of slum dwellers living in substandard houses that gives rise to unhealthy living conditions. The amount of infrastructural facilities

available in the informal settlements is grossly inadequate, while some are not available. Hence, the poor environmental conditions characterized by numerous problems such as overpopulation and inadequate basic amenities increase the socio-economic problems and pose serious threats to the slum dwellers' long-term livelihood. However, most of the challenging problems faced by low-income people could be solved using Geographical Information System (GIS) based Multi-Criteria Decision Analysis (MCDA) for calculating the simplify situations of alternative factors using Analytical Hierarchy Process (AHP) for weighting the measure of individual participant data and Weighted Linear Combination (WLC) on the socio-economic and housing characteristics in the low-income settlement. Conclusively, the informal settlement should not be considered an anomaly but rather as the necessary response. They represent the desires and needs of the poor to have access to the urban environment. Attempts to eradicate them will fail until these underlying issues of poverty and inequality are properly addressed.

References

Abbot, J. R. (2000). An Integrated Spatial Information Framework for Informal Settlement Upgrading. International Archives of Photogrammetry and Remote Sensing 33 (2) : 7–16.

Ayoola, A. and Amole, D. (2014). The Value of Housing among the Poor in Ilesa, Osun State Nigeria. Architecture Research 4 (1A):45-54. doi: 10.5923/s.arch.201401.06.

Adejuwon, S. A. (2004). Impacts of Climate Variability and Climate Change on Crop Yield in Nigeria, Stakeholders' Workshop on Assessment of Impacts and Adaptation to Climate Change (AIACC), Conference Centre Obafemi Awolowo University, Ile-Ife 20 – 21 (3 Sep. 2004).

Adelekan, I. O. (2010). The vulnerability of Poor Urban Coastal Communities to Flooding in Lagos, Nigeria. Environment and Urbanization 22(1): 433–450.

Aderogba, K. A. (2012). Qualitative Studies Of Recent Floods And Sustainable Growth And Development Of Cities And Towns In Nigeria. International Journal of Academic Research in Economics and Management Sciences 1(3):1–25.

Ackleman, H. and Anderson, M. (2008). Methods to Solve the Problem of Informal Settlements: The Case of Hangberg, South Africa.Stockholm: Royal Institute of Technology pp 23-40.

Anagnostopoulos, K.P. (2009). Land Suitability Analysis for Natural Wastewater Treatment Systems using a new GIS Add-in for supporting Criterion Weight Elicitation Method. Oper Resource International Journal 10 (10): 91-108.

Awosika, L.F., Folorunsho, R., Dublin-Green, C.O, Imevbore, V.O. (2000). Review of the Coastal Erosion at Awoye and Molume Areas of Ondo State. A Consultancy Report for Chevron Nigeria Limited. 75 pp.

Berenson, M.L., David, M.L., Krehbiel, T.C. (2006). Basic Business Statistics Concepts and Application. Prentice-Hall. Inc.Englewood Cliffs, NJ. 763 pp.

BRNCC. (2012). Towards Lagos State Climate Change Adaptation Strategy. Building Nigeria's Response to Climate Change. 10pp.

Chang, T. (2009). Improving Slum Conditions with Public-Private Partnerships. Panorama (Online).http://www.design. UPenn .edu. HTML (26 Jun. 2013).

Cochran, W.G. (1963) Sampling Techniques, 2nd Ed., New York: John Wiley and Sons, Inc. 50 pp.

Cohen, B. (2006). Urbanization in Developing Countries: Current Trends, Future Projections, and Key Challenges for Sustainability. Technology in Society 28: 63–80.

Davis, M (2004). Planet of Slums: Urban Involution and the Informal Proletariat. New Left Review 26:5-34.

Federal Republic of Nigeria (FNG). (2004). National Housing Policy. (Online).http://www.fgn.net.html (2 Feb. 1991).

Gwatkin, D.R., Rutstein, S., Johnson, K., Pande, R.P., Wagstaff, A. (2000). Socioeconomic Differences in Health, Nutrition, and Population. Hnp/Poverty Thematic Group. Washington, D.C., World Bank: 20pp.

Habitat International Coalition. (2006). Ecuador's New Constitution Includes Several Housing-Related Rights.(Online). http://www.hicnet.org/news.php.html (3 Oct. 2008).

Hill, R.(1998) What Sample Size is Enough in Internet Survey Research? Inter-Personal Computing and Technology: An Electronic Journal for the 21st Century 6(3-4): 1-10.

Idowu, O. A. and Martins, O. (2007). Hydrograph analysis for groundwater recharge in the phreatic basement aquifer of the Opeki River basin, Southwestern Nigeria. Asset Series B, 6(2): 132–141.

International Housing Coalition. (2007). Housing Challenges And Opportunities In Sub-Saharan Africa, Washington DC: IHC. 5 pp.

Karanja, I. (2010). An enumeration and mapping of informal settlements in Kisumu, Kenya, implemented by their inhabitants. Environment and Urbanization 22 (1): 217–239.

Lagos Water Corporation. (2011). LWC targets 733 million daily by 2020. http://www.lagoswater.org/news.php. (29 Mar. 2011).

Lawanson, T. O. (2005). Challenges of sustainability and urban development in Nigeria: reviewing the Millennium Development Goals. Globalization, Culture and the Nigerian Built Environment 2: 366-372.

Lawanson, T. and Olanrewaju, D. (2012). The Home as Workplace: Investigating Home-Based Enterprises in Low-Income Settlements of the Lagos Metropolis. Hbes in Lagos Metropolis 48h Isocarp Congress pp 1-30.

Liu, Y., Lv, X., Qin, X., Guo, H., Yu, Y., Wang, J., Mao, G. (2007). An Integrated GIS-Based Analysis System for Land-Use Management of Lake Areas In Urban Fringe. Land Scape Urban Plan 82(4): 233-246.

Malczewski, J. (1999). GIS and multicriteria decision analysis. John Wiley and Sons, INC. Canada and U.S.A pp 392.

Nwigwe, C. and Emberga, T. T. (2014). An Assessment of Causes and Effects of Flood in Nigeria. Standard Scientific Research and Essays 2(7): 307–315.

Odunuga, S., Oyebande, L., Omojola, A. S. (2012). Socio-Economic Indicators and Public Perception on Urban Flooding in Lagos, Nigeria. Hydrology for Disaster Management. Nigerian Association of Hydrological Sciences, pp 82–96.

Ogunleye, B. M. (2011). Analysis of the Socio-economic Characteristics and Housing Condition in the Core Neighbourhood of Akure, Nigeria. Journal of Geography and Regional Planning 6(6): 229-236.

Oladapo, A. A. (2006). A Study of Tenant Maintenance Awareness, Responsibility and Satisfaction in Institutional Housing in Nigeria. Vilnius Gediminas Technical University. International Journal of Strategic Property Management 10 (1): 217-231.

Olanrewaju, D. C. (1997). Spatial Distribution of Urban Deprivation in Akure, Ondo State, University of Sheffield, U.K.

Olotuah, A.O. (2005). Urbanisation, Urban Poverty, and Housing Inadequacy, Proceedings of Africa Union of Architects Congress, 23-28 May, Abuja, Nigeria:185-199.

Omole, K.F. (2010). An Assessment of Housing Condition and Socio-Economic Life Styles of Slum Dwellers in Akure, Nigeria. Contemporary Management Research 6(4): 272-290.

Oshodi, L . (2013). Flood Management and Governance Structure in Lagos, Nigeria. Regions Magazine 292 (1): 1-17. DOI: 10.1080/13673882.2013.10815622.

Oshodi, L. (2010). Housing, Population and Development in Lagos, Nigeria. (Online).http://oshlookman.wordpress.com/urban-spaces-innovation-usi-intervention-in-lagos-housing-crisis.html (24 Nov.2010).

Owoeye, J.O and Omole, F.K . (2012). Built Environment Decay and Health Situation of Slum Dwellers in Residential Cores of Akure, Nigeria. America Journal of Human Ecology 1(2): 33-39.

Olufemi, O. D., Ololade, O. O., Ebenezer, K. A., Tolutope, F. K., Ayodele, I. O. (2012). A Community Survey of the Pattern and Determinants of Household Sources of Energy for Cooking in Rural and Urban South-Western, Nigeria. The Pan African Medical Journal 12 (2): 5-10.

Rahman, M. M., Haughton, G., and Jonas, A. E. (2010). The challenges of local environmental problems facing the urban poor in Chittagong, Bangladesh: A scale sensitive analysis. Environment Urbanization 22(2): 561–578.

Saaty, T. L. (1977). A scaling method for priorities in hierarchical structures. Journal of Mathematical Psychology 2(15): 234-281.

Samuel, O.A. and Silvester, O.K. (2002). Informal Settlement and the Role of Infrastructure: The Case of Kibera, Kenya. Africa Journal 14 (1): 4-9.

Shummadtayar, U., Hokao, K., Iamtrakul, P. (2013). Investigating the Low-income Settlement in an Urbanization and Urban Form. A Consequences of Bangkok Growing City, Thailand. LowLand Technology International 15 (1): 45-54.

Soyinka, O., Siu, K. W. M., Lawanson, T., Olufemi, A. (2016). Assessing smart infrastructure for sustainable urban development in the Lagos Metropolis. Journal of Urban Management 5 (1): 52–64.

Tyler, R. (2011). Incorporating Local participation and GIS in Assessing Flood Vulnerability in Informal Settlement: Masiphumulele Case Study, Unpublished MPhil dissertation, University of Cape Town, Cape Town pp 20-50.

Temiz, N. and Tecim, V. (2009). The Use of GIS and Multi-Criteria Decision-Making as a Decision Tool in Forestry. Journals of Palgrave Macmillan 1: (22) 105–123.

UN-Habitat (2003) The Challenge of Slums: Global Report on Human Settlements 2003. Earthscan, London.

United Nations Human Settlement Program (UNHSP). (2003). Facing the slum challenge in Global Report on Human Settlement – Advanced draft report; UN-Habitat, Nairobi. PP 1-10.

United Nations. (2010). World Urbanization Prospects; Revision. New York: UN Department of Social and Economic Affairs. 209 pp.

Van Teijlingen, E.R., Rennie, A.M., Hundley, V., Graham, W. (2001). The Importance of Conducting and Reporting Pilot Studies: The Example of the Scottish Births Survey. Journal of Advanced Nursing 34: (1) 289-295.

World Bank (2008). Approaches to Urban Slums: A Multimedia Sourcebook on Adaptive and Proactive Strategies. Washington D. C., USA. PP 10-15.

JJEES

JJEES (2021) 12 (2): 145-153
ISSN 1995-6681

Jordan Journal of Earth and Environmental Sciences

Architectural design solutions for combating dust storms in residential buildings (case study: Abadan City, Iran)

Amena Agharabi* and Zeinab Fard

Department of Architecture, Faculy of Architecture and Arts, University of Guilan, Iran.

Received 7 March 2020; Accepted 8 November 2020

Abstract

The practice of developing urban areas without considering climate factors has contributed to global warming, increased drought, changed the pattern of rainfalls, magnified the effects of storms and in cases, paired them with dust and particle pollutants. Considering the large share of residential spaces in the urban fabric, it can be argued that revising the design methods used in residential buildings may contribute to the quality of life for the residents, improve environmental conditions, reduce energy consumption and control pollution levels. One of the main environmental issues in the dry and humid cities of South-western Iran is the winds carrying particles and dust. Therefore, in designing residential buildings, priority must be given to the factors that help combat the unpleasant effects of dust storms and particle pollution. By studying the prevailing desirable and undesirable winds blowing into Abadan city, collecting and analyzing the structural and design data from a sample group of residential buildings located in the historic fabric of the city, and by considering the latest technological advances which help to improve the quality of life for the residents in dust-prone areas, this study suggests several solutions that offer the best combination of form and direction in planning residential spaces to preserve the natural structure of the city and minimize the unwanted effects of dust storms. Recommended design solutions include methods of optimizing ventilation in the building's open spaces and corridors, paying attention to the orientation of the building's site and optimization of the building orientation relative to the desirable and undesirable winds, careful planning of the location of windows and openings, the use of wind deflectors and re-designed wind towers.

Keywords: Abadan, Climate, Residential architecture, Environmental quality, Particle pollution

1. Introduction

Dust storms and particle pollution are among the most destructive environmental issues that today, due to the close and direct relationship between their occurrence with climate change and global warming, call for promoting the practice of designing climate-friendly habitats. Given Iran's geographical latitude range which stretches from 25° 3' to 39° 47', and considering the overall dry and semi-arid climate of over 2/3 of its area, it is of utmost importance to provide the people with favourable environmental conditions, especially in residential developments. To further zoom in, given the proximity of the southern and southwestern parts of the country to the sources of dust storms in the Persian Gulf region primarily located to the west and south-west of Iran's borders, and considering the low average annual rainfall of $342^{mm}/_{year}$ in Khuzestan province (IWRM website, 2020)which is not enough to help settle the dust, improvements in designing residential buildings can be an effective step in reducing the problem of particle pollution which disrupts people's everyday lives. The city of Abadan is one of these southwestern cities in which improvements in the design of residential buildings can effectively reduce the effects of undesirable dust-carrying wind and at the same time, utilize desirable wind for natural ventilation. In line with the goals of this paper, which is to identify and recreate climate-compatible design methods for residential developments to combat the unwanted effects of dust storms and particle pollution, this study takes an investigative look into the environmental performance of the design methods and models used in the old residential fabric of the city, the prevailing desirable and undesirable winds blowing into the city throughout the year, and combined with the theoretical foundations for climatic design strategies, proposes design solutions that can help with optimization of residential developments in terms of environmental efficiency.

2. Theoretical Foundation

2.1 Quality of the Environment in Residential Spaces

Space that is designed as residential should be in direct contact with its surroundings and provide residents with a desirable environment. Housing design methods can add value to their surroundings, or reduce it if they are undesirable (Prinz, 2016). Adding quality to spaces designed for residential use encompasses a wide range of factors. Considering the damages caused to human health by dust storms and the consequent disruption of the lives of ordinary citizens, the environmental quality of residential spaces and design methods, along with other spatial, physical and social attributes, must be addressed thoroughly and design models should be determined according to the climate factors of cities to reduce the effect of dust particles.

In areas with dust storms, people's social activities outside their homes are inevitably limited to urgent and essential matters, which means that the interiors of homes

* Corresponding author e-mail: a.agharabi@guilan.ac.ir

and complexes may become the only spaces in which they can rest and relax, carry out social interactions and enjoy leisure activities. By relying on climate-friendly design principles and certain architectural solutions to mitigate and control the effects of dust storms, architects and designers can be largely successful in increasing the scope of people's activities over a wide range of hours within residential spaces (Bahraini and Khosrawi, 2015).

2.2 The Role of Climate Change in Designing Residential Spaces

Studies on climatic models have shown a temperature increase of 0.3 to 0.6 degrees Celsius in the nineteenth century and predict that by 2100, a temperature increase of 1 to 3.5 degrees Celsius should be expected as a prominent feature of climate change (Varesi and Khosrawi, 2007). Climate change in the last few decades has had significant effects on human life and has lowered the environmental quality of human settlements by reducing rainfall, increasing droughts, weakening vegetation and bringing dust storms and particle pollution (Talebzadeh, 2015).

In designing residential spaces, human response to global warming and climate change can be effective either by adapting to the new conditions or by reducing their adverse effects on the quality of life (BMZ, 2012). As shown in Figure 1, "Climate-friendly design" as a sub-category of "environmental sustainability" is at the core of sustainable development and its methods of preserving and improving environmental quality through the use of environmental technologies can play a role in reducing the impact of particles in residential spaces (Hirmandi Niasar, 2016).

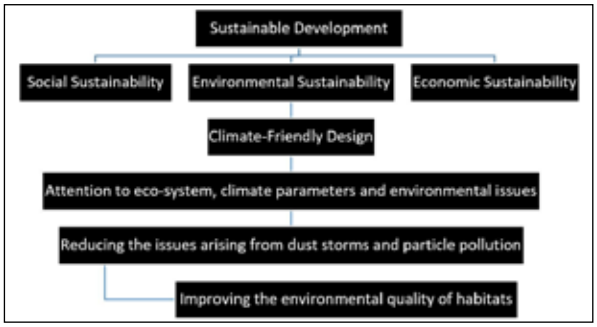

Figure 1. The Position of Climate-Friendly Design among Sustainable Development Issues (Hirmandi Niasar, 2016).

2.3 Materials

In the first stage of this case study, the current climatic features of the area have been studied and analyzed particularly concerning the issue of dust storms. Secondly, the historical climatic conditions were studied to trace back and understand the traditional methods used in the region's vernacular architecture to combat the dust problem. It was concluded then, that based on the currently available evidence and considering the aggravated problem of the dust storms both in their intensity and in frequency paired with the increasing temperature in the urban fabric, the traditional methods, despite their usefulness, cannot address the contemporary issues single handedly. They cannot also respond to the modern expectations from residential buildings nor in aesthetics neither functionality. Consequently, by studying and understanding the available technological advancements and modern solutions and fusing them with the features of vernacular architectural models used in the old fabric of the area, this study has tried to offer a solution compatible with the requirements of the modern urban fabric of the city.

3. Discussion: Site Analysis

According to the Iranian Meteorological Organization's website, Abadan is located at 30° 19' 57" N,48° 18' 8" E, and is elevated by 6.6 meters above sea level. Abadan Peninsula with its geographical location map shown in Figure 2 extends approximately 84 km from north to south along the two rivers of Bahmanshir and Arvandrood. The peninsula varies in width from 6 to 30 km (Zameni, 2015). Being part of the Khuzestan Plain, this peninsula features warm and humid climates of the southern coast of Iran and in part, shares the warm and dry central plateau climate, meaning that in general, it has a warm and semi-humid climate (Pourvahidi, 2010). Figure 3 offers a brief overview on the climatic conditions of Abadan from 1980 to 2016.

Figure 2. Location of Abadan city (Google maps).

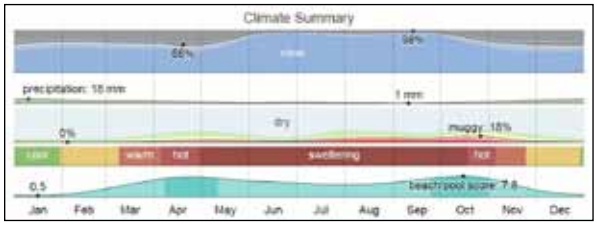

Figure 3. Climate Conditions of Abadan in Brief 1980-2016 (weatherspark.com, 2020).

Along with the severe heat and sunshine, high humidity, very low rainfall, and relatively low vegetation, winds carrying dust and particles are also considered to be among the unfavourable climatic phenomena in Abadan city. Studies have shown that with the arrival of the dust wind stream into Abadan, the density of the particles reaches 9360 micrograms/m^3 which is almost 40 times greater than the pollution standards and makes it a serious environmental threat. As such, adverse environmental effects such as general air pollution as well as the prevalence of respiratory, gastrointestinal, heart disease and other illnesses paired with lack of sunshine cannot be ignored (Tarkashvand and Kiani, 2017).

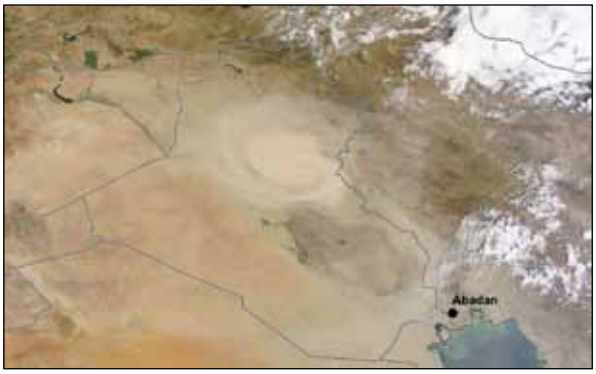

Figure 4. The dust storm, captured by NASA satellites. (NASA).

Microscopic dust particles that are lifted from drought-prone areas can travel more than a thousand kilometres through the wind to other areas. Figure 4 shows an example of dust storm formed in Northern Iraq and captured by NASA satellites. The northwest winds, as well as the wind coming from the western region of Baghdad and Hoor al-Azim, have been identified as major forces of dust storms in southwestern Iran, especially during the summer months (Mofidi and Jafari, 2011). Studies have shown that the most frequent occurrence of dust storms in the southwestern part of Iran, including Abadan, takes place during summer and decreases in spring, winter and autumn respectively. The highest rate is in mid-July and August and then in June (on average about 15 days) and the lowest in mid-December to mid-February. The highest intensity of dust and particles have been recorded between 9 am and 6 pm, usually followed by a gradual decrease in the amount of dust, and the lowest rate is recorded late at nights and early in the mornings (Azizi et al., 2012).

It should also be noted that the reduced field of view caused by high dust levels shortens the hours of outdoor activities as well as the presence of people outside their homes. This means that the leisure time for families gets almost eliminated, which in turn may have detrimental effects on people's mental health.

To achieve a proper design model that can address the issues caused by the dust phenomenon, the condition of the winds blowing into the city, especially the prevailing wind, must be examined.

The Wind Rose of Abadan city illustrated in Figure 5 shows that the winds are mostly blown in from the northwest, west and southeast of the city, classified into three general groups as per the following:

1. The Northwest wind is the Prevailing wind in the city, which is referred to as the North wind by the locals and blows during almost all months of the year. The constant dry wind that drives the Mediterranean flows into the city generally lasts for 9 months, and peaks from mid-June to mid-September. During some summer months, especially from mid-June till late July, the north wind lowers the intensity of mid-day humidity and makes the heat more tolerable compared to August and September which are characterized by high winds and humidity. The persistence of the wind is higher in late March to mid-June and its speed reaches its peak in summer. Another important point is that for most of the year since the wind passes through arid and hot regions, it is often associated with dust and particles, which greatly reduces the quality of the city's air.
2. The winds coming from the West of the city called "Samoum" or "Sam" are the second most frequent winds and blow in from the Saudi Arabian deserts with a high concentration of soil and sand and every once in a while, pollute Abadan's air in the early hours of the morning. Due to the intense heat that it carries, this wind may cause dehydration for a lot of residents, particularly when it is paired with severe sunlight. In recent years, these winds carrying dust and particles have been reducing the environmental quality of the city and disrupting living conditions.
3. The South-east wind is one of the most significant winds. Since it passes over the Persian Gulf, it brings in high humidity levels and is referred to as the "temperate wind".This wind is desirable from late winter to mid-spring as it blows into the city like a cool breeze and due to its humidity, it is often combined with clouds, fog, and even rain. The highest intensity of this wind is between mid-March and mid-May. But the same wind, with the advent of the hot summer months, especially in August and September, becomes an undesirable one which in combination with the high temperature, causes dramatic changes in the city's air. This may cause breathing difficulties and respiratory problems for the people.

Paying attention to the angular range and direction of the prevailing winds into the city as per the Figure 6 can help in choosing the optimal direction of the passages and buildings to improve the environmental quality of the residential fabric and increase the comfort level of the residents.

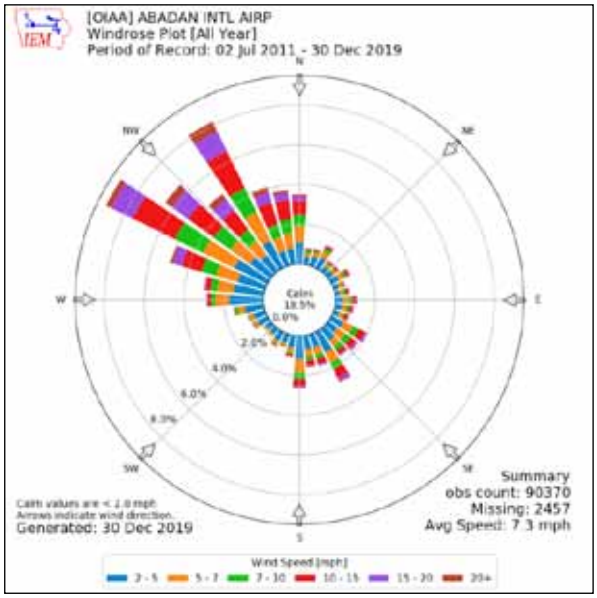

Figure 5. Speed and Direction of Wind in Abadan, 2011-2019 (Iowa Environmental Mesonet Website, 2020).

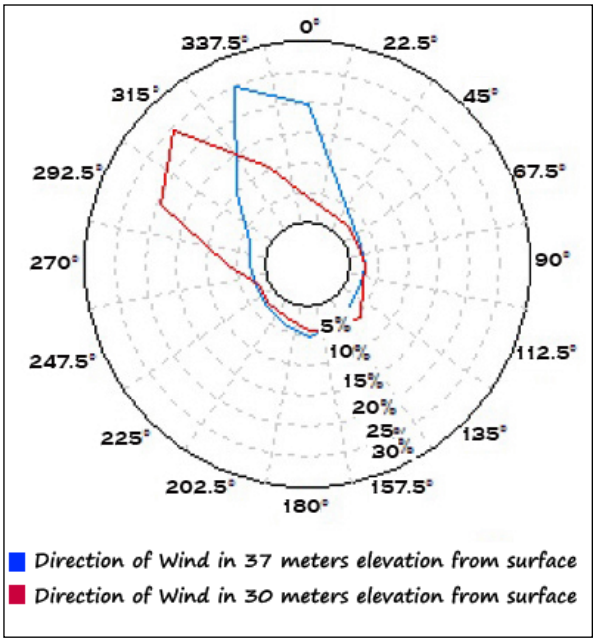

Figure 6. Direction of prevailing winds blowing into the city (Nedaei, 2012).

3.1 Role of the Wind in Designing Residential Spaces

How winds blow is influenced by the velocity, direction, intensity and quality of the airflow, and pollutants they carry. Their impact on the environmental quality of residential spaces has long been in direct contact with the urban built environment formed by the combination of mass and open spaces. The more the structure and composition of the built environment are in line with the information obtained from the city's Wind rose, the better the productivity of desirable winds and the less the impact of adverse winds. If buildings are of non-similar position and altitude in residential areas, they interrupt the direction and velocity of the airflow that will disturb residents in corridors -and even indoors-, while they inadvertently concentrate or release pollutants, reduce the thermal comfort of people and increase the costs of heating and cooling systems in buildings (Khodakarami and Asgari, 2014).

Figure 7 shows the effective range of winds on the ventilation relative to the two fronts of a given rectangular building. The maximum impact of wind on indoor airflow is when the wind angle relative to the building is between 45 and 90 degrees. If the wind blows at less than 25 degrees to the building, it will not affect the flow and the wind cannot penetrate the building (Afshari, 2012). In such a case, the building is said to be "in the shadow" of the wind, which is the best position in order to shield the building from the undesirable wind.

Wind Towers(or windcatchers) are among the most prominent examples of integration of wind in the design of traditional Iranian residential spaces and have been designed and implemented for centuries in different shapes and structures for ventilation and cooling in hot and dry or humid areas. The first examples of these Wind Towers date back to about 1,200 years ago in hot and dry regions of Iran, and later on, they spread to other countries in the Middle East and Egypt.

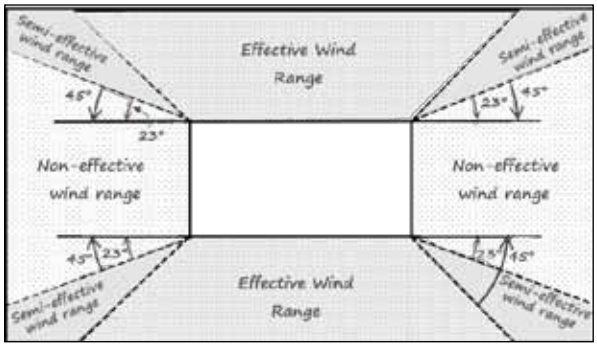

Figure 7. The effective range of winds on the ventilation relative to the two fronts of a rectangular building (Afshari, 2012).

Wind Towers come in 4 main categories:

1) One-sided Wind Towers, 2) Double-sided Wind Towers, 3) 4/6/8-sided Wind Towers, and 4) Cylindrical Wind Towers. As urban spaces in Abadan began to develop mimicking the western styles, the use of wind towers like the ones in the cities with similar warm and humid climates, such as Bushehr and Band Abbas, became less frequent. As we will discuss the matter further, it can be claimed that applying wind towers and modifying their mechanism to suit the climate of the city of Abadan will significantly improve the volume of natural ventilation in buildings. At the same time, it should be noted that the traditional wind towers, while effective to some extent, we're not flawless. If used in contemporary design, they need to be re-calibrated to meet the current climate conditions of each region. Possible flaws which need rethinking include:

1. Possibility of small birds and insects entering into the wind tower and subsequently, the building,
2. The uncontrolled entry of dust and particles into interior spaces,
3. Static nature of the crater structures and the lack of the possibility to turn the structure toward the Prevailing wind in different months,
4. Spatial limits; Limited number of Wind Towers can be used in a building,
5. Inefficiency; Some of the air may flow in and out of the Towers without getting into the building,
6. Low performance in areas with very low wind speed, and
7. Severe erosion against rain, wind and sun.

3.2 The role of wind in the design of the historical fabric of the city

Our field study on the design models and architectural methods used in the historical fabric of the city indicates that in the old days, since the winds carrying dust and particles did not constitute a major issue, climate-friendly features used in the buildings were aimed at boosting ventilation, maximizing the natural airflow, and reducing the heat and humidity inside the buildings. However, no measures were taken to combat dust and particles as the levels of dust were much lower.

3.2.1 General spatial structure and design features of the historical fabric of the city

Table 1. General spatial structure and design features of the historical fabric of the city.

Structure and Design Feature	Implementation Quality	Advantages and Disadvantages
Spatial Density	Semi-dense with high spatial extent	Advantage: Increases the chance of ventilation and reduces humidity
The ratio of the width of corridors to the height of walls	Relatively High	Advantage: Higher ventilation, Lower humidity Disadvantage: Uncontrolled natural light, requires shading
Dominant orientation of buildings and corridors	East-West	Advantage: Proper intake of sunlight and desirable wind
The volume of Green and Open Spaces (Private and Public)	High	Advantages: High per capita green space /High density of vegetation / Preservation of biodiversity / Strengthening the morale of the residents / Humidity and Temperature adjustment /Satisfaction of the residents
Number of floors	Few (1 or 2)	Advantages: Appropriate population density in residential areas / Lower Heat Island effect usually caused by activities of refineries and petrochemical complexes
Height of interior spaces	Relatively high	Advantage: Increases the chance of ventilation and reduces the temperature Disadvantage: Heating becomes difficult during winter
The ratio of openings to the surface of buildings	Relatively high	Advantage: Ease of airflow and natural ventilation to reduce humidity and temperature Disadvantage: Unwanted absorption of more heat during the warmer seasons of the year

3.2.2 Traditional small-scale design models in the old fabric of Abadan city

Below are the most significant design features in the old fabric of the city which encourage better ventilation and counter the heat and possibly, humidity:

1. Large windows at the bottom and smaller openings on top of them. As pictured in Figure 8, smaller openings are located underneath the ceiling to vent the warm air out (In recent years, all of these ventilation openings have been blocked due to heavy dust).

Figure 8. Openings for inflow and outflow of the air.

2. Positioning the rooms with high ceilings aligned with the direction of the wind and limiting the height of the buildings to two stories which will not block the wind, for better use of the airflow.

3. Narrow windows and openings designed to facilitate two-way ventilation and lower humidity. These are covered by wood, plaster or brick netting to create shade while allowing the airflow to pass through.

4. Use of aerodynamic surfaces in some parts of houses (especially in the Southern Buvardeh neighbourhood, as shown in figure 9) to direct the wind to the openings as much as possible.

Figure 9. Aerodynamic surface to direct wind (Abadantimes Website, 2019).

5. Combining shades with airflow by expanding the ceilings and porches and lattices of the porch to allow the wind to pass through and reduce the temperature of the air flowing into the interior. Examples of this can be seen in figures 10 to 12..

Figure 10. Lattice of porches (Abadantimes Website, 2019).

Figure 11. Arches of the entrance porch.

Figure 12. Shades over the northern façade at the building's entrance, Fabric of "Bahmanshir"1950´s (PMDC, 2020).

6. Maximum use of green spaces: In designing the old residential fabric of the city, pictured in figures 13 and 14, British designers tried to implement the Garden City model. Making maximum use of vegetation for the comfort (physical and mental) of the residents, along with the low density of buildings and the ability to spend leisure time around the residential fabric, have played an important role in reducing temperature and humidity.

Figure 13. Fabric of "Braim" neighborhood - 1950´s (PMDC, 2020).

Figure 14. Fabric of "Braim" neighborhood - 1950´s (PMDC, 2020).

4. Solutions

Considering the desirable and undesirable prevailing winds, the main design features of the old residential fabric of the city which have been abandoned due to the increase of dust and particle in the wind, and in line with the need of the residents to enjoy residential spaces with desirable environmental quality in the currently unfavourable climatic conditions suffering from the effect of dust and particles, the following solutions are suggested:

1. Improvements in design and organization of open spaces and corridors: It is best to build corridors parallel to desirable winds to attract and direct them to target spaces. At the same time, corridors that cross the wind's path can provide shelter against dusty winds and reduce the rate of intake of pollutants. In Abadan, due to the high humidity in summer and the need for airflow to reduce humidity, it is recommended to use passages with near-perpendicular angles along the winding paths, so that while the distribution of wind is carried out in a controlled manner, entry of particles and dust pollution is also minimized. The location and dimensions of the squares and intersections, which attract the wind and divide it into adjacent corridors, also depend on various factors such as wind speed, direction and angle, shape and dimensions of squares and intersections, and network structure of the crossings which connect to open spaces, that must be designed and structured according to the wind situation in the city.

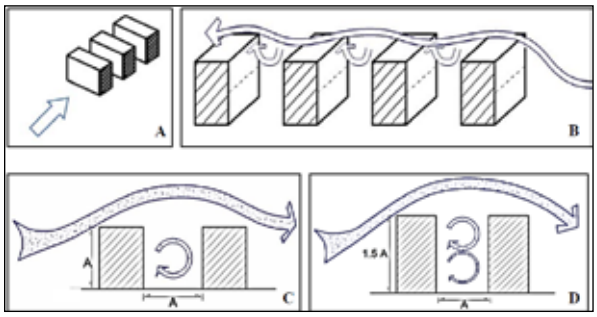

Figure 15. The rotation of the wind in different modes of corridors crossing and blocking the wind's direction (Abbaszadeh et al., 2014).

As per the illustration in Figure 15, the higher the ratio of height to width of a corridor, the better the protection against dust, while increasing the number of rotations at the cross-section and decreasing its intensity at lower rotations also prove beneficial. The optimum width to height ratio for reducing dust is between 1.5 to 1~ 2.5 to 1 (Abbaszadeh et al., 2014). To reduce the speed of the wind which carries dust and decrease the concentration of pollutants, it is advisable to gradually increase the width of the corridors relative to the crater or to change the width of the corridor in different places. Considering the intensity of sunlight in Abadan, the ratio of width to height of 1 to 2 ~ 1 to 4 is suggested (Abbaszadeh et al., 2014).

2. Appropriate orientation and form of building masses on site: Important spaces should be located on the opposite side of the building which is shielded from the dusty wind. Due to the association of wind speed with the deposition of dust particles, and the decrease in air velocity on the opposite side of the building relative to the

wind, the suspended particles remain sediment and will not be transferred to other parts of the site. Otherwise, important spaces should have properly filtered openings. Placing buildings in the shade of the undesirable wind will be another way to deal with the negative effects. Proper design and alignment of building blocks relative to each other can, even in the absence of sufficient airflow, create high-pressure and low-pressure areas in different parts of the structure, enabling accelerated airflow and better ventilation.

3. Paying attention to the structure of building blocks relative to the open spaces: Generally, in the warm and semi-humid region of Abadan, the semi-dense, semi-enclosed fabric and the relative interconnectedness of the construction blocks seem to be the most appropriate form of climate-friendly urban design. To control the winds carrying dust, the positioning of the taller building blocks should be carefully planned. Given the effect they have on the absorption and distribution of the winds blowing above the surface of the residential area, they must be placed on the edge of intersections and open spaces.
4. Optimal orientation of buildings relative to the wind: To decide on the optimal orientation of buildings to reduce the unwanted effect of winds carrying dust, attention to the direction of winds alone is insufficient. The climatic condition of the city which makes higher radiation and moisture loss in residential areas inevitable must also be taken into consideration; this means that airflow, especially in the summer, along with the reduction of the effect of the particles, is necessary. The proposed angle of orientation of the building as demonstrated earlier in Figure 7 covers a range of east-west up to 22.5 degrees southeast.

   However, due to the adverse conditions caused by winds carrying dust on the indoor air quality, some spaces can be re-orientated following the pattern of the wind-flow and the openings can get rotated to fit the desired angle of solar radiation relative to the building block.
5. Revising placement of windows and openings: Windows and openings should be moved away as far as possible from the walls facing the dusty winds, or get reduced in number and area on this front and get embedded on the opposite wall or at an angle opposite to the wind. Placing shades around the openings can also help reduce the impact of undesirable winds and improve the air quality inside the buildings.
6. Using external movable awnings: During a dust storm, awnings can allow the daylight in, while they are shut and prevent particles from entering the interior. These awnings can be made of opaque or thin glass material for the light to easily pass through.
7. Using wind deflectors: A wind deflector is most effective when it is 1.5 to 2.5 times the height of the building that it is protecting (Afshari, 2012). Studies have shown that a wall against the wind will reduce the wind speed by 15 per cent, and the maximum reducing effect over the wind by such a barrier equals 2 to 7 times its height. Also, to control the penetration of dust, a barrier of 1.7 meters high with a distance of fewer than 6 meters from the building can work effectively (Afshari, 2012). It should be noted that the windshield should not be completely impenetrable so that a low-pressure void will not be created on the less windy side of the building (Freidman, 2017). The density and structure of vegetation used as a wind deflector are the main factors that can reduce the severity of the devastating effects of dust storms. With proper design and layout, indigenous plants can provide spatial design and define margins for facing the winds, which considering Abadan's winds, can be suggested as per the Figure 16:

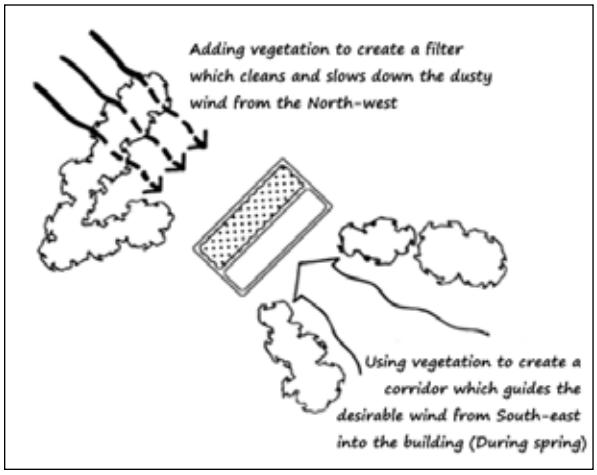

Figure 16. Low and high density of vegetation to control desirable and undesirable winds.

8. Designing an integrated shell in public spaces: This can stop or reduce the penetration of particles and dust. Such a facility could increase residents' willingness to be present in the building's outdoor spaces and promote leisure and social interactions between residents. These overall shells can be designed to incorporate transparent and non-transparent plates depending on the amount of light required in public spaces, and come with fixed and movable parts so that once the weather is fine, airflow from the outside will be possible. Examples of such shells have been well used in the Arab countries of the Persian Gulf to combat dust and particle issues by using the latest technology. These shells, illustrated in Figure 17, allow people to enjoy outdoor activities even in unfavourable climate and during dust storms.

Figure 17. Transparent overall shell in King Abdullah complex, Saudi Arabia (carloratti Website).

9. Using auto-cleaning glass and material: On a large scale, to reduce water consumption needed to clean surfaces from dust.

10. Using re-designed wind towers with filters: By combining the features of traditional wind towers with the world's latest technology, and with the correct orientation of the wind tower's openings, the wind can be trapped at optimum speed and utilized for natural and desirable ventilation. Wind towers can also operate as solar chimneys. Using innovative design methods, such as installing dark-coloured solar panels on the opposite side of the vent or by using a glass or transparent wall in the chimney body to absorb more heat, a warm air mass will be created at the top of the tower and as a result of the chimney effect, hot air gets directed outward from the building with better efficiency. Figure 18 shows the design for such a wind tower with wetted surface and a solar chimney. By improving natural ventilation in the warm months of the year which extend for a long time in the city of Abadan, will reduce the amount of energy used to cool the buildings.

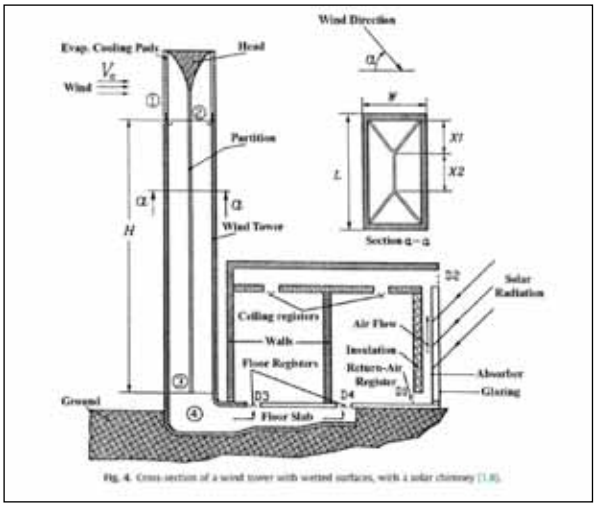

Figure 18. Wind tower with wetted surface and a solar chimney (Dehghani-Sanij et al., 2015).

On the other hand, given the high likelihood of the presence of dust and particles in the winds and the necessity of blocking them from entering the indoor space, the wind tower inlet vents must be versatile and allow opening and closing when necessary. There must also be a multi-stage filtering system mounted both at the inlet and on the walls of the tower so that clean and fresh air can flow indoors. To achieve this, redesigned wind towers updated with new technologies can be utilized which are more efficient in terms of climate-adaptability. Suggested solutions in redesigning different parts of the wind towers include:

Top of the wind tower: By incorporating a movable column or a hinge in the top part of the wind tower, this part, while separated from the body, allows the tower to be opened or closed manually or automatically, or get rotated depending on the climate, allowing it to rotate toward the prevailing wind depending on its direction. A weather vane can be used to correctly rotate the top part of the wind tower toward the desirable wind. It is best to design a pitched roof for the tower to prevent water and dirt from penetrating the structure during rainy days (Dehghani-Sanij et al., 2015).

Body of the wind tower: By using a reel mounted on the inside of the body of the wind tower, it becomes possible to easily rotate the wind tower's top part over its body toward the desired direction. Besides this, the placement of several filter sheets for fine solid particles and dust at different heights of the wind tower's body helps to better refine the quality of the air entering the building.

Openings of the wind tower: It is necessary to be able to open and close the vents using movable plates so that it will be possible to control the inflow of air. It is also advisable to use a fixed lattice plate to prevent the entry of small birds and insects (Dehghani-Sanij et al., 2015).

Samples of such redesigned wind towers are presented by Iranian researchers, two of which can be seen in Figure 19:

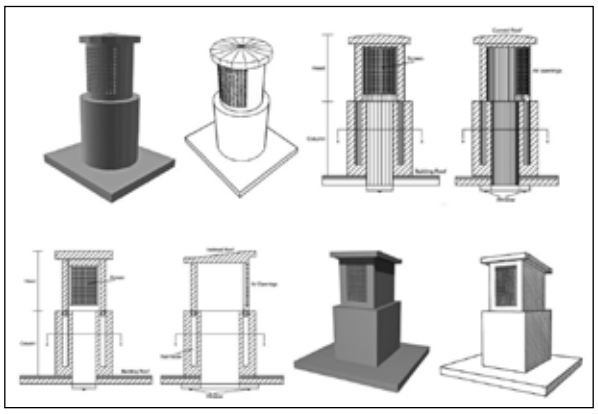

Figure 19. Sample of redesigned adjustable wind towers with filters (Dehghani-Sanij et al., 2015).

Due to the general form of wind towers in warm and humid regions of Iran, low, wide and short forms are recommended for the structure of the towers. However, in a more detailed view, wind towers' dimensions are affected by 4 factors:

1. The amount of airflow required for air conditioning and thermal comfort
2. Dimensions of the building and the building's material
3. Volume and intensity of the wind in each area
4. Security of the building (Dehghani-Sanij et al., 2015).

5. Conclusions

The study carried out on the design features of the historic fabric of the city shows that in the past, a good number of measures had been taken to utilize the wind for natural ventilation. Even though the city enjoys a good amount of natural airflow, the use of the wind towers and traditional design of openings have been abandoned due to their inefficiency against the increasing amount of dust and particles carried by the wind. To create an innovative model in all cities of this region with problems similar to that of Abadan's, integrating the traditional solutions with the latest technological advances can help in re-designing these particular features, such as wind towers, to promote eco-friendly and dust-free ventilation in residential buildings.

Other eco-friendly solutions suggested such as transparent shells and improved shading can help in controlling the intake of sunlight in public spaces of residential buildings and complexes.

Controlling the effects of particles and dust on the outdoor areas of residential buildings also allow people to enjoy being outdoors while the air quality is not within the comfort zone due to pollution. This leads to an increase in the hours of outdoor activity and allows optimum comfort and leisure time in a semi-outdoor environment.

The proposed solutions presented in this study are based on the integration of previous empirical research with the natural conditions of the city and the present problems caused by particle pollution and dust. The efficiency of each solution can be evaluated in future studies and become a foundation for generating innovative design models based on the climate of Abadan and similar cities.

References

Abadantimes Website. 2019. Abadan: Oil City Dreams and the Nostalgia for Past Futures in Iran (Part One and Two). [Online] Available at: https://abadantimes.com/2018/04/15/ [Accessed 27/02/2019].

Abbaszadeh, Sh., Zolfaghari, Gh., Pajouhankia, M. (2014). Investigating the role of wind in the arrangement of spatial-physical structure of warm and dry - warm and humid cities (Case study: Zabol and Bushehr cities). Journal of arid regions geographic studies 4 (15): 53-69.

Afshari, H. (2012). Designing a residential complex compatible with Iran'shot and semi-humid areas; Case study of Khorramshahr city. Tahan Publications. Tehran, Iran.

Azizi, Gh., Miri, M., Nabavi, S. (2012). Tracing the dust phenomenon in the western half of Iran. Journal of arid regions geographic studies 2 (7): 103-118.

Bahraini, S. and Khosrawi, H. (2015). Comparative study of sub-ecological characteristics in urban behavioral patterns. Case study: Urban spaces of cities of Yazd (warm and arid climate) and Fouman (temperate and wet climate). Journal of Environmental Studies 41 (2): 465-482.

BMZ (Federal Ministry for Economic Cooperation and Development) (2012). Land Use Planning (Concept, Tools and Applications). Published by Deutsche Gesellschaft für Internationale Zusammenarbeit (GIZ) GmbH, Bonn and Eschborn, Germany.

Carloratti Website. (2010). KA Care. [Online] Available at: https:// carloratti.com. [Accessed 27/11/2018].

Dehghani-Sanij, A. R., Soltani, M., Raahemifar, K. (2015). A new design of wind tower for passive ventilation in buildings to reduce energy consumption in windy regions. Journal of Renewable and Sustainable Energy Reviews (42): 182-195.

Freidman, A. (2017). Fundamentals of Sustainable Neighborhoods. (H. Moztarzadeh Trans.) Tahan Publications. Tehran, Iran.

Hirmandi Niasar, M. (2016). Architecture and sustainable development and their relations with human and nature. SHABAK Journal 2 (4-5): Vol 4. Art and Architecture studies.

Iowa Environmental Mesonet Website (2018). Wind Roses. [Online] Available at https://mesonet.agron.iastate.edu/sites/windrose.phtml?network=IR__ASOS&station=OIAA

IWRM (Iran Water Resources Management Company) Website (2020). Annual Rainfall Report for all Provinces. [Online] Available at: http://wrs.wrm.ir/m3/gozareshOstan.asp [Accessed 27/07/2020].

Khodakarami, J. and Asgari, S. A. M. (2014). Physical Properties of the City and its Impact on the Urban Climatic Properties. Third International Conference on New Approaches to Energy Conservation (ETEC03). [Online] Available at https://bit.ly/333NpSz

Mofidi, A. and Jafari, S. (2011). Investigating the role of regional atmospheric circulation on the Middle East in the occurrence of summer dust storms in southwestern Iran. Journal of arid regions geographic studies 2 (5): 17-45.

Nedaei, M. (2012). Wind Resource Assessment in Abadan Airport in Iran. Int. Journal of Renewable Energy Development 1(3): 87-97.

PMDC (Petroleum Museums and Documents Center) Website (2020). [Online] Available at: http://www.petromuseum.ir/content/25/ [Accessed 27/07/2020].

Pourvahidi, P. (2010). Bioclimatic analysis of vernacular Iranian architecture. Master's degree dissertation. The Institute of Graduate Studies and Research, Eastern Mediterranean University.

Prinz, D. (2016). Foundations of urban design Vol.1 (S. Shafiee Trans.) Science and Knowledge Publications. Tehran, Iran.

SOAS Research Online Website (2020). [Online] Available at: https://eprints.soas.ac.uk/17966/2/documenting-the-modern-oil-city.asp [Accessed 27/07/2020].

Talebzadeh, M. (2015). Ecological solutions for controlling the dust in south-western parts of Iran. The first International Conference on dust, Chamran University of Ahwaz, Iran.

Tarkashvand, M. and Kiani, M. (2017). Analysis of the air pollution caused by particles and dust storms in southern parts of Hamedan province. Journal of Environmental Science and Technolgy 19 (4): 80-97.

Varesi, M. and Khosrawi, H. (2007). The role of human factors in climate change and a study on its effects. Geographical Space 7 (20): 131-152.

Weatherspark Website (2018). Average Weather in Abadan-Iran-year Round. [Online] Available at https://weatherspark.com/y/104591/Average-Weather-in-Abadan-Iran-Year-Round.

Zameni, M. (2015). Defining a schema for vernacular eco-friendly architecture (case study: Abadan city). ACOB 2015 Conference of Mashhad. [Online] Available at https://www.sid.ir/Fa/Seminar/ViewPaper.aspx?ID=21853.

JJEES

JJEES (2021) 12 (2): 154-162
ISSN 1995-6681

Jordan Journal of Earth and Environmental Sciences

A designed model for identifications of *Dicarinella concavata* (Brotzen, 1934) and *Dicarinella asymetrica* (Sigal, 1952) planktic foraminifer species under thin sections: an example from the Kurdistan region, NE Iraq

Rawand Bakir Noori Jaff

Department of General Sciences, College of Education and Languages, Charmo University, Chamchamal, Kurdistan Region, Iraq.

Received 11 August 2020, Accepted 21 November 2020

Abstract

The Upper Cretaceous (Early Turonian-Early Campanian) Kometan Formation in the Kurdistan region, NE Iraq has been investigated in detail for planktic foraminiferal identifications under thin sections especially focused on the species *Dicarinella concavata* and *D. asymetrica*. The two mentioned index planktic foraminifer species for Late Turonian-Latest Santonian biozones are commonly misidentified under thin sections. For this reason, a designed model has been suggested for correct identifications between the two above mentioned species. The model shows that the *D. concavata* can be identified by steep concave spiral side and by having hemi-spherical and/or ovate early and final chambers profile. However, *D. asymetrica* can be distinguished in having flat to slightly concave spiral side, sometimes strongly convex, and early and final chambers are angular. The accurate identifications of the above index planktic foraminiferal species play a great role in the precise age determination of the Upper Cretaceous lithostratigraphic units.

Keywords: Late Cretaceous, *Dicarinella concavata*, *Dicarinella asymetrica*, Kurdistan region, NE Iraq

1. Introduction

The Upper Cretaceous (Late Turonian-Latest Santonian) *Dicarinella concavata* (Brotzen, 1934) and *D. asymetrica* (Sigal, 1952) are the two most Tethyan cosmopolitan planktic foraminiferal species, which received great attention from biostratigraphers in the last decades. *Dicarinella concavata* Zone was originally defined as the interval between the first appearances (FA) of *D. concavata* to the FA of *D. asymetrica* (Sigal, 1955). On the other hand, *D. asymetrica* is a total range zone and was first used by Postuma (1971). His *Globotruncana concavata carinata* Zone, by synonymy, is equivalent to the *D. asymetrica* Zone. Afterwards, both species were successfully used from biostratigraphers for Late Cretaceous biozonations and inter-regional correlations (e.g., Barr, 1972; Caron, 1985; Sliter, 1989; Almogi-Labin et al., 1991; Premoli Silva and Sliter, 1994, 1999; Robaszynski and Caron, 1995; Robaszynski, 1998; Robaszynski et al., 2000; Premoli Silva and Verga, 2004; Babazadeh, 2007; Sari, 2006, 2009; Farouk and Faris, 2012; Elamri et al., 2014; Jaff et al., 2015; Georgescu, 2017; Petrizzo et al., 2017; Faris et al., 2019; Fang et al., 2020; Honarmand et al., 2020; Jaff and Al-Kahtany, 2020; Jaff and Lawa, 2020). Due to the morphological similarities, several published articles indicate that the two species are commonly misidentified under thin sections and/or even sometimes as picked specimens. The objective of this study is to illustrate a designed model for accurate identifications between the two species under thin sections in the Kurdistan region, NE Iraq which might be used globally. The precise documentation of the above index planktic foraminiferal species plays a great role in better identification for the age of the Upper Cretaceous lithostratigraphic units.

2. Geological Setting and Lithostratigraphy

From structural perspective point of view, the selected sections can be allocated into two main tectonic zones which are separated from each other by major basement faults (Lawa et al., 2013). Accordingly, the Azmer section is situated in the Zagros Imbricate Zone (ZIZ) of Iraq, while the Dokan section is located in the Zagros High Folded Zone (ZHFZ) (Lawa et al., 2013; see Figure 1).

The ZIZ is intensively deformed and characterised by rock displacements and crustal thickening. Based on geomorphologic features, it is characterised by high mountains with deep-incised valleys and is a product of imbricate thrust sheets and NE-dipping thrust faults. The present structural characteristics of this zone are a result of ophiolites obduction in Late Cretaceous and Arabian-Iranian plates' collision in Late Paleogene (Lawa et al., 2013).

The ZHFZ is mainly characterised by asymmetrical, double plunging, convergent and divergent folds. Additionally, other distinctive features of this zone are NW-SE trending and SW dipping thrust faults (Lawa et al., 2013).

The Kometan Formation is broadly distributed in northeastern Iraq and is equivalent to the Khasib; Tanuma and Sa'di formations in central and southern Iraq (Figure 2). Recently the formation is dated back to the Early Turonian-Early Campanian time (Jaff et al., 2015; Jaff and Lawa, 2020).

* Corresponding author e-mail: rawand.noori@charmouniversity.org

Figure 1. Tectonic divisions in NE Iraq modified after (Lawa et al., 2013). The locations of the Dokan and the Azmer sections are shown in black circles.

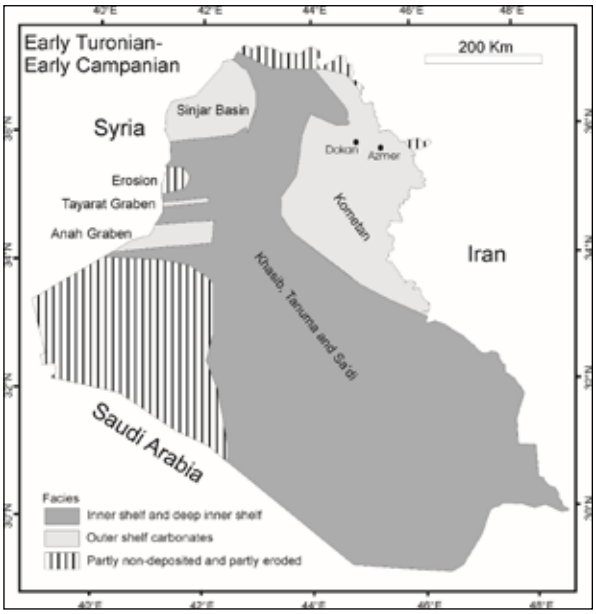

Figure 2. Paleogeographical map of Iraq during (Early Turonian-Early Campanian) with different facies and palaeoenvironments. The locations of the Dokan and Azmer sections are also shown (after Jassim and Goff, 2006).

3. Material and Methods

The present study is based on 113 samples collected from the Coniacian-Santonian pelagic limestones of the Kometan Formation in the Kurdistan region, NE Iraq. Two different localities have been selected; one at Azmer (35° 37' 30"N; 45° 31' 45"E) and the other at Dokan (35° 56' 15"N; 44° 57' 21"E; see Figure 1). First, the author tried to extract planktic foraminifera from pelagic limestones using liquid nitrogen (LN_2) method developed by (Remin et al., 2012). After several tries, the method was unsuccessful which might be related to the low quality of (LN_2) that we applied. Finally, a standard thin section size (48X28mm) prepared in MiEKiNiA Lab in Warsaw, Poland was used for planktic foraminiferal identifications. Most of the diagnostic criteria that can be used for correct planktic foraminiferal identification can be documented in axial and subaxial sections (see Figure 3). The important characteristic features that can be recognised under thin sections include the shape of the test and position and a number of marginal keels (Sliter, 1989; Sari, 2006, 2009). The images illustrated in this paper are all axial sections and were photographed with a digital Canon camera (DS126201) at the University of Leicester, UK.

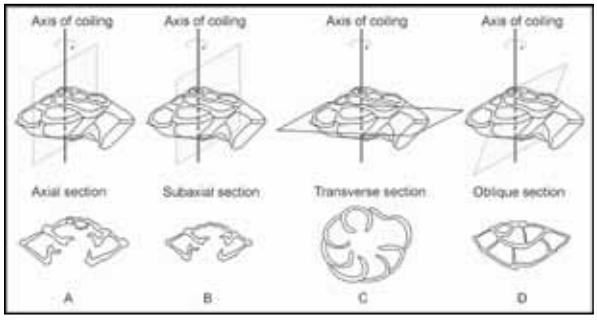

Figure 3. Planktic foraminifera test under thin sections. (A) Axial section: section passing through the axis of coiling; (B) Subaxial section: section passing parallel to the axis of coiling but not passing through the proloculus; (C) Transverse section: section passing perpendicular to the axis of coiling; (D) Oblique section: section passing neither parallel nor perpendicular to the axis of coiling (after Sari, 2006).

4. Taxonomic Notes

Planktic foraminifera noticed in the pelagic limestones of the Kometan Formation (*D. concavata* interval zone and *D. asymetrica* total range zone) are frequently abundant and have moderate diversity. Several published articles indicate that there are misidentifications between the *D. concavata* and the *D. asymetrica* species. For this reason, the present author designed a model to describe the materials in the Kurdistan region, NE Iraq and it might be used in global identifications as well (see Figure 4).

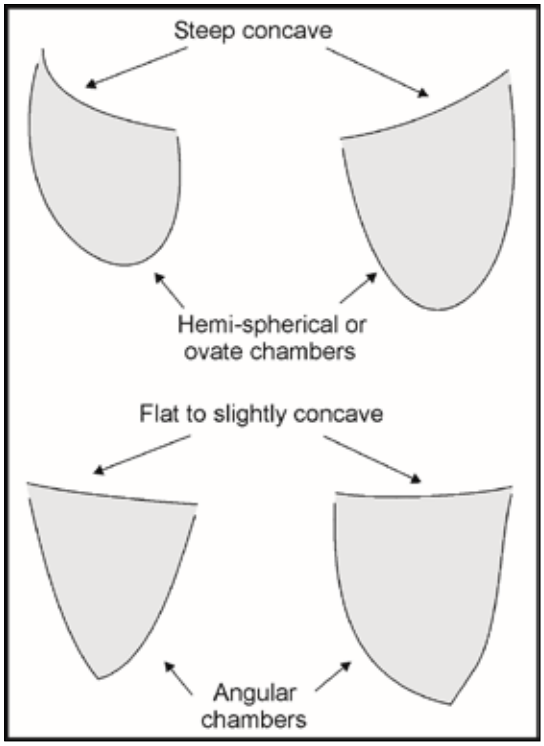

Figure 4. A designed model shows the morphological differences between *Dicarinella concavata* (top) and *Dicarinella asymetrica* (bottom) under thin sections.

The present model shows the most important characteristic features of the two species that can be easily recognised under thin sections. Furthermore, below are the original descriptions and illustrations of the holotype figured specimens of the two species by (Brotzen, 1934; Figure 5) and (Sigal, 1952; Figure 6) which are used for making strong correlations between our recorded materials in this study. Additionally, all the documented associated planktic foraminiferal species within the *D. concavata* and *D. asymetrica* zones in the Dokan and the Azmer sections are also shown in (Figures 7-8).

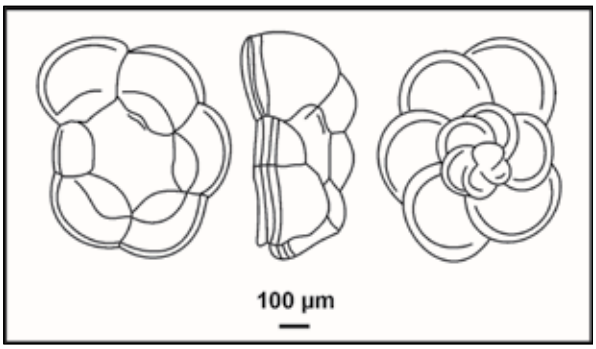

Figure 5. Holotype figured specimen of *Dicarinella asymetrica* by (Sigal, 1952).

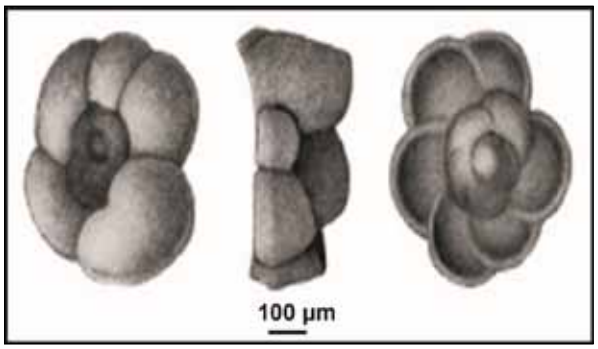

Figure 6. Holotype figured specimen of *Dicarinella concavata* by (Brotzen, 1934).

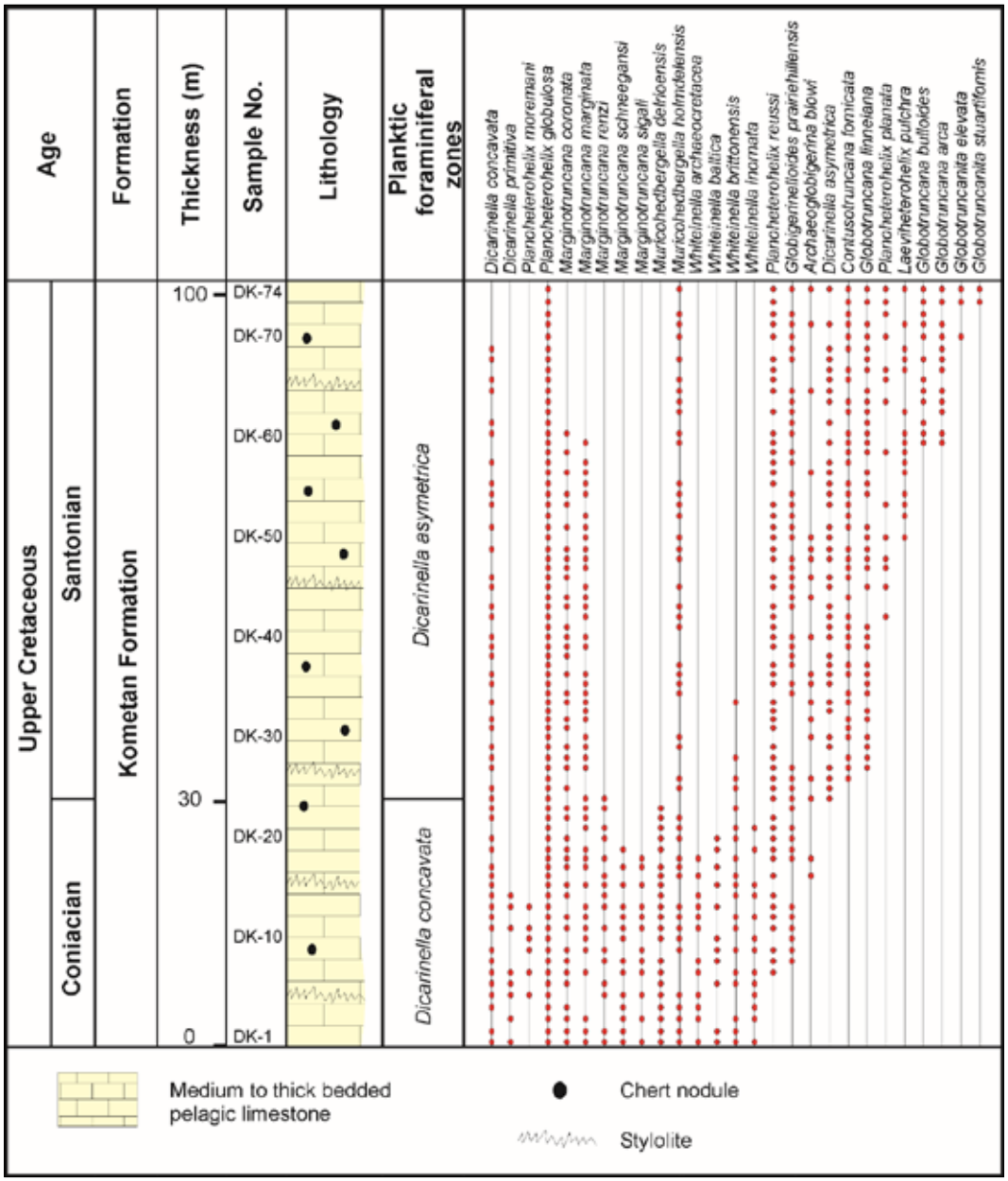

Figure 7. Coniacian to Santonian stratigraphic ranges of planktic foraminiferal species for the Kometan Formation in the Dokan section.

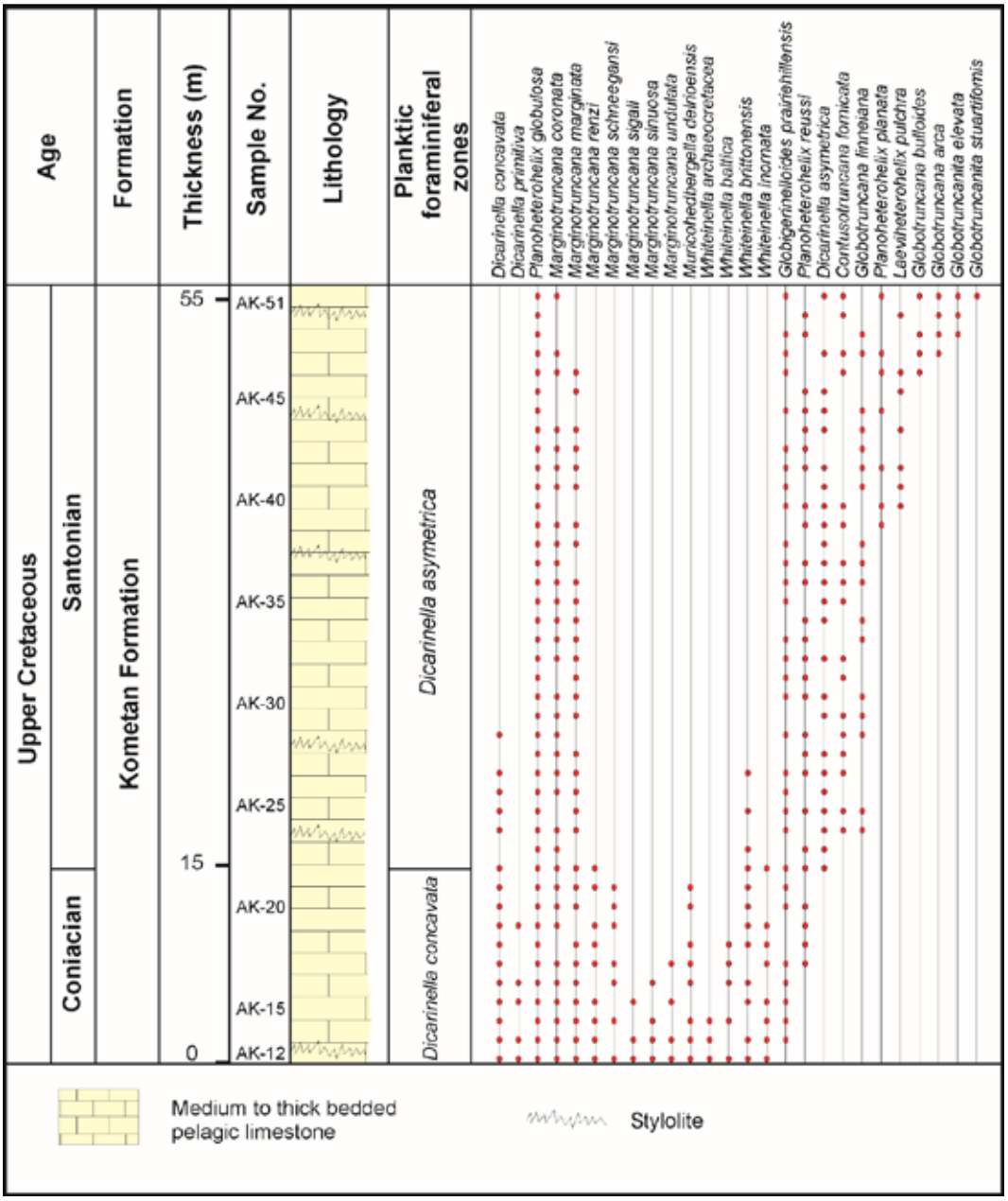

Figure 8. Coniacian to Santonian stratigraphic ranges of planktic foraminiferal species for the Kometan Formation in the Azmer section.

Genus *Dicarinella* PORTHAULT in DONZE ET AL., 1970

***Dicarinella asymetrica* (Sigal, 1952)**

Figure 9 (A-J)

Original description: *"En même temps se développe une autre espèce caractéristique par sa profonde dissymétrie du test, qui n'est pas sans présenter quelque analogie avec certains Rotalipora du Cénomanien (R. reicheli Mornad par example)".*

Original description translated from French: "A species characterised by a strong asymmetry of the test, displaying a degree of analogy with some Cenomanian *Rotalipora* (*R. reicheli* Mornad for example)".

Material: More than 130 specimens from 80 samples were recognised from the Dokan and the Azmer sections.

Description of the Kurdistani material: Large trochospiral test, spiral side flat to slightly concave, sometimes convex, umbilical side strongly convex, two well-developed widely spaced keels on the edge of the spiral side; early and final chambers angular.

Remarks: The species can be differentiated from *Dicarinella concavata* in having an angular chambers profile and in the presence of flat to slightly concave, or sometimes by strongly convex spiral side (see Figure 9).

Synonyms: *Globotruncana concavata carinata*, *Globotruncana fundiconulosa*.

Occurrence: This species is common in the upper part of the pelagic limestones of the Kometan Formation in both sections. It is restricted to the *D. asymetrica* Zone. The last appearance (LA) is at the top of the *D. asymetrica* Zone (83.64 Ma) and the FA is at the base of the *D. asymetrica* Zone (86.66 Ma) according to Gradstein et al. (2012).

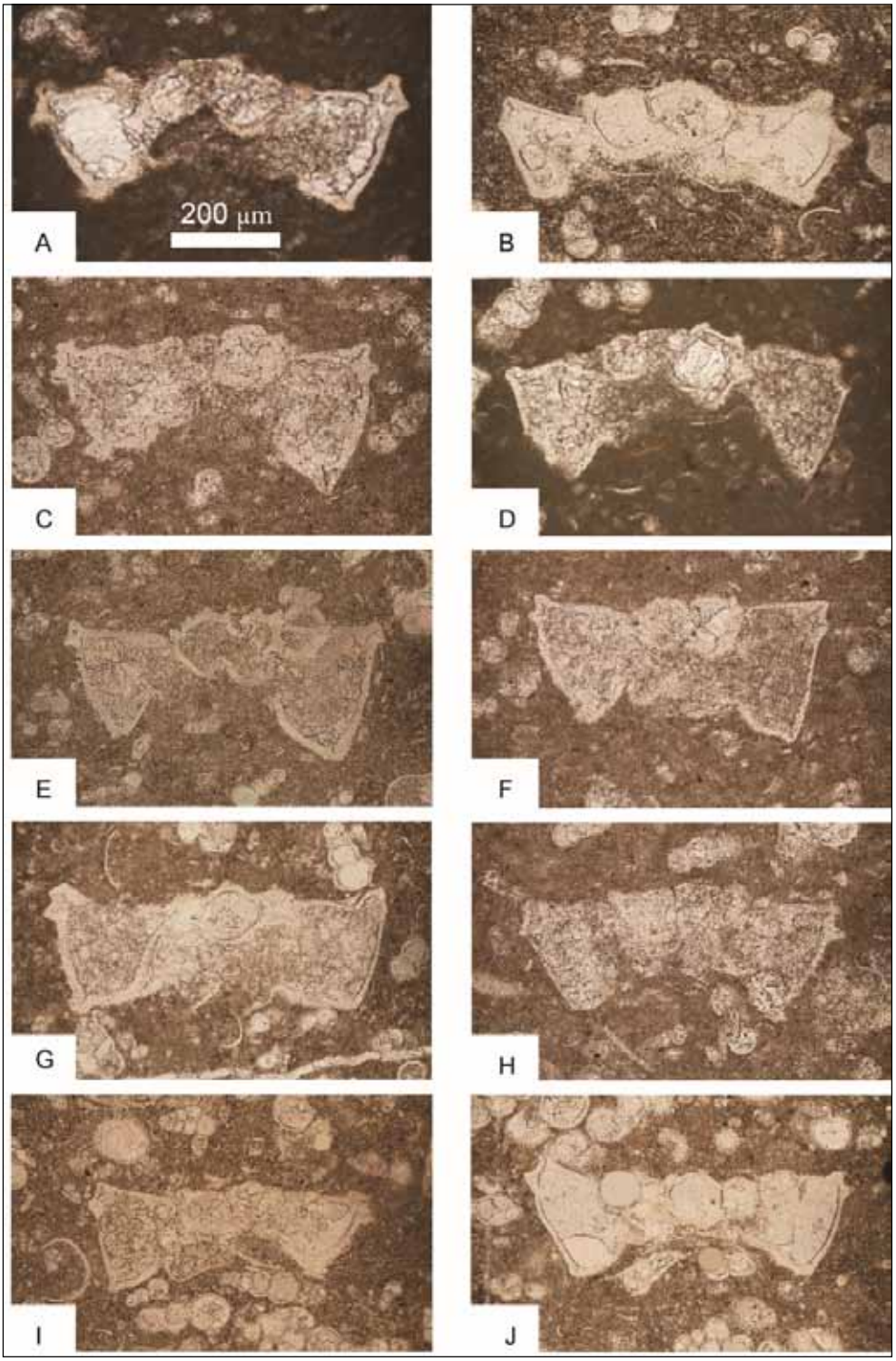

Figure 9. The axial sections of *Dicarinella asymetrica*. The scale bar is the same for all images. (A) Azmer section, sample AK-23; (B) Dokan section, sample DK-40; (C) Azmer section, sample AK-25; (D) Dokan section, sample DK-31; (E) Azmer section, sample AK-41; (F) Dokan section, sample DK-55; (G) Azmer section, sample AK-37; (H) Dokan section, sample DK-63; (I) Azmer section, sample AK-51; (J) Dokan section, sample DK-74.

***Dicarinella concavata* (Brotzen 1934)**

Figure 10 (A-J)

Original description: *"Die Spiralseite ist eingesunken und flach teller- oder schalenförmig. Sie hat eine Zentralscheibe, und der Rand ist durch einen erhobenen Saum eingefaßt. Der Nabel auf der Nabelseite ist groß und tief. Die Kammern des letzten Umganges auf der Spiralseite (6-7) sind ähnlich denen von Rotalia elevata, nur der Grat am Rande fehlt. Die Nabelseite ist wie bei R. elevata. Sie ist nahe mit dieser verwandt".*

Original description translated from German: "Spiral side depressed and flat plate or bowl-shaped. It has a central disk, and the rim is bordered by an elevated beam. The Umbilicus is on the umbilical side large and deep. Chambers of the last whorl on the spiral side (6-7) are similar to those of *Rotalia elevata* with only the ridge on the border missing.

The umbilical side is like of *R. elevata*, and is related with this species".

Material: More than 75 specimens from 33 samples were recognised from the Dokan and the Azmer sections.

Description of the Kurdistani material: Large trochospiral test, spiral side steep concave, umbilical side flat, sometimes strongly convex, two well-developed widely spaced keels on the edge of the spiral side; early and final chambers hemi-spherical and/or ovate.

Remarks: The species can be differentiated from *Dicarinella asymetrica* in having ovate and/or hemispherical chambers profile and in the presence of steep concave spiral side (see Figure 10).

Synonyms: *Globotruncana araratica, Globotruncana vridhachalensis*, *Globotruncana concavata cyrenaica*, *Marginotruncana concavata*.

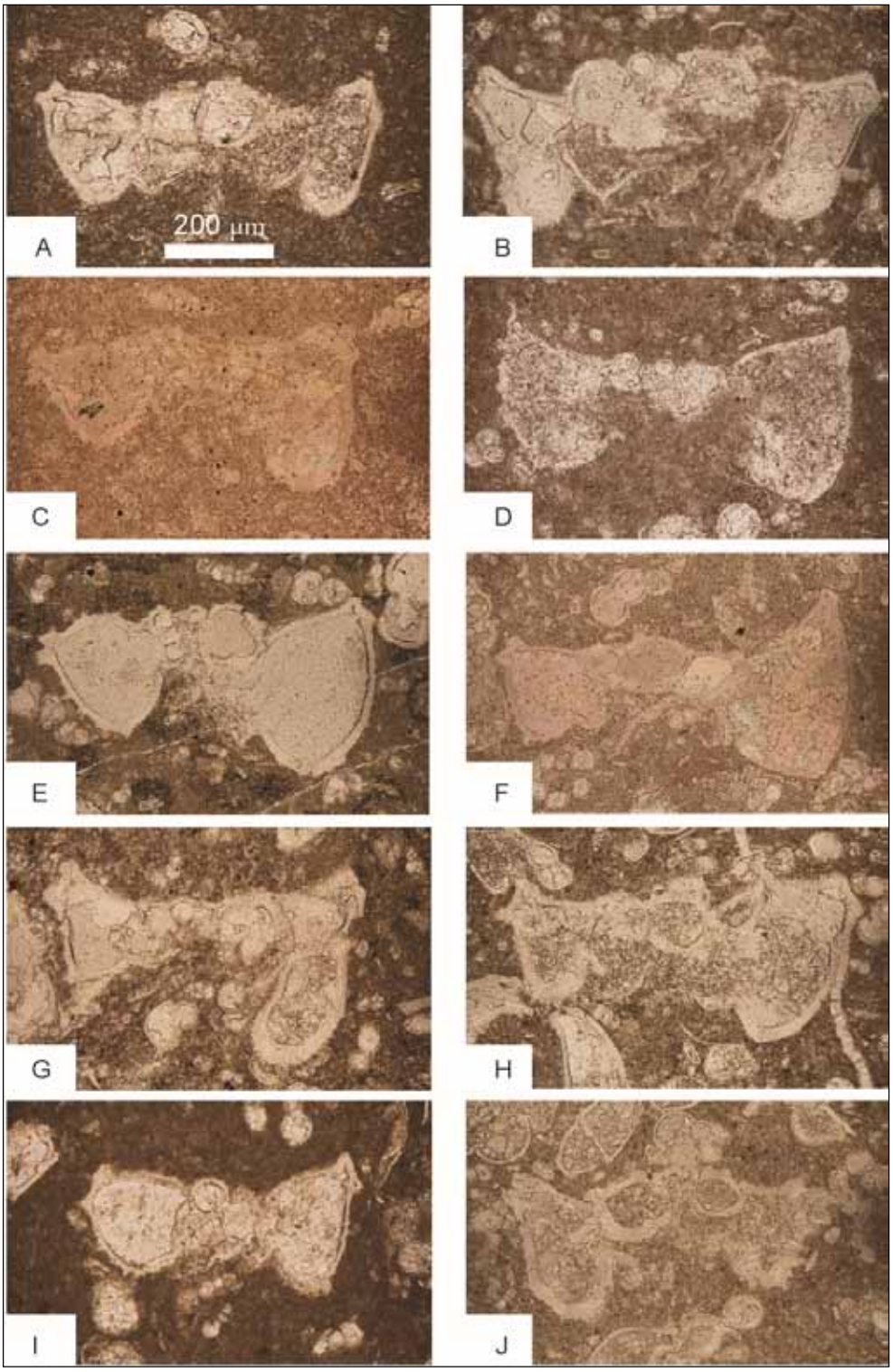

Figure 10. The axial sections of *Dicarinella concavata*. The scale bar is the same for all images. (A) Azmer section, sample AK-19; (B) Dokan section, sample DK-16; (C) Azmer section, sample AK-19; (D) Dokan section, sample DK-11; (E) Azmer section, sample AK-20; (F) Dokan section, sample DK-13; (G) Azmer section, sample AK-21; (H) Dokan section, sample DK-7; (I) Azmer section, sample AK-15; (J) Dokan section, sample DK-19.

Occurrence: This species occurs commonly throughout the pelagic limestones of the Kometan Formation in both sections. It is found in the *D. concavata* and *D. asymetrica* zones. The LA is within the *D. asymetrica* Zone (top of the Santonian Stage 83.64 Ma) and the FA is at the base of the *D. concavata* Zone (91.08 Ma) according to Gradstein et al. (2012).

5. Discussions

The two species *D. concavata* and *D. asymetrica* are widely used for Upper Turonian-Upper Santonian biozonations and inter-regional correlations in the Tethys Ocean. They also play great roles in definition of some Upper Cretaceous stages boundary interval. For instance, several authors have equated the FA of *D. concavata* with the Late Turonian (e.g., Premoli Silva and Sliter, 1994, 1999; Robaszynski and Caron, 1995; Robaszynski, 1998; Robaszynski et al., 2000; Bauer et al., 2001; Premoli Silva and Verga, 2004; Babazadeh et al., 2007; Kochhann et al., 2014). However, in some areas of Iraq, Iran, Turkey and Africa the FA of *D. concavata* has been positioned informally at the Turonian/Coniacian boundary (Salaj, 1980, 1984, 1987, 1997; Tur, 1996; Gebhardt, 2004, 2008; Sari, 2006; Farouk and Faris, 2012; Vahidinia et al., 2014; Jaff et al., 2015; El-Gammal and Orabi, 2019; Jaff and Lawa, 2020).

At the Global Boundary Stratotype Section and Point (GSSP) in Olazagutia, northern Spain and the Gubbio section in Italy the FA of *D. asymetrica* represents Latest Coniacian (Lamolda et al., 2014; Coccioni and Premoli Silva, 2015). However, Lamolda et al. (2014) used the first common occurrence of *D. asymetrica* to describe approximately the base of Santonian in the paleotropics. In other Neo-Tethyan areas, particularly in the Middle East, the FA of *D. asymetrica* is similarly used to express the Coniacian/Santonian boundary (e.g., Caron, 1985; Premoli Silva and Sliter, 1994; Robaszynski et al., 2000; Petrizzo, 2000, 2002; Sari, 2006; Farouk and Faris, 2012; Gradstein et al., 2012; Elamri et al., 2014, 2016; Jaff et al., 2015; El-Gammal and Orabi, 2019; Jaff and Lawa, 2020). Furthermore, the LA of *D. asymetrica* was proposed to describe the Santonian/Campanian boundary in the Bottaccione section of Italy (Premoli Silva and Sliter, 1994; Coccioni and Premoli Silva, 2015); Tunisia (Robaszynski et al., 2000; Elamri and Zaghbib-Turki, 2014; Elamri et al., 2014, 2016; Farouk et al., 2018); Turkey (Sari, 2006, 2009); Iran (Babazadeh et al., 2007; Honarmand et al., 2020); Egypt (Farouk and Faris, 2012; El-Gammal and Orabi, 2019); Syria (Pecimotika et al., 2014); Palestine (Meilijson et al., 2014); Kurdistan region, NE Iraq (Jaff et al., 2015; Jaff and Al-Kahtany, 2020) and in southern Tibet (Fang et al., 2020).

Due to the biostratigraphical importance of the two species as it is mentioned above, the correct identifications between them should be taking into consideration. Based on 205 specimens collected from 113 samples, the present work designed a model for accurate identifications between the two species under thin sections in the Kurdistan region, NE Iraq. The model for the Kurdistani materials are based on the illustrated holotype figured specimens of *D. concavata* by Brotzen (1934) and *D. asymetrica* by Sigal (1952). The holotype figured specimen of *D. concavata* indicates that the species should have steep concave spiral side. That is why Brotzen took the name *concavata* from the steep spiral side concavity. On the other hand, the holotype figured specimen of *D. asymetrica* appears to be flat or slightly concave in the spiral side. Based on this characterization, the latter should be differentiated from the former. The precise documentation of the above index planktic foraminiferal species play a crucial role in the exact age determination of the Upper Cretaceous lithostratigraphic units.

6. Conclusions

The achieved results of the present study can be shortened in the following:

1. Morphological similarities and misidentifications between the *D. concavata* and the *D. asymetrica* in previously published articles have allowed the author to design a model for accurate identifications.
2. From the designed model and the illustrated specimens of the Kurdistani materials, the *D. asymetrica* can be differentiated from *D. concavata* in having a flat or slightly concave spiral side, sometimes convex and in the presence of an angular early and final chambers profile.
3. The species *D. concavata* can be distinguished in having ovate and/or hemispherical chambers profile and in the presence of steep concave spiral side.
4. The correct identifications between *D. concavata* and *D. asymetrica* planktic foraminifera play great roles in the precise age determination of the Upper Cretaceous lithostratigraphic units.

Acknowledgements

The author thanks Fayez Ahmad the chief editor of the JJEES and the three anonymous reviewers for their constructive comments.

References

Almogi-Labin, A., Eshet, Y., Flexer, A., Honigstein, A., Moshkovitz, S., Rosenfeld, A. (1991). Detailed biostratigraphy of the Santonian/Campanian boundary interval in northern Israel. Journal of Micropalaeontology 10: 39-50.

Babazadeh, S.A., Robaszynski, F., Courme, M.D. (2007). New biostratigraphic data from Cretaceous planktic foraminifera in Sahlabad province, eastern Iran. Geobios 40: 445-454.

Barr, F.T. (1972). Cretaceous biostratigraphy and planktonic foraminifera of Libya. Micropaleontology 18: 1-46.

Bauer, J., Marzouk, A.M., Steuber, T., Kuss, J. (2001). Lithostratigraphy and biostratigraphy of the Cenomanian-Santonian strata of Sinai, Egypt. Cretaceous Research 22: 497-526.

Brotzen, F. (1934). Foraminiferen aus dem Senon Palastinas. Zeitschrift des Deutschen Palastina-Vereins 57: 28-72.

Caron, M. (1985). Cretaceous planktonic foraminifera. In: Bolli, H.M., Saunders, J.B., Perch-Nielsen, K. (Eds.), Plankton stratigraphy. Cambridge University Press, Cambridge: 17-86.

Coccioni, R.and Premoli Silva, I. (2015). Revised Upper Albian-Maastrichtian planktonic foraminiferal biostratigraphy and magneto-stratigraphy of the classical Tethyan Gubbio section (Italy). Newsletter on Stratigraphy 48: 47-90.

Donze, P., Porthault, B., Thomel, G., de Villoutreys, O. (1970). Le Senonien inferieur de Puget,Theniers (Alpes,Maritimes) et

sa microfaune. Geobios 2: 41-106.

Elamri, Z.and Zaghbib-Turki, D. (2014). Santonian-Campanian biostratigraphy of the Kalaat Senan area (west-central Tunisia). Turkish Journal of Earth Sciences 23: 184-203.

Elamri, Z., Farouk, S., Zaghbib-Turki, D. (2014). Santonian planktonic foraminiferal biostratigraphy of the northern Tunisia. Geologia Croatica 67: 111-126.

Elamri, Z., Abdeslam, R., Zaghbib-Turki, D. (2016). planktonic foraminiferal biostratigraphy and paleoenvironment of the Upper Coniacian–Lower Campanian succession in Northern Tunisia. Journal of African Earth Sciences 124: 234-244.

El-Gammal, M.H.and Orabi, H. (2019). Coniacian-late Campanian planktonic events in the Duwi Formation, Red Sea Region, Egypt. Journal of Geology and Geophysics 8: 1-16.

Fang, P.Y., Xu, B., Mu, L., Zhu, Y-H., Luo, H. (2020). New latest Coniacian to middle Campanian foraminiferal data from the lower Zongshan Formation in the Chaqiela section, Gamba, southern Tibet. Palaeoworld 29: 151-160.

Faris, M., Jaff, R.B.N., Farouk, S. (2019). Calcareous nannofossil biostratigraphy and bio-events of the Coniacian-lower Campanian succession in the Kurdistan region, northeastern Iraq. Arabian Journal of Geosciences 12: 153.

Farouk, S.and Faris, M. (2012). Late Cretaceous calcareous nannofossil and planktic foraminiferal bioevents of the shallow marine carbonate platform in Mitla Pass, west central Sinai, Egypt. Cretaceous Research 33: 50-56.

Farouk, S., Faris, M., Elamri, Z., Ahmad, F., Wagreich, M. (2018). Tethyan plankton bioevents calibrated to stable isotopes across the upper Santonian-lower Campanian transition in north-western Tunisia. Cretaceous Research 85: 128-141.

Gebhardt, H. (2004). Planktonic foraminifera of the Nkalagu Formation type locality (southern Nigeria, Cenomanian-Coniacian) biostratigraphy and palaeoenvironmental interpretation. Cretaceous Research 25: 191-209.

Gebhardt, H. (2008). Integrated biostratigraphy of the Cenomanian to Coniacian Nkalagu Formation in the lower Benue Trough, Nigeria. Berichte der Geologischen Bundesanstalt 74: 43-44.

Georgescu, M.D. (2017). Upper Cretaceous planktic foraminiferal biostratigraphy. Studia UBB Geologia 61: 5-20.

Gradstein, F.M., Ogg, J.G., Schmitz, M.D., Ogg, G.M. (2012). The geologic time-scale, first edition, Elsevier, 1176 pp.

Honarmand, A., Vahidinia, M., Gharaie, M.H.M., Ardestani, M.S. (2020). Biostratigraphy of Upper Cretaceous planktonic foraminifera of the Abtalkh Formation in an east-west transect, Kopet-Dagh Basin, northeastern Iran. Micropaleontology 66: 285-300.

Jaff, R.B.N., Wilkinson, I.P., Lee, S., Zalasiewicz, J., Lawa, F., Williams, M. (2015). Biostratigraphy and palaeoceanography of the early Turonian-early Maastrichtian planktonic foraminifera of NE Iraq. Journal of Micropalaeontology 34: 105-138.

Jaff, R.B.N. and Al-Kahtany, K. (2020). Coniacian/Santonian calcareous nannofossil and planktonic foraminifera in the Kurdistan region, NE Iraq: biostratigraphy and bioevents. Arabian Journal of Geosciences 13: 916.

Jaff, R.B.N. and Lawa, F.A.A. (2020). Biostratigraphy and Systematic Palaeontology of Late Cretaceous Heterohelicidae Foraminifera from Kurdistan Region Northeastern Iraq. Iraqi National Journal of Earth Sciences 20:33-63.

Jassim, S.Z.and Goff, J.C. (2006). Geology of Iraq. Brno, Czech Republic, Dolin, Prague and Moravian Museum 341 pp.

Kochhann, K.G.D., Lopes, F.M., Krahl, G., Aguiar, E., Fauth, G. (2014). Late Cretaceous-early Paleogene (Turonian? to early Danian) planktic foraminifera from DSDP site 356: A biostratigraphic reappraisal. Revista Brasileira de Paleontologia 17: 157-168.

Lamolda, M.A., Paul, C.R.C., Peryt, D., Pons, J.M. (2014). The global boundary stratotype and section point (GSSP) for the base of the Santonian stage, 'Cantera de Margas', Olazagutia, northern Spain. Episodes 37: 2-13.

Lawa, F.A., Koyi, H., Ibrahim, A. (2013). Tectono-stratigraphic evolution of the NW segment of the Zagros Fold-Thrust Belt, Kurdistan, NE Iraq. Journal of Petroleum Geology 36: 75-96.

Meilijson, A., Ashckenazi-Polivoda, S., Ron-Yankovich, L., Illner, P., Alsenz, H., Speijer, R., Almogi-Labin, A., Feinstein, S., Berner, Z., Püttmann, W., Abramovich, S. (2014). Chronostratigraphy of the Upper Cretaceous high productivity sequence of the southern Tethys, Israel. Cretaceous Research 50: 187-213.

Pecimotika, G., Tešović, B.C., Fućek, V.P. (2014). Planktonic foraminiferal biostratigraphy and paleoecology of Upper Cretaceous deposits from the Palmyride Region, Syria. Geologia Croatica 67: 87-110.

Petrizzo, M.R. (2000). Upper Turonian-lower Campanian planktonic foraminifera from southern mid-high latitudes (Exmouth Plateau, NW Australia): biostratigraphy and taxonomic notes. Cretaceous Research 21: 479-505.

Petrizzo, M.R. (2002). Palaeoceanographic and palaeoclimatic inferences from late Cretaceous planktonic foraminiferal assemblages from the Exmouth plateau (ODP Sites 762 and 763, eastern Indian Ocean). Marine Micropaleontology 45: 117-150.

Petrizzo, M.R., Jiménez Berrocoso, Á., Falzoni, F., Huber, B.T., Macleod, K.G. (2017). The Coniacian–Santonian sedimentary record in southern Tanzania (Ruvuma Basin, East Africa): Planktonic foraminiferal evolutionary, geochemical and palaeoceanographic patterns. Sedimentology 64: 252-285.

Postuma, J. (1971). Manual of Planktonic Foraminifera. Elsevier, 420 pp.

Premoli Silva, I. and Sliter, W.V. (1994). Cretaceous planktonic foraminiferal biostratigraphy and evolutionary trends from the Bottaccione section, Gubbio, Italy. Palaeontographia Italica 82: 1-89.

Premoli Silva, I.and Sliter, W.V. (1999). Cretaceous paleoceanography: Evidence from planktonic foraminiferal evolution. In: Barrera E. and Johnson C.C. (Eds.), Evolution of the Cretaceous Ocean-Climate System. Geological Society of America 332: 301-328.

Premoli Silva, I. and Verga, D. (2004). Practical manual of Cretaceous planktonic foraminifera. International school on planktonic foraminifera, 3rd course: Cretaceous. Universities of Perugia and Milan, Tiporafia Pontefelcino, Perugia, Italy, 283 pp.

Remin, Z., Dubicka, Z., Kozłowska, A., Kuchta, B. (2012). A new method of rock disintegration and foraminiferal extraction with the use of liquid nitrogen [LN_2]. Do conventional methods lead to biased paleoecological and paleoenvironmental interpretations? Marine Micropaleontology 86-87: 11-14.

Robaszynski, F. (1998). Planktonic foraminifera-upper Cretaceous, chart of Cretaceous Biochronostratigraphy. In: De Graciansky, P.C., Hardenbol, J., Vail, P.R. (Eds.), Mesozoic and Cenozoic Sequence Stratigraphy of European Basins. Sedimentary Geology 60:782.

Robaszynski, F. and Caron, M. (1995). Cretaceous planktonic foraminifera: Comments on the Europe-Mediterranean zonation. Bulletin de la SociétéGéologique de France 166: 681-

692.

Robaszynski, F., Gonzales-Donoso, J.M., Linares, D., Amedro, F., Caron, M., Dupuis, C., Dhondt, A.V., Gartner, S. (2000.

Le Crétacé supérieur de la région de Kalaat Senan, Tunisie centrale. Litho-biostratigraphie intégrée: zones d'ammonites, de foraminifè res planctoniques et de nannofossiles du Turonien supérieur au Maastrichtien. Bulletin des centres de recherches exploration-production Elf-Aquitaine, 22: 359-490.

Salaj, J. (1980). Microbiostratigraphie du Crétacé et du Paléogène de la Tunisie Septentrionale et Orientale (Hypostratotypes Tunisiens). Institut Geologique de Dionyz Stur, Bratislava 238 pp.

Salaj, J. (1984). Boundaries of upper Cretaceous hypostratotypes at the profile Djebel Fguira Salah, Tunisia. Bulletin of the Geological Society of Denmark 33: 199-201.

Salaj, J. (1987). Integrated microbiostratigraphy of the Albian to basal Santonian and its problems. Geologica Carpathica 38: 357-370.

Salaj, J. (1997). Microbiostratigraphical (Foraminifera) division of the Turonian to Santonian in Tunisia (El Kef and Dj. Fguira Salah Area). Geologica Carpathica 48: 171-178.

Sari, B. (2006). Upper Cretaceous planktonic foraminiferal biostratigraphy of the BeyDağlari autochthon in the Korkuteli area, western Taurides, Turkey. Journal of Foraminiferal Research 36: 241-261.

Sari, B. (2009). Planktonic foraminiferal biostratigraphy of the Coniacian-Maastrichtian sequences of the BeyDağlari autochthon, western Taurides, Turkey: Thin-section zonation. Cretaceous Research 30: 1103-1132.

Sigal, J. (1952). Aperçu stratigraphique sur la micropaléontologie du Crétacé. 19th Congrès Géologique International, Monographies régionales, ser. 1, Algérie, 26: 1-47.

Sigal, J. (1955). Notes micropaléontologiques nord-africaines. 1. Du Cénomanien au Santonien: zones et limites en facies pélagique. Compte Rendu Sommaire des Séances de la Société Géologique de France, 7-8: 157-160.

Sliter, W.V. (1989). Biostratigraphic zonation for Cretaceous planktonic foraminifers examined in thin section. Journal of Foraminiferal Research 19: 1-19.

Tur, N.A. (1996). Planktonic foraminifera recovery from the Cenomanian-Turonian mass extinction event, northeastern Caucasus. In: Hart, M.B. (Ed.), Biotic Recovery From Mass Extinction Events. Geological Society of London 102: 259-264.

Vahidinia, M., Youssef, M., Ardestani, M.S., Sadeghi, A., Dochev, D. (2014). Integrated biostratigraphy and stage boundaries of the Abderaz Formation, east of the Kopeh-Dagh sedimentary basin, NE Iran. Journal of African Earth Sciences 90: 87-104.

JJEES

JJEES (2021) 12 (2): 163-186
ISSN 1995-6681

Jordan Journal of Earth and Environmental Sciences

Paleocene rotaliid benthic foraminifera of Jabal Mundassa, Al Ain area, United Arab Emirates

Haidar Salim Anan

Al Azhar University-Gaza, Palestine.

Received 12 June 2020; Accepted 22 November 2020

Abstract

The micropaleontological taxa of Jabal Mundassa, Al Ain area, United Arab Emirates (UAE) indicates that the Paleocene succession bears prolific and well preserved benthic foraminifera index-species of the Danian, and its succession is considered the only outcrop that has Danian sediments in the Al Ain area, and most complete Danian rocks in UAE. The Danian succession is attributed to the shaley marl neoautochthonous sediments belong to Mundassa Member (MM) of the Muthaymimah Formation (MF), which are unconformably overlying the pre-Maastrichtian allochthonous Semail Ophiolite (SO, serpentinites and serpentinized peridotites). Forty six rotaliid benthic foraminiferal species belonging to twenty six genera are identified from fourteen samples collected from the Paleocene succession of the Mundassa section. Based on the planktic foraminiferal zonation, the duration of the hiatus at the Cretaceous/Paleogene (K/P) boundary includes the two early Danian biozones (P0 and Pa, about 0.02 Ma). This depositional gap is most probably due to submarine erosion (not to subaerial denudation), and correspond to an interval of tectonic activity that exists in most localities in the Middle East and other sites in the world.

In current study, an attempt is made to identify the rotaliid Danian calcareous benthic foraminifers of the Mundassa section, and it is possible to illustrate twenty eight of them in two plates (1, 2), for the first time, with some additional remarks on paleontology, stratigraphy and paleogeography in the UAE and other Tethyan localities.

Keywords: Rotaliina, foraminifera, Danian, Paleocene, Mundassa, Al Ain area, United Arab Emirates, Tethys.

1. Introduction

The Late Maastrichtian to Paleogene post nappe rocks outcrop as a discontinuous belt in jabals (mountains) and qarns (hills) around the western front of the Northern Oman Mountains (NOM) in the United Arab Emirates (UAE). The folded anticlines of Jabal Mundassa and J. Malaqet in Al Ain area are a part of the (NOM) and located approximately 25 km due south of Al Ain city (UAE), and about 20 km to the east of J. Hafit (Figure 1). These jabals outcrops on the eastern side of the Al Jaww Plain, near the border with the Sultanate of Oman. The pre-Maastrichtian Semail Ophiolite Nappe (SO, gabbro and serpentinites) forms the core of the breached anticline of J. Mundassa and J. Malaqet. In the last stage of the emplacement of the SO onto the passive continental margin of the Arabian platform, several foredeep basins (Ras Al Khaima Basin and Mundassa Basin) were developed on the northwestern flank of the NOM. These basins hosted deposition of upper Cretaceous–Paleogene sedimentary successions, which unconformably overlying sequences were later deformed by thrust faults and folds in that time. The previous works of Nolan et al. (1990), Hamdan and Anan (1993), Anan and Hamdan (1992, 1993), Anan (1993a,b, 1995, 1996, 2015a,b, 2016, 2019b), Warrak (1996), Noweir and Eloutefi (1997), Boukhary et al. (2003) are pertinent to the present study. Current study in the Mundassa area aims to elucidate the paleontology and paleogeography during the Danian and correlated with other Danian successions inside and outside of the UAE.

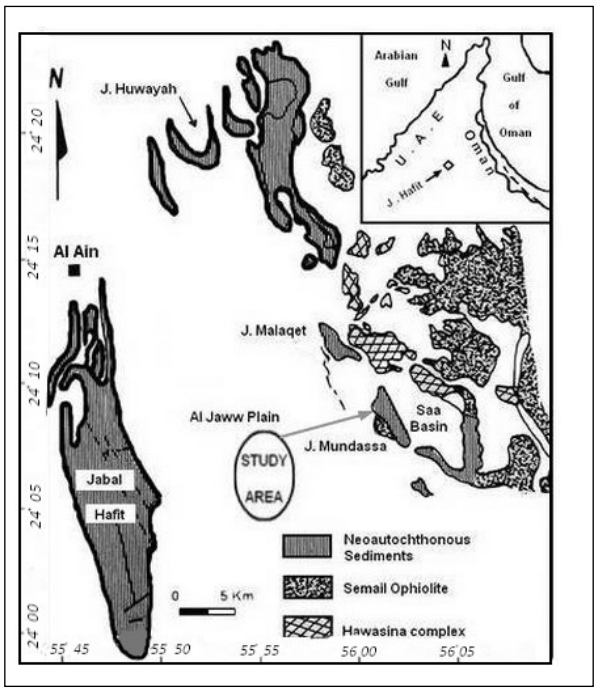

Figure 1. Location of the study section at Jabal Mundassa, Al Ain area, UAE.

* Corresponding author e-mail: profanan@gmail.com

2. Geology and stratigraphy

The Paleocene post-nappe shaley marl sediments of J. Mundassa are attributed here to the Danian, but to the Late Paleocene by Noweir and Eloutefi (1997), while to the Early-Middle Paleocene based on the planktic foraminiferal biozonation (after Berggren and Pearson, 2005). On the other hand, the green shale in J. Malaqet (which unconformably overlies the Late Maastrichtian Simsima Formation, not SO) was attributed to the Middle Paleocene (Hamdan and Anan, 1993; Anan and Hamdan, 1993 and Anan,1993a), or the Late Paleocene (Noweir and Eloutefi, 1997, and Boukhary et al., 2003).

During the last stage of the emplacement of the Semail Ophioliteonto the passive continental margin of the Arabian platform, some foredeep basins were developed including the Ras Al Khaima basin, in the north of UAE (Alsharhan and Nairn, 1995), and the Mundassa basin in the south (Anan, 2015a). These basins hosted deposition of a Paleocene sedimentary sequence, which is an unconformably overlying sequence that deformed later by thrust faults and folds. The Danian rocks are attributed to the shaley marl neoautochthonous sediments belong to the Mundassa Member (MM) of the Muthaymimah Formation (MF), which are unconformably overlying the Pre-Maastrichtian allochthonus SO. In current study, 46 rotaliid benthic foraminiferal species are recorded, and 28 of them are illustrated in Plates (1, 2) from the Danian (Early Paleocene, P1a-P3a) of the shaley marl succession in J. Mundassa.

Based on the planktic foraminiferal biozones (Anan, 2016), the duration of the hiatus at the Cretaceous/Paleogene (K/P) boundary includes the two earliest Danian biozones (P0 and Pα), about 0.02 Ma (Figure 2). This depositional gap is most probably due to submarine erosion, not to subaerial denudation, and corresponds to an interval of tectonic activity that exists in most localities in the world.

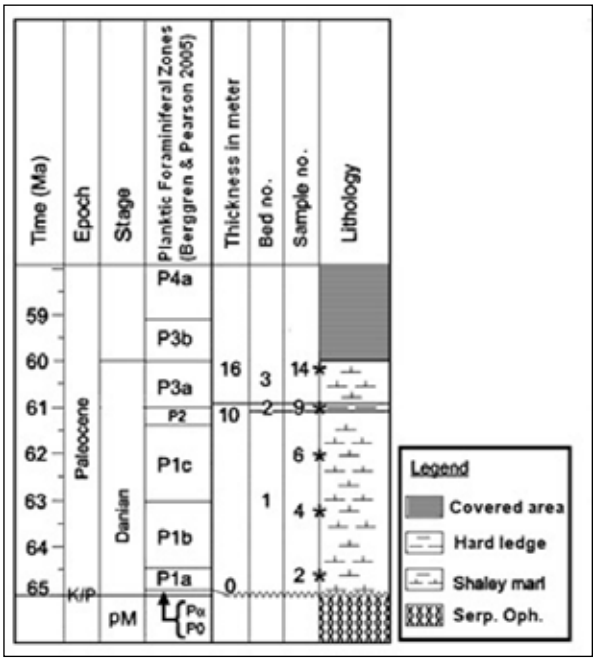

Figure 2. Stratigraphic log of the Danian on Stage the eastern limb of J. Mundassa anticline, Al Ain area, UAE. The standard earliest Danian zones (P0 and Pα)are absent from the study section (pM= pre-Maastrichtian, K/P= Cretaceous/Paleogene boundary, Serp. Oph.= serpentine Semail Ophiolite).

3. Material and methods

The present study is the fourth part from the series concerning the Paleocene foraminiferal assemblages of J. Mundassa: agglutinated and lagenid foraminifera (2015a, b, respectively), planktic foraminifera (Anan, 2016) and rotaliid foraminifera (current study). Fourteen samples of shaley marl were collected from the exposed neoautochthonous rocks of the J. Mundassa (beds 1, 3; samples 1-8, 10-14, about 26 m thick) (74-94% insoluble residue), except bed no. 2 (sample 9) is characterized by its yellow-brown hard ledge (99% insoluble residue). This succession belongs to the Paleocene MM of the MF and rests unconformably on a peniplaned allochthonus Pre-Maastrichtian SO (Figure 3).

Figure 3. View of the Paleocene (Danian) sediments (Mundassa Member of the Muthaymimah Formation) which nonconformably overly the obducted Pre-Maastrichtian Semail Ophiolite.

4. Taxonomy

Forty six rotaliid benthic foraminiferal species in J. Mundassa are identified and 28 of them are illustrated in Plates 1, 2. The classification of Loeblich and Tappan (1987) and Bolli et al. (1994) are followed in current study.

Order Foraminiferida Eichwald, 1830

Suborder Rotaliina Delage and Hérouard, 1896

Superfamily Bolivinacea Glaessner, 1937

Family Bolivinoididae Loeblich and Tappan, 1984

Genus *Bolivinoides* Cushman, 1927

Type species. *Bolivina draco* Marsson, 1878

***Bolivinoides curtus* Reiss, 1954**

(Pl. 1, fig. 1)

1954 *Bolivinoides curta* Reiss, p. 158, pl. 30, figs. 15-16.

1956 *Bolivinoides curtus*; Said and Kenawy, p. 140, pl. 3, fig. 43.

1963 *Bolivinoides delicatulus curtus*; Hiltermann, p. 217, pl. 3, figs. 8-9.

1992 *Bolivinoides curtus*; Anan and Hamdan, p. 205, text-fig. 5.

1994 *Bolivinoides delicatulus curtus*; Bolli et al., p. 129, fig. 34. 36.

1993a *Bolivinoides curtus*; Anan, p. 316, pl. 2, fig. 15.

2011b *Bolivinoides curtus*; Anan, p. 134, pl. 1, fig. 1.

Remarks: This Paleocene species is closely related to *Bolivinoides delicatulus* Cushman but differs by its smaller and shorter test. Hiltermann (1963) noted that both species *B. delicatulus* and *B. curtus* start in the Upper Cretaceous rocks in Europe (France and Germany) and continue to the

Danian, but *B. curtus* is not recorded in the Upper Cretaceous at some Middle East localities, but only in Paleocene rocks: Negev (Reiss, 1954), Sinai (Said and Kenawy, 1956), J. Malaqet (Anan and Hamdan, 1992; Anan, 1993a) as well as J. Mundassa, UAE (current study).

Superfamily Turrilinacea Cushman, 1927
Family Turrilinidae Cushman, 1927
Genus *Praebulimina* Hofker, 1953
Type species. *Bulimina ovulum* Reuss, 1844

***Praebulimina carseyae* (Plummer, 1931)**

1931 *Buliminella carseyae* Plummer, p. 179, pl. 8, fig. 9.
1946 *Buliminella carseyae*; Cushman, p. 119, pl. 50, figs. 17, 20.
1956 *Buliminella carseyae*; Said and Kenawy, p. 142, pl. 4, fig. 8.
1968 *Praebulimina carseyae*; Sliter, p. 83, pl. 11, fig. 16.
1970 *Praebulimina carseyae*; Al-Omari, p. 85, pl. 3, fig. 29.
1993b *Praebulimina carseyae*; Anan, p. 659, pl. 3, fig. 5.

Remarks: This Maastrichtian–Paleocene species was recorded from the USA (Plummer, 1931), Mexico (Sliter, 1968), Egypt (Said and Kenawy, 1956), Iraq (Al-Omari, 1970), and also Qarn El Barr section, UAE (Anan, 1993b). It is recorded in the Paleocene of the studied section.

Superfamily Buliminacea Jones, 1977
Family Siphogenerenoididae Saidova, 1981
Subfamily Siphogenerenoidinae Saidova, 1981
Genus *Orthokarstenia* Dietrich, 1935
Type species. *Orthocerina ewaldi* Karsten, 1858

***Orthokarstenia applinae* (Plummer, 1927)**

1927 *Bolivina applinae* Plummer, p. 69, pl. 4, fig. 1.
1948 *Loxostoma applinae*; Brotzen, p. 69, pl. 10, fig. 11.
1953 *Loxostomum applinae*; LeRoy, p. 27, pl. 8, fig. 1.
1956 *Loxostomum applinae;* Haque, P. 134, pl. 15, figs. 24-25.
1975 *Loxostomoides applinae*; Berggren and Aubert, p. 420, pl. 4, fig. 11.
1976 *Loxostomoides applinae*; Futyan, p. 521.
1985 *Loxostomoides applinae*; Luger, p. 106, pl. 7, fig. 1.
1992 *Loxostomoides applinae*; Saint-Marc, p. 485, pl. 1, fig. 12.
1993a *Loxostomoides applinae*; Anan, p. 316, pl. 2, fig. 14.
1994 *Loxostomoides applinae*; Speijer, p. 109, pl. 1, fig. 11.
1998 *Orthokarsteni aapplinae*; Anan, p. 371, fig. 3. 3.
2012 *Orthokarstenia applinae*; Ismail, p. 48, pl. 4, fig. 7.
2020 *Orthokarsteni aapplinae*; Anan, p. 6, pl. 2.2.

Remarks: The initial part of this species is, however, obscure. Plummer (1927) noted that the chambers are smooth except for distinct striae extended from the initial extremity upward over several chambers and its crenulated base of the biserial part and longitudinal striae. It has a triserial part that becomes biserial and uniserial, for this reason, it should belong to the genus *Orthokarstenia*. Anan (1998) regarded the species *applinae* is an evolutionary development from the Maastrichtian *O. oveyi* (Nakkady). He also added that all members of the latter genus in Egypt seem to be restricted to south Egypt (*Orthokarstenia* province of Hewaidy, 1997). This Paleocene–Early Eocene species was recorded from the USA (Plummer, 1927), Sweden (Brotzen, 1948), Tunisia (Berggren and Aubert, 1975), Egypt (LeRoy, 1953), Jordan (Futyan, 1976), UAE (J. Malaqet, Anan, 1993a) and Pakistan (Haque, 1956). It is recorded in the Paleocene of the studied section.

Family Buliminidae Hofker, 1951
Genus *Bulimina* d'Orbigny, 1826
Type species. *Bulimina marginata* d'Orbigny, 1826

***Bulimina mexicana* Cushman, 1922**

(Pl. 1, fig. 2)

1922 *Bulimina inflata* Seguenza var. *mexicana* Cushman, p. 95, pl. 21, fig. 2.
2006 *Bulimina mexicana*; Ortiz and Thomas, p. 114, pl. 4, figs. 15, 16.

Remarks: This Paleocene–Early Eocene species can be distinguished by its conspicuous well-developed costae extending downward as sharp spines and inflated chambers. It was recorded, so far, from the US and Spain. It is recorded from the Paleocene of the study section.

Bulimina midwayensis Cushman and Parker, 1936

(Pl. 1, fig. 3)

1936 *Bulimina arkadelphiana* var. *midwayensis* Cushman and Parker, p. 42, pl. 7, figs. 9-10.
1956 *Bulimina arkadelphiana* var. *midwayensis;* Said and Kenawy, p. 142, pl. 4, fig. 11.
1975 *Bulimina midwayensis;* Berggren and Aubert, p. 175, pl. 14, fig. 8.
1976 *Bulimina midwayensis;* Aubert and Berggren, p. 422, pl. 5, fig. 7.
1983 *Bulimina midwayensis;* Tjalsma and Lohmann, p. 6, pl. 3, fig. 1.
1985 *Bulimina midwayensis;* Luger, p. 106, pl. 7, fig. 4.
1990 *Bulimina midwayensis;* Thomas, p. 539, pl. 2, fig. 8.
1993a *Bulimina midwayensis;* Anan, p. 316, pl. 2, fig. 16.
1993b *Bulimina midwayensis;* Anan, p. 659, pl. 3, fig. 7.
1994 *Bulimina midwayensis;* Bolli et al., p. 136, fig. 36. 19-21.
2003 *Bulimina midwayensis;* Ali, p. 118, pl. 8, fig. 17.
2005 *Bulimina midwayensis;* Sztrákos, p. 187, pl. 6, fig. 13.
2006 *Bulimina midwayensis;* Alegret and Ortiz, p. 440, pl. 1, fig. 22.
2007 *Bulimina midwayensis;* Valchev, p. 131, pl. 1, fig. 9.
2020 *Bulimina midwayensis;* Anan, p. 7.

Remarks: The Campanian-Paleocene *B. midwayensis* shows less distinct costae and more spines than *B. mexicana* and has re-entrants along the sutures. It was recorded from the USA (Cushman and Parker, 1936), Trinidad (Bolli et al., 1994), Atlantic Ocean (Tjalsma and Lohmann, 1983), France (Sztrákos, 2005), Bulgaria (Valchev, 2007), Tunisia (Aubert and Berggren, 1975), Egypt (Said and Kenawy, 1956) and the UAE (J. Malaqet and Qarn El Barr sections, Anan, 1993a,b), and also the Paleocene of J. Mundassa, UAE.

***Bulimina trinitatensis* Cushman and Jarvis, 1928**

(Pl. 1, fig. 4)

1928 *Bulimina trinitatensis* Cushman and Jarvis, p. 102, pl. 14, fig. 12.
1956 *Bulimina stokesi;* Said and Kenawy, p. 143, pl. 4, fig. 14.
1976 *Bulimina trinitatensis;* Aubert and Berggren, p. 423, pl. 5, fig. 12.

1978 *Bulimina trinitatensis;* Proto Decima and Bolli, p. 791, pl. 2, figs. 15-16.
1983 *Bulimina trinitatensis;* Tjalsma and Lohmann, p. 7, pl. 3, fig. 4.
1993a *Bulimina stokesi;* Anan, p. 316, pl. 2, fig. 17.
1994 *Bulimina stokesi;* Bolli et al., p. 136, fig. 36. 24-26.
1994 *Bulimina trinitatensis;* Speijer, p. 154, pl. 2, fig. 3.

Remarks: Tjalsma and Lohmann (1983) noted that this Paleocene–Early Eocene species has a wide bathymetric distribution during the Paleocene, becoming restricted to the shallow and intermediate sites during the Eocene. Speijer (1994) treated the Egyptian species *Bulimina stokesi* of Said and Kenawy (1956) as a junior synonym of *B. trinitatensis* Cushman and Jarvis. This species is distinguished from the similar *B. midwayensis* in its coarser ornamentation and somewhat larger size. It was recorded in the Early Eocene in Trinidad, but in the Paleocene in Egypt, and also the studied section J. Mundassa, UAE.

Family Buliminellidae Hofker, 1951
Genus *Buliminella* Cushman, 1911
Type species. *Bulimina elegantissima* d'Orbigny, 1839
***Buliminella grata* Parker andBermúdez, 1937**
(Pl. 1, fig. 5)
1937 *Buliminella grata* Parker and Bermúdez, p. 515, pl. 59, fig. 6.
1982 *Praebulimina grata*; Proto Decima and Bolli, p. 118, pl. 7, fig. 4.
1983 *Buliminella grata*; Tjalsma and Lohmann, p. 26, pl. 12, fig. 7.
1993 *Buliminella grata*; Boltovskoy and Vera Ocampo, p. 148, pl. 2, fig. 2.
1994 *Buliminella grata*; Bolli et al., p. 137, fig. 37. 3.
2000 *Elongobula grata*; Sztrákos, p. 110, pl. 15, fig. 8.

Remarks: This Paleocene–Oligocene species has a slender test, somewhat inflated chambers without costae or spine, but with a peculiar protuberance in the apertural face of the last chamber, while the genus *Elongobula* Finlay (1939) has an elongate test in a high troche spiral coil, circular to oval in section (Loeblich and Tappan, 1987, p. 570). *B. grata* was recorded from the Caribbean region (Bolli et al., 1994), Atlantic Ocean (Tjalsma and Lohmann, 1983), France (Sztrákos, 2000), Italy (Proto Decima and Bolli, 1982) and the Arabian Sea (Boltovskoy and Vera Ocampo, 1993). It is recorded in the Paleocene of the studied section, UAE.

Genus *Globobulimina* Cushman, 1927
Type species. *Globobulimina pacifica*Cushman, 1927
***Globobulimina suteri* (Cushman and Renz, 1946)**
(Pl. 1, fig. 6)
1946 *Bulimina (Desinobulimina) suteri* Cushman and Renz, p. 38, pl. 6, fig. 15.
1994 *Globobulimina* (?) *suteri*; Bolli et al., p. 137, figs. 34-36.
2007 *Globobulimina suteri*; Valchev, p. 132, pl. 1, fig. 11.

Remarks: Bolli et al. (1994) noted that this Campanian-Late Paleocene species presents an unusual combination of features of the Buliminidae (coiling mode) and the Pleurostomellidae (apertural characteristics). Our specimens have an oval test in outline and round in cross-section, triserial arrangement, inflated chambers, sharply increasing in size, with a smooth surface. This species was recorded from the USA (Cushman and Renz, 1946), Caribbean region (Bolli et al., 1994), and Bulgaria (Valchev, 2007). It is recorded in the Paleocene of the studied section, UAE.

Family Fursenkoinidae Loeblich and Tappan, 1961
Genus *Coryphostoma* Loeblich and Tappan, 1962
Type species. *Bolivina platium* Carsey, 1926
***Coryphostoma midwayensis* (Cushman, 1936)**
(P1. I, fig. 7)
1936 *Bolivina midwayensis* Cushman, p. 50, pl. 7, fig. 12.
1976 *Bolivina midwayensis*; Aubert and Berggren, p. 240, pl. 4, fig. 10.
1988 *Coryphostoma midwayensis*; Kaiho, p. 554, fig. 1.
1993a *Bolivina midwayensis;* Anan, p. 316, pl. 2, fig. 13.
1993b *Bolivina midwayensis;* Anan, p. 659, pl. 3, fig. 2.
1994 *Coryphostoma midwayensis*; Bolli et al., p. 138, fig. 37.13-15.
1995 *Coryphostoma midwayensis*; Nomura and Brohi, p. 227, pl. 1, fig. 10.
2001 *Coryphostoma midwayensis*; Shahin, p. 12, fig. 6. 18.
2004 *Coryphostoma midwayensis* (Cushman). - Anan, p. 44, pl. 1, fig. 4.
2007 *Bolivina midwayensis;* Valchev, p.131, pl. 1, fig. 5.

Remarks: The test of the genus *Coryphostoma* has biserial arranged with a tendency to become uniserial. This cosmopolitan Paleocene species *C. midwayensis*is characterized by its elongate, very slightly tapering, much-compressed test, periphery rounded, biserial throughout. It is recorded from the Paleocene of the USA (Cushman, 1936), Trinidad (Bolli et al., 1994), Bulgaria (Valchev, 2007), Tunisia (Aubert and Berggren, 1975), Egypt (Shahin, 2001), J. Malaqet and Qarn El Barr sections, UAE (Anan, 1993a,b), Pakistan (Nomura and Brohi, 1995), and also in the studied section, UAE.

***Coryphostoma nekhliana* (Said and Kenawy, 1956)**
(Pl. 1, fig. 8)
1956 *Bolivina decurrens parallela* Said and Kenawy, p. 143, pl. 4, fig. 18.
1959 *Bolivina decurrens nekhliana;* Thalmann, p. 130.

Remarks: Thalmann (1959) presented new names for some foraminiferal homonyms. Consequently, this subspecies was assigned a new name: *Bolivina decurrens nekhliana* (non *B. parallela* Perner, 1892). This species has an elongate test and the sutures in the early portion not strongly oblique than *C. midwayensis.* It was originally recorded from the Maastrichtian of Sinai in Egypt (Said and Kenawy, 1956), but for the first time, from the Paleocene of the studied section.

Superfamily Pleurostomellacea Reuss, 1860
Family Pleurostomellacea Reuss, 1860
Subfamily Pleurostomellacea Reuss, 1860
Genus *Ellipsoglandulina* Silvestri, 1900
Type species. *Ellipsoglandulina laevigata* Silvestri, 1900
***Ellipsoglandulina arafati* Anan, 2009**
2009b *Ellipsoglandulina arafati* Anan, p. 111, fig. 2.
2011a *Ellipsoglandulina arafati;* Anan, p. 62, pl. 3, fig. 30.

Remarks: This species is characterized by its widest size in the middle portion of the test and pointed initial end. It

differs from the Italian Pliocene *E. laevigata* Silvestri (1900) by its lesser lunate aperture and more spherical test than the variable dimensional test of the latter, which have more elongated and wider tests. *E. arafati* was originally recorded from the Lower Eocene of the Abu Zenima section, Sinai of Egypt (Anan, 2009b). It is recorded also here, for the first time, from the Paleocene of the studied section, UAE.

***Ellipsoglandulina ellisi* Said and Kenawy, 1956**

1956 *Ellipsoglandulina ellisi* Said and Kenawy, p. 146, pl. 4, fig. 34.

Remarks: The Early Eocene *E. arafati* Anan differs from the Maastrichtian–Paleocene *E. ellisi* Said and Kenawy by its more spherical test with rapidly increasing nodosarian chambers, semilunate aperture to the longer elongate test with gradually increasing nodosarian chambers, and slit-like aperture of the latter. It was originally recorded from the Sinai in Egypt (Said and Kenawy, 1956). It is recorded here outside Egypt, for the first time, from the Paleocene of the studied section, UAE.

Genus *Nodosarella* Rzehak, 1895

Type species. *Lingulina tuberosa* Gümbel, 1870

***Nodosarella gracillima* Cushman, 1944**

1944 *Nodosarella gracillima* Cushman, p. 13, pl. 2, fig. 32.

1946 *Nodosarella gracillima;* Cushman, p. 134, pl. 55, figs. 19-21.

1956 *Nodosarella gracillima;* Said and Kenawy, p. 145, pl. 4, fig. 27.

Remarks: This Maastrichtian-Paleocene species is characterized by its slender and slightly tapering test, aperture semielliptical at one side of the end of the last-formed chamber. It was recorded from the USA (Cushman, 1944) and Egypt (Said and Kenawy, 1956). It is also found for the first time, in the Paleocene of the studied section, UAE.

***Nodosarella paleocenica* Cushman and Todd, 1946**

(Pl. 1, fig. 9)

1946 *Nodosarella paleocenica* Cushman and Todd, p. 60, pl. 10, fig. 23.

1951 *Nodosarella paleocenica*; Cushman, p. 46, pl. 12, fig. 38.

1956 *Ellipsonodosaria paleocenica;* Haque, p. 139, pl. 23, figs. 10, 11.

1994 *Nodosarella paleocenica*; Bolli et al., p. 142, fig. 37.43, 44.

Remarks: This Maastrichtian-Paleocene species is characterized by its slender and slightly tapering test, aperture semielliptical at one side of the end of the last-formed chamber. It was recorded from the USA (Cushman, 1944) and Egypt (Said and Kenawy, 1956). It is also found for the first time, in the Paleocene of the studied section, UAE.

***Nodosarella subnodosa* (Guppy, 1894)**

(Pl. 1, fig. 10)

1894 *Ellipsoidina subnodosa* Guppy, p. 650, pl. 41, fig. 13.

1945 *Nodosarella subnodosa*; Cushman and Stainforth, p. 53, pl. 9, fig. 3.

1956 *Nodosarella subnodosa;* Said and Kenawy, p. 146, pl. 4, fig. 31.

1992 *Nodosarella subnodosa;* Gawor-Biedowa, p. 135, pl. 26, fig. 5.

1993b *Nodosarella subnodosa;* Anan, p. 659, pl. 3, fig. 10.

1994 *Nodosarella subnodosa;* Bolli et al., p. 142, fig. 37.45, 46.

Remarks: This Maastrichtian–Oligocene species has a more compact test than *N. paleocenica.* It was recorded from Eocene-Oligocene of Trinidad (Bolli et al., 1994), the Maastrichtian from Poland (Gawor-Biedowa, 1992), thePaleocene-Eocene of Egypt (Said and Kenawy, 1956), and Maastrichtian–Paleocene of the Qarn El Barr section, UAE (Anan, 1993b). It is recorded also from the Paleocene of J. Mundassa, UAE.

Genus Pleurostomella Reuss, 1860

Type species. *Dentalina subnodosa Reuss*, 1851

***Pleurostomella naranjoensis* Cushman and Bermúdez, 1937**

(Pl. 1, fig. 11)

1937 *Pleurostomella naranjoensis* Cushman and Bermúdez, p. 16, pl. 1, figs. 59-60

1948 *Pleurostomella naranjoensis*; Cushman and Renz, p. 30, pl. 5, fig. 21.

1994 *Pleurostomella naranjoensis*; Bolli et al., p. 143, figs. 38. 6-7.

2019a *Pleurostomella naranjoensis*; Anan, p. 175, pl. 1, fig. 11.

Remarks: This species has a short test, but more width than P. cubensis Cushman and Bermúdez (1937) and its biserial portion has a rounded periphery. It was recorded from the Paleocene-Eocene of Cuba (Cushman and Bermúdez, 1937), Trinidad (Bolli et al., 1994), and now, for the first time, from the Paleocene of J. Mundassa, UAE.

***Pleurostomella subnodosa* Reuss, 1860**

(Pl. 1, fig. 12)

1860 *Pleurostomella subnodosa* Reuss, p. 204, pl. 8, fig. 2.

1946 *Pleurostomella subnodosa;* Cushman, p. 132, pl. 55, figs. 1-9.

1956 *Pleurostomella subnodosa;* Said and Kenawy, p. 145, pl. 4, fig. 26.

1968 *Pleurostomella subnodosa;* Sliter, p. 110, pl. 19, fig. 10.

1993b *Pleurostomella subnodosa;* Anan, p. 663, pl. 3, fig. 11.

2003 *Pleurostomella subnodosa;* Ali, pl. 7, fig. 21.

2019a *Pleurostomella subnodosa;* Anan, p. 177, pl. 2, fig. 18.

Remarks: This species slender, elongate and small to medium size smooth test with hooded aperture. It was recorded from the upper part of the Cretaceous in Europe (Reuss, 1860), USA (Cushman, 1946), Mexico (Sliter, 1968), but Paleocene of Egypt (Said and Kenawy, 1956), and Qarn El Barr section, UAE (Anan, 1993b). It is recorded also, for the first time, from the Paleocene of J. Mundassa, UAE.

Superfamily Stilostomellacea Finlay, 1947

Family Stilostomellidae Finlay, 1947

Genus *Orthomorphina* Stainforth, 1952

Type species. *Orthomorphina havanensis* (Cushman and Bermúdez, 1937)

***Orthomorphina rohri* (Cushman and Stainforth, 1945)**

1945 *Nodogenerina rohri* Cushman and Stainforth, p. 39, pl. 5, fig. 26.

1953 *Orthomorphina rohri*; Beckmann, p. 365, pl. 21, fig. 8.

1956 *Orthomorphina rohri*; Said and Kenawy, p. 142, pl. 4, fig. 4

1978 *Orthomorphina rohri*; Proto Decima and Bolli, p. 795, pl. 1, fig. 17.
1980 *Orthomorphina* sp.; Barr and Berggren, p. 187, pl. 3, fig. 5.
1989 *Orthomorphina rohri*; Hulsbos et al., p. 272, pl. 3, fig. 1
1994 *Orthomorphina rohri*; Bolli et al., p. 358, fig. 62. 17.
2000 *Nodogenerina rohri*; Sztrákos, p. 167.
2007 *Orthomorphina rohri*; Ozsvárt, p. 71, pl. 8, fig. 17.
2007 *Orthomorphina rohri*; Valchev, p. 133, pl. 1, fig. 13.
2010 *Orthomorphina rohri*; Anan, p. 163.
2020 *Orthomorphina rohri*; Anan, p. 8, pl. 2.8.

Remarks: The holotype of this Oligocene species from Trinidad was erected to belong to the genus *Nodogenerina.* Later on, this species was treated, by many authors, to belong to the genus *Orthomorphina* due to showing the characters of this genus in its irregular arranged chambers and the simple terminal aperture. It is also recorded from the Middle to Upper Eocene of J. Hafit, UAE (Anan, 2010), the Lower Eocene of Libya (Barr and Berggren, 1980), France (Sztrákos, 2000), Norwegian Sea (Hulsbos et al., 1989), Bulgaria (Valchev, 2007), Hungary (Ozsvárt, 2007), Trinidad (Bolli et al., 1994), but from the Paleocene of Egypt (Said and Kenawy, 1956) and the studied Mundassa section.

Genus *Stilostomella* Guppy, 1894
Type species. *Stilostomella rugosa* Guppy, 1894
***Stilostomella paleocenica* (Cushman and Todd, 1946)**
(Pl. 1, fig. 13)
1946 *Ellipsonodosaria paleocenica* Cushman and Todd, p. 61, pl. 10, fig. 26.
1956 *Stilostomella paleocenica;* Said and Kenawy, p. 146, pl. 4, fig. 39.
1994 *Stilostomella paleocenica;* Bolli et al., p. 145, figs. 38. 29, 30.
1996 *Stilostomella paleocenica;* Aref and Youssef, p. 568, pl. 3, fig. 30.
2001 *Stilostomella paleocenica;* Khalil, p. 329, fig. 8. 12.
2003 *Stilostomella paleocenica;* Ali*,* p.124, pl. 7, fig. 25.
2007 *Siphonodosaria paleocenica*; Valchev, p. 133, pl. 1, fig. 15.
2020 *Stilostomella paleocenica;* Anan, p. 8.

Remarks: Loeblich and Tappan (1987) treated the genus *Ellipsonodosaria* Silvestri (1900) as a junior synonym of the genus *Nodosarella* Rzehak (1895). The genus *Stilostomella* differs from the genus *Siphonodosaria* mainly by its straight test rather than slightly arcuate, not broadening initial chambers and arcuate aperture rather than phialine with a crenulated apertural lip. This Paleocene-Miocene species has a slim smooth elongated straight uniserial test, slightly tapered in the initial portion then slightly broadening with around 10 spherical chambers which gradually increase in size, straight horizontal deep sutures, and terminal aperture on a short neck with a lip. It was recorded from the USA (Cushman and Todd, 1946), Trinidad (Bolli et al., 1994), Bulgaria (Valchev, 2007) and Egypt (Said and Kenawy, 1956). It is recorded, for the first time, from the Paleocene of J. Mundassa, UAE.

Family Bagginidae Cushman, 1927
Subfamily Baggininae Cushman, 1927

Genus *Valvulineria* Cushman, 1926
Type species. *Valvulineria californica* Cushman, 1926
***Valvulineria scrobiculata* (Schwager, 1883)**
(Pl. 2, fig. 1)
1883 *Anomalina scrobiculata* Schwager, p. 129, pl. 29, fig. 18.
1953 *Valvulineria scrobiculata;* LeRoy, p. 53, pl. 9, figs. 18-20.
1956 *Valvulineria scrobiculata*; Said and Kenawy, p. 147, pl. 4, fig. 42.
1976 *Valvulineria scrobiculata*; Salaj, pl. 8, figs. 1, 2.
2001 *Valvulineria scrobiculata;* Hewaidy and Strougo, p. 17, pl. 2, figs. 18, 19.
2003 *Valvulineria scrobiculata;* Ali, p.125, pl. 9, figs. 17-19.
2006 *Valvulineria scrobiculata;* Ernst et al., p. 102, pl. 2, figs. c, d.
2012 *Valvulineria scrobiculata;* Stassen et al., p. 158, fig. 5. 3, 9.

Remarks: This Paleocene-Eocene species has a slightly longer than the broad test, slightly convex both dorsally and ventrally, with 7-8 chambers in the last whorl enlarging slowly as added, aperture ventral at the last chamber. It is recorded from Egypt (LeRoy, 1953) and Tunisia (Salaj, 1976), and now, for the first time, from the Paleocene of J. Mundassa, UAE.

Superfamily Discorbinellacea Sigal, 1952
Family Parrelloididae Hofker, 1956
Genus *Cibicidoides* Thalmann, 1939
Type species. *Truncatolina mundula* Brady, Parker and Jones, 1890
***Cibicidoides libycus* (LeRoy, 1953)**
(Pl. 2, fig. 2)
1953 *Cibicides libycus* LeRoy, p. 24, pl. 5, figs. 1-3.
1956 *Cibicidoides libycus*; Said and Kenawy, p. 156, pl. 7, fig. 17.
1980 *Heterolepa libyca*; Saperson and Janal, p. 404, pl. 2, fig. 4.
2005 *Heterolepa libyca*; Sztrákos, p. 189, pl. 9, fig. 9.
2008 *Cibicidoides libycus*; Anan, p. 365, pl. 1, fig. 8.
2019b *Cibicidoides libycus*; Anan, p. 268, pl. 3, fig. 81.

Remarks: According to Loeblich and Tappan (1987), the genus *Cibicidoides* Thalmann differs from the genus *Gavelinella* Brotzen by its biconvex, biumbonate test and angular periphery than rounded in the other. Moreover, the genus *Heterolepa* has a slit-like aperture extending about half of the distance to the umbilicus and extending a short distance across periphery on the dorsal side, but without biumbonate test. Both *C. alleni* and *C. libycus* have conspicuous biumbonate test and a low interiomarginal equatorial arch aperture. The Paleocene–Early Eocene *C. libycus* is characterized by its depressed sutures in both sides than elevated and taper sutures in the dorsal side and slightly in the ventral side in *C.alleni* (Plummer). *Cibicidoides libycus* was recorded from Egypt (LeRoy, 1953), France (Sztrákos, 2005) and Turkmenia (Saperson and Janal, 1980). It was originally recorded from Egypt (LeRoy, 1953), and now, for the first time, from the Paleocene of J. Mundassa, UAE.

***Cibicidoides pharaonis* (LeRoy, 1953)**

1953 *Cibicides pharaonis* LeRoy, p. 24, pl. 7, figs. 9-11.
1988 *Cibicidoides pharaonis*; Anan and Sharabi, p. 215, pl. 2, fig. 20.
1994 *Cibicidoides pharaonis*; Speijer, p. 156, pl. 4, fig. 3.
2001 *Cibicidoides pharaonis*; Hewaidy and Strougo, p. 17, pl. 2, figs. 27, 28.
2006 *Cibicidoides pharaonis*; Alegret and Ortiz, p. 440, pl. 1, fig. 24.
2008 *Cibicidoides pharaonis*; Anan, p. 366, pl. 1, fig. 9.
2016 *Cibicidoides pharaonis*; Orabi and Zaky, p. 188, pl. 3, fig. 18.
2019b *Cibicidoides pharaonis*; Anan, p. 268, pl. 3, fig. 82.

Remarks: This Paleocene–Early Eocene species has a medium test with 8-10 chambers in the last whorl, ventrally more convex than dorsally, sutures flush with the surface. It is characterized by its moderately wide, curved ventral sutures and coarse punctuation. It was recorded by LeRoy (1953) from the Lower Eocene of the Maqfi section, and later from many sites in Egypt. This species is recorded for the first time outside Egypt, in the Paleocene of the studied Mundassa section, UAE.

***Cibicidoides pseudoacutus* (Nakkady, 1950)**

1950 *Anomalina pseudoacuta* Nakkady, p. 691, pl. 90, figs. 29-32.
1953 *Anomalina pseudoacuta*; Le Roy p. 18, pl. 3, figs. 29 -31.
1994 *Cibicidoides pseudoacutus*; Speijer, p. 54, pl. 7, fig. 6.
1996 *Anomalina pseudoacuta*; Aref and Youssef, p. 551, pl. 4, fig. 12.
2001 *Cibicidoides pseudoacutus*; El-Dawy, p. 45, pl. 2, fig. 17
2002 *Cibicidoides pseudoacutus*; Galeotti and Coccioni, p. 198, fig. 1.
2002 *Cibicidoides pseudoacutus*; Alegret et al., p. 132, fig. 5. 3.
2004 *Cibicidoides pseudoacutus*; Anan, p. 45, pl. 1, fig. 6.
2005 *Gavelinella pseudoacuta*; Sztrákos, p. 214, pl. 9, fig. 14.
2006 *Cibicidoides pseudoacutus*; Ernst et al., p. 95, pl. 1, figs. J, k.
2006 *Cibicidoides pseudoacutus*; Alegret and Ortiz, p. 440, pl. 2, fig. 2.
2007 *Cibicidoides pseudoacutus*; Anan, p. 306, pl.1, fig. 6.
2019b *Cibicidoides pseudoacuta*; Anan, p. 268, pl. 3, fig. 83.

Remarks: This Maastrichtian–Eocene species is distinguished by biconvex test, the central boss on the dorsal side, fine beads on the ventral side. It was described by Nakkady (1950) from the Abu Durba (Sinai) and Luxor section (Nile Valley). Later, it was recorded in different localities in Egypt: Farafra Oasis (LeRoy, 1953), Red Sea coast (Aref and Youssef, 1996; Anan, 2004), Dababiya section (Ernst et al., 2006), but Paleocene-Eocene (Alegret and Ortiz, 2006). It is interesting to note that it was also recorded in the Maastrichtian–Paleocene of Tunisia (Speijer, 1994), but in the Paleocene–Eocene of France (Sztrákos, 2005). It is recorded for the first time, from the Paleocene of J. Mundassa, UAE.

Superfamily Asterigerinacea d'Orbigny, 1839
Family Epistomariidae Hofker, 1954
Subfamily Nuttallidinae Saidova, 1981
Genus *Nuttallides* Finlay, 1939
Type species. *Nuttallides truempyi* Nuttall, 1930

***Nuttallides truempyi* (Nuttall, 1930)**

(Pl. 2, fig. 3)

1930 *Eponides truempyi* Nuttall, p. 274, 287, pl. 24, figs. 9, 13-14.
1975 *Nuttallides truempyi*; Proto Decima and De Biase, p. 95. pl. 2, fig. 9.
1976 *Nuttallides truempyi*; Berggren and Aubert, p. 315, pl.2, figs.12-13.
1978 *Nuttallides truempyi*; Proto Decima and Bolli, p. 795, pl. 3, figs, 1, 2..
1983 *Nuttallides truempyi*; Miller, p. 439, pl. 1, figs. 4-7.
1983 *Nuttallides truempyi*; Tjalsma and Lohmann, p.17, pl. 6, fig. 4, pl. 17, figs. 4-5, pl. 21, figs. 1-4.
1988 *Nuttallides truempyi*; Kaiho, p. 554.
1988 *Nuttallides truempyi*; Parisi and Coccioni, p. 103, pl. 2, figs. 12-17.
1988 *Nuttallides truempyi*; Saint-Marc and Berggren, p. 110, pl. 4, figs. 7-9.
1989 *Nuttallides truempyi*; Hulsbos et al., p. 272.
1990 *Nuttallides truempyi*; Thomas, p. 594, pl. 3, figs. 1, 2.
1993 *Nuttallides truempyi*; Boltovskoy and Vera Ocampo, p. 152, pl. 4, fig. 15.
1993b *Nuttallides truempyi*; Anan, p. 665, pl. 3, fig. 14.
1994 *Nuttallides truempyi*; Bolli et al., p. 370, fig. 88. 13.
1996 *Nuttallides truempyi*; Anan, p. 154, fig. 4. 4.
2005 *Nuttallides truempyi*; Sztrákos, p. 188, pl. 17, fig. 22.
2007 *Nuttallides truempyi*; Anan, p. 76, pl. 1, fig. 7.
2008 *Nuttallides truempyi*; Alegret et al., p. 96.
2010 *Nuttallides truempyi*; Anan, p. 166.

Remarks: Berggren and Aubert (1976) noted that the extinction of *Nuttallides truempyi* serves as a useful marker in determining the approximate position of the Eocene/ Oligocene boundary, which is confirmed by Proto Decima and Bolli (1978), Alegret et al. (2008). Tjalsma and Lohmann (1983) added that this extinction is diachronous, and it is frequent abundant during the Paleocene and rare to abundant in the Middle-Late Eocene (MLE). Miller (1983) noted that the Eocene *N. truempyi* is replaced by the Oligocene *N. umbonifera*. Saint-Marc and Berggren (1988) recorded it from the Paleocene of Tunisia and UAE (Qarn El Barr section). Berggren and Miller (1989) considered the last appearance of this species is at the end of Late Eocene. Bolli et al. (1994) noted that it ranges in Trinidad from Maastrichtian through Late Eocene. It was recorded also by Sztrákos (2005) from the Paleocene–Upper Eocene in France. It is recorded in the Upper Eocene of J. Malaqet and MLE of J. Hafit, UAE. It is recorded here for the first time, from the Paleocene of J. Mundassa, UAE.

Family Alfredinidae S. N. Singh and Kalia, 1972
Genus *Epistomaroides* Uchio, 1952
Type species. *Discorbina polystomelloides* Parker and Jones, 1865

***Epistomaroides spissiformis* Cushman and Stainforth, 1945**

1945 *Anomalina alazanensis* Nuttall var. *spissiformis* Cushman and Stainforth, p. 71, pl. 14, fig.5.

1951 *Anomalina alazanensis* Nuttall var. *spissiformis*; Cushman and Stainforth, p. 162, pl. 28, fig. 6.

1975 *Anomalina alazanensis spissiformis*; Proto Decima and De Biase, p. 97. pl. 2, fig. 24.

1978 *Anomalina alazanensis spissiformis*; Proto Decima and Bolli, p. 789, pl.5, figs. 12-13.

1983 *Anomalina spissiformis*; Tjalsma and Lohmann, p. 23, pl. 20, fig. 4.

1988 *Anomalina spissiformis*; Parisi and Coccioni, p. 104, pl. 4, figs. 4-9.

1994 *Anomalina alazanensis spissiformis*; Bolli et al., p. 373, pl. 59, figs. 10-12.

2006 *Anomalinoides spissiformis*; Ortiz and Thomas, p. 112, pl. 3, fig. 7.

2010 *Epistomaroides spissiformis*; Anan, p. 167, pl. 2, fig. 2.

Remarks: Loeblich and Tappan (1987) noted that the type specimen of *Anomalina* was lost, and a petition was submitted to the ICZN for the suppression of the genus *Anomalina* d'Orbigny (1826) and retention of the genus *Epistomaroides* Uchio (1952) as a valid genus. This Paleocene–Oligocene species was recorded from Oligocene of Trinidad (Cushman and Stainforth, 1945), Ecuador (Cushman and Stainforth, 1951), Trinidad (Bolli et al.,1994), Atlantic (Tjalsma and Lohmann, 1983), Italy (Parisi and Coccioni, 1988), and J. Hafit, UAE (Anan, 2010). It is recorded here from the Paleocene of J. Mundassa, UAE.

Superfamily Nonionacea Schultze, 1854

Family Nonionidae Schultze, 1854

Subfamily Pulleniinae Schwager, 1877

Genus *Pullenia* Parker and Jones, 1862

Type species. *Nonionina bulloides* d'Orbigny, 1846

***Pullenia angusta* Cushman and Todd, 1943**

(Pl. 2, fig. 4)

1943 *Pullenia quinqueloba* (Reuss) *angusta* Cushman and Todd, p. 10, pl. 2, fig. 3.

1956 *Pullenia quinqueloba angusta*; Said and Kenawy, p. 157, pl. 7, fig. 23.

1994 *Pullenia angusta*; Bolli et al., p. 151, fig. 41. 21, 22.

Remarks: This Maastrichtian–Early Eocene species has a closed coiled test, periphery rounded, flush suture, aperture a long narrow slit extending over the periphery at the base of the septal face with some deep umbilical extending to the periphery. It was recorded from the USA (Cushman and Todd, 1943), Caribbean (Bolli et al., 1994), Egypt (Said and Kenawy, 1956). It is recorded for the first time, from the Paleocene of J. Mundassa, UAE.

***Pullenia coryelli* (White, 1929)**

(Pl. 2, fig. 5**)**

1929 *Pullenia coryelli* White, p. 58, pl. 5, fig. 22.

1946 *Pullenia coryelli*; Cushman, p. 147, pl. 60, figs. 10-11.

1956 *Pullenia* cf. *coryelli*; Said and Kenawy, p. 156, pl. 7, fig. 24.

1988 *Pullenia coryelli*; Kaiho, p. 554, fig. 1.

1990 *Pullenia coryelli*; Thomas, p. 594, pl. 3, fig. 6.

1993b *Pullenia coryelli*; Anan, p. 665, pl. 3, fig. 15.

1994 *Pullenia coryelli*; Bolli et al., p. 151, fig. 41. 23, 24.

2002 *Pullenia coryelli*; Alegret et al., p. 132, fig. 5. 9.

2005 *Pullenia coryelli*; Waśkowska-Oliwa, p. 312, fig. 9. 9.

2006 *Pullenia coryelli*; Valchev, p. 44, pl. 2, fig. 18.

2012 *Pullenia coryelli*; Drobne et al., p. 222, pl. 4, fig. 56.

2020 *Pullenia coryelli*; Anan, p. 10.

Remarks: Tjalsma and Lohmann (1983) noted that *P. coryelli*can be differentiated from *P. eocenica* mainly by its lobulate periphery. This late Maastrichtian–Eocene species was recorded from Mexico (White, 1929), the USA (Cushman, 1946), Trinidad (Bolli et al., 1994), Bulgaria (Valchev, 2006), Slovenia (Drobne et al., 2012), Poland (Waśkowska-Oliwa, 2005), Tunisia (Alegret et al., 2002), Egypt (Said and Kenawy, 1956), Qarn El Barr, UAE section (Anan, 1993b), Japan and New Zealand (Kaiho, 1988). It is recorded here from the Paleocene of J. Mundassa, UAE.

***Pullenia eocenica* Cushman and Siegfus, 1939**

1939 *Pullenia eocenica* Cushman and Siegfus, p. 31, pl. 7, fig. 1.

1975 *Pullenia eocenica*; Proto Decima and De Biase, p. 97. pl. 3, fig. 1.

1978 *Pullenia eocenica*; Proto Decima and Bolli, p. 795, pl. 4, figs. 7-8.

1983 *Pullenia eocenica*; Miller, p. 439, pl. 4, fig. 11.

1983 *Pullenia eocenica*; Tjalsma and Lohmann, p. 36. pl. 16, fig. 1.

1985 *Pullenia eocenica*; Boltovskoy and Watanabe, p. 299, pl. 3, fig. 26.

1988 *Pullenia eocenica*; Parisi and Coccioni, p. 104, pl. 3, figs. 8, 9.

1994 *Pullenia eocenica;* Bolli et al., p. 152, fig. 41. 29, 30.

2000 *Pullenia eocenica*; Sztrákos, p. 170, pl. 16, fig. 8.

2010 *Pullenia eocenica*; Anan, p. 168.

Remarks: This Maastrichtian–Eocene species is characterized by its non-lobate equatorial periphery. It was recorded from the USA (Cushman and Siegfus, 1939), Trinidad (Bolli et al., 1994), Atlantic (Tjalsma and Lohmann, 1983), Spain (Miller, 1983), France (Sztrákos, 2000), Italy (Proto Decima and De Biase, 1975), and J. Hafit, UAE (Anan, 2010). It is recorded here from the Paleocene of J. Mundassa, UAE.

***Pullenia quinqueloba* (Reuss, 1851)**

(Pl. 2, fig. 6)

1851 *Nonionina quinqueloba* Reuss, p. 47, pl. 5, fig. 31.

1953 *Pullenia quinqueloba*; Le Roy, p. 45, pl. 11, figs. 10-11.

1956 *Pullenia quinqueloba*; Haque, p. 171, pl. 34, fig. 5.

1978 *Pullenia quinqueloba*; Proto Decima and Bolli, p. 795, pl. 4, fig. 9.

1980 *Pullenia quinqueloba*; Ingle et al., p. 142, pl. 5, fig. 8.

1983 *Pullenia quinqueloba*; Miller, p. 439, pl. 4, figs. 9, 10.

1983 *Pullenia quinqueloba*; Tjalsma and Lohmann, p. 36. pl. 16, fig. 2.

1985 *Pullenia quinqueloba*; Boltovskoy and Watanabe, p. 299, pl. 3, fig. 16.

1988 *Pullenia quinqueloba*; Parisi and Coccioni, p. 104, pl. 3, figs. 10-11.

1989 *Pullenia quinqueloba*; Hulsbos et al., p. 273, pl. 3, fig. 8.

1993a *Pullenia quinqueloba*; Anan, p. 316, pl. 3, fig. 7.

1993b *Pullenia quinqueloba*; Anan, p. 665, pl. 3, fig. 16.

1994 *Pullenia quinqueloba*; Bolli et al., p. 152, fig. 41. 31-32.
2000 *Pullenia quinqueloba*; Sztrákos, p. 170.
2006 *Pullenia quinqueloba*; Cimerman et al., p. 38, pl. 10, figs. 10.
2006 *Pullenia quinqueloba*; Ortiz and Thomas, p. 128, pl. 10, 10.
2010 *Pullenia quinqueloba*; Anan, p. 168.
2020 *Pullenia quinqueloba*; Anan, p. 10.

Remarks: This cosmopolitan species is characterized by its 5-chambers in the last whorl, with semi-compressed test and semi-lobate periphery. Tjalsma and Lohmann (1983) included the 4-chambers in this species, while Hulsbus et al. (1989) include 5-6 chambers in the last whorl. On the other hand, this species was recorded from Maastrichtian–Paleocene in the Qarn El Barr section, UAE (Anan, 1993b), but the Paleocene in J. Malaqet (Anan, 1993a), in Pacific (Boltovskoy and Watanabe, 1985), but from Eocene in Egypt (LeRoy, 1953), in Atlantic(Tjalsma and Lohmann, 1983) in the Norwegian Sea (Hulsbus et al., 1989) and at J. Hafit, UAE (Anan, 2010). It is recorded here in the Paleocene of J. Mundassa, UAE.

***Pullenia reussi* Cushman and Todd, 1943**

(Pl. 2, fig. 7)

1943 *Pullenia reussi* Cushman and Todd, p. 4, pl. 1, figs. 10-13.
1956 *Pullenia reussi*; Said and Kenawy, p. 156, pl. 7, fig. 22.
1993a *Pullenia reussi;* Anan, p. 317.

Remarks: This Cretaceous–Eocene species has few chambers (4 chambers), a broadly rounded periphery, and a low convex apertural face. It was recorded from the USA (Cushman and Todd, 1943), Egypt (Said and Kenawy, 1956) and J. Malaqet, UAE (Anan, 1993a). It is recorded here in the Paleocene of J. Mundassa, UAE.

Superfamily Chilostomellidae Brady, 1881
Family Quadrimorphinidae Saidova, 1981
Genus *Quadrimorphina* Finlay, 1939
Type species. *Valvulina allomorphinoides* Reuss, 1860

***Quadrimorphina esnehensis* (Nakkady, 1950)**

1950 *Valvulineria esnehensis* Nakkady, p. 689, pl. 90, figs. 11-13.
1953 *Valvulineria esnehensis*; LeRoy,p. 53, pl. 7, figs. 29-30.
1956 *Valvulineria esnehensis*; Said and Kenawy, p. 147, pl. 4, fig. 41.
1994 *Valvulineria esnehensis*; Hewaidy, p. 55, fig. 4.
1976 *Quadrimorphina esnehensis*; Futyan, p. 521.
2009a *Quadrimorphina esnehensis*; Anan, p. 42.
2020 *Quadrimorphina esnehensis*; Anan, p. 10.

Remarks: Anan (2009a) regarded this species to the genus *Quadrimorphina* (non *Valvulineria*, as originally described by Nakkady, 1950), due to its biconvex test, not flattened to moderately umbilical side, with 5-6 chambers in the last whorl and inflated ventral chambers.This Maastrichtian–Early Eocene species was recorded from many sites in Egypt (Nakkady, 1950; LeRoy, 1953; Anan, 2009a), and Jordan (Futyan, 1976). It is recorded from the Paleocene of J. Mundassa, UAE.

Family Alabaminidae Hofker, 1951
Genus *Alabamina* Toulmin, 1941
Type species. *Alabamina wilcoxensis* Toulmin, 1941

***Alabamina midwayensis* Brotzen, 1948**

1948 *Alabamina midwayensis* Brotzen, p. 99, pl. 16, figs. 1, 2.
1976 *Alabamina midwayensis;* Aubert and Berggren, p. 428, pl. 8, fig. 3.
1976 *Alabamina midwayensis;* Salaj, pl. 15, figs. 1, 2.
1993a *Alabamina midwayensis;* Anan, p. 317.
1994 *Alabamina midwayensis;* Bolli et al., p. 155, fig. 42. 33, 34.
2001 *Alabamina midwayensis;* Alegret and Thomas, p. 276, pl. 1, fig. 2.
2003 *Alabamina midwayensis;* Ali, p. 118, pl. 12, figs. 4-6.
2020 *Alabamina midwayensis;* Anan, p. 10.

Remarks: This Paleocene species was recorded from Sweden (Brotzen, 1948), Trinidad (Bolli et al., 1994), Tunisia (Aubert and Berggren, 1975), Egypt (Ali, 2003) and J. Malaqet, UAE (Anan, 1993a). It is also recorded from the Paleocene of J. Mundassa, UAE.

Genus *Valvalabamina* Reiss, 1963
Type species. *Rotalina lenticula* Reuss, 1845

***Valvalabamina planulata* (Cushman and Renz, 1941)**

(Pl. 2, fig. 8)

1941*Gyroidina planulata* Cushman and Renz, p. 23, , pl. 4, fig. 1.
1953 *Gyroidina planulata*; LeRoy, p. 35, pl. 11, figs. 1-3.
1956 *Gyroidina planulata;* Said and Kenawy, p. 149, pl. 5, fig. 8.
1994 *Valvalabamina planulata*; Speijer, p. 160, pl. 7, fig. 3.
2001 *Valvalabamina planulata*; Hewaidy and Strougo, p. 17, pl. 2, figs. 31, 32.

Remarks: This Paleocene–Eocene species has a flattened smooth test, rounded periphery, more convex ventral side than dorsal side, flush spiral and ventral sutures and slightly curved, and narrow elongate umbilical-extraumbilical slit aperture, and less peripheral lobulation than *V. depressa* (Alth). These species characters belong to the genus *Valvalabamina* more than the planoconvex test and nearly radial sutures of the genus *Gyroidina*with its low interiomarginal slit aperture. It was recorded from the USA (Cushman and Renz, 1941), Egypt (LeRoy, 1953; Speijer, 1994). It is recorded here, for the first time, from the Paleocene of J. Mundassa, UAE.

Family Osangulariidae Loeblich and Tappan, 1946
Genus *Osangularia*Brotzen, 1940
Type species. *Osangularia lens*Brotzen, 1940

***Osangularia plummerae* Brotzen, 1940**

1940 *Osangularia plummerae* Brotzen, p. 30, text-fig. 8.
1976 *Osangularia plummerae;* Aubert and Berggren, p. 429, pl. 8, fig. 5.
1976 *Osangularia plummerae*; Salaj, pl. 8, fig. 4.
1985 *Osangularia plummerae;* Luger, p. 110, pl. 8, fig. 6.
1988 *Osangularia plummerae;* Keller, pl. 1, figs. 1-3.
1993a *Osangularia plummerae;* Anan, pl.317, pl. 3, fig. 9.

1994 *Osangularia plummerae;* Speijer, p. 56, pl. 7, fig. 5; p. 161, pl. 4, fig. 1.
2005 *Osangularia plummerae;* Sztrákos, p. 189, pl. 9, fig. 1; pl. 16, fig. 19.
2006 *Osangularia plummerae;* Alegret and Ortiz, p. 441, pl. 2, fig. 41.
2006 *Osangularia plummerae;* Ortiz and Thomas, p. 124, pl. 9, fig. 4.
2011 *Osangularia plummerae;* Sprong et al., p. 179, pl. 1, fig. 15.

Remarks: This Paleocene species is characterized by its biconvex test and distinct aperture. It was recorded from Sweden (Brotzen, 1940), Spain (Ortiz and Thomas, 2006), France (Sztrákos, 2005), Tunisia (Aubert and Berggren, 1975), Egypt (Luger, 1985) and J. Malaqet, UAE (Anan, 1993a). It is recorded from thePaleocene of J. Mundassa.

Superfamily Chilostomellacea Bandy, 1881
Family Heterolepidae Gonzáles-Donoso, 1969
Genus *Anomalinoides*Brotzen, 1942
Type species. *Anomalinoides plummerae* Brotzen, 1942

***Anomalinoides acutus* (Plummer, 1927)**

1927 *Anomalina ammonoides* Reuss var. *acuta* Plummer, p. 149, pl. 10, fig. 2.
1948 *Anomalinoides acuta*; Brotzen, p. 87, pl. 14, fig. 2.
1976 *Anomalinoides acuta*; Aubert and Berggren, p. 430, pl. 9, fig. 1.
1993a *Anomalinoides acuta*; Anan, p. 317, pl. 3, fig. 10. 276, pl. 1, fig. 9.
2006 *Anomalinoides acutus*; Alegret and Ortiz, p. 438, pl. 1, fig. 12.
2011 *Anomalinoides acutus*; Aly et al., p. 116, pl. 8, fig. 1.

Remarks: This Paleocene–Late Eocene species was recorded from the USA (Plummer, 1927), Sweden (Brotzen, 1940), Tunisia (Aubert and Berggren, 1975), Egypt (Alegret and Ortiz, 2006), and J. Malaqet, UAE (Anan, 1993a). It is recorded from the Paleocene of J. Mundassa, UAE.

***Anomalinoides rubiginosus* (Cushman, 1926)**
(Pl. 2, fig. 9**)**

1926 *Anomalina rubiginosa* Cushman, p. 607, pl. 2, fig. 6.
1940 *Cibicides danica* Brotzen, p. 31, pl. 25, text-fig. 2.
1948 *Anomalinoides danica*; Brotzen, p. 87, pl. 14, fig. 13.
1953 *Anomalinagranosa;* LeRoy, p. 17, pl. 6, figs. 1-3.
1956 *Anomalina dorri aragonensis;* Haque, p. 191, pl. 33, fig. 1.
1975 *Gavelinella danica*; Berggren and Aubert, p. 155, pl. 6, fig. 3.
1976 *Gavelinella rubiginosa*; Aubert and Berggren, p. 433, pl. 12, fig. 3.
1982 *Gavelinella rubiginosa*; Beckmann, p. 111, pl. 5, fig. 26.
1983 *Gavelinelladanica*; Tjalsma andLohmann, p. 13, pl. 5, fig. 7.
1988 *Anomalinoides rubiginosus*; Kaiho, p. 554, fig. 1.
1993a *Gavelinelladanica*; Anan, p. 317, pl. 3, fig. 12.
1993b *Gavelinelladanica*; Anan, p. 666, pl. 3, fig. 18.
1994 *Anomalinoides rubiginosus*; Bolli et al., p.158, fig. 44. 18,19.
2001 *Anomalinoides rubiginosus*; Shahin, p. 14, fig. 7. 18.
2001 *Anomalinoides rubiginosus*; Alegret and Thomas, p. 276, pl. 2, fig. 6.
2001 *Gavelinella rubiginosa*; El-Dawy, p. 46, pl. 3, figs. 15, 16.
2004 *Anomalinoides rubiginosus*; Anan, p. 45, pl. 1, figs. 7, 8.
2005 *Anomalinoides rubiginosus*; Sztrákos, p. 214, pl. 9, fig. 7.
2012 *Gavelinella rubiginosa*; Ismail, p. 41, pl. 3, fig. 27.
2012 *Gavelinella rubiginosa*; Youssef and Taha, pl. 5, fig. 7, 8.
2016 *Anomalinoidesgranosa;* Orabi and Zaky, p. 188, pl. 3, fig. 21.
2020 *Anomalinoides rubiginosus*; Anan, p. 11, pl. 2.16.

Remarks: Berggren and Aubert (1975) noted that this Campanian–Eocene species has been recorded under several names in the literature. They also noted that the early Eocene*Gavelinelladanica* appears to have evolved into another species which the majority of workers have identified as *Gavelinella* or *Anomalinoides*. This form has been identified as the species *rubiginosa* and variously ascribed to the genus *Anomalinoides* or *Gavelinella*. These two species *danica* and *rubiginosus* have slightly differing morphology due to a function of depth. Bolli et al. (1994) noted that the shape variation from moderately planoconvex (predominant in the Late Cretaceous) to thick biconvex and pseudoplanispiral (mostly in the Paleocene) and the coiling are usually nearly involute. They also added that Cushman's *rubiginosus* may indicate a relationship to the *A. dorri aragonensis* group. The author believes that: 1) *A.danica* is a junior synonym of *A.rubiginosus*, 2) the shape of Late Cretaceous *A.rubiginosus* with moderately planoconvex and closely coiled test varies to a thick biconvex pseudo-planispiral Paleocene test, 3) the different shapes of the two forms are most probably related to water depth, 4) some Paleogene forms have slightly raised sutures in the early chambers. Anan (2004) proposed six benthic foraminiferal lineages, and one of them is the Maastrichtian–Paleocene *Anomalinoides rubiginosus* (Cushman) to Paleocene*A. midwayensis* (Plummer). This cosmopolitan species was recorded from the USA (Cushman, 1926), the Caribbean sea (Bolli et al., 1994), North and South Atlantic (Tjalsma and Lohmann, 1983), Sweden (Brotzen, 1948), Italy (Beckmann, 1982), Tunisia (Aubert and Berggren, 1975), Egypt (Shahin, 2001), J. Malaqet and Qarn El Barr sections, UAE (Anan, 1993a,b), Pakistan (Haque, 1956), New Zealand (Kaiho, 1988). It is recorded here from the Paleocene of J. Mundassa, UAE.

***Anomalinoides umboniferus* (Schwager, 1883)**

1883 *Discorbina praecursoria* var. *umbonifera* Schwager, p. 126, pl. 27 (4), fig. 14.
1953 *Anomalina umbonifera;* LeRoy, p. 18, pl. 7, figs. 15-17.
1985 *Anomalinoides umboniferus*; Luger , p. 111, pl. 8, figs. 10, 11.
2003*Anomalinoides umboniferus*; Ali, p. 118, pl. 9, figs. 11-14.
2011 *Anomalina umbonifera;* Aly et al.,p. 117, pl. 8, gig. 6.
2016 *Anomalinoides umboniferus*; Orabi and Zaky, p. 188, pl. 3, fig. 17.

Remarks: This Eocene species was recorded originally from Egypt. It is recorded here for the first time, outside Egypt from the Paleocene of J. Mundassa, UAE.

Family Gavelinellidae Hofker, 1956
Subfamily Gyroidinoidinae Saidova, 1981
Genus *Gyroidinoides* Brotzen, 1942
Type species. *Rotalia nitida* Reuss, 1844

***Gyroidinoides bollii* (Cushman and Renz, 1946)**

1946 *Eponides bollii* Cushman and Renz,p.44, pl. 7, fig. 23.
1988 *Gyroidinoides bollii;* Kaiho, p. 554, fig. 1.
1994 *Gyroidina bollii;* Bolli et al., p. 165, fig. 47. 20-22.

Remarks: According to Said and Kenawy (1956, p. 149), Reuss's original *Rotalia nitida,* which represents the type species of the genus *Gyroidinoides* Brotzen (1942) has been removed to a new generic name *Gyroidinoides.* Bolli et al. (1994) noted that the Maastrichtian *'Eponides' sigali* Said and Kenawy (1956) is a possible junior synonym of this Campanian–Paleocene species. It was recorded from the USA (Cushman and Renz, 1946), the Caribbean area (Bolli et al., 1994) and Japan (Kaiho, 1988). It is recorded for the first time in the Middle East, from the Paleocene of J. Mundassa, UAE.

***Gyroidinoides depressus* (Alth, 1850)**

1850 *Rotalina depressa* Alth, p. 266, pl. 13, fig. 21.
1946 *Gyroidina depressa*; Cushman, p. 139, pl. 58, figs. 1, 2.
1956 *Gyroidina depressa*; Said and Kenawy, p. 149, pl. 5, fig. 11.
1985 *Gyroidinoides depressus*; Luger, p. 109, pl. 8, fig. 1.
1993b *Gyroidinoides depressus*; Anan, p. 666.
2001 *Gyroidinoides depressus*; Alegret and Thomas, p. 286, pl. 6, fig. 9.
2012 *Gyroidinoides depressus*; Ismail, p. 40, pl. 3, fig. 22.

Remarks: This Maastrichtian–Early Eocene species is characterized by its compressed trochoid test with the rounded periphery, 10-12 chambers in the last-formed whorl, sutures curved and nearly flush in the dorsal side, but nearly radial in the ventral side. It was recorded from western Ukraine (Alth, 1850), the USA (Cushman, 1946), Mexico (Alegret and Thomas, 2001), Egypt (Said and Kenawy, 1956) and the Qarn El Barr section, UAE (Anan, 1993b). It is recorded from the Paleocene of J. Mundassa, UAE.

Gyroidinoides girardanus (Reuss, 1851)
(Pl. 2, fig. 10)

1851 *Rotalia girardana* Reuss, p. 73, pl. 5, fig. 34.
1946 *Gyroidina girardana*; Cushman, p. 140, pl. 58, fig. 9.
1951*Gyroidina girardana*; Cushman and Stainforth, p. 158, pl. 27, fig. 24.
1953 *Gyroidina girardana*; LeRoy, p. 35, pl. 5, figs. 10-12.
1956 *Gyroidina girardana*; Haque, p. 149, pl. 17, fig. 2.
1956 *Gyroidina girardana*; Said and Kenawy, p. 148, pl. 5, fig. 7.
1985 *Gyroidinoides girardanus;* Luger, p. 110, pl. 8, figs. 2, 3.
1988 *Gyroidinoides girardanus;* Kaiho, p. 554, fig. 1.
1993a *Gyroidinoides girardanus;* Anan, p. 317.
1994 *Gyroidinoides girardanus;* Speijer, p. 118, pl. 3, fig. 3.
2002 *Gyroidinoides girardanus;* Al-Hitmi, 49, pl. 3, fig. 15.
2004 *Gyroidinoides girardanus;* Anan, p. 47, pl. 1, figs. 11, 12.
2006 *Gyroidinoides girardanus;* Ortiz and Thomas, p. 119, pl. 7, fig. 4.
2011 *Gyroidinoides girardanus*; Aly et al., p. 117, pl. 8, fig. 8.
2012 *Gyroidinoides girardanus;* Ismail, p. 40, pl. 3, fig. 23.
2020 *Gyroidinoides girardanus;* Anan, p. 11.

Remarks: This Maastrichtian–Oligocene species has a planoconvex and high trochospiral test. It is easily distinguished from other *Gyroidinoides* species by its conspicuous concave apertural face and by the overhanging lower edges of the ventral chambers. Anan (2004) proposed six benthic foraminiferal lineages, and one of them is the Maastrichtian–Oligocene G. *girardanus* (Reuss) to Paleocene *G. luterbacheri* Anan. This cosmopolitan species was recorded from Germany (Reuss, 1851), the USA (Cushman, 1946), Ecuador (Cushman and Stainforth, 1951), Trinidad (Cushman and Stainforth, 1945), Egypt (LeRoy, 1953), J. Malaqet, UAE (Anan, 1993a), Qatar (Al-Hitmi, 2002), Pakistan (Haque, 1956) and New Zealand (Kaiho, 1988). It is recorded here from the Paleocene of J. Mundassa, UAE.

***Gyroidinoides globosus* (Hagenow, 1842)**
(Pl. 2, fig. 11**)**

1842 *Nonionina globose* Hagenow, p. 574.
1946 *Gyroidina globosa;* Cushman, p. 140, pl. 58, figs. 6-8.
1956 *Gyroidina globosa;* Said and Kenawy, p. 149, pl. 5, fig. 5.
1968 *Gyroidinoides globosus*; Sliter, p. 675, pl. 10, figs. 7, 8.
1983 *Gyroidinoides globosus*; Tjalsma and Lohmann, p. 58, pl. 7, fig. 5.
1988 *Gyroidinoides globosus*; Kaiho, p. 556, fig. 2.
1993b *Gyroidinoides globosus*; Anan, p. 666.
1994 *Gyroidinoides globosus*; Bolli et al., p. 159, fig. 45. 1-3.
1995 *Gyroidinoides globosus*; Nomura and Brohi, p. 220, fig. 4.
2005 *Gyroidinoides globosus*; Alegret and Thomas, p. 61, 72.
2011d *Gyroidinoides globosus*; Anan, p. 303, pl. 1, fig. 10.
2012 *Gyroidinoides globosus*; Youssef and Taha, pl. 6, fig. 1.

Remarks: The Maastrichtian–Eocene cosmopolitan species *globosus* differs from other species of the genus *Gyroidinoides* by it's very broadly rounded periphery, tight umbilical area and very rounded test. It was recorded from Germany (Hagenow, 1842), the USA (Cushman, 1946), Atlantic Ocean (Tjalsma and Lohmann, 1983), Trinidad (Bolli et al., 1994), Mexico (Sliter, 1968), Egypt (Said and Kenawy, 1956), the Qarn El Barr section, UAE (Anan, 1993b), Pakistan (Nomura and Brohi, 1995), and Japan (Kaiho, 1988). Itis recorded here for the first time, from the Paleocene of J. Mundassa, UAE.

***Gyroidinoides reussi* (Said and Kenawy, 1956)**
(Pl. 2, fig. 12)

1956 *Gyroidina reussi* Said and Kenawy, p. 149, pl. 5, fig. 10.

Remarks: This Paleocene species has a plano-convex smooth test, periphery broadly rounded, sutures slightly curved, aperture a low slit at the base of the last chamber from the 6 chambers in the last whorl. This species was originally recorded from Egypt (Said and Kenawy, 1956). It is recorded for the first time outside Egypt, from the Paleocene of J. Mundassa, UAE.

***Gyroidinoides subangulatus* (Plummer, 1927)**

(Pl. 2, fig. 13)

1927 *Rotalia soldanii* (d'Orbigny) var. *subangulata* Plummer, p. 154, pl. 12, fig. 1.

1953 *Gyroidina subangulata;* LeRoy, p. 35, pl. 3, figs. 23-25.

1956 *Gyroidina subangulata;* Said and Kenawy, p. 149, pl. 5, fig. 9.

1976 *Gyroidinoides subangulatus;* Aubert and Berggren, p. 429, pl. 8, fig. 6.

1976 *Gyroidinoides subangulatus;* Salaj, pl. 8, fig. 5.

1993b *Gyroidinoides subangulatus;* Anan, p. 666.

1994 *Gyroidinoides subangulatus;* Bolli et al., p. 159, fig. 45. 25-27.

2001 *Gyroidinoides subangulatus;* El-Dawy, p. 46, pl. 3, fig. 10.

2003 *Gyroidinoides subangulatus;* Ali, p. 120, pl. 11, figs. 1-3.

2005 *Gyroidinoides subangulatus;* Sztrákos, p. 189, pl. 17, fig. 9.

2005 *Gyroidinoides subangulatus;* Clemmensen and Thomsen, p.358, pl.3, figs. 20-22.

2006 *Gyroidinoides subangulatus;* Karoui-Yaakoub, p. 584, pl.2, figs.13,14.

2016 *Gyroidinoides subangulatus;* Orabi and Zaky, p. 188, pl. 3, fig. 20.

2020 *Gyroidinoides subangulatus;* Anan, p. 11, pl. 2.18.

Remarks: This Paleocene species has a plano-convex smooth test, with 8-9 chambers in the final whorl, and sutures slightly depressed. It was recorded from the USA (Plummer, 1927), North Sea Basin (Clemmensen and Thomsen, 2005), France (Sztrákos, 2005), Tunisia (Aubert and Berggren, 1976), Egypt (Said and Kenawy, 1956) and the Qarn El Barr section, UAE (Anan, 1993b). It is recorded here, from the Paleocene of J. Mundassa, UAE.

Genus *Stensiöeina* Brotzen, 1942

Type species. *Rotalia exsculpta* Reuss, 1860

***Stensiöeina esnehensis* Nakkady, 1950**

1950 *Stensiöeina esnehensis* Nakkady, p. 689, pl. 90, figs.8-10.

2009a *Stensiöeina esnehensis*; Anan, p. 43.

2011c *Stensiöeina esnehensis*; Anan, p. 23, pl. 2, fig. 14.

Remarks: This species has plano-convex test with 10 chambers, dorsal side flat, but dome-shaped ventral side, curved, raised and ornate dorsal sutures, but slightly raised and gently curved ventral side. It was recorded originally from the Maastrichtian rocks of Wadi Danili and Abu Zenima sections, Sinai, Egypt. It is recorded here for the first time outside Egypt, from the Paleocene of J. Mundassa, UAE.

Subfamily Gavelinellinae Hofker, 1956

Genus *Angulogavelinella* Hofker, 1957

Type species. *Discorbis gracilis* Marsson, 1878

***Angulogavelinella abudurbensis* (Nakkady, 1950)**

(Pl. 2, fig. 14)

1950 *Cibicides abudurbensis* Nakkady, p. 691, pl. 90, figs. 35-38.

1956 *Cibicides* cf. *abudurbensis*; Said and Kenawy, p. 154, pl. 7, fig. 7.

1993b *Cibicidoides abudurbensis*; Anan, p. 663, pl. 3, fig. 13.

1994 *Cibicidoides abudurbensis*; Speijer, p. 54, pl. 4, fig. 6.

2003 *Angulogavelinella abudurbensis*; El-Dawy and Hewaidy, p. 79, pl. 1, figs. 4-6.

2004 *Cibicidoides abudurbensis*; Anan, p. 44, pl. 1, fig. 5.

2005 *Gavelinella abudurbensis*; Sztrákos, p.230, pl. 17, fig. 11.

2009a *Cibicidoides abudurbensis*; Anan, p. 40, pl. 1, fig. 12.

2016 *Cibicidoides abudurbensis*; Orabi and Zaky, p. 188, pl. 3, fig. 15.

Remarks: The genus *Cibicidoides* Thalmann differs from *Gavelinella* Brotzen by its biconvex and biumbonate test and angular periphery than rounded in the other (Loeblich and Tappan, 1987). Weidich (1995) referred the species *abudurbensis* to the genus *Angulogavelinella* due to its apertural characteristics, functional morphology and bilamellar wall ultrastructure of the test. Nakkady (1950) originally recorded his species *abudurbensis* from the Maastrichtian of Abu Durba and Wadi Danili sections, Sinai, Egypt. It was also recorded from the Qarn El Barr section, UAE (Anan, 1993b), Tunisia (Speijer, 1994), France (Sztrákos, 2005). It is recorded here from the Paleocene of J. Mundassa, UAE.

***Angulogavelinella avnimelechi* (Reiss, 1952)**

(Pl. 2, fig. 15)

1952 *Pseudovalvulineria avnimelechi* Reiss, p. 269, text-fig. 2.

1976 *Angulogavelinella avnimelechi*; Aubert and Berggren, p. 431, pl. 8, figs. 8, 9.

1988 *Angulogavelinella avnimelechi*; Saint-Marc and Berggren, p. 111, pl. 4, figs. 13-16.

1993a *Angulogavelinella avnimelechi*; Anan, p. 317, pl. 3, fig. 11.

1994 *Angulogavelinella avnimelechi*; Bolli et al., p.161, fig. 45. 34-36.

2001 *Angulogavelinella avnimelechi*; Hewaidy and Strougo, p. 17, pl. 2, fig. 35.

2003 *Angulogavelinella avnimelechi*; Ali, pl. 10, figs. 18-20.

2004 *Angulogavelinella avnimelechi*; Anan, p. 49, pl. 1, fig. 14.

2005 *Angulogavelinella avnimelechi*; Sztrákos, p. 214, pl. 9, fig. 13.

2006 *Angulogavelinella avnimelechi*; Alegret and Ortiz, p. 442, pl. 1, figs. 10, 11.

2012 *Angulogavelinella avnimelechi*; Youssef and Taha, pl. 6, figs. 14, 15.

2020 *Angulogavelinella avnimelechi*; Anan, p. 12.

Remarks: This Maastrichtian–Paleocene species is characterized by its high conical planoconvex test, with flat dorsal side, keeled periphery, limbate ventral sutures with irregular depressions radiating from the umbilicus. Many authors, i.e., Berggren and Miller (1989), Anan (1993a; 2004), Alegret and Ortiz (2006), considered the last occurrence of the *avnimelechi* species marks the Paleocene/Eocene boundary. Anan (2004) proposed six benthic foraminiferal lineages, and one of them is the Maastrichtian *Angulogavelinella nekhliana* (Said and Kenawy) to Maastrichtian–Paleocene *A. avnimelechi* (Reiss). It was recorded in the Caribbean region (Bolli et al., 1994), France (Sztrákos, 2005), Tunisia (Saint-Marc and Berggren, 1988), Egypt (Alegret and Ortiz, 2006),

J. Malaqet, UAE (Anan, 1993a). It is recorded here from the Paleocene of J. Mundassa, UAE.

Genus *Paralabamina* Hansen, 1970

Type species. *Eponides lunata* Brotzen, 1948

***Paralabamina lunata* (Brotzen, 1948)**

1948 *Eponides lunata* Brotzen, p. 77, pl. 10, figs. 17, 18.

1953 *Eponides lunatus;* LeRoy, p. 30, pl. 9, figs. 24-26.

1956 *Eponides lunatus;* Said and Kenawy, p. 148, pl. 5, fig. 3.

1987 *Paralabamina lunata;* Loeblich and Tappan, p. 641, pl. 721, figs. 1-7.

1990 *Neoeponides lunata;* Thomas, p. 593, pl. 2, figs. 5, 6.

2011 *Eponides lunata;* Aly et al.,p. 109, pl. 6, fig. 4.

2020 *Paralabamina lunata;* Anan, p. 12, pl. 2.20.

Remarks: This Paleocene-Middle Eocene species has biconvex test, 5-6 chambers in the last whorl with a low slit aperture at the base of the last chamber. According to Loeblich and Tappan (1987), the species *lunata* was treated as the type species of the genus *Paralabamina* Hansen (1970). It was recorded from Sweden (Brotzen, 1948), Antarctica (Thomas, 1990), Egypt (LeRoy, 1953). It is also recorded here from the Paleocene of J. Mundassa, UAE.

5. Eustatic changes and tectonism in the Al Ain area

The deposition of the Paleocene Mundassa Member (MM) of the Muthaymimah Formation (MF) at both J. Mundassa and J. Malaqet in the Al Ain area reflect the effects of tectonic movements and sea-level changes. The pattern of sediments was driven by relatively rapid subsidence punctuated by eustatic sea-level variation.

1. The Tertiary sea began with the deposition of the neoautochthonous sediments of the lower Danian shaley marl succession (about 20 meters thick) in the Mundassa Basin, while the Malaqet area was still land. The Mundassa Basin hosted deposition of a Danian sedimentary sequence, which rests nonconformity on the obducted pre-Maastrichtian Semail Ophiolite (SO) that was deformed later by thrust faults and folds (Anan, 1993a).
2. The duration of the hiatus at the Cretaceous/Paleogene (K/P) boundary in Mundassa section includes the two earliest Danian biozones: P0 and Pα, about 0.02 Ma (Figure 2), while at J. Malaqet a marked basal conglomerate bed (about 0.50 cm) between the obducted pre-Maastrichtian SO and the upper Maastrichtian neoautochthonous limestone sediments of the Simsima Formation (SF) is observed. This depositional gap in the Al Ain area corresponds to an interval of tectonic activity that existed at most localities throughout the Middle East and other parts of the world (Anan, 2016).
3. The eustatic sea-level rise more and more in the Mundassa area and deposited the Selandian succession (covered area). The seawater also covered the Malaqet area (north of the Mundassa area) which rests on the shallow environment upper Maastrichtian neoautochthonous limestone sediments SF, and the deposition of the upper Danian MM exposed sediments in J. Malaqet took place with about 6 m thick (*Morozovella angulata* Zone) which may represent continued subsidence below sea level (Anan, 1993a; 2014).
4. After that, an intraformational bed (about 10 meters thick) in the Malaqet area accumulated upon the 6 m of upper Danian sediments, which represents rapid tectonics (Anan, 2015a).

6. Temporal distribution of the Paleocene species in J. Mundassa

Table 1 shows the distribution of forty six rotaliid benthic foraminiferal species belonging to twenty six genera from the Paleocene (Danian) in J. Mundassa. The following remarks can be presented:

1. Ten species are recorded in the Paleocene sediments of three exposed sections in the UAE (J. Mundassa, J. Malaqet and Qarn El Barr sections): *Pleurostomella subnodosa, Nuttallides truempyi, Pullenia coryelli, P. quinqueloba, Alabamina midwayensis, Osangularia plummerae, Anomalinoides rubiginosus, Gyroidinoides subangulata, Angulogavelinella abudurbensis* and *A. avnimelechi.*

Table 1. The distribution of the rotaliid Paleocene benthic foraminiferal species in Jabal Mundassa section, Al Ain area, UAE (samples number 1-14), x = recorded, Θ = illustrated.

p. No.	Paleocene rotaliid benthic foraminiferal species / Sample no		Jabal Mundassa section													
			1	2	3	4	5	6	7	8	9	10	11	12	13	14
1	*Bolivinoides*	*curtus*	-	-	-	-	-	-	-	-	-	-	-	x	Θ	x
2	*Praebulimina*	*carseyae*	-	-	-	-	-	-	-	-	-	x	-	x	x	-
3	*Orthokarstenia*	*applinae*	-	-	-	**x**	-	-	**x**	x	x	-	-	-	-	-
4	*Bulimina*	*mexicana*	-	-	-	-	-	-	-	x	-	x	x	-	x	Θ
5		*midwayensis*	x	-	**x**	-	-	x	-	x	-	Θ	x	-	-	-
6		*trinitatensis*	-	-	-	-	-	-	-	x	-	x	Θ	-	-	x
7	*Buliminella*	*grata*	-	-	-	-	-	-	-	-	Θ	-	-	x	x	x
8	*Globobulimina*	*suteri*	-	-	-	-	-	-	-	-	-	-	-	x	-	Θ

Continue Table 1

p. No.	Paleocene rotaliid benthic foraminiferal species / Sample no		Jabal Mundassa section													
			1	2	3	4	5	6	7	8	9	10	11	12	13	14
9	*Coryphostoma*	*midwayensis*	-	-	-	-	-	-	x	-	-	-	-	-	x	Θ
10		*nekhliana*	-	-	-	-	-	-	-	-	-	-	-	x	Θ	x
11	*Ellipsoglandulina*	*arafati*	-	-	-	-	-	-	-	-	-	-	x	x	-	x
12		*ellisi*	-	-	-	-	-	-	x	-	-	-	-	-	-	x
13	*Nodosarella*	*gracillima*	-	-	-	-	-	-	-	-	-	x	-	-	-	Θ
14		*paleocenica*	-	-	-	-	-	-	-	-	-	-	-	-	x	x
15		*subnodosa*	-	-	-	-	-	-	-	-	-	-	-	Θ	-	-
16	*Pleurostomella*	*naranjoensis*	-	-	-	-	-	-	-	-	-	-	-	-	-	Θ
17		*subnodosa*	-	-	-	-	-	-	-	-	-	-	-	x	Θ	x
18	*Orthomorphina*	*rohri*	-	-	-	x	-	-	-	-	x	x	-	-	-	x
19	*Stilostomella*	*paleocenica*	-	-	-	-	-	-	-	-	-	-	-	-	-	Θ
20	*Valvulineria*	*scrobiculata*	x	-	-	x	x	-	-	-	-	-	x	x	x	Θ
21	*Cibicidoides*	*pharaonis*	-	-	-	x	x	-	-	x	x	x	x	x	x	x
22		*pseudoacutus*	x	x	-	x	x	-	x	x	-	x	-	-	-	-
23	*Nuttallides*	*truempyi*	-	-	-	-	-	-	Θ	-	-	-	-	x	-	-
24	*Epistomaroides*	*spissiformis*	-	-	-	-	-	-	-	-	-	-	-	-	-	x
25	*Pullenia*	*angusta*	-	-	-	-	-	-	-	-	-	-	-	Θ	-	-
26		*coryelli*	-	-	-	-	-	-	-	-	-	-	Θ	-	-	-
27		*eocenica*	-	-	-	x	-	-	-	-	-	-	-	-	-	-
28		*quinqueloba*	-	-	-	-	-	-	-	-	-	Θ	-	-	-	-
29		*reussi*	-	-	-	-	-	-	-	-	-	-	-	Θ	-	-
30	*Quadrimorphina*	*esnehensis*	-	-	-	-	-	-	-	-	-	-	-	-	-	x
31	*Alabamina*	*midwayensis*	-	-	-	-	-	-	-	x	-	-	-	x	x	-
32	*Valvalabamina*	*planulata*	-	-	-	-	-	-	-	-	-	-	-	-	-	Θ
33	*Osangularia*	*plummerae*	-	-	-	-	-	-	-	-	-	-	-	-	-	x
34	*Anomalinoides*	*acutus*	-	-	-	-	-	-	-	-	-	-	-	-	x	x
35		*rubiginosus*	-	-	-	-	-	-	-	-	-	-	-	-	-	Θ
36		*umbonifera*	-	-	x	-	-	-	-	-	-	-	-	-	-	-
37	*Gyroidinoides*	*bollii*	-	-	-	-	-	-	-	-	-	-	-	x	-	-
38		*depressus*	-	-	-	-	-	-	-	-	-	-	-	-	-	x
39		*girardanus*	-	-	x	-	-	-	Θ	-	-	x	-	-	-	-
40		*globosus*	-	-	-	-	-	-	Θ	-	-	-	-	-	-	x
41		*reussi*	-	-	-	-	-	-	-	-	-	-	-	-	-	Θ
42		*subangulatus*	-	x	-	-	-	-	-	Θ	-	x	-	-	-	-
43	*Stensiöeina*	*esnehensis*	-	-	-	-	-	-	-	-	-	-	-	-	-	x
44	*Angulogavelinella*	*abudurbensis*	x	x	-	x	-	-	-	x	x	x	x	x	x	Θ
45		*avnimelechi*	-	-	-	-	-	-	-	-	-	-	-	-	-	Θ
46	*Paralabamina*	*lunata*	-	-	-	-	-	-	x	x	-	x	-	x	x	x

2. The UAE Paleocene benthic foraminiferal species are of the Midway type is suggested (according to Berggren and Aubert, 1975) and characteristic of essentially middle to outer shelf depth varying from 50–200 meters in the Danian, which due to variations in the depositional conditions throughout the Paleocene time.

Table 2 shows the paleogeographic distribution of the Paleocene rotaliid benthic foraminiferal species in the UAE and some other Tethyan localities. The following remarks can be presented:

1- The diversity of the identified rotaliid species gradually increased upward throughout the Paleocene of J. Mundassa, which may be explained by an increase in water depth.

2- The Paleocene succession of UAE yields 59 rotaliid species compared with 46 species from J. Mundassa, 27 species from J. Malaqet, and 21 species of Qarn El Barr section (Anan, 1993a,b)

3- The identified rotaliid Paleocene species from UAE (59 species) compared with 50 species that recorded from Egypt (LeRoy, 1953; Said and Kenawy, 1956), 27 species from the USA (Plummer, 1927; Cushman, 1922, 1927, 1936, 1946, 1951), 26 species from Tunisia (Berggren and Aubert, 1975), 24 species from Caribbean (Bolli et al., 1994), 15 species from each of EU (Reuss, 1851,1860; Sztrákos, 2000, 2005; Proto Decima and Bolli, 1982) and Atlantic Ocean (Tjalsma and Lohmann, 1983), 9 species from Pakistan (Haque, 1956; Nomura and Brohi, 1995), 7 from Japan and New Zealand (Kaiho, 1988), 5 species from Iraq (Al-Omari, 1970), 4 species from the Arabian Sea (Boltovskoy and Watanabe, 1985) and only 3 species from Jordan (Futyan, 1976). The unclosed number of Paleocene rotaliid species in the different localities in the Tethys may due to lack of available study, different latitudes, differences in paleoenvironmental conditions (depth, salinity, temperature, dissolved oxygen, nutrients).

Table 2. Paleogeographic distribution of the Paleocene rotaliid benthic foraminifera in the United Arab Emirates = UAE (MN = Mundassa and MQ = Malaqet, QB = Qarn El Barr sections) and some other Tethyan localities: USA = United States of America and Mexico, C = Caribbean region (Trinidad, Cuba), AO = Atlantic Ocean,EU = Europe(Sweden, Spain, France, Germany, Italy, Poland, Bulgaria, Slovenia, Czech), T = Tunisia, E= Egypt, J = Jordan, I = Iraq, AS = Arabian Sea, P = Pakistan, JZ = Japan and New Zealand (x = recorded species, - = not recorded).

Sp. No.	Paleocene rotaliidBenthic foraminiferal species		United Arab Emirates				Some Tethyan localities										
			MN	MQ	Q B	UAE	USA	C	AO	EU	T	E	J	I	AS	P	JZ
1	*Bolivinoides*	*curtus*	x	x	-	x	-	-	-	x	-	x	-	-	-	-	-
2	*Aragonia*	*velascoensis*	-	-	x	x	x	-	x	x	x	-	-	-	-	-	-
3	*Eouvigerina*	*aegyptiaca*	-	x	x	x	-	-	-	-	-	x	-	-	-	-	-
4	*Praebulimina*	*carseyae*	x	-	x	x	x	-	-	x	-	x	-	x	-	-	-
5	*Orthokarstenia*	*applinae*	x	x	-	x	x	-	-	x	x	x	x	-	-	x	-
6	*Bulimina*	*mexicana*	x	-	-	x	x	-	-	x	-	x	-	-	-	-	-
7		*midwayensis*	x	x	-	x	x	x	x	x	x	x	-	-	-	-	x
8		*quadrata*	-	-	x	x	x	-	-	-	x	x	-	-	-	-	-
9		*trinitatensis*	x	x	-	x	x	x	-	x	-	x	-	-	-	-	-
10	*Buliminella*	*grata*	x	-	-	x	-	x	x	-	-	-	-	-	x	-	-
11	*Globobulimina*	*suteri*	x	-	-	x	-	x	-	-	x	x	-	-	-	-	-
12	*Trifarina*	*esnaensis*	-	x	-	x	-	-	-	-	-	x	-	-	-	-	-
13	*Coryphostoma*	*midwayensis*	x	-	-	x	x	x	-	x	x	x	-	-	-	x	-
14		*nekhliana*	x	-	-	x	-	-	-	-	-	x	-	-	-	-	-
15	*Ellipsoglandulina*	*arafati*	x	-	-	x	-	-	-	-	-	x	-	-	-	-	-
16		*ellisi*	x	-	-	x	-	-	-	-	-	x	-	-	-	-	-

Continue Table 2

Sp. No.	Paleocene rotaliidBenthic foraminiferal species		United Arab Emirates				Some Tethyan localities										
			MN	MQ	Q B	UAE	USA	C	AO	EU	T	E	J	I	AS	P	JZ
17	*Nodosarella*	*gracillima*	x	-	-	x	x	-	-	-	-	x	-	-	-	-	-
18		*paleocenica*	x	-	-	x	x	x	-	-	-	x	-	-	-	x	-
19		*subnodosa*	x	-	-	x	x	x	x	X	-	x	-	-	-	-	-
20	*Pleurostomella*	*naranjoensis*	x	-	-	x	-	x	-	-	x	-	-	-	-	x	-
21		*subnodosa*	x	x	x	x	x	-	-	-	x	x	-	x	-	-	-
22	*Orthomorphina*	*rohri*	x	-	-	x	-	x	x	x	-	-	-	-	-	-	-
23	*Stilostomella*	*paleocenica*	x	-	-	x	x	x	-	x	x	x	-	-	-	x	-
24	*Valvulineria*	*aegyptiaca*	-	x	-	x	-	-	-	-	-	x	-	-	-	-	-
25		*scrobiculata*	x	-	-	x	-	-	-	-	x	x	-	-	-	-	-
26	*Discorbis*	*newmanae*	-	x	-	x	-	-	-	-	-	-	-	-	-	-	-
27	*Cibicidoides*	*alleni*	-	x	x	x	-	-	x	x	x	x	-	-	-	-	-
28		*howelli*	-	x	x	x	-	-	-	-	x	x	-	-	-	-	-
29		*mellahensis*	-	-	x	x	-	-	-	-	-	-	-	-	-	-	-
30		*pharaonis*	x	-	-	x	-	-	-	-	x	x	-	-	-	-	-
31		*pseudoacutus*	x	-	-	x	-	-	-	x	x	x	-	-	-	-	-
32	*Nuttallides*	*truempyi*	x	x	x	x	-	x	x	x	x	x	-	-	-	-	x
33	*Epistomaroides*	*spissiformis*	x	-	-	x	x	x	x	x	-	x	-	-	-	-	-
34	*Pullenia*	*angusta*	x	-	-	x	-	x	-	-	-	x	-	-	-	-	-
35		*coryelli*	x	x	x	x	x	x	x	x	-	x	-	x	-	-	x
36		*eocenica*	x	-	-	x	x	x	x	x	-	x	-	-	x	-	-
37		*quinqueloba*	x	x	x	x	-	x	x	x	x	x	-	-	-	x	-
38		*reussi*	x	x	-	x	-	-	-	-	-	-	-	-	-	-	-
39	*Quadrimorphina*	*allomorphinoides*	-	x	x	x	x	x	-	-	x	x	x	-	-	-	-
40		*esnehensis*	x	-	-	x	-	-	-	-	-	-	x	-	-	-	-
41	*Alabamina*	*midwayensis*	x	x	x	x	x	-	-	-	x	x	-	-	-	-	-
42	*Valvalabamina*	*planulata*	x	-	-	x	x	x	-	x	x	x	-	-	-	-	-
43	*Osangularia*	*plummerae*	x	x	x	x	-	-	-	x	x	x	-	-	-	-	-
44	*Anomalinoides*	*acutus*	x	x	-	x	x	-	-	x	x	x	-	-	-	-	-
45		*rubiginosus*	x	x	x	x	x	x	-	x	x	x	-	-	-	x	x

Continue Table 2

Sp. No.	Paleocene rotaliidBenthic foraminiferal species		United Arab Emirates				Some Tethyan localities										
			MN	MQ	Q B	UAE	USA	C	AO	EU	T	E	J	I	AS	P	JZ
46		*sinaensis*	-	-	x	x	-	-	-	-	-	x	-	-	-	-	-
47		*umboniferus*	x	-	-	x	-	-	-	-	-	x	-	-	-	-	-
48		*velascoensis*	-	-	x	x	x	-	-	-	-	x	-	x	-	-	-
49	*Gyroidinoides*	*bollii*	x	-	-	x	x	x	-	-	-	x	-	-	-	-	x
50		*depressus*	x	x	-	x	x	-	-	-	-	x	-	-	-	-	-
51		*girardanus*	x	x	-	x	-	x	x	-	-	x	-	-	-	-	x
52		*globosus*	x	x	-	x	x	x	x	-	x	x	-	-	x	x	x
53		*nitidus*	-	-	x	x	x	-	-	x	x	x	-	x	-	-	-
54		*reussi*	x	-	-	x	-	-	-	-	-	x	-	-	-	-	-
55		*subangulatus*	x	x	x	x	x	x	x	x	x	x	-	-	-	-	-
56	*Stensiöeina*	*esnehensis*	x	-	-	x	-	-	-	-	-	x	-	-	-	-	-
57	*Angulogavelinella*	*abudurbensis*	x	x	x	x	-	-	-	-	-	x	-	-	-	-	-
58		*avnimelechi*	x	x	x	x	-	x	x	x	x	x	-	-	x	x	-
59	*Paralabamina*	*lunata*	x	x	-	x	-	-	-	x	-	x	-	-	-	-	-

4- The close resemblance of the Paleocene rotaliid species of the UAE (59 species) with the synchronous age assemblage from Egypt (50 species) shows that they most probably were parts of the same paleogeographic province at that time.

5- Twenty five species have wide geographic distribution, having been found at more than four localities):*Aragon iavelascoensis, Praebulimina carseyae, Orthokarstenia applinae, Bulimina midwayensis, Coryphostoma midwayensis, Nodosarella paleocenica, N. subnodosa, Pleurostomella subnodosa, Stilostomella paleocenica, Cibicidoides alleni, Nuttallides truempyi, Epistomaroides spissiformis, Pullenia coryelli, P. eocenica, P. quinqueloba, Quadrimorphina allomorphinoides, Valvalabamina planulata, Anomalinoides acutus, A. rubiginosus, Gyroidinoides bollii, G. girardanus, G. globosa, G. nitidus, G. subangulata* and *Angulogavelinella avnimelechi.*

6- The wide geographic distribution of the recorded rotaliid assemblage emphasizes the interpretations that have been presented by some authors (i.e. Berggren, 1971; Adams et al.,1983; Rögl, 1999; Meulenkamp and Sissingh, 2003) about the extended realms of the Indo-Pacific with the Atlantic via the Tethys during the Paleocene.

7. Summary and Conclusions

- The studied section Jabal Mundassa represents the only outcrop in the Al Ain area (UAE) containing Danian sediments (Fig. 3, samples 1-14).
- Forty six rotaliid benthic foraminiferal species belonging to twenty six genera are identified and most of them (28 species, about 60 %) are illustrated.
- The K/P boundary in J. Mundassa is represented by a nonconformity, which is located between the pre-Maastrichtian allochthonus igneous rocks (SO) and the neoautochthonous Danian sedimentary rocks of the MM of the MF. The missing horizon includes the two early Danian biozones: *G. cretacea* (P0) and *P. eugubina* (Pα) as documented by Anan (2015a, b, 2016 and current study). This missing horizon at K/P boundary was most probably controlled by active tectonic (mainly synsedimentary faulting) and eustatic sea-level changes at that time (Vail et al., 1977).
- The studied section (J. Mundassa) has the only Danian outcrop in the Al Ain area, UAE (*Parasubbotina pseudobulloides* (P1a), *Subbotina triloculinoides* (P1b), *Globanomalina compressa*/*Praemurica inconstans*

(P1c) *Praemurica uncinata* (P2) Zones, and *Morozovella angulate* Zone (P3a) rest unconformably on the pre-Maastrichtian Serpentine Semail Ophiolite (Anan, 2016). On the other hand, the Paleocene sediments in the Qarn El Barr section (located about 6 km southwest of Al Dhayd city, in eastern Sharjah Emirate, UAE) is represented by the latest Danian *Morozovella angulata* Zone (P3a) (Anan, 1993b).

- The Cenozoic history of the Arabian Gulf area began with regression at the K/P boundary, which left most of Arabia emergent, except for the basinal areas in the northern UAE (Ras Al Khaima Basin) and in the southern UAE (Mundassa Basin), which left a Danian marine basin.

Acknowledgements

The author would like to express his sincere appreciation to the United Arab Emirates University for facilitating in the photography of the rotaliid foraminiferal assemblage, and the editor of the JJEES for his contribution and efforts, and also for the anonymous reviewers for valuable comments. Thanks are extended to my daughter Dr. Huda Anan for her help in the development of the figures and plates.

References

Adams, C.G., Gentry A.W., Whybrow, P.J. (1983): Dating the terminal Tethys event. Utrecht Micropaleontological Bulletin 30: 273-298.

Alegret, L., Arenillas, I., Arz, J.A., Molina, E. (2002): Eventoestratigrafia del limite Cretácico/Terciario en Aïn Settara, Tunicia: ¿diminución de produvtividad y/o de la oxigenación oceánicas?. Revista Mexicana de Ciencias Geológicas 19. 2: 121-136.

Alegret L., Cruz L. E., Fenero R., Molina E., Ortiz S., Thomas E. (2008). Effects of the Oligocene climatic events on the foraminiferal record from Fuente Caldera section (Spain, western Tethys). Palaeogeography, Palaeoclimatology, Palaeoecology 269: 94-102.

Alegret L.and Ortiz S. (2006). Global extinction event in benthic foraminifera across the Paleocene /Eocene boundary at the Dababiya Stratotype section. Micropaleontology 52 (5): 433-447.

Alegret L., Ortiz S., Arenillas I., Molina E. (2005). Paleoenvironmental turnover across the Paleocene /Eocene boundary at the Stratotype section in Dababiya (Egypt) based on benthic foraminifera. Terra Nova 17: 526-536.

Alegret, L. and Thomas, E. (2001). Upper Cretaceous and lower Paleogene benthic foraminifera from northeastern Mexico. Micropaleontology 47 (4): 269-316.

Alegret, L. and Thomas, E. (2005). Cretaceous/Paleogene boundary bathyal paleo-environments in the central North Pacific (DSDP Site 465), the Northwestern Atlantic (ODP Site 1049), the Gulf of Mexico and the Tethys: The benthic foraminiferal record. Palaeogeography, Palaeoclimatology, Palaeoecology 224: 53-82.

Al-Hitmi, H. (2002). Foraminiferal biostratigraphy of the Upper Cretaceous succession in southwest Qatar, Arabian Gulf. Egyptian Journal of Paleontology 2: 41-54.

Ali, M.Y. (2003). Micropaleontological and stratigraphical analyses of the Late Cretaceous/Early Tertiary succession of the Southern Nile Valley (Egypt). Der Fakultät für Geowissenschaften der Ruhr-Universität Bochum vorgelegte Dissertation zur Erlangung des Grades eines: 1-197.

Al-Omari, F.S. (1970). Upper Cretaceous and lower Cenozoic foraminifera of three oil wells in northwestern Iraq. Missouri University of Science and Technology, Doctoral Dissertations 2207: 1-213.

Alsharhan, A. and Nairn, A. (1995). Tertiary of the Arabian Gulf: sedimentology and hydrocarbon potential. Palaeogeography, Palaeoclimatology, Palaeoecolog 114: 369-384.

Alth, A. (1850). Geognostisch-paläontologische Beschreibung der nächsten Umgebing von Lemberg. Haidinger's Naturwissenschaftlich Abhandllungen Vienna 3: 171-284.

Aly, H.A., Abd el-Aziz, S.M., Abd El-Gaied, I.M. (2011). Middle and Upper Eocene benthic foraminifera from Wadi Bayad El Arab-Gebel Homret Shaibon area, Northeastern Beni Suef, Nile Valley, Egypt. Egyptian Journal of Paleontology 11: 79-131.

Anan, H.S. (1993a). Paleocene benthonic foraminifera of Jabal Malaqet, Al Ain region, United Arab Emirates. Al Azhar Bulletin of Science, Al Azhar University, Cairo 4(1): 293-320.

Anan, H.S. (1993b). Maastrichtian-Paleocene micropaleontology and biostratigraphy of Qarn El Barr section, Al Dhayd area, United Arab Emirates. Al Azhar Bulletin of Science, Al Azhar University, 4(2): 639-670.

Anan, H.S. (1995). Late Eocene biostratigraphy of Jabals Malaqet and Mundassa of Al Ain region, United Arab Emirates. Revue de Micropaléontologie 38 (1): 3-14.

Anan, H.S. (1996). Early Eocene foraminifera of Jabal Hafit, United Arab Emirates. Middle East Research Center Ain Shams University, Earth Science Series Cairo 10: 147-162.

Anan, H.S. (1998). Accelerated evolution in representatives of the genera Orthokarstenia and Discorbis (Benthic foraminifera) in the Maastrichtian and Paleocene of Egypt (Misr). Neues Jahrbuch für Geologie und Paläontologie, Mh. 6: 365-375.

Anan, H.S. (2004). A lineage phylogeny for some Maastrichtian to Ypresian benthic foraminifera in Egypt. Egyptian Journal of Paleontology 4:39-57.

Anan, H.S. (2007). Paleontological and biostratigraphical remarks on some diagnostic Tethyan benthic foraminifera. 2nd International Conference on the Geology of the Tethys, Cairo University 2007: 303-308.

Anan, H.S. (2008). Maastrichtian-Paleogene LeRoy's benthic foraminiferal species from Egypt and Tethyan-Atlantic regions. Revue de Paléobiologie 27 (2): 357-376.

Anan, H.S. (2009a). Paleontology, paleogeography, paleoenvironment and stratigraphical implications of the Nakkady's benthic foraminiferal fauna in Egypt and Tethys. Egyptian Journal of Paleontology 9: 31-52.

Anan, H.S. (2009b). Early Eocene Ellipsoglandulina arafati n. sp. (benthic foraminifera) from Abu Zenima section, west central Sinai, Egypt. Egyptian Journal of Paleontology 9: 111-117.

Anan, H.S. (2010). Paleontology and stratigraphical distribution of suborder Rotaliina (benthic foraminifera) from the Middle-Late Eocene Mazyad Member of the Dammam Formation in Jabal Hafit (Al Ain area), United Arab Emirates, Northern Oman Mountains. Revue dePaléobiologie 29 (1): 157-184.

Anan, H.S. (2011a). Paleontology, paleoenvironments, palaeogeography and stratigraphic value of the Maastrichtian-Paleogene and Recent foraminiferal species of Anan in the Middle East. Egyptian Journal of Paleontology 11: 49-78.

Anan, H.S. (2011b). Paleontology and stratigraphic significance of the Maastrichtian-Paleocene genus Bolivinoides in Egypt and Tethys. Egyptian Journal of Paleontology 11: 133-144.

Anan, H.S. (2011c). Maastrichtian small benthic foraminifera from Middle East and their distribution in the Tethys. Revue de Paléobiologie 30 (1): 13-30.

Anan, H.S. (2011d). additional to the Maastrichtian foraminiferaof the Middle East. Revue de Paléobiologie 30 (1): 295-311.

Anan, H.S. (2014). Significant episodes of tectonic activities in the Paleogene of Al Ain area, United Arab Emirates. International Journal of Chemical and Natural Science 2 (6): 180-188.

Anan, H.S. (2015a). Paleocene agglutinated foraminifera from Jabal Mundassa, Al Ain Area, United Arab Emirates. Spanish Journal of Paleontology 30 (2): 239-256.

Anan, H.S. (2015b). Paleocene Lagenid benthic foraminifera of Jabal Mundassa, Al Ain Area, United Arab Emirates. Egyptian Journal of Paleontology15: 61-83.

Anan, H.S. (2016). Planktic foraminifera of the Danian/ Selandian transition in Jabal Mundassa Al Ain area, United Arab Emirates. Neues Jahrbuch für Geologie und Paläontologie, Mh. 282, 3: 305- 318.

Anan, H.S. (2019a). On the variability of benthic foraminiferal species of the genus Pleurostomella in the Tethys. Journal of Microbiology and Experimentation 7 (3): 173-181.

Anan, H.S. (2019b). Maastrichtian-Paleogene benthic foraminifera from the Middle East and its distribution in the Tethys, a review. Journal of Microbiology and Experimentation 7 (6): 255-278.

Anan, H.S. (2020). Early Paleogene benthic foraminifera of Duwi section, Red Sea coast, Egypt. Journal of American Sciences 16 (2): 1-22.

Anan, H.S. and Hamdan, A.R. (1992). *Bolivinoides curtus* Reiss from the Paleocene of Jabal Malaqet, East of Al Ain, west of the Northern Oman Mountains, United Arab Emirates. Journal of Faculty of Science, U.A.E. University 4 (1): 200-211.

Anan, H.S. and Hamdan, A.R. (1993). Paleocene planktonic foraminifera of Jabal Malaqet, East of Al Ain, United Arab Emirates. Neues Jahrbuch für Geologie und Paläontologie H.1: 27-48.

Anan, H.S and Sharabi, S.A. (1988). Benthonic foraminifera from Upper Cretaceous-Lower Tertiary rocks of northwest Kharga Oasis, Egypt. Middle East Research Center, Ain Shams University, Earth Science Series, Cairo, 2: 191-218.

Aref, M. and Youssef, M. (1996). Benthic foraminiferal biostratigraphy of the Late Cretaceous / Early Tertiary succession along the Red Sea coastal area, Egypt. 3rd International Conference of the Geology of Arab World, Cairo University, Cairo: 539-573.

Aubert, J. and Berggren, W.A. (1976). Paleocene benthonic foraminiferal biostratigraphy and paleoecology of Tunisia. Bulletin de Centre de Recherches, Pau-SNPA 10(2): 379-469.

Barr, F.T. and Berggren, W.A. (1980). Lower Tertiary Biostratigraphy and Tectonics of Northeastern Libya. The Geology of Libya 1: 163-192.

Beckmann, J-P. (1953). Die Foraminiferen der Oceanic Formation (Eocaen-Oligocaen) von Barbados, Kl. Antillen. Ecoglae Geologicae Helvetiae 46: 301-412.

Beckmann, J-P. (1982). Campanian-Maastrichtian smaller benthic foraminifera. Micropaleontology and biostratigraphy of the Campanian to Paleocene of the Monte Giglio, Pergamo Province, Italy. Memorie di Scienze Geologiche. In: Beckmann, J-P. et al. (Eds.), Padova 35: 107-113.

Berggren, W.A. (1971). Micropaleontology and Cenozoic palaeoclimatology, part 2: 277-299 (In Berggren and Phillips: Influence of the Continental drift on the distribution of the Tertiary benthic foraminifera in the Caribbean and Mediterranean regions). In: Gray, C. (Ed.), Symposium on the geology of Libya, Tripoli, University of Libya, Faculty of Science 263-299.

Berggren, W.A. and Aubert, J. (1975). Paleocene benthonic foraminiferal biostratigraphy, paleobiogeography and paleoecology of Atlantic-Tethyan regions: Midway-type fauna. Palaeogeography, Palaeoclimatology, Palaeoecology 18: 73-192.

Berggren, W.A. and Miller, K.G. (1989). Cenozoic bathyal and Abyssal calcareous benthic foraminiferal zonation. Micropaleontology 35 (4): 308-320.

Berggren, W.A. and Pearson, P.N. (2005). A revised tropical to subtropical Paleogene planktonic foraminiferal zonation. Journal of Foraminiferal Research 35 (4): 279-298.

Boltovskoy, E. and Vera Ocampo, J. (1993). Benthic foraminifers from DSDP site 219 (Eocene-Pleistocene, Arabian Sea). Revista Española de Micropaleontologia 25 (1): 127-156.

Boltovskoy, E. and Watanabe, S. (1985). Foraminiferos bentonicos del Cenozoico (Paleoceno superior-Cuartario) del sitio 305 del DSDP (Pacifico Noroccidental). Revista Española de Micropaleontologia 27 (2): 281-314.

Boukhary, M., Abdeen, M.M., Alsharhan, A.S. (2003). Stratigraphical setting and structural evolution of Jabal Malaqet, northern Oman Mountains, United Arab Emirates. Neues Jahrbuch für Geologie und Paläontologie, Mh. 8: 477-497.

Bolli, H.M., Beckmann, J-P., Saunders, J.B. (1994). Benthic foraminiferal biostratigraphy of the south Caribbean region. Cambridge University: 1-408.

Brotzen, F. (1940). Flinträннaus och Trindelrännans geologi (Öresund). Sveriges Geologiska Undersökning, Stockholm 34: 3-33.

Brotzen, F. (1948). The Swedish Paleocene and its foraminiferal fauna. Sweden Sveriges Geologiska Undersökning, series C, no. 493: 1-140.

Cimerman, F., Jelen, B., Skaberne, D. (2006). Late Eocene benthic foraminiferal fauna from clastic sequence of the Socka-Dobrna area and its chronostratigraphic importance (Slovenia). Geologija 49 (1): 7-44.

Clemmensen, A. and Thomsen, E. (2005). Paleoenvironmental changes across the Danian-Selandian boundary in the North Sea Basin. Palaeogeography, Palaeoclimatology, Palaeoecology

219: 351-394.

Cushman, J.A. (1922). The Byram calcareous marl of Mississippi and its Foraminifera. United States Geological Survey, Professional Paper 129E: 87-105.

Cushman, J.A. (1926). The foraminifera of the Velasco Shale of the Tampico Embayment. American Association of Petroleum Geology Bulletin 10: 581-612.

Cushman, J.A. (1927). An outline of the re-classification of the Foraminifera. Contributions from the Cushman Laboratory for Foraminiferal Research 3: 1-105.

Cushman, J.A. (1936). New genera and species of the families Verneuilinidae and Vulvulinidae and of the subfamily Virgulininae. Cushman Foundation for Foraminiferal Research, Special Publication 6: 1-71.

Cushman, J.A. (1944). A Paleocene foraminiferal fauna from the Coal Bluff Marl Member of Alabama. Contributions from the CushmanLaboratory for Foraminiferal Research 20 (2): 29-50.

Cushman, J.A. (1946). Upper Cretaceous foraminifera of the Gulf Coastal Region of the United States and adjacent areas.

United States Geological Survey, Professional Paper 206: 1-241.

Cushman, J.A. (1951). Tertiary foraminifera of coastal Ecuador, Eocene. Journal of Paleontology 25: 129-164.

Cushman, J.A. and Bermúdez, P.J. (1937). Further new species of foraminifera from the Eocene of Cuba. Contributions from the Cushman Laboratory for Foraminiferal Research, 13: 1-29.

Cushman, J.A. and Jarvis, P.W. (1928). Cretaceous foraminifera from Trinidad. Contributions from the Cushman Laboratory for Foraminiferal Research 4 (4): 84-103.

Cushman, J.A. and Parker, F.L. (1936). Some American Eocene Buliminas. Contributions from the Cushman Laboratory for Foraminiferal Research 12 (2): 39-45

Cushman, J.A. and Renz, H.H. (1941). New Oligocene-Miocene Foraminifera from Venezuela. Cushman Foundation for Foraminiferal Research 17 (1): 1-27.

Cushman, J.A. and Renz, H.H. (1946). The foraminiferal fauna of the Lizard Springs Formation of Trinidad, British West Indies. Contributions from the Cushman Laboratory for Foraminiferal Research, Special Publication 18: 1-48.

Cushman, J.A. and Renz, H.H. (1948). Eocene foraminifera of the Navet and Hospital Hill formations of Trinidad. Cushman Laboratory for Foraminiferal Research, Special Publication 24: 1-42.

Cushman, J.A. and Stainforth, R.M. (1945). The Foraminifera of the Cipero marl formation of Trinidad, British West Indies. Cushman Laboratory for Foraminiferal Research, Special Publication 14: 1-74.

Cushman, J.A. and Stainforth, R.M. (1951). Tertiary foraminifera of the coastal Ecuador: Part 1, Eocene. Journal of Paleontology 25 (2): 129-164.

Cushman, J.A. and Todd, R. (1943). The genus Pullenia and its species. Contributions from the Cushman Laboratory for Foraminiferal Research 241: 1-28.

Cushman, J.A. and Todd, R. (1946). A foraminiferal fauna from the Paleocene of Arkansas. Contributions from the Cushman Laboratory for Foraminiferal Research 22: 45-69.

Cushman, J.A. and Siegfus, S.S. (1939). Some new and interesting foraminifera from the Kreyenhagen Shale of California. Contributions from the Cushman Laboratory for Foraminiferal Research 15 (2): 23-33.

Drobne, K., Bartol, M., Premec-Fućek, V., Schenk, B., Ćosović, V., Pugliese, N. (2012). Microfauna and nannoplankton below the Paleocene/Eocene transition in hemipelagic sediments at the southern slope of Mt. Nanos (NW part of the Paleogene Adriatic carbonate platform, Sloveni. Austrian Journal of Earth Sciences Vienna 105 (1): 208-223.

El-Dawy, M.H. (2001). Paleocene benthic foraminiferal biostratigraphy and paleobathymetry, El Sheikh Fadl and Ras Gharib, Eastern Desert, Egypt. Micropaleontology 47 (1): 23-46.

El-Dawy, M. H. and Hewaidy, A. A. (2003). Biostratigraphy, paleobathymetry and biogeography of some Late Maastrichtian - Early Eocene Rotaliina from Egypt. Egyptian Journal of Paleontology 3: 55-86.

Ernst, S.R., Guasti, E., Dupuis, C., Speijer, R.P. (2006). Environmental perturbation in the southern Tethys across the Paleocene/Eocene boundary (Dababiya, Egypt): Foraminiferal and clay mineral records. Marine Micropaleontology 60: 89-111.

Futyan, A.I. (1976). Late Mesozoic and Early Cainozoic benthonic foraminifera from Jordan. Palaeontology 19 (3): 53-66.

Galeotti, S. and Coccioni, R. (2002). Changes in coiling direction of *Cibicidoides pseudoacutus* (Nakkady) across the Cretaceous-Tertiary boundary of Tunisia: palaeoecological and biostratigraphic implications. Palaeogeography, Palaeoclimatology, Palaeoecology 178: 197-210.

Gawor-Biedowa, E. (1992). Campanian and Maastrichtian foraminifera from the Lublin Upland, Eastern Poland. Palaeotologica Polonica 52: 1-226.

Guppy, R.J.L. (1894). On some foraminifera from the microzoic deposits of Trinidad, West Indies. Proceedings of the Zoological Society of London: 647-653.

Hagenow, F. von (1842). Monographie der Rügen'sche Kreide-Versteinerungen. Abt 3: Mollusken. Neues Jahrbuch für Mineralogie, Geognosie, Geologie und Petrefactenkunde, Stuttgart 528-575.

Hamdan, A.R. and Anan, H.S. (1993). Cretaceous/Tertiary boundary in the United Arab Emirates. Middle East Research Center Ain Shams University, Earth Science Series Cairo 7: 223-231.

Haque, A.F.M.M. (1956). The foraminifera of the Ranikot and the Laki of the Nammal Gorge, Salt Range, Pakistan. Pakistan Geological Survey Memoir, Palaeontologica Pakistanica 1: 1-229.

Hewaidy, A.A. (1994). Biostratigraphy and paleobathymetry of the Garra-Kurkur area, southeast Aswan, Egypt. Middle East Research Center, Ain Shams University, Earth Science Series, Cairo 8:48-73.

Hewaidy, A.A. (1997). A proposed paleoecologic scheme for the Upper Cretaceous-Lower Tertiary sequences in Egypt. Middle East Research Center, Ain Shams University, Earth Science Series, Cairo 11: 159-168.

Hewaidy, A.A. and Strougo, A. (2001). Maastrichtian-Lower Eocene benthic foraminiferal distribution and paleoecology of three outcrop sections in Farafra. Egyptian Journal of Paleontology 1: 1-22.

Hiltermann, H. (1963). Zur Entwicklung der Benthos-Foraminifere Bolivinoides: Evolutionary trends in Foraminifera. Elsevier Publisher Company, Amsterdam: 198-222.

Hulsbos, R.E., Kroon, D., Jansen, H.S.M., Van Hinte, J.E. (1989). Lower Eocene benthic foraminifera and paleoenvironment of the outer Vøring Plateau, Norwegian Sea (DSDP Site 338). Micropaleontology 35 (3): 256-273.

Ingle, J.C., Keller, G., Kolpack, R.L. (1980). Benthic foraminiferal biofacies, sediments and water masses of the southern Peru-Chile Trench area, southeastern Pacific Ocean. Micropaleontology 26 (2): 113-150.

Ismail, A.A. (2012). Late Cretaceous-Early Eocene benthic foraminifera from Esh El Mallaha area, Egypt. Revue de Paléobiologie 31 (1): 15-50.

Kaiho, K. (1988). Uppermost Cretaceous to Paleocene bathyal benthonic foraminiferal biostratigraphy of Japan and New Zealand: Latest Paleocene-Middle Eocene benthic foraminiferal species turnover. Revue de Paléobiologie, Special Volume 2 (Benthos'86): 553-559.

Karoui-Yaakoub, N. (2006). Effet du réchauffement climatique global sur le comportement des foraminiféres benthiques l'intervalle de passage Paléocène-Eocene de la coupe d'Ellès (Tunisie). Revue de Paléobiologie Genéve 25 (2): 575-591.

Keller, G. (1988). Biotic turnover in benthic foraminifera across the Cretaceous/Tertiary boundary at El Kef, Tunisia. Palaeogeography, Palaeoclimatology, Palaeoecology 66: 153-171.

LeRoy, L.W. (1953). Biostratigraphy of Maqfi section, Egypt. Geological Society of American Memoir 54: 1-73.

Loeblich, A.R. and Tappan, H. (1987). Foraminiferal genera and their classification. Van Nostr and Reinhold (VNR), New York, part 1: 970 p., part 2: 847 p.

Luger, P. (1985). Stratigraphie der marinen Oberkreide und des Alttertiars im sudwestlichen Obernil-Becken (SW-Agypten) under besondere Berucksichtig, undder Micropaläontologie, Palökologie und Micro-paläogeographie. Berliner Geowissenschaftliche Abhandlungen A. 63: 1-151.

Meulenkamp, J.E. and Sissingh, W. (2003). Tertiary palaeogeography and tectonostratigraphic evolution of the Northern and Southern Peri-Tethys platforms and the intermediate domains of the African-Eurasian convergent plate boundary zone. Palaeogeography, Palaeoclimatology, Palaeoecology 196: 209-228.

Miller, K.G. (1983). Eocene-Oligocene paleoceanography of the deep bay of Biscay: Benthic foraminiferal evidence. Marine Micropaleontology 7 (5): 403-440.

Nakkady, S.E. (1950). A new foraminiferal fauna from the Esna Shale and Upper Cretaceous chalk of Egypt. Journal of Paleontology 24 (6): 675-692.

Nolan, S.C., Skelton, P.W., Clissold, B.P., Smewing, J. D. (1990). Maastrichtian to early Tertiary stratigraphy and paleogeography of the Central and Northern Oman Mountains. In: Robertson, A.H.F., Searle M.P., Ries A.C. (Eds.), The Geology and Tectonics of the Oman Region. Geological Society of London, Special Publication 49: 495-519.

Nomura, R. and Brohi, I. A. (1995). Benthic foraminiferal fauna during the time of the Indian-Asian contact, in southern Balochistan, Pakistan. Marine Micropaleontology 24: 215-238.

Noweir, M.A. and Eloutefi, N.S. (1997). The structure and stratigraphy of Jabal Malaqet-Jabal Mundassa area, Southeast Al-Ain, Northern Oman Mountains, United Arab Emirates. Neues Jahrbuch für Geologie und Paläontologie, Abhandlungen 204 (2): 263-284.

Nuttall, W.L.F. (1930). Eocene foraminifera from Mexico. Journal of Paleontology 4: 271-293.

Orabi, H.O. and Zaky, A.S. (2016). Differential dissolution susceptibility of Paleocene foraminiferal assemblage from Farafra Oasis, Egypt. Journal of African Earth Sciences 113: 181-193.

Ortiz, S. and Thomas, E. (2006). Lower-middle Eocene benthic foraminifera from the Fortuna Section (Betic Cordillera, southeastern Spain). Micropaleontology 52 (2): 97-150.

Ozsvárt, P. (2007). Middle and Late Eocene benthic foraminiferal fauna from the Hungarian Paleogene Basin: systematics and paleoecology. Geologica Pannonica, Special Publication 2, 129 p.

Parisi, G. and Coccioni, R. (1988). Deep-water benthic foraminifera of the Eocene-Oligocene boundary in the Massignano section (Ancona, Italy). International Subcommittee on Paleogene stratigraphy, E/O Meeting, Special Publication, Ancona 2 (3): 97-109.

Parker, F.L. and Bermúdez,P. J. (1937). Eocene Species of the genera *Bulimina* and *Buliminella* from Cuba. Journal of Paleontology 11 (6): 513-516.

Plummer, H.J. (1927). Foraminifera of the Midway Formation in Texas. Bulletin University of Texas 2644: 3-206.

Plummer, H.J. (1931). Some Cretaceous foraminifera in Texas. Bulletin University of Texas 3101: 109-203.

Proto Decima, F. and Bolli, H.M. (1978). Southeast Atlantic DSDP Leg 40 Paleogene benthic foraminifers. In: Bolli H.M., Ryan, W.B.F. et al. (Eds.), Washington, D. C. Initial Report of the DSDP, United States Government Printing Office 40: 783-809.

Proto Decima, F. and Bolli, H.M. (1982). Paleocene smaller benthic foraminifera. In: Beckmann, J-P. et al. (Eds.), Micropaleontology and biostratigraphy of the Campanian to Paleocene of the Monte Giglio, Bergamo Province, Italy. Memorie de Scienze Geologiche, Padova, 35: 114-120.

Proto Decima, F. and De Biase, R. (1975). Foraminiferi bentonici del Paleocene, dell' Eocene inferiore e medio. In: Braga, G. et al.: Foraminiferi bentonici del Paleocene ed Eocene della sezione di Possagno. Schweizerische Paläontologische Abhandlungen 97: 87-98.

Reiss, Z. (1952). Two new species of foraminifera from Israel. Bulletin Research Council, Israel, 2: 269-270.

Reiss, Z. (1954). Upper Cretaceous and Lower Tertiary Bolivinoides from Israel. Contributions from the Cushman Foundation for Foraminiferal Research 5 (4): 154-164.

Reuss, A.E. (1851). Ober die fossilen foraminiferen und Entomostraceen der Septarienthone der Umgegend von Berlin. Zeitschrift der Deutschen Geologischen Gesellschaft, Berlin 3: 49-92.

Reuss, A.E. 1860. Die foraminiferen der westphälischen Kreideformation. Sitzungsber Bayerischen Akademie der Wissenschaften mathematisch naturwissenschaften, Vienna 40: 147-238.

Rögl, F. (1999). Mediterranean and Paratethys. Facts and hypotheses of an Oligocene to Miocene paleogeography (short overview). Geologica Carpathica 50 (4): 339-349.

Said, R. and Kenawy, A. (1956). Upper Cretaceous and Lower Tertiary foraminifera from northern Sinai, Egypt. Micropaleontology 2(2): 105-173.

Saint-Marc, P. (1992). Biogeographic and bathymetric distribution of benthic foraminifera in Paleocene El Haria Formation of Tunisia. Journal of African Earth Sciences 15 (3/4): 473-487.

Saint-Marc, P. and Berggren, W.A. (1988). A quantitative analysis of Paleocene benthic foraminiferal assemblages in central Tunisia. Journal of Foraminiferal Research 18 (2): 97-113.

Salaj, J. 1976. Foraminiferida, zonation and subzonation of the Paleocene of Tunisia. Acta Palaeotologica Polonica 21 (2): 127-190.

Saperson, E. and Janal, M. (1980). Biostratigraphy of the Anomalinidae and Cibicididae in Soviet Tethyan Paleogene. Micropaleontology, 26 (4): 392-413.

Schwager, C. 1883. Die Foraminiferen aus dem Eocaenable-gerungen der Libyschen wuste und Agyptens. Paleontographica 30: 81-153.

Shahin, A. (2001). Mass extinction and bioevents across the Paleocene-Eocene boundary in the Western Sinai, Egypt. Neues Jahrbuch für Geologie und Paläontologie, Monatshefte 1: 1-20.

Sliter, W.V. (1968). Upper Cretaceous foraminifera from Southern California and Northwestern Baja California, Mexico. Kansas Paleontological Contribution 49(7): 1-171.

Speijer, R.P. (1994). Extinction and recovery patterns in benthic foraminiferal paleocommunities across the Cretaceous/ Paleocene and Paleocene/Eocene boundaries. Geologica Ultraiectina, Universität Utrecht 124: 1-191.

Sprong, J., Youssef, M.A., Bornemann, A., Schulte, P., Steurbaut, E., Stassen, P., Kouwenhoven, T.J., Speijer, R.P. (2011). A multi-proxy record of the Latest Danian Event at Gebel Qreiya, Eastern Desert, Egypt. Journal of Micropalaeontology 30: 167–182.

Stassen, P., Etienne, S., Morsi, A-M., Schulte, P., Speijer, R.P. (2012). Biotic impact of Eocene thermal maximum 2 in a shelf

setting (Dababiya, Egypt). Austrian Journal of Earth Sciences

105(1):154-160.

Sztrákos, K. (2000). Eocene foraminifers in the Adour Basin (Aquitaine, France): biostratigraphy and taxonomy. Revue de Micropaléontologie 43 (1-2): 71-172.

Sztrákos, K. (2005). Paleocene and lowest Eocene foraminifera from the north Pyrenean trouph (Aquitaine, France). Revue de Micropaléontologie 48: 175-236.

Thalmann, H.E. (1959). New names for foraminiferal homonyms. Contributions from the Cushman Laboratory for Foraminiferal Research 4: 130-131.

Thomas, E. (1990). Late Cretaceous through Neogene Deep-Sea benthic foraminifers (Maud Rise, Weddell Sea, Antractica). Proceeding of the Ocean Drilling Program, Scientific Results 113: 571-594.

Tjalsma, R.C. and Lohmann, G. P. (1983). Paleocene-Eocene bathyal and abyssal benthic foraminifera from the Atlantic Ocean. Micropaleontology, Special Publication 4: 1-90.

Vail, P.R. and Hardenbol, J. (1979). Sea level change during the Tertiary. Oceanus, 22: 71-79.

Vail, P.R., Mitchum, R.M., Thompson, III S. (1977). Seismic stratigraphy and global changes of sea level. In: Payton, C.E. (Ed.), Stratigraphic Interpretation of Seismic Data. American Association of Petroleum Geologists Memoir, 26: 83-97.

Valchev, B. (2006). Benthic foraminiferal morphogroups from the Paleocene of the coastal part of East Stara Planina Mts. Geologica Balcanica 35(3-4): 41-48.

Valchev, B. (2007). Midway-Type Benthic foraminifera from the Paleocene of the coastal part of East Stara Planina (Eastern Bulgaria). Family Textulariidae Ehrenberg, 1838 to Family Stilostomellidae Finlay, 1947. Annual of the University of Mining and Geology “St. Ivan Rilski”, Geology and Geophysics 50(1): 129-137.

Waśkowska-Oliwa, A. (2005). Foraminiferal palaeodepth indicators from the lower Palaeogene deposits of the Subsilesian Unit (Polish Outer Carpathians). Studia Geologica Polonica, Kraków 124: 297–324.

Warrak,M. (1996). Origin of the Hafit structure: implications for timing the Tertiary deformation in the Northern Oman Mountains. Journal of Structural Geology 18 (6): 803-818.

Weidich, K.F. (1995). The genus *Angulogavelinella* Hofker, 1957 and its species (Foraminiferida: Rotaliina, Upper Cretaceous-Lower Tertiary). Journal of Foraminiferal Research, 25 (4): 309-333.

White, P.M. (1929). Some index foraminifera of the Tampico Embayment area of Mexico. Journal of Paleontology 3: 30-58.

Youssef, M. and Taha, S. (2012). Biostratigraphy and Paleoecology of Paleocene/Eocene (P/E) interval of some geological sections in Central Egypt. Arabian Journal of Geosciences: 1- 23.

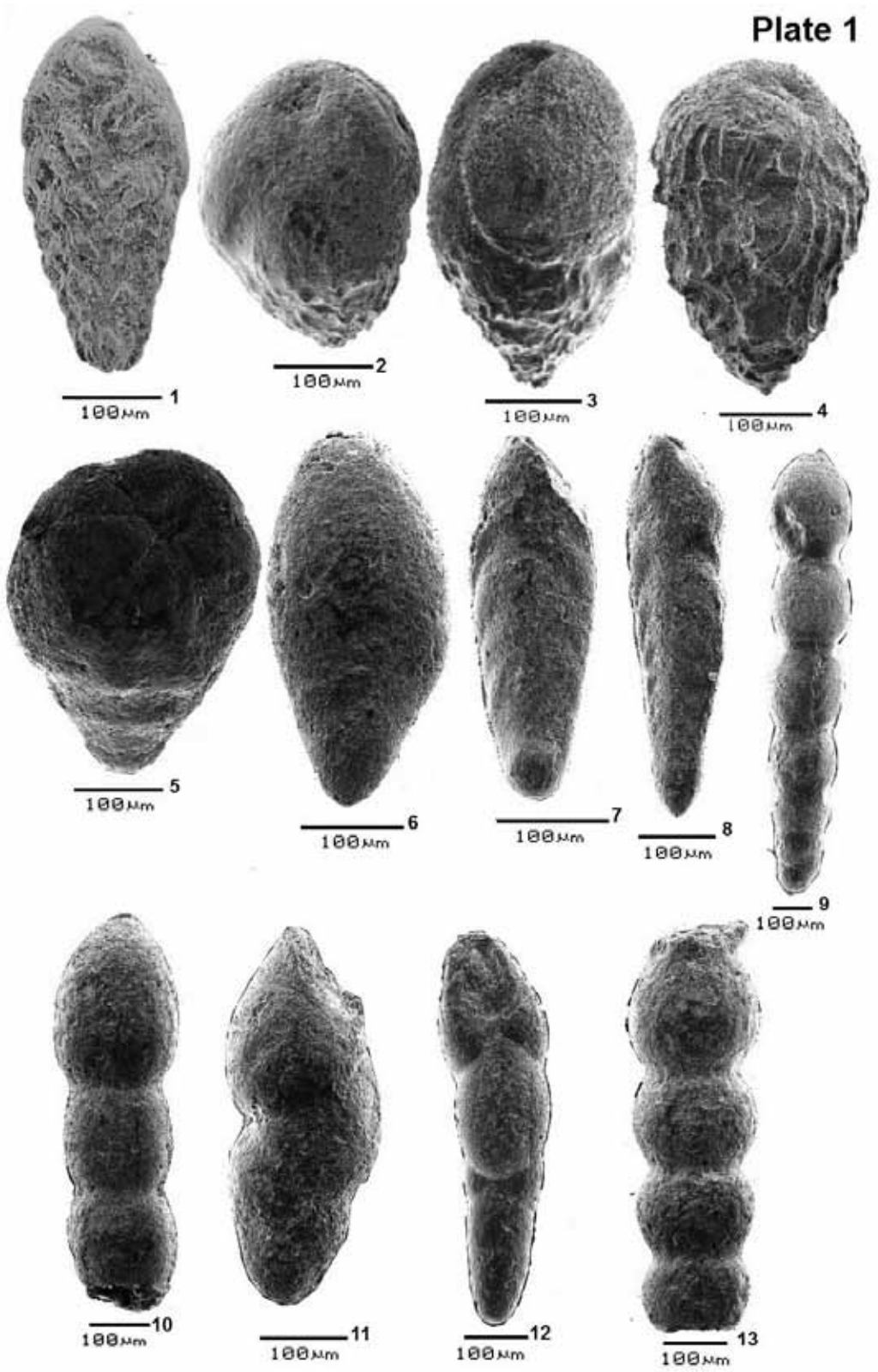

Explination of Plate 1

Fig. 1. *Bolivinoides curtus* Reiss, 1954, Sample 13, Danian of J. Mundassa, UAE.
Fig. 2. *Bulimina mexicana* Cushman, 1922, S. 14.
Fig. 3. *Bulimina midwayensis* Cushman and Parker, 1936, S. 10.
Fig. 4. *Bulimina trinitatensis* Cushman and Jarvis, 1928, S. 11.
Fig. 5. *Buliminella grata* Parker and Bermúdez, 1937, S. 9.
Fig. 6. *Globobulimina suteri* (Cushman and Renz, 1946), S. 14.
Fig. 7. *Coryphostoma midwayensis* (Cushman, 1936), S. 14.
Fig. 8. *Coryphostoma nekhliana* (Said and Kenawy, 1956), S. 13.
Fig. 9. *Nodosarella gracillima* Cushman, 1944, S. 14.
Fig. 10. *Nodosarella subnodosa* (Guppy, 1894), S. 12.
Fig. 11. *Pleurostomella naranjoensis* Cushman and Bermúdez, 1937, S. 14.
Fig. 12. *Pleurostomella subnodosa* Reuss, 1860, S. 13.
Fig. 13. *Stilostomella paleocenica* (Cushman and Todd, 1946), S. 14.

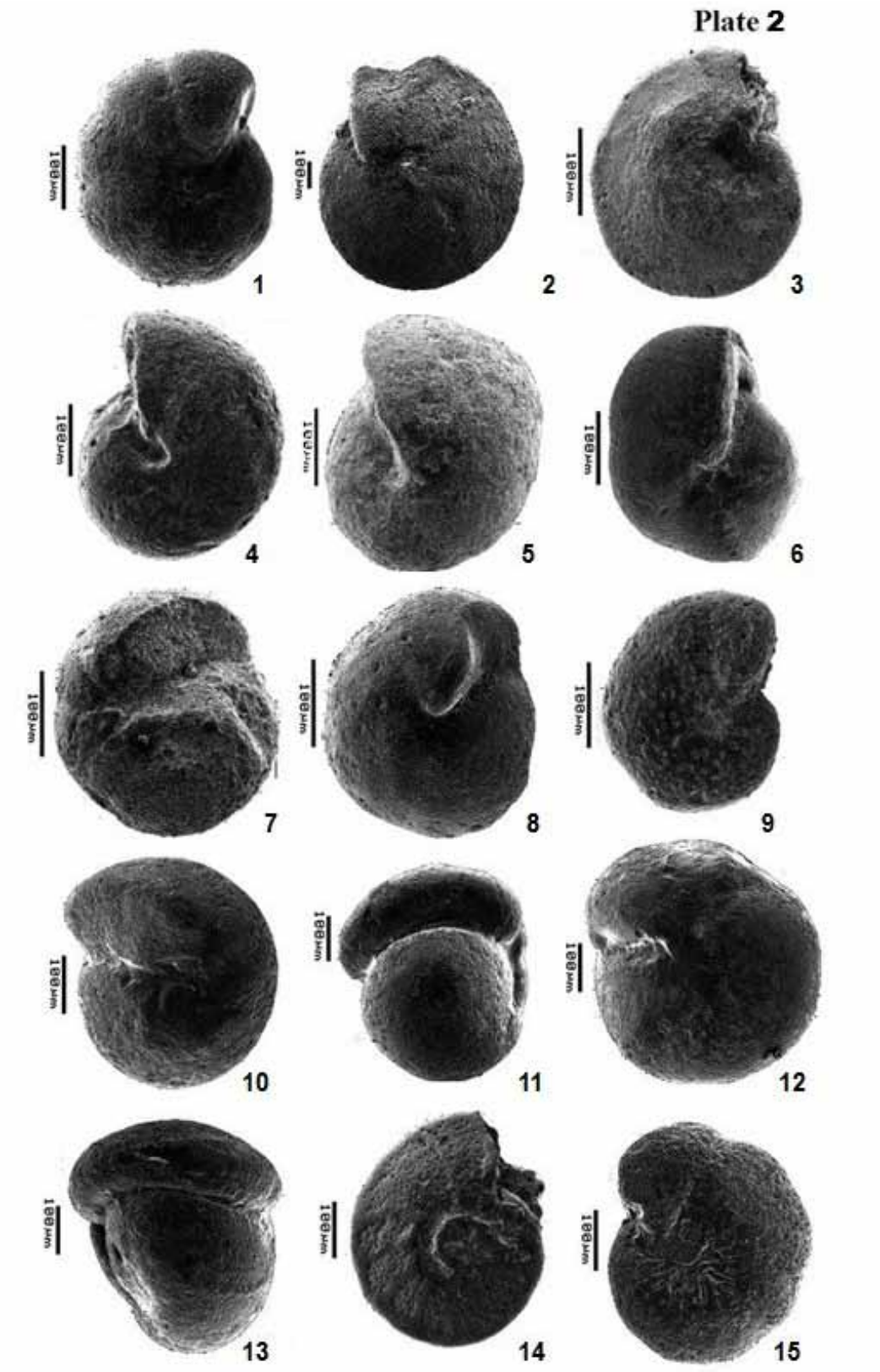

Explination of Plate 2

Fig. 1. *Valvulineria scrobiculata* (Schwager, 1883), Sample 14, Danian of J. Mundassa, UAE.
Fig. 2. *Cibicidoides libycus* (LeRoy, 1953), S. 14.
Fig. 3. *Nuttallides truempyi* Nuttall, 1930, S. 7.
Fig. 4. *Pullenia angusta* Cushman and Todd, 1943, S. 12.
Fig. 5. *Pullenia coryelli* (White, 1929), S. 11.
Fig. 6. *Pullenia quinqueloba* (Reuss, 1851), S. 10.
Fig. 7. *Pullenia reussi* (Cushman and Todd, 1943), S. 12.
Fig. 8. *Valvalabamina planulata* (Cushman and Renz, 1941), S. 12.
Fig. 9. *Anomalinoides rubiginosus* (Cushman, 1926), S. 14.
Fig. 10. *Gyroidinoides girardanus* (Reuss, 1851), S. 7, Danian.
Fig. 11. *Gyroidinoides globosus* (Hagenow, 1842), S. 7, Danian.
Fig. 12. *Gyroidinoides reussi* (Said and Kenawy, 1956), S. 14.
Fig. 13. *Gyroidinoides subangulatus* (Plummer, 1927), S. 8, Danian.
Fig. 14. *Angulogavelinella abudurbensis* (Nakkady, 1950), S. 14.
Fig. 15. *Angulogavelinella avnimelechi* (Reiss, 1952),S. 14, Danian of J. Mundassa, UAE.

المملكة الأردنية الهاشمية

صندوق دعم البحث العلمي

الجامعة الهاشمية

المجلة الأردنية
لعلوم الأرض والبيئة

JJEES

مجلة علمية عالمية محكمة

المجلد (١٢) العدد (٢)

http:// jjees.hu.edu.jo/

ISSN 1995-6681

المجلة الأردنية لعلوم الأرض والبيئة

مجلة علمية عالمية محكمة

المجلة الأردنية لعلوم الأرض والبيئة: مجلة علمية عالمية محكمة ومفهرسة ومصنفة، تصدر عن عمادة البحث العلمي في الجامعة الهاشمية وبدعم من صندوق البحث العلمي - وزارة التعليم العالي والبحث العلمي، الأردن.

ترسل البحوث إلكترونيا إلى البريد الإلكتروني التالي:

رئيس تحرير المجلة الأردنية لعلوم الأرض والبيئة

jjees@hu.edu.jo

لمزيد من المعلومات والأعداد السابقة يرجى زيارة موقع المجلة على شبكة الانترنت على الرابط التالي:

www.jjees.hu.edu.jo

المملكة الأردنية الهاشمية صندوق دعم البحث العلمي الجامعة الهاشمية

JJEES

المجلة الأردنية لعلوم الأرض والبيئة

المجلد (١٢) العدد (٢)

مجلة علمية عالمية محكمة تصدر بدعم من صندوق دعم البحث العلمي

ISSN 1995-6681 jjees.hu.edu.jo حزيران ٢٠٢١